Cationic Titanium Amidinate and Guanidinate Complexes

Adam F. Russell MSci ARCS AMRSC

Thesis submitted to the University of Oxford for the degree of
Doctor of Philosophy, May 2014.

Statement of confidentiality

Some of the work described in this Thesis is of a commercially sensitive nature. The examiners are requested to respect the confidentiality of this information and not to disclose the information to individuals outside the Board of Examiners.

The work described in this Thesis was carried out in the Chemistry Research Laboratory, University of Oxford from October 2010 to May 2014 under the supervision of Professor Philip Mountford. All work is my own unless stated to the contrary, and has not previously been submitted for any degree at this or any other university.

Adam F. Russell

May 2014

Abstract

Adam Francis Russell Trinity 2014

Balliol College D.Phil. Thesis

This Thesis describes the synthesis and characterisation of half-sandwich complexes supported by κ^1-amidinate and κ^1-guanidinate ligands as well as the cationic species produced on activation. The chemistry of the cationic species is detailed and DFT studies which have also been carried out to elucidate the bonding in relevant complexes are also presented.

Chapter 1 introduces Ziegler-Natta catalysis with a focus on Group 4 metals. The development of post-metallocene catalysts is also detailed and the activation chemistry of metallocene and post-metallocene homogenous catalysts is discussed.

Chapter 2 details the synthesis and characterisation of half-sandwich dichloride and dimethyl complexes supported by κ^1-amidinate and κ^1-guanidinate ligands. Obtained X-ray structures are also presented and discussed. DFT studies on the electronic structure of dicationic metallocene and post-metallocene fragments, as well as a comprehensive study on the nature of the Ti-N bonding in a variety of complexes, are also detailed.

Chapter 3 describes the activation of κ^1-amidinate and κ^1-guanidinate complexes with methyl abstracting agent TBF_{20} to produce cationic species. The trapping of these species with $OPPh_3$, py and THF to form isolable complexes has also been detailed. DFT studies on the electronic and geometrical structures of relevant post-metallocene dications, monocations and dimers are presented alongside the thermodynamics of the dimerisation processes. The formation of bimetallic monoalkyl-bridged monocations and alkyl-bridged alkylaluminium trapped cations is also presented alongside relevant DFT investigations.

Chapter 4 describes the reaction of alkyl cations with unsaturated substrates including carbodiimides, isocyanates, nitriles and alkynes to produce κ^2-amidinate, κ^2-acetamido, ketimide and alkenyl complexes, respectively. DFT studies are also presented to investigate the thermodynamics of intramolecular agostic and Lewis basic interactions present in these species.

Chapter 5 presents full experimental procedures and characterising data for the new complexes reported in this Thesis.

CD Appendix contains .cif files for all new crystallographically characterised complexes described.

Contents

Chapter 4 - Reactions of amidinate and guanidinate titanium cations with unsaturated substrates and polymerisation studies

Acknowledgements

I would firstly like to thank my supervisor, Prof. Philip Mountford, for his help and guidance over my time in Oxford. He has taught me many things which will undoubtedly prove priceless in my future career. The opportunity to work in the Mountford group is something I will appreciate for years to come.

Thank you to all the members of the Mountford group that I have had the pleasure to share a lab with; working with many people whom I can call friends as well as colleagues has certainly made my DPhil experience a less stressful one. The enthusiasm of people in the group to discuss each other's chemistry whether good or bad is an invaluable asset and of course a trip to the 'uni-club' on a particularly bad day is always well accompanied. I would particularly like to single out Dr Andrew Schwarz and Dr Matthew Blake, who during their time as post-docs in the group have really been a great help and a listening ear; their time and commitment to helping the entire group on a day to day basis has really been admirable.

Of course I must thank Dr Richard Scott (now at Lanxess Elastomers) who got me on my feet when I first arrived in Oxford and who has been a friend first, a boss second and probably entertainer third. I have had the pleasure to supervise Richard Collins who never stops smiling even in the face of some of the funniest lab-based calamities I might have witnessed; he is truly a good and funny man. I would also like to mention Dr Laura Groom who has been a great friend but who also has persistently been willing to sit down time after time to discuss my chemistry with me even when I'm sure she had other things she'd rather be doing. She, alongside Dr Matthew Blake, must also be thanked for doing an excellent job on proof reading my Thesis. Thank you to Dr Nick Rees who amongst being generally entertaining has also been great at keeping the Inorganic NMR service up and running and who will always be more than willing to help with an experiment (provided he can be located). Dr Tim Claridge has been a great help with running DOSY NMR spectra during my project and my gratitude also goes to him. Thanks also to Dr Jeff Harmer who helped with running EPR spectra. My thanks also go to Prof. John McGrady who really helped with getting my DFT work off the mark.

Thanks go to our collaborators Lanxess Elastomers, particularly Dr Gerard van Doremaele, Dr Alexandra Berthoud, Dr Martin Zuideveld, Dr Victor Quiroga, Dr

Richard Scott, Mr John van de Moosdijk, Mr Hans Leduc, Ms Emma de Koning and Mr Ralph Franssen whom have all been friendly and helpful during my time as part of the collaboration. Dr Betty Coussens at DSM should also be thanked for her abundance of DFT work that has helped with the understanding of my chemistry.

My family, of course, have been a great support to me and even though they have blank expressions when I begin to talk about chemistry they still nod along to humour me. I know I can always count on them to share in the good times and the bad times. My brother in particular has always helped me keep perspective throughout my years in higher education. Thanks go to my friends and housemates Tom Adams, Adam Levy, Tom Cuthbertson and Nick Davies who have kept me busy outside of labs and have also been a lifeline on many occasions. Last but by no means least I thank my lovely girlfriend Raffaella who amongst many other things has always managed to keep me grounded; her love and support has been indispensible.

Abbreviations

General

Å	Ångstrom
av.	average
ca.	*circa*, about
calcd.	calculated
cf.	*confer*, compare to
Cp_{cent}	computed cyclopentadienyl ring carbon centroid
°C	degrees Celsius
°	degrees
d	day(s)
D	Diffusion coefficient
DFT	Density Functional Theory
equiv(s)	equivalent(s)
g	gram(s)
GPC	Gel Permeation Chromatography
h	hour(s)
k	kilo
K	Kelvin
κ	denticity
l	litre(s)
μ	bridging
mg	milligram(s)
min	minute(s)
ml	millilitre(s)
mmol	millimole(s)
μl	microlitre(s)
RT	room temperature
T	temperature

vs.	*versus*

Chemical

Ar	aryl
Ar^{F_2}	$C_6H_3F_2$
BF_{15}	tris(pentafluorophenyl)borane, $B(C_6F_5)_3$
$[BF_{20}]^-$	tetra(pentafluorophenyl)borate, $[B(C_6F_5)_4]^-$
BHT	2,6-di-*tert*-butyl-4-methylphenol
Bn	benzyl
^{i}Bu	*iso*-butyl
^{n}Bu	*n*-butyl
^{t}Bu	*tert*-butyl
CGC	constrained geometry catalyst
Cp	cyclopentadienyl
Cp*	pentamethylcyclopentadienyl
Cy	cyclohexyl
EHT	extended Hückel theory
EP	ethylene-propylene
EPDM	ethylene-propylene-diene monomer
Et	ethyl
Et_2O	diethyl ether
i	*iso*
IBAO	isobutylaluminoxane
Ind	Indenyl, C_9H_7
L	ligand
M	metal or mol dm^{-3}
MAO	methylaluminoxane
Me	methyl
Me_3[9]aneN_3	trimethyl 1,4,7-triazacyclononane
M_n	number average molecular weight

M_w	weight average molecular weight
PDI	polydispersity index
Ph	phenyl
PMH	pentamethylheptane
^{i}Pr	*iso*-propyl
py	pyridine
R	generic alkyl group or hydrogen atom
TBF_{20}	trityl tetrakis(pentafluorophenyl)borate, $[Ph_3C][BF_{20}]$
TIBA	tri(*iso*butyl)aluminium
TMA	trimethylaluminium, $AlMe_3$
THF	tetrahydrofuran
Tol	4-C_6H_4Me
Tp	tris(pyrazolyl)borate
X	generic halide or alkyl ligand
Xyl	2,6-$C_6H_3Me_2$

Nuclear Magnetic Resonance Spectroscopy

app	apparent
br	broad
^{13}C-{^{1}H}	proton-decoupled ^{13}C
COSY	correlation spectroscopy
DOSY	Diffussion ordered spectroscopy
d	doublet
δ	chemical shift in ppm
HMBC	heteronuclear multiple bond correlation
HSQC	heteronuclear single quantum coherence
Hz	Hertz
i	*ipso*
J	coupling constant
m	*meta*

m	multiplet
MHz	Megahertz
NMR	Nuclear Magnetic Resonance
NOE	nuclear Overhauser effect
o	*ortho*
p	*para*
ppm	parts per million
q	quartet or quaternary
ROESY	rotating-frame nuclear Overhauser Effect spectroscopy
s	singlet
sept	septet
SST	spin saturation transfer
t	triplet
VT	variable temperature

Calculations

AO	atomic orbital
DFT	density functional theory
eV	electron volts
HOMO	highest occupied molecular orbital
LUMO	lowest unoccupied molecular orbital
MO	molecular orbital
TS	transition state(s)

Mass Spectrometry

EI	Electron Impact
m/z	mass to charge ratio
MS	Mass spectrometry

Infrared Spectroscopy

cm^{-1}	wavenumbers
FT-IR	Fourier transform infrared
IR	Infrared
m	medium
s	strong
w	weak

Notes

Literature compounds described in this Thesis are numbered **1.x**, **2.x**, **3.x**, **4.x** according to the Chapter in which they occur. The new compounds described in this Thesis are numbered **1-59**. Ionic compounds are either numbered as an ion-pair e.g. **8-[BF_{20}]** or as $\mathbf{8}^+$ if referring to the cation alone. In the case where monomeric or dimeric cations need to be distinguished subscript labels are added to the compound number alongside the appropriate charge e.g. $\mathbf{21}_{\mathbf{dim}}^{2+}$ or $\mathbf{21}_{\mathbf{mono}}^{+}$. In ionic compounds, again when required, monomers and dimers are labelled with appropriate subscripts e.g. $\mathbf{21}_{\mathbf{dim}}\mathbf{-[BF_{20}]_2}$ or $\mathbf{21}_{\mathbf{mono}}\mathbf{-[BF_{20}]}$. DFT calculated compounds are numbered **I-XXI** for hypothetical/non-experimentally observed species, or according to the number of the experimentally observed compound on which they are based with the suffix **Q** (for the full experimental systems) or **q** (for simplified model systems). X-ray data was collected and solved by either Dr Andrew Schwarz (**3**, **7**, **15-[BF_{20}]** and **45-[BF_{20}]**), Dr Matthew Blake ($\mathbf{21}_{\mathbf{dim}}\mathbf{-[BF_{20}]_2}$), Dr Richard Scott (**1**, **5**, **37-[$MeBF_{15}$]** and **54-[BF_{20}]**) or Mr Richard Collins (**2**). In all cases the molecular drawings were produced by Prof. Philip Mountford. Density functional theory (DFT) calculations were carried out by Dr Betty Coussens or by the author. Polymerisations were carried out by Lanxess Elastomers under the supervision of Dr Alexandra Berthoud.

Chapter 1

Introduction

1.1 General introduction

The discovery of transition metal catalysed polymerisation of olefins in the 1950s by Ziegler and Natta is of utmost importance in the world of organometallic and, more generally, inorganic chemistry as a whole.[1-4] In the last thirty years the interest in homogenous polymerisation has not only grown but has changed focus from primarily studying the metallocene complexes of Group 4 to widespread exploration of post-metallocene systems. This is a consequence of extensive patenting of the metallocene catalyst systems, as well as for general interest in the improvement of polyolefin catalysis. The plastics industry produces 1.3×10^7 tonnes of polyethylene, polypropylene and polystyrene each year worldwide and the study of well defined homogenous catalysts is invaluable in uncovering the mechanism of polymerisation and the fundamental properties of the active species.

Recently Lanxess Elastomers B.V. introduced a new class of κ^1-amidinate complexes (as Keltan ACE^{TM}) which are very active olefin polymerisation catalysts and this Thesis concerns the study of closely related compounds. Post-metallocene complexes containing κ^1-amidinate ($NC(NR_2)Ar$, R = alkyl) and κ^1-guanidinate ($NC(NR_2)_2$, R = alkyl or aryl) supporting ligands have been synthesised and fully characterised. Studies involving stoichiometric reactivity of the cationic monoalkyl species ($[L_2MR]^+$, L = supporting ligand, R = alkyl, M = Group 4 metal) have been carried out in order to probe the nature of this catalytically active species. This Thesis will compare and contrast the reactivity of the different species that have been synthesised as well as look at how they compare to the more traditional metallocene and post-metallocene systems.

This Chapter will give an introduction to homogenous Ziegler-Natta catalysis in general as well as an overview of a selection of Group 4 post-metallocene catalysts. The activation of Group 4 dialkyl precatalysts by the formation of monoalkyl cations will be discussed alongside any precedential reactivity of such species. Finally this Chapter will discuss amidinate- and guanidinate-supported complexes and also detail previous reactivity studies of a base-free κ^1-amidinate-supported titanium catalyst. The reader is directed to several review articles for a more comprehensive overview of homogenous Ziegler-Natta catalysis.[5-14]

1.2 Ziegler-Natta catalysis

Ziegler and Natta were awarded the Nobel Prize in Chemistry in 1963 "for their discoveries in the field of the chemistry and technology of high polymers". Ziegler and Natta discovered that heterogeneous polymerisation of ethylene and propylene could be achieved by mixtures of transition metal and trialkylaluminium compounds; such systems included $TiCl_4/AlEt_3$.[1, 3, 15, 16] To this day the majority of industrially produced polyolefins are produced in this way. These systems have been widely developed over the last 50 years and act as efficient and selective catalysts for many types of olefin polymerisation. The main problem with these catalysts is the lack of definition in the active site. Without a well-defined active site rational catalyst design and characterisation is difficult and the polymer produced by such a system has a broad molecular weight distribution. This is where the study of homogenous catalysis finds its benefits. The molecules which now act as the active sites for catalysis can be completely defined and characterised by methods such as NMR spectroscopy or X-ray crystallography with relative ease leading to logical catalyst design.

1.3 Metallocene catalysts

Geoffrey Wilkinson, who won a Nobel prize in 1973 together with Ernst Otto Fischer "for their pioneering work, performed independently, on the chemistry of the organometallic, so called sandwich compounds", reported the synthesis of Cp_2TiBr_2 and Cp_2ZrBr_2 in 1953.[17] In 1957 Natta and Breslow both reported that the bent metallocene Cp_2TiCl_2 in conjunction with Et_2AlCl or $AlEt_3$ could polymerise ethylene but not propylene.[18, 19] This system was not ideal, however, as the polymerisation was slow. Unexpectedly in 1980 Sinn and Kaminsky discovered that addition of a small amount of water to metallocene/alkylaluminum systems vastly increased the system's polymerisation activity.[20-22] This was due to the formation of methyl aluminoxane (MAO) which is formed from the partial hydrolysis of trimethylaluminium (TMA) and can be prepared prior to polymerisation or *in situ*. MAO can be used in general to activate a variety of Group 4 metallocenes towards ethylene or α-olefin polymerisation.[23, 24]

Metallocene systems activated with MAO are also capable of polymerising propylene. One such system is the zirconocene system Cp_2ZrCl_2/MAO. An extra consideration when polymerising propylene, due the presence of an extra methyl group per

monomer, is tacticity. This is defined by the relative chiral arrangement of adjacent pendant methyl groups. Examples of the principal different stereochemistry possible in polypropene can be seen in Figure 1.1.

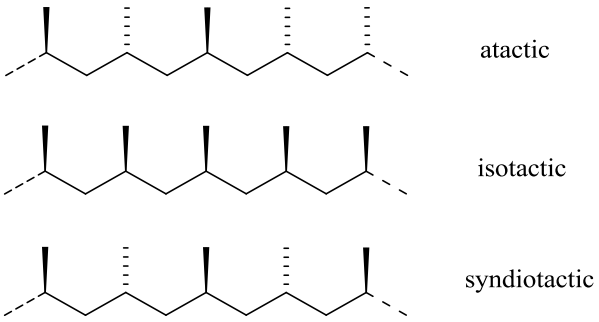

Figure 1.1 Tacticity variation in polypropylene.

1.4 Constrained Geometry Catalysts (CGCs) and *ansa*-metallocenes

Following the discovery of metallocene catalysts, the 1980s saw a considerable amount of research into catalysts that could control the stereochemistry and thus microstructure of the resulting polyolefin. Variation of metallocene symmetry was discovered to be the main factor in determining the spatial arrangement of the final polymer.[11]

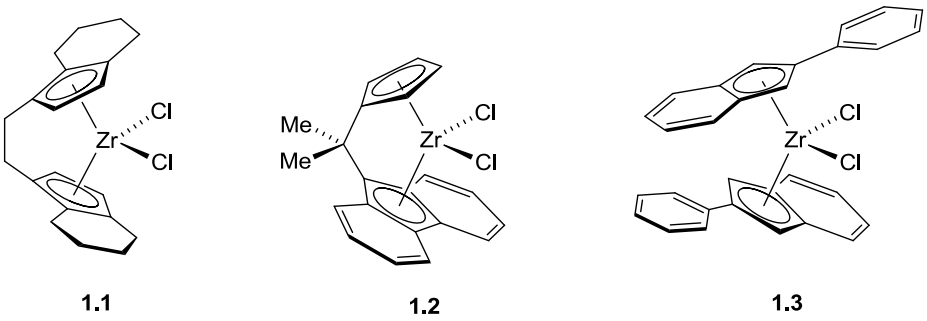

1.1 **1.2** **1.3**

Figure 1.2 Post-metallocene catalysts which can control the tacticity of polypropylene.

The ligand sets investigated were metallocene based but the two supporting ligands were linked by an *ansa*-bridging moiety. This connection prevents rotation of the ligands helping to well define the steric environment of the active site. Kaminsky and Brintzinger developed the C_2 symmetric zirconocene catalyst **1.1** which produced highly isotactic polypropylene; the sterics defined in the active site control the insertion of each monomer to give this microstructure.[25] Ewen *et al.* later found that C_s symmetric complex **1.2** produced highly syndiotactic polypropylene.[26] Although not an *ansa* compound, in 1995 Coates and Waymouth described a sterically crowded

metallocene compound **1.3** which acted in a similar fashion; although this was not constrained by a physical bridge the bulky groups led to restricted rotation.[27] In the absence of a physical link the top and bottom ligands could rotate intermittently and thus the catalyst fluctuates between chiral and achiral producing a block polymer containing isotactic and atactic sections.

Limited temperature stability and the production of low molecular weight polymers under commercially relevant conditions by the metallocene *ansa*-catalysts resulted in the development of a new catalyst type, the constrained geometry catalysts (CGCs). Steven *et al.* define a CGC as "a complex in which a π-bonded moiety is linked to one of the other ligands on the same metal centre in such a way that the angle measured between the centroid of the π-system and the additional ligand is smaller than the comparable unbridged complex".[28, 29] This important class of catalyst was developed by Dow[28, 30-33] and Exxon[34-37] following the discovery of silane-bridged cyclopentadienyl-amido scandium and titanium catalysts by Bercaw and Okuda respectively.[38, 39] The general form of a CGC is illustrated in Figure 1.3.

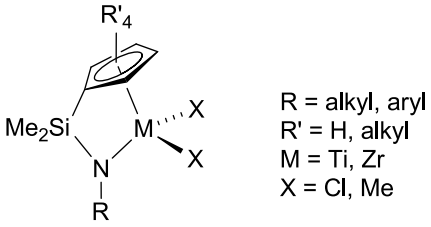

Figure 1.3 General form of a constrained geometry catalyst (CGC).

CGC catalysts have outstanding performance in ethylene polymerisation and in copolymerisations with higher α-olefins. The reasons for superior performance in these areas when compared to metallocenes are: a more open coordination sphere, a small Cp_{cent}-M-N angle and a reduced propensity to undergo chain transfer.[40] The amido group acts as a maximum three electron donor, *cf.* cyclopentadienide (5 electron donor), which yields a highly electrophilic metal centre and thus results in its high productivity as a catalyst. CGCs can be used in high temperature polymerisation processes because of their high thermal stability and produce higher molecular weight polymers than their metallocene counterparts.[41, 42]

1.5 Post-metallocene catalysts and the isolobal analogy

Due in part to extensive patenting of the more traditional Group 4 metallocene systems and CGCs new post-metallocene systems were of great research interest in the 1990s and onwards.[10, 12] Research efforts directed at new types of catalyst also allowed for a chance to improve and control resultant polymer properties and to explore new monomer combinations. Post-metallocene systems aim to replace one or more of the cyclopentadienyl ligands on the metal centre with a different moiety. A strategy that has been successfully employed in new ligand design is the isolobal analogy developed by Hoffman for which he was awarded a Nobel prize alongside Fukui "for their theories, developed independently, concerning the course of chemical reactions".[43] When two electronically defined systems are isolobal to one another the symmetry, shape and energies of the frontier orbitals are similar. This principle, when combined with the correct steric properties, can be powerful in ligand design for new catalysts.

Ligands relevant to this project, which have been employed because they fulfil the criteria put forward by the isolobal analogy, consist of an anionic heteroatom binding to the metal centre in a κ^1-mode. If one considers the cyclopentadienide ligand and compares the electronic properties to the general form of a κ^1-bound anionic donor, for example an imido ligand, the isolobal analogy can be seen in operation (See Figure 1.4). The frontier orbitals of each ligand comprise of a single σ-donor and two π-donor orbitals which can interact with the metal centre.

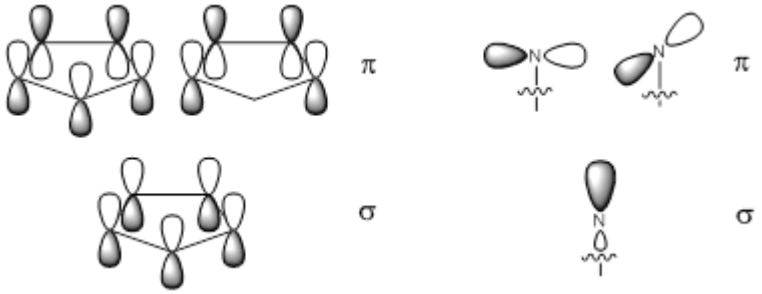

Figure 1.4 Frontier orbitals of cyclopentadienide and NR^{2-} ligands.

Previous work in the Mountford group has utilised this analogy in the synthesis of titanium imido compounds such as **1.4**.[14, 44, 45] In this compound the imido ligand is isolobal to Cp but is formally dianionic and so the other supporting ligand, 1,4,7-triazacyclononane, must be neutral to keep the charges balanced in the compound. DFT calculations show that that the frontier molecular orbitals of

dicationic imido compound $[Ti(NMe)(H_3[9]aneN_3)]^{2+}$ ($H_3[9]aneN_3$ = 1,4,7-triazacyclononane) are broadly similar to that of $[Cp_2Ti]^{2+}$ in line with the isolobal analogy.[46] For in depth computational studies on $[Cp_2M]^{n+}$ the reader is directed to a review article by J. C. Green.[47]

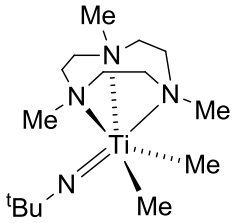

1.4

1.5.1 Half-sandwich catalysts

Group 4 complexes of the form $CpM(L)X_2$ (M = Group 4 metal, L = supporting ligand, X = halide or alkyl), which are supported by one cyclopentadienyl and one κ^1-bound monoanionic ligand have been well studied.[10, 12, 48] The monoanionic ligands act as an isolobal analogue of cyclopentadienide and also posses the same charge, thus they can be directly substituted without the need to change the other supporting ligand. Prominent examples comprise of amide (**1.5**),[49-51] ketimide (**1.6**),[52-56] guanidinate (**1.7**),[57] iminoimidazolidide (**1.8**),[58-63] phosphinimide (**1.9**)[64-72] and aryloxide (**1.10**)[73-78] supported half-sandwich compounds (Figure 1.5). The most relevant to this Thesis are the κ^1-bound N-donor ligands which will be discussed briefly below.

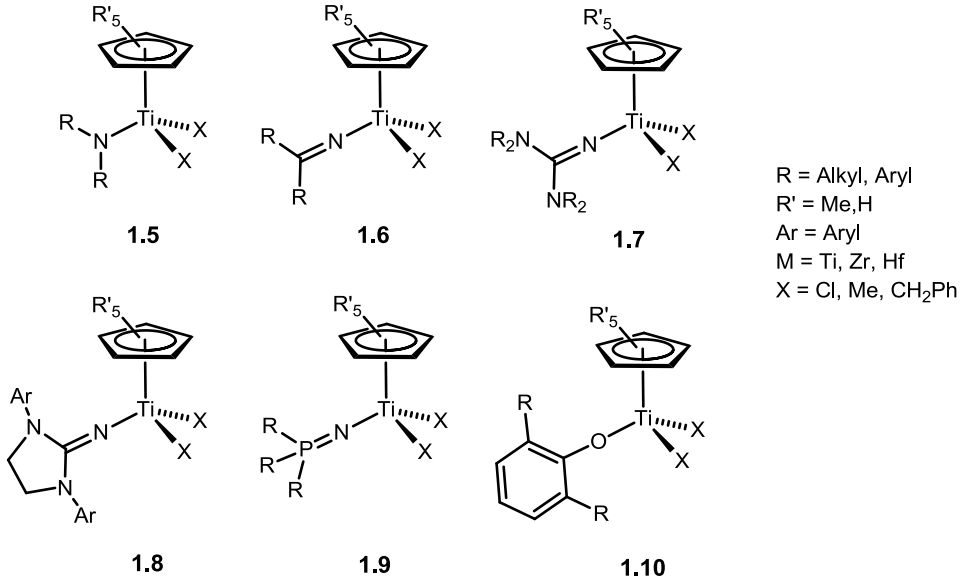

1.5 **1.6** **1.7**

1.8 **1.9** **1.10**

Figure 1.5 Half-sandwich post-metallocene precatalysts.

The first half-sandwich ketimide complex of the form $Cp^RM(NCR_2)Cl_2$ ($Cp^R = C_5R'_5$, R′ = H or alkyl, R = alkyl) was reported in 1986 by Leigh *et al.*; namely $CpTi\{NC(^nBu)^tBu\}Cl_2$.[79] Since then a large number of compounds of this type have been reported and the area has been reviewed.[56] In $CpTi\{NC(^nBu)^tBu\}Cl_2$ the bonding of the ketimide to the metal is *ca.* linear (Ti-N-C, 171.3(4)°) indicating that the nitrogen atom is effectively *sp* hybridised and suggests Ti-N multiple bonding. Another important system where the ketimide supporting ligand is $-NC^tBu_2$ was reported by Dias, Nomura and Zhang.[52, 54, 80, 81] However it was over a decade between the first reported synthesis of half-sandwich ketimide complexes and their recognition as polyolefin catalysts.

Another important and comprehensively studied ligand is the phosphinimide (**1.9**, $-NPR_3$, R = alkyl or aryl). Stephan *et al.* have investigated $CpTi(NPR_3)X_2$ (R = alkyl or aryl, X = halide or alkyl) complexes since the 90s regarding their general reactivity and polymerisation ability.[65] Phosphinimide ligands have been shown to bind in a linear fashion to the metal centre with a short M-N bond.[71, 72] These attributes are evidence of a $\sigma+2\pi$ bonding mode between ligand and metal just like Cp. The steric influence of the phosphinimides have also been shown to be comparable with Cp and it is argued that the steric influence of the ligand is the most important factor in determining the polymerisation activity in these particular systems.[67, 69]

The steric influence of the ligand is also thought to be important in aryloxide supported half-sandwich systems (**1.10**) but in others it appears to be the electronic effects that are considered key to catalyst productivity. Hessen,[59] Tamm[61, 62] and Nomura[60] have all investigated iminoimidazolidide ligands (cyclic guanidinates, **1.8**, Figure 1.6) and it has been suggested that an increase in π-bonding between the ligand and titanium can lead to an increase in catalytic activity.[59-62] The significant π-bonding in these complexes originates from formal lone pair donation of the amino nitrogens towards the π_{CN} system which means the ligand can be considered up to a $5e^-$ donor *via* a $\sigma+2\pi$ interaction (Figure 1.6). This electronic arrangement is supported experimentally by short Ti-N bond lengths and linear Ti-N-C angles. The activity of complex $CpTi\{NC(N(Xyl)CH_2)_2\}Bn_2$ is higher than ketimide supported $CpTi(NC^tBu_2)Bn_2$ (1600 and 1128 kg mol^{-1} h^{-1} bar^{-1}, respectively) due to the addition of amino nitrogen donors.[59]

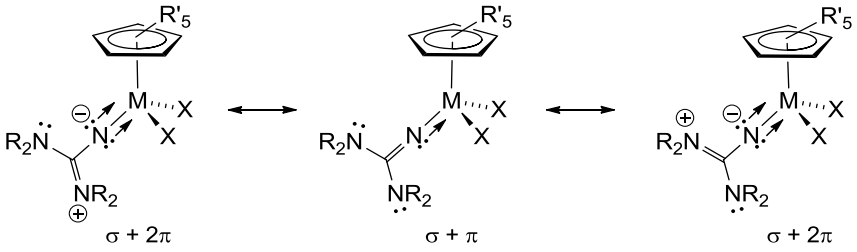

1.7

Figure 1.6 Metal-ligand bonding interactions for guanidinate supported complexes (**1.7**).

1.5.2 Other post-metallocene catalysts

Many post-metallocene catalysts have also been developed which do not contain a cyclopentadienyl supporting ligand.[10, 12] In some instances these have contained ligands that still aim to imitate Cp, for example boratobenzene[82-84] and phosphacyclopentadienyl[85-88] supported catalysts **1.11** and **1.12**.

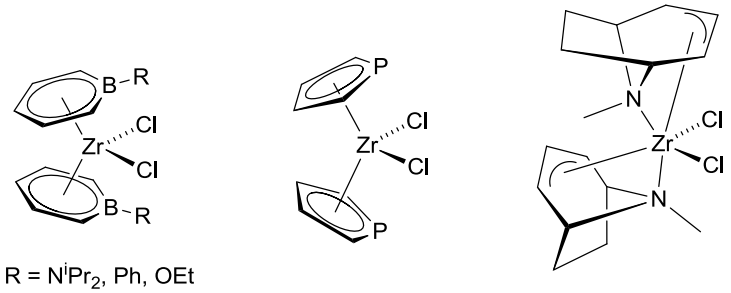

1.11 **1.12** **1.13**

Boratobenzenes are formed by the addition of a boron atom into a cyclopentadienide ring. Since boron contributes only an empty p-orbital to the π system the aromaticity is not disturbed. When activated with MAO the catalysts give reasonably high activities (105 kg mol^{-1} h^{-1} bar^{-1}).[82] When changing the N^iPr_2 substituent on boron (**1.11**) to less sterically demanding substituents Ph or OEt there is an increased rate of β-hydrogen elimination resulting in α-olefin production.[82-84] Phosphacyclopentadienes are obtained by the exchange of a single carbon in a cyclopentadienide ring by a P atom; this maintains the same ring size as Cp as well as the aromaticity. Catalysts supported by these ligands can give productivities similar to their Cp analogues. Tropidinyl ligands have been utilised by Bergman *et al.* as a Cp mimic in complexes such as **1.14**; despite having a separate σ and π system the ligand has been described as an analogue of Cp.[89] An alternative ligand that can be used in place of Cp is the monoanionic

tris(pyrazol)borate (Tp).[90-92] Although this is a face-capping ligand it isolobal with Cp; the relevant σ- and π-orbitals are shown alongside the ligand in Figure 1.7.

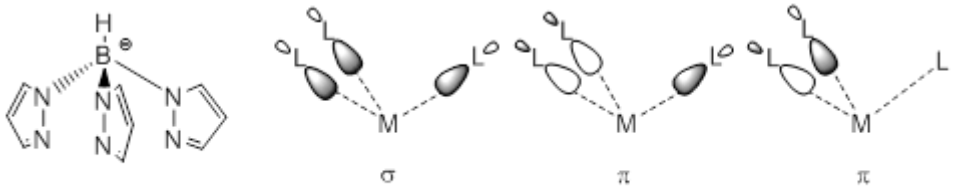

1.14

Figure 1.7 $[Tp]^-$ ligand shown alongside donor orbitals of σ- and π-symmetry for a *fac*-L_3 moiety.

These ligands have been used in the Mountford group as Cp surrogates in production of Group 4 polymerisation catalysts that are supported by Tp and κ^1-amidinate ligands.[93, 94] Other Tp-supported Group 4 polyolefin catalysts have also been investigated by other groups.[95-98]

1.6 Metallocene and post-metallocene alkyl cations

It is generally acknowledged that the active species in Group 4 based olefin polymerisation catalysis is of the form $[L_nMR]^+$ (L = supporting ligands, M = Group 4 metal, R = alkyl group). The nature of the active species is of great importance in the fundamental understanding of the mechanism of olefin polymerisation. Once one understands the mechanisms, deactivation reactions and structure activity relationships better catalysts can be designed. This Section will present a concise introduction into the area of cationic Group 4 metal alkyl complexes and their reactivity. This subject area has been extensively reviewed.[5, 9, 99, 100]

1.6.1 Historical background

The suggestion of a cationic active species in olefin catalysis occurred not long after initial reports of the polymerisation activity of $TiCl_4/AlEt_3$ by Ziegler in 1953.[15] Newburg, Long and Breslow suggested that the active agent was a highly polarised bimetallic species (**1.15**) containing Ti and Al bridged by chlorine (Scheme 1.1).[101, 102]

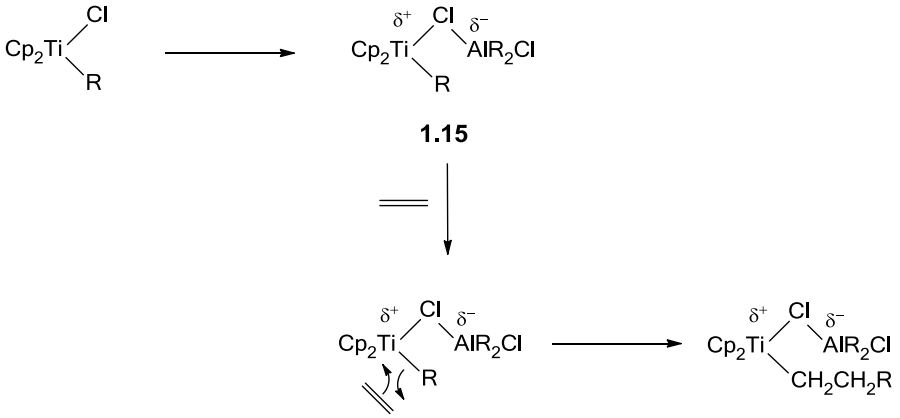

Scheme 1.1 Insertion of ethylene into a highly polarised bimetallic species (**1.15**).

Conductivity and electrodialysis studies by Shilov *et al.* suggested that the catalytically active species in polymerisations is actually cationic.[103, 104] Direct evidence for the involvement of a cationic active species was provided by electrochemical synthesis of $[Cp_2TiMe]^+$ in CH_2Cl_2 carried out by Dyachovskii accordingly; polymerisation only occurred only in the cathode chamber.[105] The idea of an ionic active species in a process which was carried out in non-polar solvents was not well accepted at the time. Curiosity was revitalised in 1985 when Eisch *et al.* provided chemical evidence for the existence of a cationic active species by isolating $[Cp_2Ti\{Me_3SiCC(Ph)Me\}][AlCl_4]$ (**1.16**); this was synthesised by the insertion of the alkyne $PhCCSiMe_3$ into the then postulated $[Cp_2TiMe]^+$ (Scheme 1.2).[106] This type of reaction models the insertion of ethylene into the Ti-C bond.

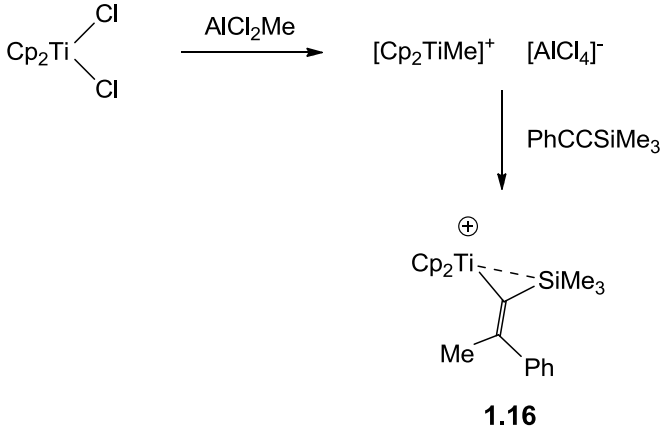

Scheme 1.2 The first example of an isolable insertion product (**1.16**) formed by insertion into the Ti-C bond of a titanium methyl cation.

In 1986 both Bochmann and Jordan made important contributions in this area. Jordan *et al.* reported the synthesis of $[Cp_2ZrMe(THF)][BPh_4]$ (**1.17**) which was structurally

characterised and shown to have polymerised ethylene.[107] This was the first time that Group 4 cations were shown to polymerise ethylene without alkyl aluminium cocatalysts. Bochmann *et al.* reported titanocene analogues in the same year, $[Cp_2TiMe(L)][X]$ (L = NH_3, NCR, pyridine, X = BPh_4, PF_6); however, the presence of the stronger Lewis bases meant these complexes showed no activity towards ethylene polymerisation.[108, 109]

1.6.2 Preparation of Group 4 alkyl cations

The possibility of performing polymerisation in the absence of MAO combined with the potential to undertake mechanistic investigations has led to a large amount of research into the different methods of preparing monoalkyl cations. There are a number of general synthetic routes to Group 4 alkyl cations which have been reviewed and will be discussed below.[110]

1.6.2.1 Protonolysis

Ammonium salts have been used to generate alkyl cations *via* protonolysis of M-R bonds; an example of this is the generation of $[Cp_2TiMe(NH_3)][PF_6]$ from Cp_2TiMe_2 and $[NH_4][PF_6]$ reported by Bochmann *et al.* in 1987.[109] Other ammonium salts have been used to this effect such as $[PhNMe_2H]^+$ and $[^nBu_3NH]^+$. Treatment of Cp_2ZrMe_2 with $[PhNMe_2H][BF_{20}]$ ($[BF_{20}]^- = [B(C_6F_5)_4]^-$) produces the cation $[Cp_2ZrMe]^+$ with a $[BF_{20}]^-$ counterion .[110-113] Using protonolysis to generate the alkyl cation leads to the generation of a Lewis base side product which can bind to the cation. The Lewis base must be removed from the cation to allow binding of the olefin for polymerisation and therefore the presence of Lewis bases reduces catalytic activity.[114] As an alternative to ammonium salts phosphonium salts can be used in the same vein.[115] If one employs bulky phosphonium ions such as $[Cy_3PH]^+$ and $[Mes_3PH]^+$ the resulting phosphine does not coordinate to the generated cation which then leads to a productive catalytic system.[115]

1.6.2.2 Lewis acids

The borane compound tris(pentafluorophenyl)borane (BF_{15}) is a strong Lewis acid and as such can be used for the activation of Group 4 alkyl based olefin polymerisation precatalysts. This was employed by Marks *et al.* in 1991 to synthesise $[\{1,2\text{-}(CH_3)_2C_5H_3\}_2ZrCH_3][MeBF_{15}]$ (**1.18**) which was the first example of an isolable and crystallographically characterised (Figure 1.8) cation-like species.[116] Activating in

this fashion leads to no side products that could interfere with the cation; on the other hand the anion itself ($[MeBF_{15}]^-$) is known to interact with the cation. If there is an interaction the complex is best considered as a zwitterionic molecule containing a methyl bridge between the metal and boron. The extent of interaction between the anion and the cation can be determined by the separation of the *meta* and *para* ^{19}F NMR chemical shifts.[114] This type of interaction is important to consider since it can obstruct close approach of an olefin monomer to the metal centre during polymerisation and therefore generally the presence of this anion leads to an inhibitory effect on the polymerisation.

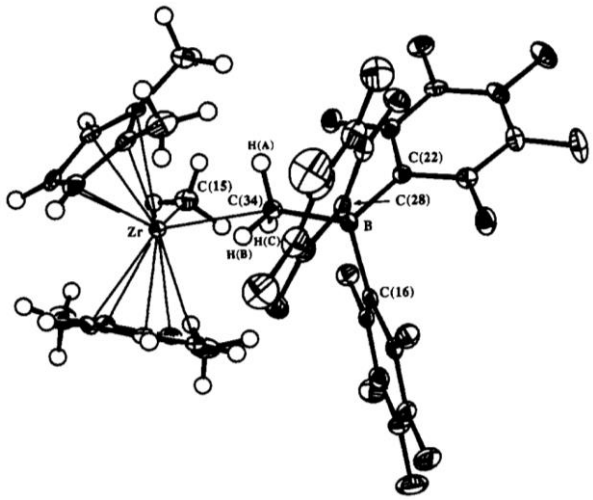

Figure 1.8 Molecular structure of **1.18**.[117]

1.6.2.3 Alkyl abstraction

The most commonly employed agent used to abstract methyl groups is the trityl cation, $[Ph_3C]^+$. Abstraction of the alkyl group (R) from the precatalyst yields the formation of Ph_3CR alongside the corresponding cation.[110] This method of activation is the most relevent to this Thesis and is utilised in Chapters 3 and 4. Equation 1.1 shows activation of *rac*-ethylenebis(indenyl)dimethylzirconium by way of example. If the trityl cation is coupled with an anion such as tetrakis(pentafluorophenyl)borate ($[BF_{20}]^-$) the product is a cation accompanied by a non-interacting anion, which acts as highly active polymerisation catalyst.

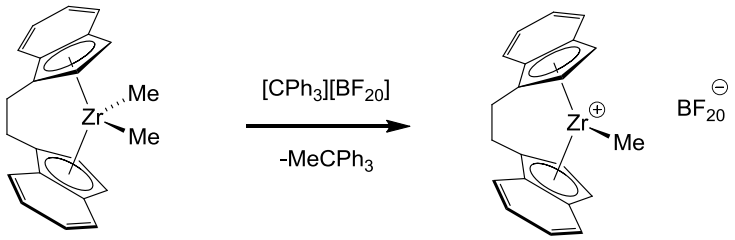

Equation 1.1

1.6.2.4 Other methods

Early methods of producing cations involved oxidative reagents such as $[Cp_2Fe]^+$ (Equation 1.2) or Ag^+.[118] Activation of dimethyl zirconocene was carried out by Jordan *et al.* in 1986 with $Ag[BPh_4]$ yielding ethane and silver metal as side products, which occurred *via* oxidative cleavage of the Zr-Me bond.[119] The titanium (III) species Cp^*_2TiMe has also been shown to be oxidised by $AgBPh_4$ in THF to yield the monoalkyl titanocenium (IV); this process occurs *via* a one-electron oxidation.[120]

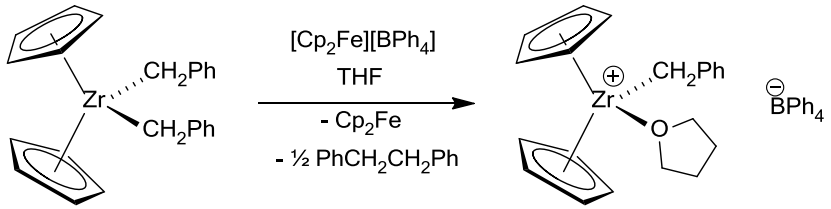

Equation 1.2

Another method employed to generate cations is displacement of chloride by strong neutral donors e.g. PMe_3 in complexes such as $Cp_2TiMe(Cl)$ and $Ind_2TiMe(Cl)$ as shown in Equation 1.3.

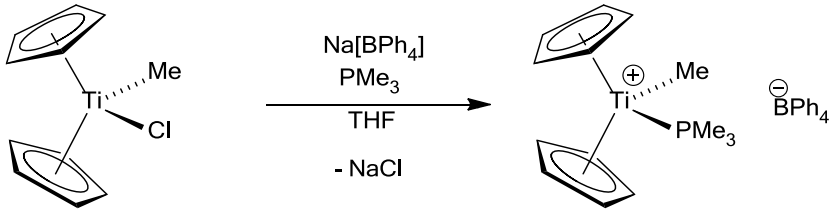

Equation 1.3

1.6.3 $AlMe_3$ and its effects on alkyl cations and polymerisation

The alkyl aluminium compound Al_2Me_6 (from now on referred to as $AlMe_3$) is present in polymerisation reactions that use MAO as a co-catalyst. Although this can help the process by scavenging oxygen and water from the reaction it can also cause complications for example $AlMe_3$ can cause variation in catalytic productivity and also

changes in the properties of the polymer.[121-123] Activation of zirconocene complexes with $AlMe_3$ can lead to a small amount of activity but are significantly less productive than their MAO activated analogues.[124] The presence of $AlMe_3$ leads to the formation of heterobimetallic species of the type $[L_nM(\mu\text{-}Me_2)AlMe_2]^+$ (M = Group 4 metal, L = supporting ligand) which themselves are not catalytically active, result in chain transfer and can also act to deactivate the active species; they are also considered to be catalytic resting states.[125-127] Alkyl aluminium compounds can also have a negative effect on the polymerisation performance of Group 4 catalysts by acting as reducing agents; titanium (III) compounds are not electrophilic enough to achieve high polymerisation activities. The more $AlMe_3$ present in solution the more of the polymerisation inactive heterobimetallic species will be present.

The first adduct of $AlMe_3$ with a Group 4 alkyl cation was reported in 1994 by Bochmann *et al.* ($[Cp_2Zr(\mu\text{-}Me_2)AlMe_2]^+$, **1.19**, Figure 1.9). However, this was not structurally characterised.[128] In 2006 Mountford *et al.* reported the first cationic transition metal compound containing a $M(\mu\text{-}Me_2)AlMe_2$ moiety characterised by X-ray crystallography (**1.20**, Figure 1.9).[129]

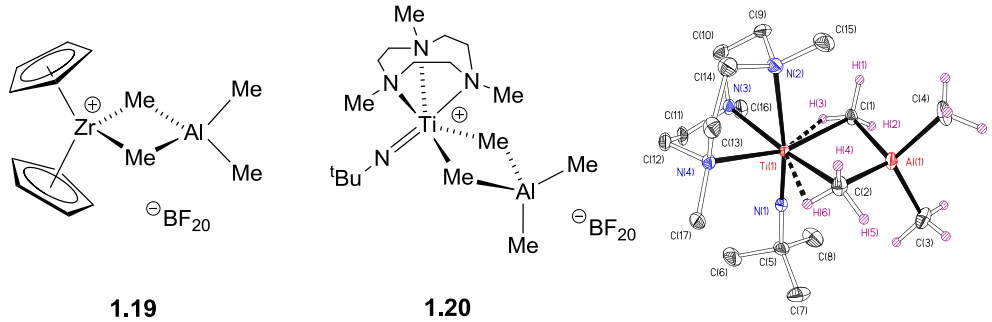

Figure 1.9 $AlMe_3$ adducts of alkyl cations 1.[130, 131]

To reduce the effect of $AlMe_3$ on the polymerisation process scavengers can be added; one such scavenger is 2,6-di-*tert*-butyl-4-methylphenol which is more commonly referred to as butylated hydroxytoluene (BHT-H). This phenol reacts with $AlMe_3$ to produce $(BHT)_2AlMe$ [132] which does not interfere with the active site but can still scavenge unwanted impurities.[133, 134]

1.6.4 Anion and solvent interactions

Interaction of the anion with the cation is important to consider as it can have a substantial effect on the polymerisation process. These types of interaction occur

because of a low number of valence electrons in the metal centre. If a significant interaction exists between the anion and cation, and the active site is blocked, the anion must be removed from the active site before polymerisation can take place[135] which has been shown in various metallocene and post-metallocene systems to involve quite substantial energies.[136-138] It has already been discussed above that $[MeBF_{15}]^-$ forms a strong interaction with the cationic metal centre to form a zwitterionic molecule. Equally if the anion reacts with the cation to give a different non-active species then this too has to be circumvented by the use of a different anion. It is also worth noting that anions that are usually considered non-coordinating such as $[BF_4]^-$ and $[PF_6]^-$ have been shown to react with $[Cp_2MR]^+$, e.g. reaction of $[Cp_2ZrMe(CH_3CN)]^+$ with $[PF_6]^-$ produces Cp_2ZrMeF *via* fluoride abstraction.[119] Even anions such a $[BPh_4]^-$ have been shown to interact with the cationic centres. Treatment of $ZrBn_4$ with dimethylanilinium tetraphenylborate leads to the formation of $[ZrBn_3(\eta^6\text{-}C_6H_5)BPh_3)]$ (**1.21**) in which the cationic centre is stabilised by the anion. This type of interaction has also been demonstrated with $C_2H_4(Ind)_2ZrMe_2$.[139] Hlatky and Turner reported that $[BPh_4]^-$ can even react with cationic species such as $[Cp^*_2ZrMe]^+$ to form **1.22** which is formed as a result of C-H activation.[112]

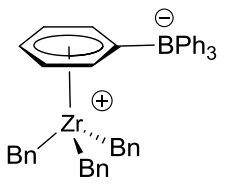

1.21

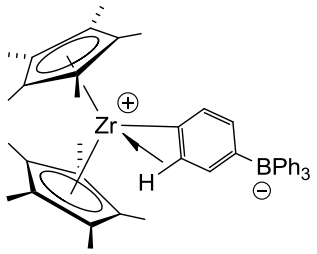

1.22

In a search of non-interacting and non-coordinating anions perfluorinated species, the most popular of which is $[BF_{20}]^-$, were investigated.[140-143] $[BF_{20}]^-$ has been used extensively in the work discussed in this Thesis, *vide infra*. Indeed in some cases it has been shown that a molecule of solvent would rather bind to the vacant site of the cation than $[BF_{20}]^-$; this is testament to the anion's non-coordinating nature.[144-146] Despite its weakly coordinating nature there have been reports of reactivity with $[BF_{20}]^-$ for example by McConville and Stephan yielding **1.23** and **1.24** respectively.[66, 147] **1.23** was formed by the extraction of $C_6F_5^-$ from $[BF_{20}]^-$ by $[(^tBu_3PN)_3Ti]^+$ followed by phosphinimide ligand abstraction and B-C bond cleavage.

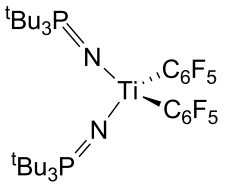

1.23

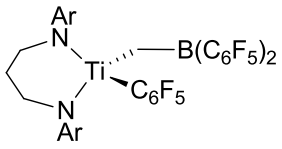

1.24

Work by Brintzinger and Geyer in 1999 showed using Pulsed Gradient Spin Echo (PGSE) NMR spectroscopy that the compound $[Cp_2ZrMe][BF_{20}]$ exists as a dimer in C_6D_6, in this case an ion quadruple. Thus the weakly coordinated anion $[BF_{20}]^-$ can interact with cations sufficiently to form higher aggregates.[148] Marks *et al.* reported using similar PGSE NMR measurements in C_6D_6 that $[Cp^*ThMe][BF_{20}]$ exists as only monomeric tight ion pairs.[149] PGSE reveals that PPh_3, THF, benzene and toluene adducts of various zirconocene type systems can exists as ion quadruples or even hextuples in solution at higher concentrations. It is worth noting that the previously mentioned PGSE experiments were carried out at concentrations above that usually used in single site catalysis and the existence of these aggregates at lower, more relevant, concentrations is more unlikely. Bochmann has carried out extensive research into a series of more complex fluorinated anions based around BF_{15} which are of the form $[X(BAr_3)_2]^-$ (X = CN, NH_2, $N(CN)_2$; Ar = C_6F_5, 2-$C_6F_4(C_6F_5)$). The idea was to create very weakly coordinating anions by delocalising the negative charge over multiple atoms. Accordingly in the case of $[CN(BF_{15})_2]^-$ the contribution of the anion to the activation energy of propene polymerisation with zirconocene catalysts was actually 1.1 $kJmol^{-1}$ less than $[BF_{20}]^-$. These anions can have an effect on both the activity and stereoselectivity during polymerisations.[9, 150-154]

The solvents generally used in this chemistry are polar due to the ionic nature of the compounds and have been shown to form adducts with Group 4 cations in order to stabilise the active species. One such example that has been crystallographically characterised is $[Cp_2ZrBn(C_6H_5Cl)][BF_{20}]$ (**1.25**, Figure 1.10).[155] Other examples of halocarbon solvents bound to transition metals are known.[155-158] It is possible that the solvent stabilised cations are resting states in the catalytic cycle and that the solvent needs to be removed from the metal centre before binding and subsequent polymerisation of the olefin can occur.[5, 135, 159] The cations in $[Cp^*ZrMe_2][MeBF_{15}]$ and $[\{Me_2Si(^tBuN)(C_5Me_4)\}ZrMe][BF_{20}]$ are even stabilised by a molecule of hydrocarbon solvent (toluene) in solution and the former also in the solid state.[144-146]

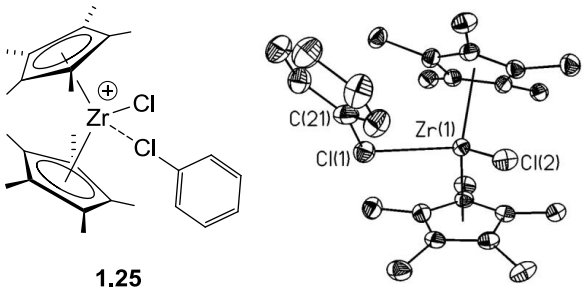

1.25

Figure 1.10 Structure of $[Cp_2ZrCl(C_6H_5Cl)]^+$.[155]

1.6.5 Non-classical interactions

Agostic interactions have been shown to be important in stabilising highly electrophilic cations.[160, 161] These interactions have also been proposed to play a key role in the polymerisation process. The μ-Me dication, $[Cp^*_2Ti_2\{NC(N^iPr_2)Ar^{F_2}\}_2\text{-}Me_2][BF_{20}]_2$ (**1.26_{dim}-$[BF_{20}]_2$**, Figure 1.11), which is relevant to this Thesis, has been characterised by X-ray crystallography and displays two agostic interactions for each methyl group, respectively.[162] $[Cp_2TiMe][MeBF_{15}]$ also exhibits α-agostic interactions which were not crystallographically characterised but determined using IR spectroscopy; neutral compounds such as $CpTiMe_3$ and $CpTiMeCl_2$ have also been shown to display α-agostic interactions using the same method.[161]

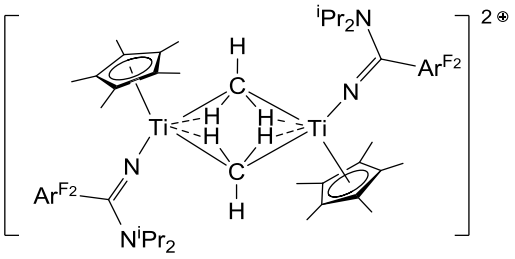

1.26_{dim}^{2+}

Figure 1.11 Structurally characterised compound containing α-agostic interactions.[162]

Computational studies by Clot and Eisenstein have predicted that the α-agostic interaction is not so much a result of electron donation from the C-H σ-bond into the electron deficient metal centre, although this does occur, but is in fact better viewed as a second order Jahn-Teller distortion.[163] Agostic interactions are identified by a short M···HC distance, these occur not primarily because the C-H bond is acting as a base but because the tilt of the CH_3 group allows the σ_{CH_3} orbital to pick up an additional stabilising interaction from a different lower energy d-orbital. The extent to which this tilting occurs is a balance of the overlap and energetics involved. This is illustrated in

Figure 1.12. Tilting of the CH_3 group also allows a more efficient σ(C-H) interaction to occur with the metal centre.

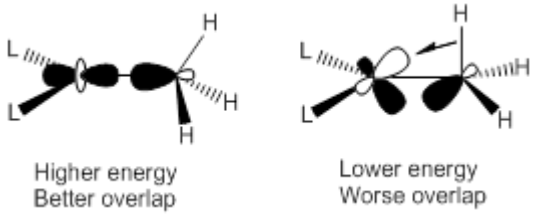

Figure 1.12 Frontier orbitals involved in the formation of an α-agostic interaction.

Jordan *et al.* have reported the β-C-H agostically stabilised species $[Cp'_2Zr(PMe_3)C_2H_5]^+$ (Cp′ = C_5H_4Me) which contains a structurally characterised β-C-H agostic interaction.[164] Green *et al.* have used pendant phenyl groups to study agostic interactions in Group 4 alkyl cations.[159] Another somewhat more prominent example of a non-classical interaction is that of the so called *ipso*-interaction which involves the η^2-coodination of a benzyl group. An example of such an interaction was reported by Horton *et al.* in an alkylzirconium complex supported by a tridentate diamide ligand (**1.27**) .[165] The Ti···C_{ipso} interaction manifests itself in the ^{13}C NMR spectrum showing a large $^1J_{CH}$ for the $ZrCH_2$ group (142 Hz) and an unusually upfield *ipso* carbon chemical shift (137.5 ppm).

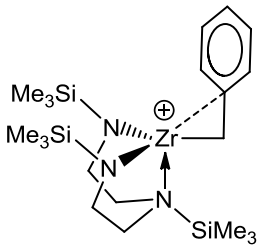

1.27

Agostic interactions are also possible between Si-Me bonds and the metal centre. Compound **1.16** synthesised by Eisch *et al.* displays a β-Si-C agostic interaction with the metal centre which is reflected in the upfield ^{29}Si NMR resonance (δ = -54.9 ppm).[106] Bochmann and Macchioni also suggested their systems contained Si-Me agostic interactions which manifested itself as restricted rotation in the NMR spectra of compound $[\{rac\text{-}Me_2Si(1\text{-}Ind)_2\}M\{CH_2SiMe_3\}]^+$ (M = Zr or Hf).[166] Likewise Marks *et al.* also suspected the presence of an agostic interaction in the complex $[(C_5H_3Me_2)_2Zr\{CH_2(SiMe_3)\}]^+$ which became evident in the low temperature NMR spectra.[136] Work by Mountford *et al.* in 2005 showed that treatment of

$Ti(N^tBu)(Me_3[9]aneN_3)(CH_2SiMe_3)_2$ ($Me_3[9]aneN_3$ = 1,4,7-trimethyltriazacyclononane) with TBF_{20} ($[Ph_3C][B(C_6F_5)_4]$) gave species $[Ti(N^tBu)(Me_3[9]aneN_3)(CH_2SiMe_3)][BF_{20}]$ which is stabilised by a β-Si-C agostic interaction as characterised by a high field ^{29}Si NMR resonance (-17.5 ppm).[167, 168]

1.6.6 Reactivity of alkyl cations

Prior to this Section this introduction has centred on the formation and solution behaviour of Group 4 alkyl cations. This Section will aim to give a brief introduction into the types of reactivity that have been observed with these species. Reactivity of base-free cations is not only interesting from a fundamental point of view but can also help reveal mechanistic aspects of the polymerisation process.

1.6.6.1 Insertion chemistry of alkyl cations

The study of the insertion of unsaturated substrates into the metal alkyl bond is applicable to the understanding of the chain growth processes present in Ziegler-Natta polymerisation. As mentioned previously, in 1985 Eisch *et al.* showed that insertion of $Me_3SiCCPh$ into the Ti-Me bond resulted in the formation of alkenyl complex **1.16**. Shortly after this discovery Bochmann *et al.*[108, 109] showed that base stabilised cation $[Cp_2TiMe(NCMe)]^+$ would react with CO to yield complex **1.28** and with ^{t}BuNC to yield complex **1.29**.

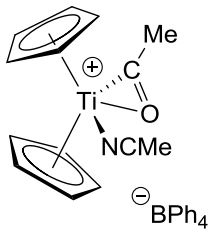

1.28

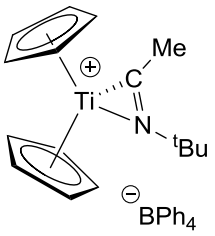

1.29

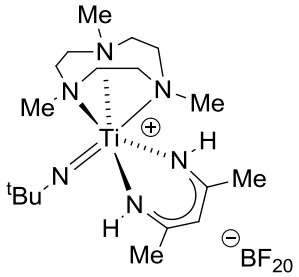

1.30

Treatment of $[Cp_2TiMe(NCMe)]^+$ with nitriles PhCN and ^{t}BuCN produced a Lewis base adduct. However, with indenyl supporting ligands and in the presence of excess nitrile both PhCN and ^{t}BuCN undergo insertion into the Ti-Me bond within 1 hour; this increase in reactivity is explained by the increased donor ability of indenyl *vs.* Cp. Insertion of MeCN and PhCN into the Ti-Me bond of $[Cp_2TiMe][BPh_4]$ can occur but a longer reaction time is observed; for example acetonitrile takes 2 weeks to react with the cation.[108, 109, 169] In 2006 Mountford *et al.* showed that imido complex

$[Ti(N^tBu)(Me_3[9]aneN_3)(NCMe_2)(NCMe)]^+$, produced initially from the insertion of acetonitrile into the Ti-Me bond of $[Ti(N^tBu)(Me_3[9]aneN_3)Me]^+$, would rearrange to create a β-diketiminato complex (**1.30**) over 1 month.[168] Insertion chemistry equivalent to that described above was exhibited by the analogous base stabilised zirconocene compound **1.17** by Jordan *et al.*[100, 119, 170] This reactivity is illustrated in Scheme 1.3.

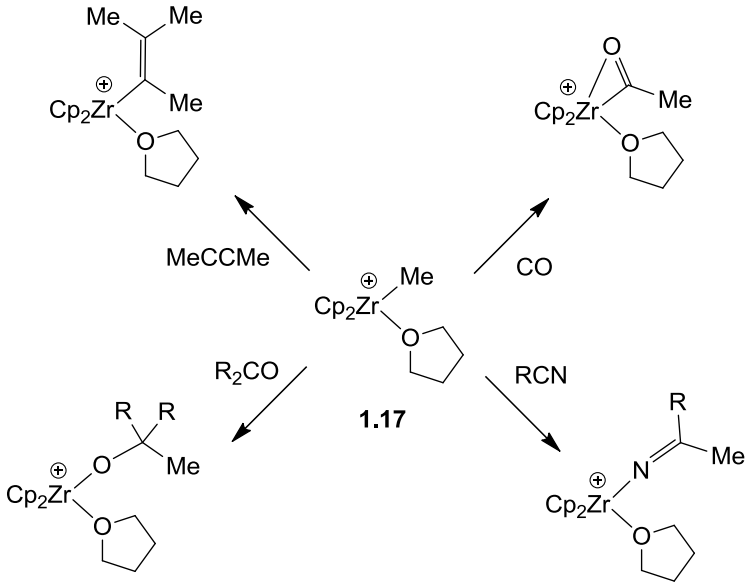

Scheme 1.3 Reaction of **1.17** with unsaturated substrates. $[BPh_4]^-$ omitted.

Donor ligands (e.g. ethylene or nitrile) bond to $[Cp_2TiMe]^+$ by interacting with the metal's d_σ orbital.[171] In the case of nitriles this complex is stable and isolable whereas with ethylene this is not the case (with electron poor metals). The metal-nitrile complexes consequently experience a more significant activation barrier to migratory insertion than the unstable metal-ethylene complex. This crucially results in a much faster insertion into the metal alkyl bond for ethylene than nitriles and thus facile polymerisation of the ethylene. These nitrile reactions help show, therefore, that it is important to have an unstable metal-alkene intermediate in order for polymerisation of unsaturated species to occur. Post-metallocene species have also had their insertion chemistry studied. Stephan *et al.* have shown their ubiquitous phosphinimide supported titanium and zirconium complexes will undergo insertion chemistry with carbodiimides and alkynes to give κ^2-amidinate and alkenyl complexes, respectively; an example of a carbodiimide insertion to form **1.31** is shown in Equation 1.4.[70, 172]

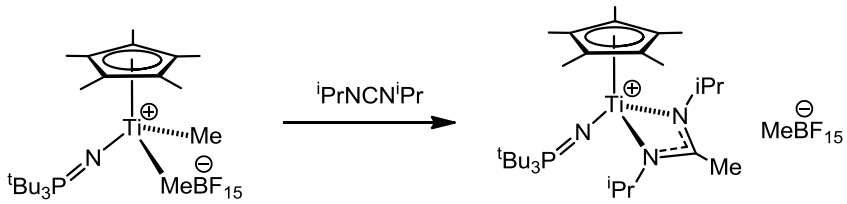

1.31

Equation 1.4

The insertion of alkenes into M-C bonds of Group 4 cations has also been investigated. In 1994 Pellacchia *et al.* reported the synthesis of $[Zr(Bn)_2(CH_2CHMeCH_2Ph)]$-$[PhCH_2B(C_6F_5)_3)]$ by the insertion of propene into the Zr-C bond of $[ZrBn_3\{(\eta^6$-$PhCH_2)B(C_6F_5)_3\}]$. Compound **1.32** was also synthesised by the insertion of propene into the Zr-C bond of $[Cp^*ZrBn_2]^+$ and was isolated and characterised by NMR spectroscopy and shown to contain a back-biting Ph-Zr interaction which acts to stabilise the cationic metal centre; this compound was later characterised by X-ray crystallography. The Ph-Zr interaction results in a stability in the complex towards both β-hydrogen elimination and further propene insertion. Other higher olefin insertion products could also be isolated and characterised.[173, 174]

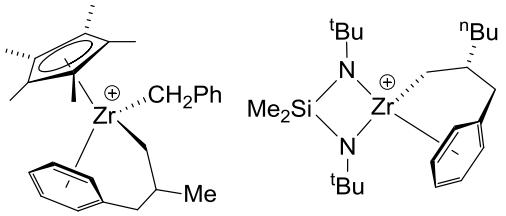

1.32 **1.33**

Horton *et al.* reported the products of alkene insertion into the Ti-Me bond of diamide supported complex $[\{Me_2Si(NCMe_3)\}ZrBn][BF_{20}]$. Reaction with 1-hexene produced the isolable product **1.33**; the insertions of ethylene and propylene could be observed on the NMR scale but the products could not be isolated. Compound **1.33** was also found to be stabilised by a Ph-Zr interaction as evident in the ^{13}C NMR. An interesting point to note is that the alkenes only reacted with the monomeric catalyst and the dimeric catalyst persisted in solution.[175] Baird and Budzelaar have also published papers in the last few years regarding the formation of titanium alkyl species resulting from alkene insertion into the Ti-Me bond.[176-178]

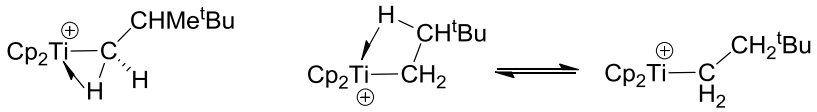

Figure 1.13 Cations **1.34** and **1.35** stabilised by agostic interactions.

Insertion of 3,3-dimethyl-1-butene (DMB) into the Ti-Me bond of the solvent stabilised monomethyl cation $[Cp_2TiMe(CD_2Cl_2)]^+$ results in the formation of complex **1.34**, which can be characterised by NMR spectroscopy at 195-205 K. **1.34** is thought to be stabilised by an α-agostic interaction which is reflected in the 7 ppm separation of the α-CH_2 protons and in the geminal coupling constant. On standing **1.34** is thought to undergo β-hydrogen elimination to give $[Cp_2TiH]^+$ which then inserts excess DMB to yield **1.35** which exists as a β-agostic stabilised species in fast exchange with its non-agostic analogue.[176] A similar β-agostic stabilised species is also formed from reaction of $[Cp_2TiMe(CD_2Cl_2)]^+$ with 2,4-dimethyl-1-pentene (DMP). In this reaction Cp_2TiMe_2 is treated with $[Ph_3C][BF_{20}]$ (TBF_{20}) in the first step resulting in a mixture of species which are assigned as $[Cp_2TiMe(CD_2Cl_2)][BF_{20}]$, $[Cp_2TiMe][BF_{20}]$ and $[(Cp_2TiMe)_2(\mu\text{-}Me)][BF_{20}]$. On addition of alkene DMP only $[Cp_2TiMe(CD_2Cl_2)][BF_{20}]$ reacted; $[Cp_2TiMe][BF_{20}]$ did not react with DMP nor did it re-equilibrate to form $[Cp_2TiMe(CD_2Cl_2)][BF_{20}]$. In the publication it does note that a reviewer is not compelled by the existence of both $[Cp_2TiMe(CD_2Cl_2)][BF_{20}]$ and $[Cp_2TiMe][BF_{20}]$ and suggested the existence of a dimeric species.[178]

1.6.6.2 Lewis acid-base chemistry

Alkyl cations are well known to form adducts with Lewis bases as previously mentioned and the early examples of alkyl cations were isolated as adducts as previously discussed. Examples of Lewis bases used in this chemistry include RCN, PR_3, THF, pyridine, NR_3. Stronger donors such as PR_3 will replace moderately labile donors such as MeCN but THF, being a weaker donor, will not.[109] The number of Lewis base donors that can bond to the metal centre is dependent on the ionic radius of the metal. For example titanium can form 16 valence electron complexes with a single Lewis base whereas zirconium can fit another ligand if small donor ligands are used and thus form 18 valence electron cations, e.g. $[Cp_2ZrMe(PMe_3)_2]^+$.[100, 179]

1.7 Project introduction

Lanxess Elastomers has recently introduced κ^1-amidinate ($NC(NR_2)Ar$, R = alkyl) catalysts in the form of Keltan ACE^{TM}.[63, 162, 180, 181] In these compounds the amidinate ligand binds to the metal thorough only the imide nitrogen with a single σ-interaction and two π-interactions. Amidinate ligands are in theory isolobal with ketimide, guanidinate, phosphinimide and cyclopentadienyl type ligands (discussed further in Chapter 2). The reason for the κ^1-amidinates ability to act as σ+2π donor is the same as previously discussed for the iminoimidazolidides (cyclic guanidinates) in Section 1.51; in this case the single amino nitrogen can mesomerically donate into the π_{CN} system as displayed in Figure 1.14.

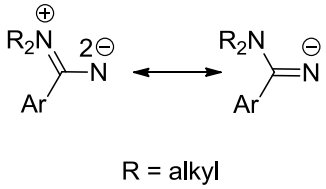

Figure 1.14 Mesomeric forms of an anionic amidinate ligand.

The steric properties can be adjusted on both the aryl and amine substituents of the ligand with relative ease. Lanxess Elastomers' interest in guanidinate-supported titanium catalysts has also grown recently and resulted in a published patent on some κ^1-guanidinate supported catalysts in 2011.[57] The general forms of the amidinate (**1.36**) and guanidinate (**1.37**) supported precatalysts are shown in Figure 1.15.

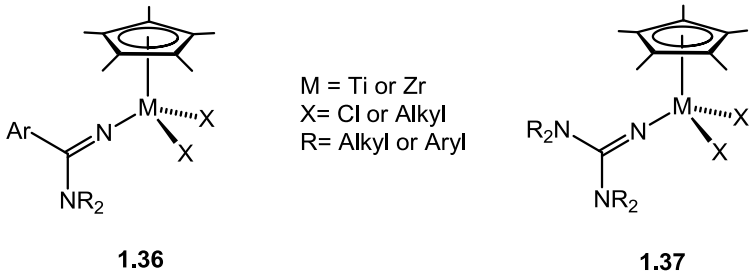

1.36 **1.37**

Figure 1.15 Representation of pentamethylcyclopentadienyl κ^1-amidinate- (**1.36**, left) and κ^1-guanidinate- (**1.37**, right) supported catalysts.

The titanium amidinate complexes have ultra-high molecular weight capabilities in the polymerisation of ethylene and also perform very well in the co-polymerisation of ethylene, propylene and dienes ethylidenenorborene (ENB), vinyl norbornene (VNB) and dicyclopentadiene (DCPD) to make the elastomer EPDM (Figure 1.16).

Prior to this technology, Lanxess's EPDM was produced using more traditional heterogeneous vanadium based catalysts. The corresponding zirconium complexes are much less active than their titanium counterparts.[182]

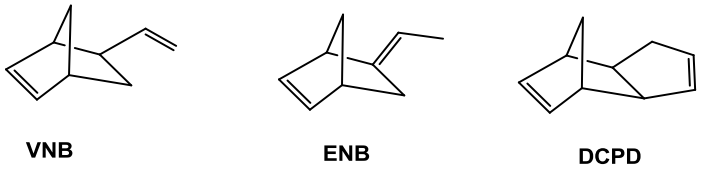

Figure 1.16 Dienes used in the production of EPDM

1.7.1 General chemistry of amidinates and guanidinates

Both amidines and guanidines can be described as an sp^2-carbon bonded to an imine nitrogen alongside either one (amidine) or two (guanidine) amine nitrogens. The neutral compounds have been used as ligands for organometallic compounds. However, this is not so relevant to this Thesis and the reader is directed to review articles for further information.[183, 184]

The ligands are usually utilised in their monoanionic state,[185-188] which in reality is best represented as a mixture of resonance forms as seen in Figure 1.17 for a *N,N′*-disubstituted amidinate. This representation sees the monoanionic charge spread over the central NCN unit and as such they are considered isoelectronic with carboxylate and allyl ligands.

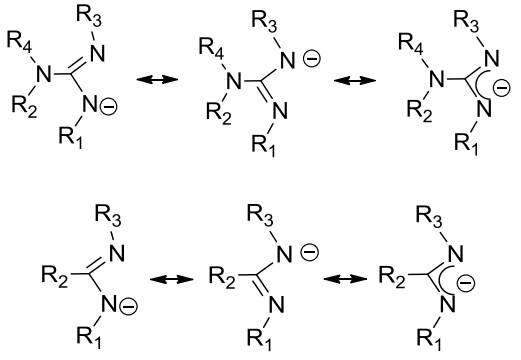

Figure 1.17 N,N′-disubstituted amidinate resonance forms

Given this one would then expect, and indeed it is so, that the most common binding mode to a metal centre for these amidinates involves a κ^2- interaction (Figure 1.18 (a)) consisting of two σ-bonds. A single σ bond between the ligand and metal centre is possible but rare (Figure 1.18 (b)); for example Group 10 platinum complex $\{C_6H_3(NMe_2)\}Pt\{TolNCHNTol\}$ displays such an interaction.[189] Chelating amidinates

are easily synthesised by nucleophilic addition to carbodiimides and thus allows the production of a large variety of ligands with different steric and electronic environments. It is also possible, but more unusual, to have the amidinate ligand bond through a discrete σ_X and discreet σ_L type interaction with the metal centre (Figure 1.18 (c)). The more common κ^2-amidinate supported complexes have been utilised as olefin polymerisation catalysts and have been well reviewed.[185-187, 190]

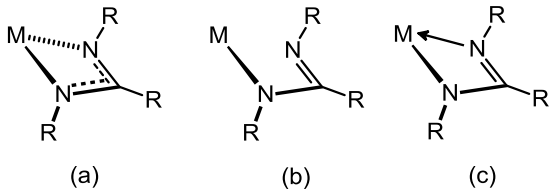

Figure 1.18 Ligand binding modes

If the amidinate is *N,N*-disubstituted binding *via* a single anionic imine nitrogen in a κ^1-mode, as in **1.36**, is possible but examples are quite rare and only a handful of similar compounds have been crystallographically characterised; some examples are illustrated in Figure 1.19.

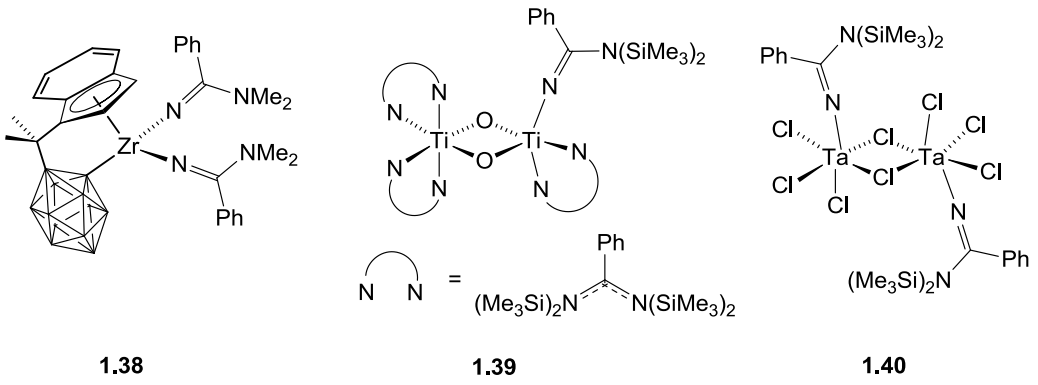

Figure 1.19 Crystallographically characterised complexes containing a κ^1-amidinate ligand.

These complexes have been synthesised by a variety of different methods; **1.38** was synthesised by the insertion of a nitrile into a Zr-amide bond, **1.39** was synthesised by silyl migration in a κ^2-amidinate and **1.40** by reaction of Me_3Si-NCPh$(NSiMe_3)_2$ with tantalum pentachloride. Similar to the cyclic guanidinates (iminoimidazolidides) already discussed in Section 1.5.1 κ^1-amidinate ligands can also act as $\sigma+2\pi$ donors to a metal centre. Although the amidinate (**1.36**) has only one amino nitrogen it can donate into the π_{CN} system in a similar fashion to a guanidinate (Figure 1.20).

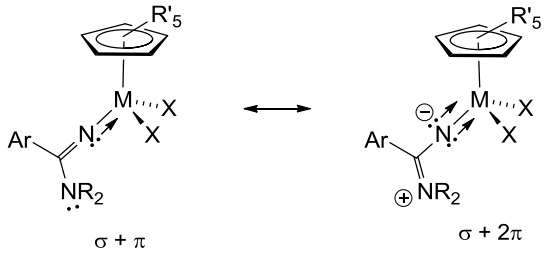

1.36

Figure 1.20 Resonance forms of a κ^1-amidinate ligand (**1.36**) acting as a σ+π (left) and σ+2π (right) donor to a metal centre.

Literature precedence for Group 4 κ^1-guanidinate complexes is far from extensive. There are only 14 crystallographically characterised titanium κ^1-guanidinate compounds in the literature (See Figure 1.21) and 12 of them contain only small variations of the iminoimidazolidide type ligand. The other two compounds contain a mono- and bis-tetramethylguanidine ligand set (**1.46** and **1.47**, respectively)[191] In total only *ca.* 50 titanium κ^1-guanidinate compounds have ever been reported in literature and nearly all of these are contained in a single patent or in papers by Tamm, Hessen and Nomura.[57-63] The compounds **1.46** and **1.47** have been synthesised by Zhang *et al.* and are the only structurally characterised non-cyclic guanidinate supported titanium species.[191]

$Cp_2Ti\{NC(NMe_2)_2\}Cl$ (**1.46**) was synthesised by treatment of Cp_2TiCl_2 with $LiNC(NMe_2)_2$. Interestingly, the addition of a second equivalent of lithiated ligand resulted in the formation of $CpTi\{NC(NMe_2)_2\}_2Cl$ (**1.47**) *via* the loss of one Cp ligand.[191] In the reported patent as well as in the other reported instances the synthesis of all the precatalysts proceeds *via* a similar salt metathesis route.[57-63]

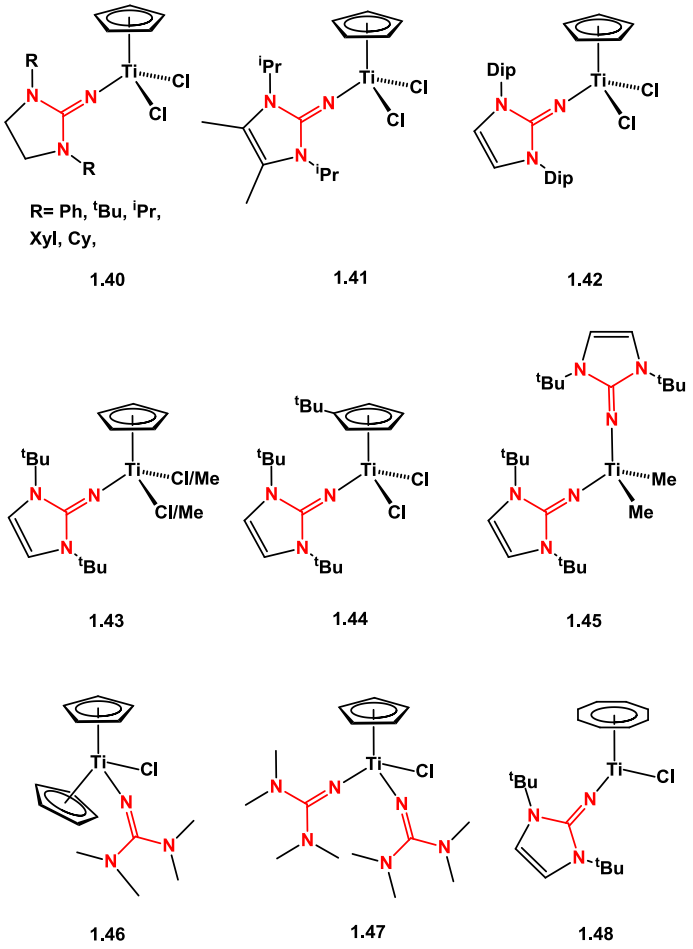

Figure 1.21 Structurally characterised titanium κ^1-guanidinate complexes (**1.40**-**1.48**).

1.7.2 Chemistry of the κ^1-amidinate catalysts

Due to the importance of base-free cationic species in polymerisation reactions it is important to understand how they behave both in solution and in the solid state. In 2010 in order to explore the underlying chemistry of κ^1-amidinate polymerisation catalysts the dimethyl precatalyst Cp*Ti{NC(N^{i}Pr$_2$)Ar^{F_2}}Me$_2$ (**1.49**, Ar^{F_2} = 2,6-C$_6$H$_3$F$_2$) was treated with TBF$_{20}$ under various conditions. The general reactivity investigated is summarised in Scheme 1.4. Treating **1.49** with 1 equiv of TBF$_{20}$ resulted in the formation of the first example of a crystallographically characterised base-free Group 4 dimeric dimethyl-bridged dication [Cp*$_2$Ti$_2${NC(N^{i}Pr$_2$)Ar^{F_2}}$_2$Me$_2$]$^{2+}$ (**1.26$_{dim}$**$^{2+}$, Figure 1.22). This isolable compound can be used as a catalyst with the same polymerisation capabilities as the *in situ* generated catalyst. The bridging methyl groups in this compound form 3-centre-2-electron bonds with the titanium centres and interestingly also contain two α-agostic interactions each to the titanium centres. Reaction of **1.26$_{dim}$**$^{2+}$ with **1.49** yields the dimeric monomethylbridged monocation

$[Cp^*_2Ti_2\{NC(N^iPr_2)Ar^{F_2}\}_2Me_2(\mu\text{-}Me)]^+$ (**1.50**$^+$). Further treatment of **1.50**$^+$ with $OPPh_3$ results in the formation of Lewis base stabilised cation $[Cp^*Ti\{NC(N^iPr_2)Ar^{F_2}\}(OPPh_3)Me][BF_{20}]$ (**1.51**$^+$) alongside the dimethyl precatalyst **1.49**. Alternatively direct treatment of **1.26**$^+$ with $OPPh_3$ or activation of **1.49** in the presence of $OPPh_3$ also yields **1.51**$^+$.

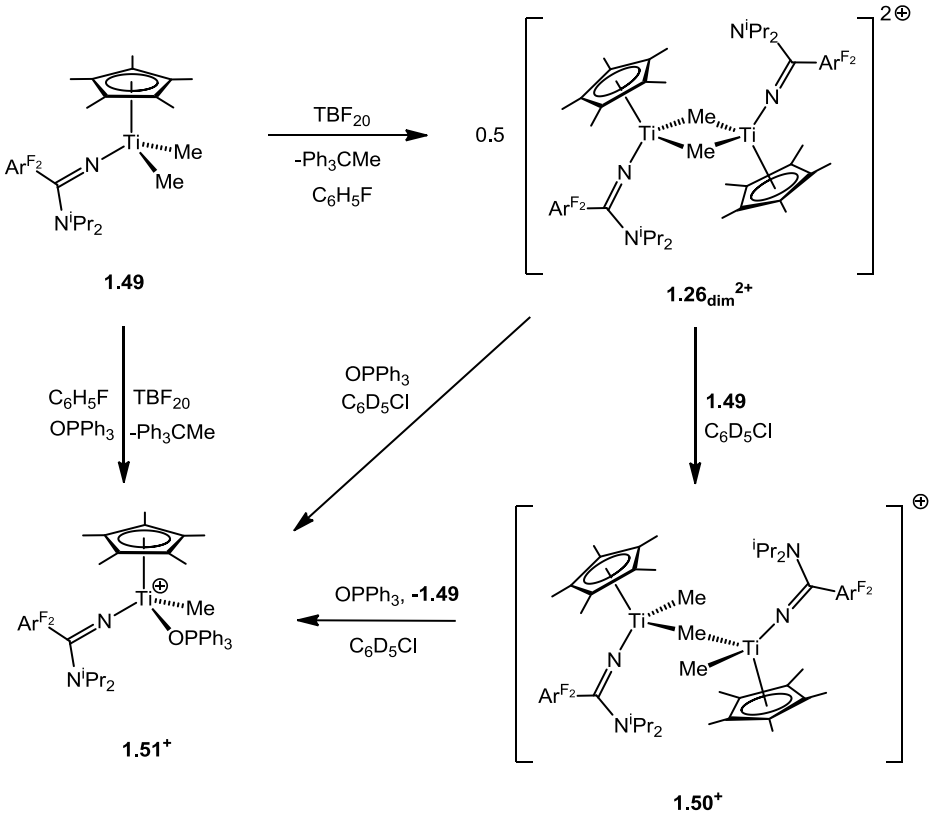

Scheme 1.4 Synthesis of titanium methyl cations **1.26**$_{dim}^{2+}$, **1.50**$^+$ and **1.51**$^+$. $[BF_{20}]^-$ anions omitted for clarity.

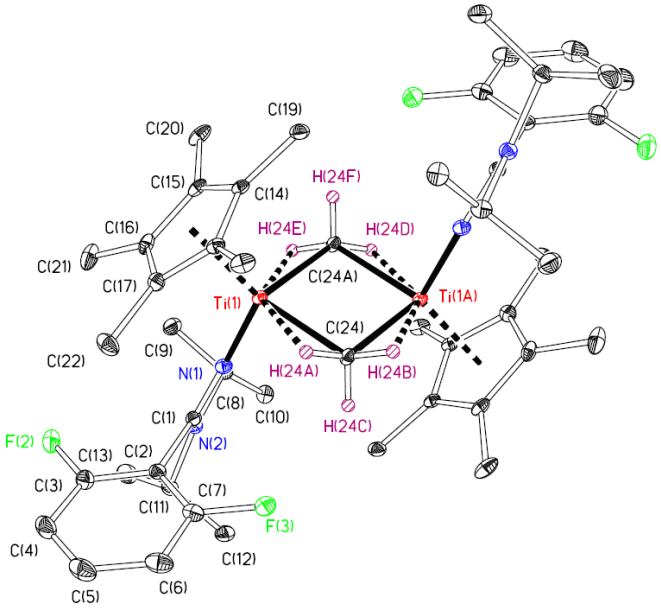

Figure 1.22 Crystal structure of $\mathbf{1.26_{dim}}^{2+}$.

Even though a lot of effort has been put into the chemistry of alkyl cations since the early 1980s only one other Group 4 dication has been reported. Sita *et al.* reported the half-sandwich zirconocene dication $[Cp^*_2Zr_2\{MeC(N^tBu)(NEt)\}_2(\mu\text{-}Me)_2]^{2+}$, in 2000 which also contained bridging methyl groups.[192] The methyl groups were said to have an unusual trigonal bipyramidal geometry and two α-agostic interactions but DFT studies on this system coupled with the fact that the hydrogens weren't positionally refined has led to scepticism over the true nature of these methyl groups.[162]

1.8 Summary and objectives

This Chapter has described the expansion of polyolefin catalysis from heterogeneous Ziegler-Natta systems to homogenous metallocene and post-metallocene catalysts. The isolobal analogy between metallocene and post-metallocene catalysts has been introduced. A variety of different methods for the activation of precatalysts has also been described as well as the interactions that can lead to stabilisation of the active monoalkyl cation. Various facets of the reactivity of the monoalkyl cations has be detailed and the development of a new series of κ^1-amidinate and κ^1-guanidinate catalysts has also been presented. Chapter 2 will discuss the synthesis and characterisation of a series of amidinate and guanidinate supported Ti(IV) complexes. A DFT study of the bonding in these compounds has also been carried out and will be presented in Chapter 2. Chapter 3 will focus on the base-free monoalkyl cation chemistry of various complexes in order to elucidate their behaviour and will also

describe the synthesis and characterisation of various Lewis base adducts. Chapter 3 will also present DFT calculations to reveal the electronic structures of the active cationic species; these calculations will also explain monomer-dimer equilibria. The end of Chapter 3 concentrates on the formation of alkyl bridged species initially discussing monomethylbridged monocations and later alkyl aluminium adducts. The reaction of the alkyl cations with unsaturated substrates is detailed in Chapter 4 along with DFT studies to facilitate understanding. The polymerisation ability of the amidinate and the guanidinate supported catalysts will be discussed at the end of Chapter 4.

1.9 References

1. K. Ziegler, E. Holzkamp, H. Breil and H. Martin, *Angew. Chem. Int. Ed.*, 1955, **67**, 541-547.
2. K. Ziegler, *Angew. Chem.*, 1964, **76**, 545-553.
3. G. Natta, *Angew. Chem. Int. Ed.*, 1956, **68**, 393-403.
4. G. Natta, *Angew. Chem.*, 1964, **76**, 553-566.
5. M. Bochmann, *J. Chem. Soc., Dalton Trans.*, 1996, 255-270.
6. W. Kaminsky, *J. Chem. Soc., Dalton Trans.*, 1998, 1413-1418.
7. G. W. Coates, *J. Chem. Soc., Dalton Trans.*, 2002, 467-475.
8. H. H. Brintzinger, D. Fischer, R. Mülhaupt, B. Rieger and R. M. Waymouth, *Angew. Chem. Int. Ed. Engl.*, 1995, **34**, 1143-1170.
9. M. Bochmann, *J. Organomet. Chem.*, 2004, **689**, 3982-3998.
10. G. J. P. Britovsek, V. C. Gibson and D. F. Wass, *Angew. Chem. Int. Ed.*, 1999, **38**, 428-447.
11. A. L. McKnight and R. M. Waymouth, *Chem. Rev.*, 1998, **98**, 2587-2598.
12. V. C. Gibson and S. K. Spitzmesser, *Chem. Rev.*, 2003, **103**, 283-315.
13. M. Mitani, J. Saito, S.-i. Ishii, Y. Nakayama, H. Makio, N. Matsukawa, S. Matsui, J.-i. Mohri, R. Furuyama, H. Terao, H. Bando, H. Tanaka and T. Fujita, *Chem. Rec.*, 2004, **4**, 137-158.
14. P. D. Bolton and P. Mountford, *Adv. Synth. Catal.*, 2005, **347**, 355-366.
15. K. Ziegler, H. Breil, E. Holzkamp and H. Martin, *German Pat. Appl.*, 1953.
16. G. Wilke, *Angew. Chem. Int. Ed.*, 2003, **42**, 5000-5008.
17. G. Wilkinson, P. L. Pauson, J. M. Birmingham and F. A. Cotton, *J. Am. Chem. Soc.*, 1953, **75**, 1011-1012.

18. D. S. Breslow and N. R. Newburg, *J. Am. Chem. Soc.*, 1957, **79**, 5072-5073.
19. G. Natta, P. Pino, G. Mazzanti and U. Giannini, *J. Am. Chem. Soc.*, 1957, **79**, 2975-2976.
20. K. H. Reichert and K. R. Meyer, *Makromol. Chem.*, 1973, **169**, 163-176.
21. W. P. Long and D. S. Breslow, *Justus Liebigs Ann. Chem.*, 1975, **1975**, 463-469.
22. A. Andresen, H.-G. Cordes, J. Herwig, W. Kaminsky, A. Merck, R. Mottweiler, J. Pein, H. Sinn and H.-J. Vollmer, *Angew. Chem. Int. Ed. Engl.*, 1976, **15**, 630-632.
23. H. Sinn, W. Kaminsky, F. G. A. Stone and W. Robert, in *Advances in Organometallic Chemistry*, Academic Press, 1980, vol. Volume 18, pp. 99-149.
24. H. Sinn, W. Kaminsky, H.-J. Vollmer and R. Woldt, *Angew. Chem. Int. Ed. Engl.*, 1980, **19**, 390-392.
25. W. Kaminsky, K. Külper, H. H. Brintzinger and F. Wild, *Angew. Chem. Int. Ed. Engl.*, 1985, **24**, 507-508.
26. J. A. Ewen, R. L. Jones, A. Razavi and J. D. Ferrara, *J. Am. Chem. Soc.*, 1988, **110**, 6255-6256.
27. G. W. Coates and R. M. Waymouth, *Science*, 1995, **267**, 217-219.
28. J. C. Stevens, F. J. Timmers, D. R. Wilson, G. F. Schmidt, P. N. Nickias, R. K. Rosen, G. W. Knight and S. Y. Lai, *Dow Chemical Co., EP416815A2*, 1991.
29. H. Braunschweig and F. M. Breitling, *Coord. Chem. Rev.*, 2006, **250**, 2691-2720.
30. J. C. Stevens, F. J. Timmers and R. K. Rosen, *Dow Chemical Co., EP416815A2*, 1991.
31. J. C. Stevens and D. R. Neithamer, *Dow Chemical Co., EP418044A2*, 1991.
32. R. K. Rosen, P. N. Nickias, D. D. Devore and F. J. Timmers, *Dow Chemical Co., WO9319104A1*, 1993.
33. R. K. Rosen, P. N. Nickias, D. D. Devore, J. C. Stevens and F. J. Timmers, *Dow Chemical Co., US5374696A*, 1994.
34. J. A. M. Canich, *Exxon Chemical Patents Inc., EP420436A1*, 1991.
35. J. A. M. Canich, *Exxon Chemical Patents Inc., US5026798A*, 1991.
36. J. A. M. Canich, *Exxon Chemical Patents Inc., US5096867A*, 1992.

37. J. A. M. Canich, H. W. Turner and G. G. Hlatky, *Exxon Chemical Patents Inc.*, *US5621126A* 1997.
38. P. J. Shapiro, E. Bunel, W. P. Schaefer and J. E. Bercaw, *Organometallics*, 1990, **9**, 867-869.
39. J. Okuda, *Chem. Ber.*, 1990, **123**, 1649-1651.
40. H. Braunschweig and F. M. Breitling, *Coord. Chem. Rev.*, 2006, **250**, 2691-2720.
41. P.-J. Sinnema, d. V. L. van, A. L. Spek, N. Veldman and J. H. Teuben, *Organometallics*, 1997, **16**, 4245-4247.
42. D. B. Millward, A. P. Cole and R. M. Waymouth, *Organometallics*, 2000, **19**, 1870-1878.
43. R. Hoffmann, *Angew. Chem. Int. Ed.*, 1982, **21**, 711-724.
44. N. Adams, H. J. Arts, P. D. Bolton, D. Cowell, S. R. Dubberley, N. Friederichs, C. M. Grant, M. Kranenburg, A. J. Sealey, B. Wang, P. J. Wilson, M. Zuideveld, A. J. Blake, M. Schroeder and P. Mountford, *Organometallics*, 2006, **25**, 3888-3903.
45. H. R. Bigmore, S. R. Dubberley, M. Kranenburg, S. C. Lawrence, A. J. Sealey, J. D. Selby, M. A. Zuideveld, A. R. Cowley and P. Mountford, *Chem. Commun.*, 2006, 436-438.
46. P. D. Bolton, E. Clot, N. Adams, S. R. Dubberley, A. R. Cowley and P. Mountford, *Organometallics*, 2006, **25**, 2806-2825.
47. J. C. Green, *Chem. Soc. Rev.*, 1998, **27**, 263-272.
48. K. Nomura and J. Liu, *Dalton Trans.*, 2011, **40**, 7666-7682.
49. P. J. Sinnema, T. P. Spaniol and J. Okuda, *J. Organomet. Chem.*, 2000, **598**, 179-181.
50. K. Nomura and K. Fujii, *Organometallics*, 2002, **21**, 3042-3049.
51. K. Nomura and K. Fujii, *Macromolecules*, 2003, **36**, 2633-2641.
52. S. Zhang, W. E. Piers, X. Gao and M. Parvez, *J. Am. Chem. Soc.*, 2000, **122**, 5499-5509.
53. K. W. Henderson, A. Hind, A. R. Kennedy, A. E. McKeown and R. E. Mulvey, *J. Organomet. Chem.*, 2002, **656**, 63-70.
54. A. R. Dias, M. T. Duarte, A. C. Fernandes, S. Fernandes, M. M. Marques, A. M. Martins, J. F. da Silva and S. S. Rodrigues, *J. Organomet. Chem.*, 2004, **689**, 203-213.

55. K. Nomura, K. Fujita and M. Fujiki, *J. Mol. Catal. A: Chem.*, 2004, **220**, 133-144.
56. M. J. Ferreira and A. M. Martins, *Coord. Chem. Rev.*, 2006, **250**, 118-132.
57. G. H. J. van Doremaele, M. A. Zuideveld, N. V. F. Quiroga and A. Leblanc, *LANXESS Elastomers, WO2011054927A1*, 2011.
58. W. P. Kretschmer, *Stichting Dutch Polymer Institute, US20040192541A1*, 2004.
59. W. P. Kretschmer, C. Dijkhuis, A. Meetsma, B. Hessen and J. H. Teuben, *Chem. Commun.*, 2002, 608-609.
60. K. Nomura, H. Fukuda, S. Katao, M. Fujiki, H. J. Kim, D.-H. Kim and S. Zhang, *Dalton Trans.*, 2011, **40**, 7842-7849.
61. M. Tamm, S. Randoll, T. Bannenberg and E. Herdtweck, *Chem. Commun.*, 2004, 876-877.
62. M. Tamm, S. Randoll, E. Herdtweck, N. Kleigrewe, G. Kehr, G. Erker and B. Rieger, *Dalton Trans.*, 2006, 459-467.
63. K. Nomura, H. Fukuda, W. Apisuk, A. G. Trambitas, B. Kitiyanan and M. Tamm, *J. Mol. Catal. A: Chem.*, 2012, **363–364**, 501-511.
64. D. W. Stephan, F. Guérin, R. E. v. H. Spence, L. Koch, X. Gao, S. J. Brown, J. W. Swabey, Q. Wang, W. Xu, P. Zoricak and D. G. Harrison, *Organometallics*, 1999, **18**, 2046-2048.
65. D. W. Stephan, J. C. Stewart, F. Guérin, R. E. v. H. Spence, W. Xu and D. G. Harrison, *Organometallics*, 1999, **18**, 1116-1118.
66. F. Guerin, J. C. Stewart, C. Beddie and D. W. Stephan, *Organometallics*, 2000, **19**, 2994-3000.
67. N. L. S. Yue and D. W. Stephan, *Organometallics*, 2001, **20**, 2303-2308.
68. N. Yue, E. Hollink, F. Guerin and D. W. Stephan, *Organometallics*, 2001, **20**, 4424-4433.
69. D. W. Stephan, J. C. Stewart, F. Guerin, S. Courtenay, J. Kickham, E. Hollink, C. Beddie, A. Hoskin, T. Graham, P. Wei, R. E. v. H. Spence, W. Xu, L. Koch, X. Gao and D. G. Harrison, *Organometallics*, 2003, **22**, 1937-1947.
70. E. Hollink, P. Wei and D. W. Stephan, *Organometallics*, 2004, **23**, 1562-1569.
71. K. Dehnicke and F. Weller, *Coord. Chem. Rev.*, 1997, **158**, 103-169.
72. K. Dehnicke, M. Krieger and W. Massa, *Coord. Chem. Rev.*, 1999, **182**, 19-65.

73. K. Nomura, N. Naga, M. Miki, K. Yanagi and A. Imai, *Organometallics*, 1998, **17**, 2152-2154.
74. K. Nomura, N. Naga, M. Miki and K. Yanagi, *Macromolecules*, 1998, **31**, 7588-7597.
75. K. Nomura, M. Tsubota and M. Fujiki, *Macromolecules*, 2003, **36**, 3797-3799.
76. Y. Qian, H. Zhang, X. Qian, J. Huang and C. Shen, *J. Mol. Catal. A: Chem.*, 2003, **192**, 25-33.
77. A. E. Fenwick, K. Phomphrai, M. G. Thorn, J. S. Vilardo, C. A. Trefun, B. Hanna, P. E. Fanwick and I. P. Rothwell, *Organometallics*, 2004, **23**, 2146-2156.
78. W. Wang, T. Tanaka, M. Tsubota, M. Fujiki, S. Yamanaka and K. Nomura, *Adv. Synth. Catal.*, 2005, **347**, 433-446.
79. I. A. Latham, G. J. Leigh, G. Huttner and I. Jibril, *J. Chem. Soc., Dalton Trans.*, 1986, 377-383.
80. K. Nomura, K. Fujita and M. Fujiki, *J. Mol. Catal. A: Chem.*, 2004, **220**, 133-144.
81. K. Nomura, K. Fujita and M. Fujiki, *Catal. Commun.*, 2004, **5**, 413-417.
82. G. C. Bazan, G. Rodriguez, A. J. Ashe, S. Al-Ahmad and C. Müller, *J. Am. Chem. Soc.*, 1996, **118**, 2291-2292.
83. G. C. Bazan, G. Rodriguez, A. J. Ashe, S. Al-Ahmad and J. W. Kampf, *Organometallics*, 1997, **16**, 2492-2494.
84. R. A. Lee, R. J. Lachicotte and G. C. Bazan, *J. Am. Chem. Soc.*, 1998, **120**, 6037-6046.
85. C. Janiak, K. C. H. Lange, U. Versteeg, D. Lentz and P. H. M. Budzelaar, *Chem. Ber.*, 1996, **129**, 1517-1529.
86. T. Wada, T. Tsukhara, T. Sugano, T. Takahama, K. Yamamoto and H. Kurokawa, *(Mitsubishi Kagaku Kk), Jpn. Kokai Tokkyo Koho JP-A 07,188335*, 1995.
87. T. Wada, T. Tsukhara, T. Sugano, T. Takahama, K. Yamamoto and H. Kurokawa, *(Mitsubishi Kagaku Kk), Jpn. Kokai Tokkyo Koho JP-A 07,188319*, 1995.
88. E. J. M. D. Boer, H. J. Heeres and H. J. R. D. B. (Shell), *EP-B 638, 593*, 1995.
89. S. J. Skoog, C. Mateo, G. G. Lavoie, F. J. Hollander and R. G. Bergman, *Organometallics*, 2000, **19**, 1406-1421.

90. S. Trofimenko, *J. Am. Chem. Soc.*, 1966, **88**, 1842-1844.
91. S. Trofimenko, *J. Am. Chem. Soc.*, 1967, **89**, 3904-3905.
92. S. Trofimenko, *J. Am. Chem. Soc.*, 1967, **89**, 6288-6294.
93. H. Bigmore, *DPhil Thesis, University of Oxford*, 2007.
94. L. Clark, Part II Thesis, University of Oxford, 2008.
95. H. Nakazawa, S. Ikai, K. Imaoka, Y. Kai and T. Yano, *J. Mol. Catal. A: Chem.*, 1998, **132**, 33-41.
96. M. P. Gil, S. J. H. Z. Dos and O. L. Casagrande, Jr., *Macromol. Chem. Phys.*, 2001, **202**, 319-324.
97. M. P. Gil and O. L. Casagrande, *J. Organomet. Chem.*, 2004, **689**, 286-292.
98. M. P. Gil, S. J. H. Z. dos and O. L. Casagrande, *J. Mol. Catal. A: Chem.*, 2004, **209**, 163-169.
99. E. Y.-X. Chen and T. J. Marks, *Chem. Rev.*, 2000, **100**, 1391-1434.
100. R. F. Jordan, F. G. A. Stone and W. Robert, in *Advances in Organometallic Chemistry*, Academic Press, 1991, vol. Volume 32, pp. 325-387.
101. W. P. Long and D. S. Breslow, *J. Am. Chem. Soc.*, 1960, **82**, 1953-1957.
102. D. S. Breslow and N. R. Newburg, *J. Am. Chem. Soc.*, 1959, **81**, 81-86.
103. A. K. Zefirova and A. E. Shilov, *Dokl. Akad. Nauk*, 1961, **136**, 599-602.
104. F. S. Dyachkovskii, A. K. Shilova and A. E. Shilov, *J. Polym. Sci., Polym. Symp.*, 1967, **No. 16**, 2333-2339.
105. F. S. Dyachkovskii, *in 'Coordination Polymerisation'*, ed. J. C. W. Chien, 1975.
106. J. J. Eisch, A. M. Piotrowski, S. K. Brownstein, E. J. Gabe and F. L. Lee, *J. Am. Chem. Soc.*, 1985, **107**, 7219-7221.
107. R. F. Jordan, C. S. Bajgur, R. Willett and B. Scott, *J. Am. Chem. Soc.*, 1986, **108**, 7410-7411.
108. M. Bochmann and L. M. Wilson, *J. Chem. Soc., Chem. Commun.*, 1986, 1610-1611.
109. M. Bochmann, L. M. Wilson, M. B. Hursthouse and R. L. Short, *Organometallics*, 1987, **6**, 2556-2563.
110. E. Y.-X. Chen and T. J. Marks, *Chem. Rev.*, 2000, **100**, 1391-1434.
111. H. W. Turner, *Exxon Chemical Co.*, 1988, **EP 0 277 004 A1**.
112. G. G. Hlatky, H. W. Turner and R. R. Eckman, *J. Am. Chem. Soc.*, 1989, **111**, 2728-2729.

113. G. G. Hlatky, D. J. Upton and H. W. Turner, *Exxon Chemical Co.*, 1991, **WO 91/09882**.

114. A. D. Horton, J. de With, A. J. van der Linden and H. van de Weg, *Organometallics*, 1996, **15**, 2672.

115. J. S. J. McCahill, G. C. Welch and D. W. Stephan, *Dalton Trans.*, 2009, 8555-8561.

116. X. Yang, C. L. Stern and T. J. Marks, *J. Am. Chem. Soc.*, 1991, **113**, 3623-3625.

117. X. Yang, C. L. Stern and T. J. Marks, *J. Am. Chem. Soc.*, 1991, **113**, 3623-3625.

118. R. F. Jordan, R. E. LaPointe, C. S. Bajgur, S. F. Echols and R. Willett, *J. Am. Chem. Soc.*, 1987, **109**, 4111-4113.

119. R. F. Jordan, W. E. Dasher and S. F. Echols, *J. Am. Chem. Soc.*, 1986, **108**, 1718-1719.

120. M. Bochmann, A. J. Jaggar, L. M. Wilson, M. B. Hursthouse and M. Motevalli, *Polyhedron*, 1989, **8**, 1838-1843.

121. A. R. Barron, *Organometallics*, 1995, **14**, 3581-3583.

122. F. Zhu, Q. Huang and S. Lin, *J. Polym. Sci., Part A: Polym. Chem.*, 1999, **37**, 4497-4501.

123. I. Tritto, M. C. Sacchi, P. Locatelli and S. X. Li, *Macromol. Chem. Phys.*, 1996, **197**, 1537-1544.

124. L. Resconi, S. Bossi and L. Abis, *Macromolecules*, 1990, **23**, 4489-4491.

125. M. Bochmann, *J. Organomet. Chem.*, 2004, **689**, 3982-3998.

126. G. J. P. Britovsek, S. A. Cohen, V. C. Gibson and M. van Meurs, *J. Am. Chem. Soc.*, 2004, **126**, 10701-10712.

127. K. P. Bryliakov, N. V. Semikolenova, D. V. Yudaev, V. A. Zakharov, H. H. Brintzinger, M. Ystenes, E. Rytter and E. P. Talsi, *J. Organomet. Chem.*, 2003, **683**, 92-102.

128. M. Bochmann and S. J. Lancaster, *Angew. Chem. Int. Ed. Engl.*, 1994, **33**, 1634.

129. P. D. Bolton, E. Clot, A. R. Cowley and P. Mountford, *J. Am. Chem. Soc.*, 2006, **128**, 15005-15018.

130. M. Bochmann and S. J. Lancaster, *Angew. Chem. Int. Ed. Engl.*, 1994, **33**, 1634-1637.

131. P. D. Bolton, E. Clot, A. R. Cowley and P. Mountford, *J. Am. Chem. Soc.*, 2006, **128**, 15005-15018.
132. A. P. Shreve, R. Mulhaupt, W. Fultz, J. Calabrese, W. Robbins and S. D. Ittel, *Organometallics*, 1988, **7**, 409-416.
133. V. C. Williams, C. Dai, Z. Li, S. Collins, W. E. Piers, W. Clegg, M. R. J. Elsegood and T. B. Marder, *Angew. Chem. Int. Ed.*, 1999, **38**, 3695-3698.
134. R. A. Stapleton, B. R. Galan, S. Collins, R. S. Simons, J. C. Garrison and W. J. Youngs, *J. Am. Chem. Soc.*, 2003, **125**, 9246-9247.
135. M. Bochmann and A. J. Jaggar, *J. Organomet. Chem.*, 1992, **424**, C5-C7.
136. C. L. Beswick and T. J. Marks, *J. Am. Chem. Soc.*, 2000, **122**, 10358-10370.
137. P. A. Deck, C. L. Beswick and T. J. Marks, *J. Am. Chem. Soc.*, 1998, **120**, 1772-1784.
138. C. Beddie, E. Hollink, P. Wei, J. Gauld and D. W. Stephan, *Organometallics*, 2004, **23**, 5240-5251.
139. A. D. Horton and J. H. G. Frijns, *Angew. Chem.*, 1991, **103**, 1181-1183.
140. X. Yang, C. Stern and T. J. Marks, *Organometallics*, 1991, **10**, 840-842.
141. J. C. W. Chien, W. M. Tsai and M. D. Rausch, *J. Am. Chem. Soc.*, 1991, **113**, 8570-8571.
142. G. G. Hlatkey, D. J. Upton and H. W. Turner, *PCT. Int. Appl*, WO 91/09882, 1991.
143. M. J. Elder and J. A. Ewen, *Eur. Pat. Appl. 0 426 637*, 1991.
144. L. Jia, X. Yang, C. L. Stern and T. J. Marks, *Organometallics*, 1997, **16**, 842-857.
145. D. J. Gillis, M. J. Tudoret and M. C. Baird, *J. Am. Chem. Soc.*, 1993, **115**, 2543-2545.
146. S. J. Lancaster, O. B. Robinson, M. Bochmann, S. J. Coles and M. B. Hursthouse, *Organometallics*, 1995, **14**, 2456-2462.
147. J. D. Scollard, D. H. McConville and S. J. Rettig, *Organometallics*, 1997, **16**, 1810-1812.
148. S. Beck, A. Geyer and H.-H. Brintzinger, *Chem. Commun.*, 1999, 2477-2478.
149. N. G. Stahl, C. Zuccaccia, T. R. Jensen and T. J. Marks, *J. Am. Chem. Soc.*, 2003, **125**, 5256-5257.
150. A. Rodriguez-Delgado, M. D. Hannant, S. J. Lancaster and M. Bochmann, *Macromol. Chem. Phys.*, 2004, **205**, 334-346.

151. F. Song, M. D. Hannant, R. D. Cannon and M. Bochmann, *Macromol. Symp.*, 2004, **213**, 173-185.
152. S. Garratt, A. G. Carr, G. Langstein and M. Bochmann, *Macromolecules*, 2003, **36**, 4276-4287.
153. S. J. Lancaster, A. Rodriguez, A. Lara-Sanchez, M. D. Hannant, D. A. Walker, D. H. Hughes and M. Bochmann, *Organometallics*, 2002, **21**, 451-453.
154. M. H. Hannant, J. A. Wright, S. J. Lancaster, D. L. Hughes, P. N. Horton and M. Bochmann, *Dalton Trans.*, 2006, 2415-2426.
155. F. Wu, A. K. Dash and R. F. Jordan, *J. Am. Chem. Soc.*, 2004, **126**, 15360-15361.
156. M. D. Butts, B. L. Scott and G. J. Kubas, *J. Am. Chem. Soc.*, 1996, **118**, 11831-11843.
157. R. J. Kulawiec, J. W. Faller and R. H. Crabtree, *Organometallics*, 1990, **9**, 745-755.
158. P. T. Witte, A. Meetsma, B. Hessen and P. H. M. Budzelaar, *J. Am. Chem. Soc.*, 1997, **119**, 10561-10562.
159. L. H. Doerrer, M. L. H. Green, D. Haussinger and J. Sassmannshausen, *J. Chem. Soc., Dalton Trans.*, 1999, 2111-2118.
160. M. Brookhart, M. L. H. Green and L.-L. Wong, *Prog. Inorg. Chem.*, 1988, **36**, 1.
161. W. Scherer and G. S. McGrady, *Angew. Chem. Int. Ed.*, 2004, **43**, 1782-1806.
162. E. G. Ijpeij, B. Coussens, M. A. Zuideveld, G. H. J. van Doremaele, P. Mountford, M. Lutz and A. L. Spek, *Chem. Commun.*, 2010, **46**, 3339-3341.
163. E. Clot and O. Eisenstein, in *Principles and Applications of Density Functional Theory in Inorganic Chemistry II*, Springer Berlin Heidelberg, 2004, vol. 113.
164. R. F. Jordan, P. K. Bradley, N. C. Baenziger and R. E. LaPointe, *J. Am. Chem. Soc.*, 1990, **112**, 1289-1291.
165. A. D. Horton, W. J. de, d. L. A. J. van and d. W. H. van, *Organometallics*, 1996, **15**, 2672-2674.
166. F. Song, S. J. Lancaster, R. D. Cannon, M. Schormann, S. M. Humphrey, C. Zuccaccia, A. Macchioni and M. Bochmann, *Organometallics*, 2005, **24**, 1315-1328.
167. P. D. Bolton, E. Clot, A. R. Cowley and P. Mountford, *Chem. Commun.*, 2005, 3313-3315.

168. P. D. Bolton, E. Clot, N. Adams, S. R. Dubberley, A. R. Cowley and P. Mountford, *Organometallics*, 2006, **25**, 2806-2825.
169. M. Bochmann, L. M. Wilson, M. B. Hursthouse and M. Motevalli, *Organometallics*, 1988, **7**, 1148-1154.
170. Y. W. Alelyunas, R. F. Jordan, S. F. Echols, S. L. Borkowsky and P. K. Bradley, *Organometallics*, 1991, **10**, 1406-1416.
171. K. Tatsumi, A. Nakamura, P. Hofmann, P. Stauffert and R. Hoffmann, *J. Am. Chem. Soc.*, 1985, **107**, 4440-4451.
172. L. Cabrera, E. Hollink, J. C. Stewart, P. Wei and D. W. Stephan, *Organometallics*, 2005, **24**, 1091-1098.
173. C. Pellecchia, A. Grassi and A. Zambelli, *Organometallics*, 1994, **13**, 298-302.
174. C. Pellecchia, A. Immirzi and A. Zambelli, *J. Organomet. Chem.*, 1994, **479**, c9-c11.
175. A. D. Horton and J. de With, *Organometallics*, 1997, **16**, 5424-5436.
176. A. F. Dunlop-Brière, P. H. M. Budzelaar and M. C. Baird, *Organometallics*, 2012, **31**, 1591-1594.
177. M. Vatamanu, G. Stojcevic and M. C. Baird, *J. Am. Chem. Soc.*, 2007, **130**, 454-456.
178. F. Sauriol, J. F. Sonnenberg, S. J. Chadder, A. F. Dunlop-Brière, M. C. Baird and P. H. M. Budzelaar, *J. Am. Chem. Soc.*, 2010, **132**, 13357-13370.
179. R. F. Jordan, C. S. Bajgur, W. E. Dasher and A. L. Rheingold, *Organometallics*, 1987, **6**, 1041-1051.
180. E. G. Ijpeij, P. J. H. Windmuller, H. J. Arts, F. Van der Burgt, G. H. J. Van Doremaele and M. A. Zuideveld, *LANXESS ELASTOMERS, WO/2005/090418*, 2005.
181. K. Nomura and J.-Y. Liu, *Dalton Trans.*, 2011, **40**, 7666-7682.
182. R. T. W. Scott and P. Mountford, in *Unpublished Results*, 2012.
183. M. P. Coles, *Dalton Trans.*, 2006, 985-1001.
184. J. Barker and M. Kilner, *Coord. Chem. Rev.*, 1994, **133**, 219-300.
185. S. Collins, *Coord. Chem. Rev.*, 2011, **255**, 118-138.
186. E. Smolensky and M. S. Eisen, *Dalton Trans.*, 2007, 5623-5650.
187. F. T. Edelmann, *Chem. Soc. Rev.*, 2009, **38**, 2253-2268.
188. D. A. Kissounko, M. V. Zabalov, G. P. Brusova and D. A. Lemenovskii, *Usp. Khim.*, 2006, **75**, 395-421.

189. D. M. Grove, G. van Koten, H. J. C. Ubbels, K. Vrieze, L. C. Niemann and C. H. Stam, *J. Chem. Soc., Dalton Trans.*, 1986, 717-724.

190. F. T. Edelmann, *Adv. Organomet. Chem.*, 2008, **57**, 183-352.

191. J. Zhang, F. Han, Y. Han, Z. Chen and X. Zhou, *Dalton Trans.*, 2009, 1806-1811.

192. R. J. Keaton, K. C. Jayaratne, J. C. Fettinger and L. R. Sita, *J. Am. Chem. Soc.*, 2000, **122**, 12909-12910.

Chapter 2

Titanium complexes supported by κ^1-amidinate and κ^1-guanidinate ligands

2.1 Overview

This Chapter describes the synthesis and characterisation of a series of cyclopentadienyl-supported κ^1-amidinate, κ^1-guanidinate and κ^1-iminoimidazolidide post-metallocene titanium complexes that can be used in the production of polyolefins. The structures of $Cp^*Ti\{NC(NMe_2)_2\}Cl_2$ (**1**), $Cp^*Ti\{NC(NMe_2)_2\}Cl_2$ (**2**), $Cp^*Ti\{NC(N(Xyl)CH_2)_2\}Cl_2$ (**3**), $Cp^*Ti\{NC(NMe_2)_2\}Bn_2$ (**5**) and $Cp^*Ti\{NC(N(Xyl)\text{-}CH_2)_2\}Me_2$ (**7**) are also described and various structural parameters used to help interpret the Ti-N bonding in this series of complexes. A detailed computational study of the bonding in a range of dimethyl complexes using DFT methods will also be presented and discussed.

2.2 Synthesis of ligand precursors

2.2.1 Amidines

The synthesis of amidines, the precursors to amidinates, can be carried out straightforwardly by the nucleophilic attack of aryl nitriles by magnesiated secondary amines, followed by quenching with a protic reagent e.g. $MeOH/H_2O$ (Scheme 2.1). This simple synthetic method is advantageous when screening for new ligands and as such, Lanxess Elastomers published a patent in 2005 covering the synthesis of a large number of amidines as well as the preparation of their corresponding Group 4 precatalysts.[1] However, this synthetic route can be problematic if the amine is very sterically demanding; for example, di*tert*butylamine cannot be used in this synthesis.

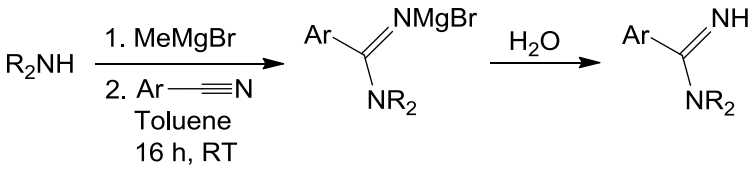

Scheme 2.1 Synthesis of an amidine protio-ligand, R = alkyl.

These compounds can be purified by a variety of methods including vacuum distillation and recrystallisation. The protio-ligands of particular interest in this Thesis are those synthesised from di*iso*propylamine and either benzonitrile, to produce $HNC(N^iPr_2)Ph$ (**2.1**), or *ortho*fluorobenzonitrile to produce $HNC(N^iPr_2)Ar^{F_2}$ (**2.2**). Work by Mountford *et al.*, alongside Lanxess Elastomers, previously described the synthesis and full characterisation of **2.1** including the crystal structure followed by the synthesis and characterisation of the corresponding dichloro and dimethyl complexes

Cp*Ti{NC(N^{i}Pr$_2$)Ph}Cl$_2$ (**2.3**) and Cp*Ti{NC(N^{i}Pr$_2$)Ph}Me$_2$ (**2.4**), respectively.[2] Compound **2.2** has been utilised previously, as described in Section 1.7.2, for the synthesis of the dimethyl precatalyst **1.49** and the dimethyl-bridged dication **1.26$_{dim}^{2+}$**.[3]

2.2.2 Guanidines

Recently Lanxess Elastomers has tested and patented a series of half-sandwich κ^1-guanidinate catalysts utilising high-throughput screening methods.[4] It was thought the addition of the second amine donor to the ligand should help modify the electronic properties, and hence catalytic activity, of the precatalysts by increasing the electron density in the Ti-N bond. The synthesis of guanidines is somewhat more complex than that for the amidines and generally involves the use of phosgene, thiophosgene and ammonia.[5] The ligand precursor 1,1,3,3-tetramethylguanidine (HNC(NMe$_2$)$_2$, **2.5**) is commercially available and so acted as a good initial point for the investigation of κ^1-guanidinate-supported catalysts. The ligand precursor HNC(N^{i}BuMe)$_2$ (**2.6**) was also utilised in the work to follow and was supplied by Lanxess Elastomers.

2.3 Synthesis of metal complexes

All the κ^1-amidinate and κ^1-guanidinate metal complexes discussed in this Thesis were synthesised from the corresponding protio-ligand and Cp*TiCl$_3$. Initially the ligand is deprotonated using an alkyl lithium reagent such as ^{n}BuLi to yield the lithiated ligand. This can then be reacted directly with the Cp*TiCl$_3$ to form the dichloride compounds, by way of example the synthesis of Cp*Ti{NC(NMe$_2$)$_2$}Cl$_2$ (**1**) is shown in Scheme 2.2.

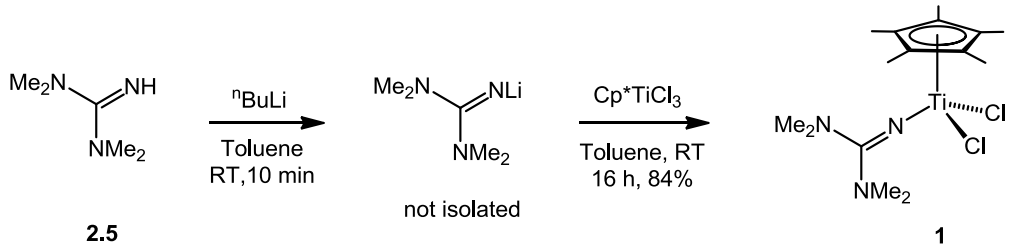

Scheme 2.2 Synthesis of Cp*Ti{NC(NMe$_2$)$_2$}Cl$_2$ (**1**)

Although the corresponding magnesiated salts of the ligands can also be used to form such complexes it has been found that using the lithiated ligand generally leads to higher isolated yields. Another alternative approach to the synthesis of κ^1-amidinate and κ^1-guanidinate titanium complexes is to react the protio-ligand with Cp*TiCl$_3$ in the presence of an excess of NEt$_3$.[2] For example, the synthesis of

Cp*Ti{NC(N^{i}Pr$_2$)Ph}Cl$_2$ (**2.3**) *via* this method is displayed in Equation 2.1. This method, although negating the use of ^{n}BuLi, generally leads to lower yields of the dichloride complexes and as such was not used as a matter of routine for work carried out in this Thesis.

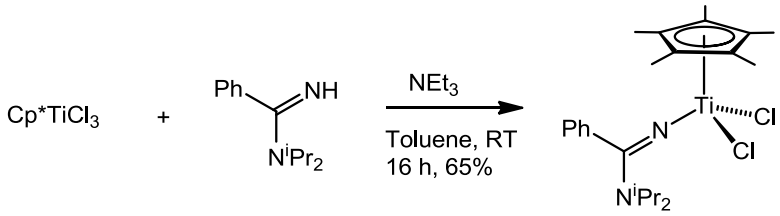

2.3

Equation 2.1

As already mentioned, Mountford *et al.* have previously synthesised and fully characterised compounds **2.4** and **1.49** [2, 3] which will be utilised for further studies in later Chapters and so will be included in the following discussions where appropriate.

2.3.1 Synthesis and characterisation of Cp*Ti{NC(NMe$_2$)$_2$}Cl$_2$ (1)

Stoichiometric reaction of Cp*TiCl$_3$ with *in situ* generated LiNC(NMe$_2$)$_2$ produced the dichloride compound Cp*Ti{NC(NMe$_2$)$_2$}Cl$_2$ (**1**) which could be isolated in a 82% yield after separation from LiCl. Compound **1** has been characterised by NMR spectroscopy, IR spectroscopy, EI mass spectrometry and elemental analysis in collaborative work involving the author and Dr Richard Scott. The room temperature ^{1}H NMR spectrum of **1** (Figure 2.1) is straightforward due to fast rotation about the Me$_2$N-C(sp^2) bonds and is consistent with C_s symmetry in solution. The spectrum therefore consists of two singlets at 2.34 and 2.09 ppm which correspond to NMe$_2$ and Cp* environments, respectively (Figure 2.1). The simplicity of this spectrum might be surprising as one could expect there to be a reasonably large bond rotation energy about the Me$_2$N-C(sp^2) bond due to conjugation of the amine lone pair into the π_{CN} system; the nature of this bonding will be discussed more in Section 2.5.2.

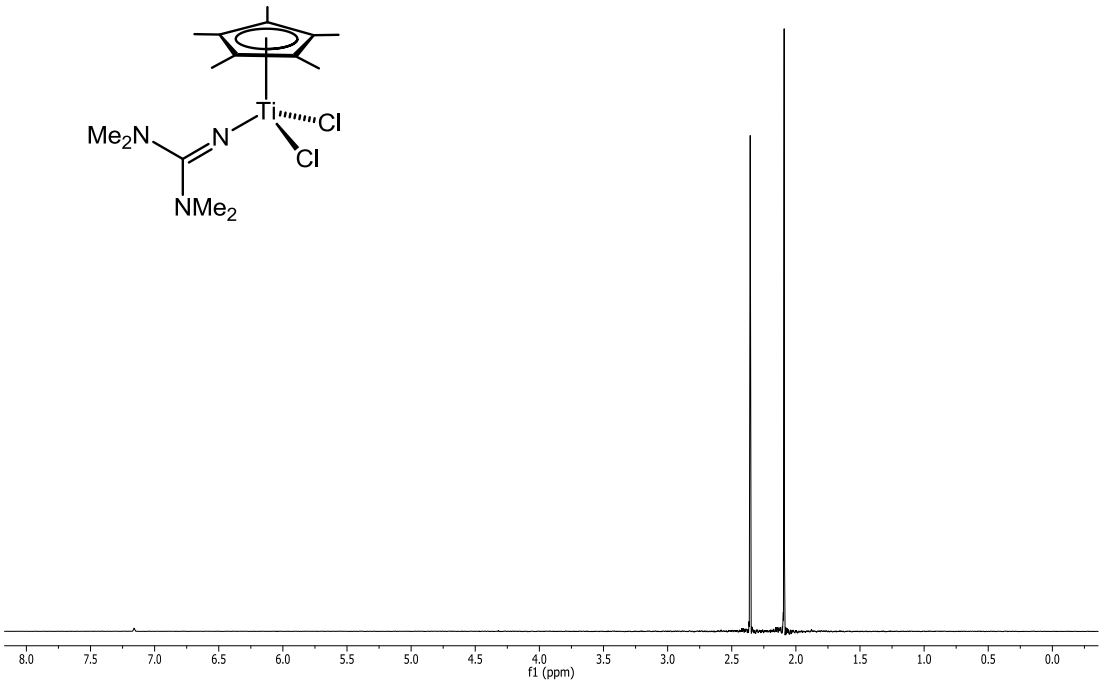

Figure 2.1 ^{1}H NMR spectrum (299.9 MHz, 293 K, C_6D_6) of Cp*Ti{NC(NMe_2)$_2$}Cl_2 (**1**).

2.3.2 Crystal structure of Cp*Ti{NC(NMe_2)$_2$}Cl_2 (1)

Diffraction-quality crystals of **1** were grown from a saturated benzene solution at room temperature. Surprisingly this is only the third example of a crystallographically characterised non-cyclic guanidinate titanium complex, the first two being reported by Zhang *et al.* in 2009 (**1.46** and **1.46**, Figure 1.21).[6] The molecular structure of **1** is displayed in Figure 2.2 and selected distances and angles are listed in Table 2.1.

Complex **1** exhibits a three-legged piano stool arrangement around titanium, with a *pseudo*-tetrahedral coordinated sphere and is consistent with the solution NMR data discussed previously. The ligand NMe_2 groups are slightly pyramidalised as quantified by the sum of the C-N-C bond angles (354.6°), the N-Me bonds also deviate from the plane of the C-N π-system as shown by the average dihedral angles of the proximal (8.5°, C(12)-N(2)-C(11)-N(1) and C(14)-N(3)-C(11)-N(1)) and the distal (35.2°, C(13)-N(2)-C(11)-N(1) and C(15)-N(3)-C(11)-N(1)) methyl groups. The pyramidalisation at nitrogen and the slight rotation of the NMe_2 groups away from the π_{CN} plane is a result of sterics and some sp^3 character in the amino nitrogen atoms as a result of the presence of two amino nitrogen atoms adjacent to the π_{CN} system

(discussed in more detail in Section 2.5.2). The reason for the larger deviation of the distal methyl groups from planarity of the π_{CN} system is to minimise the steric clash between both groups. The Ti(1)-N(1)-C(11) bond angle is nearly linear (170.3(3)°) which suggests a pπ-dπ contribution to the metal-ligand bond which is also reflected in the Ti(1)-N(1) (1.782(3) Å), N(1)-C(11) (1.324(5) Å), C(11)-N(2) (1.361(5) Å) and C(11)-N(3) (1.357(5) Å) bond lengths. The Ti(1)-N(1) bond length in **1** is much shorter than the average Ti-amide bond length (1.90(3) Å).[7] This is because guanidinate ligands can act as σ+2π donors rather than amides which are only σ+π donors. The Ti(1)-N(1) bond length is however significantly longer than that found in titanium imides (1.69-1.76 Å).[8, 9] Both ligands can act as σ+2π donors but the bonding is far more efficient in the case of the imide. The Ti(1)-N(1) bond in **1** is only slightly shorter than that found for the amidinate complex **2.4** (1.800(3) Å) but the difference is significant. This shows that the addition of the extra amine donor to the ligand makes a small difference to the Ti-N bond order but not as much as going from amide to a guanidinate or indeed from an amidinate to an imide (discussed further in Section 2.5.2). This small change in bonding is also reflected in the N(1)-C(11) distance in **1** which although slightly longer is the same within error to the equivalent N(1)-C(11) distance in **2.4** (1.310(4) Å). The Ti(1)-Cp_{cent} distances for **1** and **2.4** are both 2.05 Å.

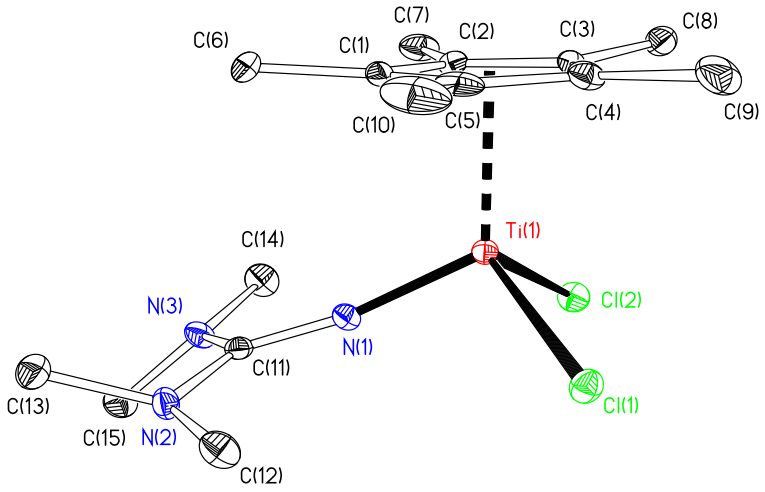

Figure 2.2 Displacement ellipsoid plot (20% probability) of Cp*Ti{$NC(NMe_2)_2$}Cl_2 (**1**). H atoms omitted for clarity.

Table 2.1 Selected bond lengths (Å) and angles (°) for Cp*Ti{NC(NMe$_2$)$_2$}Cl$_2$ (**1**). Cp$_{cent}$ is the computed Cp* ring carbon centroid.

Ti(1)-Cp$_{cent}$	2.05	Cp$_{cent}$-Ti(1)-Cl(1)	114.9
Ti(1)-Cl(1)	2.3181(11)	Cp$_{cent}$-Ti(1)-Cl(2)	114.2
Ti(1)-Cl(2)	2.3149(11)	Cp$_{cent}$-Ti(1)-N(1)	117.5
Ti(1)-N(1)	1.782(3)	Ti(1)-N(1)-C(11)	170.3(3)
N(1)-C(11)	1.324(5)	N(1)-Ti(1)-Cl(1)	102.87(11)
N(2)-C(11)	1.361(5)	N(1)-Ti(1)-Cl(2)	103.45(11)
N(3)-C(11)	1.357(5)	Cl(1)-Ti(1)-Cl(2)	101.91(4)

2.3.3 Synthesis and characterisation of Cp*Ti{NC(N^{i}BuMe)$_2$}Cl$_2$ (2)

To create a larger steric environment around the metal centre whilst maintaining similar electronic properties to the ligand NC(NMe$_2$)$_2$, the guanidinate ligand NC(N^{i}BuMe)$_2$ was utilised. The larger hydrocarbon chain is also useful to increase solubility in organic solvents aiding the study of the cations discussed later in Chapter 3. The titanium complex was again synthesised by lithiation of the protio-ligand (**2.6**) followed by treatment with Cp*TiCl$_3$. Cp*Ti{NC(N^{i}BuMe)$_2$}Cl$_2$ (**2**) was isolated as an orange powder in 82% yield and characterised by NMR spectroscopy, IR spectroscopy, EI mass spectrometry, elemental analysis and X-ray diffraction. The room temperature ^{1}H NMR spectrum is again consistent with a C_s symmetric complex in solution. The NC(N^{i}BuMe)$_2$ resonances consist of a doublet at 2.95 ppm (NC$\underline{H}_2{}^i$Pr), a singlet at 2.42 ppm (N$\underline{Me}$), a multiplet at 1.65 ppm (C$\underline{H}$Me$_2$) and a doublet at 0.81 ppm (CH$\underline{Me}_2$). A single Cp* environment is also present in the spectrum at 2.10 ppm, *cf*. Cp*Ti{NC(NMe)$_2$}Cl$_2$, 2.09 ppm.

2.3.4 Crystal structure of Cp*Ti{NC(N^{i}BuMe)$_2$}Cl$_2$ (2)

Diffraction-quality crystals of **2** were grown from a saturated benzene solution at 4 °C. The molecular structure is displayed in Figure 2.3 and selected distances and angles are listed in Table 2.2.

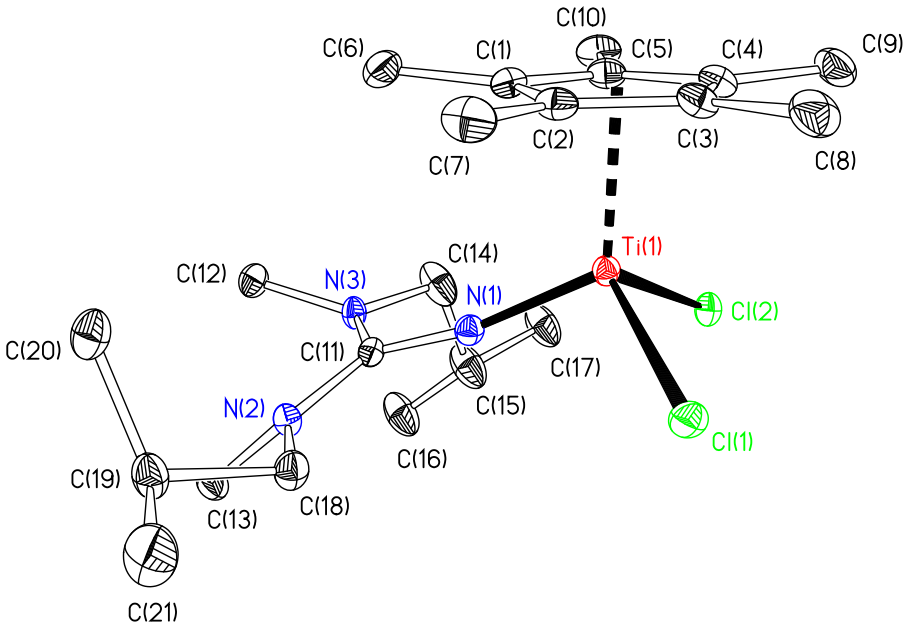

Figure 2.3 Displacement ellipsoid plot (20% probability) of Cp*Ti{NC(N^{i}BuMe)$_2$}Cl$_2$ (**2**). H atoms omitted for clarity.

Table 2.2 Selected bond lengths (Å) and angles (°) for Cp*Ti{NC(N^{i}BuMe)$_2$}Cl$_2$ (**2**). Cp$_{cent}$ is the computed Cp* ring carbon centroid.

Ti(1)-Cp$_{cent}$	2.06	Cp$_{cent}$-Ti(1)-Cl(1)	113.7
Ti(1)-Cl(1)	2.3171(13)	Cp$_{cent}$-Ti(1)-Cl(2)	113.40
Ti(1)-Cl(2)	2.3184(11)	Cp$_{cent}$-Ti(1)-N(1)	119.41
Ti(1)-N(1)	1.781(3)	Ti(1)-N(1)-C(11)	169.3(2)
N(1)-C(11)	1.324(4)	N(1)-Ti(1)-Cl(1)	103.39(9)
N(2)-C(11)	1.345(4)	N(1)-Ti(1)-Cl(2)	101.60(9)
N(3)-C(11)	1.363(4)	Cl(1)-Ti(1)-Cl(2)	103.44(4)

The structure shows a three legged piano stool arrangement around titanium with a *pseudo*-tetrahedral coordination sphere. The two sterically bulky *iso*butyl groups of the guanidinate are pointing away from one another in a proximal position to the metal centre presumably to avoid the steric clash that would occur if they were distal. The natural comparison to be made is between this structure and that of **2**, where the only difference is the introduction of the two bulky *iso*butyl groups on the amine nitrogens rather than methyl groups. The Ti(1)-N(1) bond length is almost identical in **2** (1.781(3) Å) and **1** (1.782(3) Å); this is also true for the N(1)-C(11) distances which are 1.324(4) Å and 1.324(5) Å, respectively. The Ti(1)-N(1)-C(11) angle is nearly linear (169.3(2)°) which, alongside the short Ti(1)-N(1) bond length, is indicative of a pπ-dπ ligand metal interaction. Similar to **1** the NR$_2$ groups are not in the plane of the

π_{CN} system and the effect is more exaggerated for the distal methyl groups; the sum of the NCN angles is 357.6° and the dihedral CNCN angles are 14.5° (proximal) and 32.1° (distal).

2.3.5 Synthesis and characterisation of Cp*Ti{NC(N(Xyl)CH$_2$)$_2$}Cl$_2$ (3)

To allow comparison of the non-cyclic guanidinate compounds **1** and **2** with a well established iminoimidazolidide compound, Cp*Ti{NC(N(Xyl)CH$_2$)$_2$}Cl$_2$ (**3**) was synthesised according to the literature procedure found in a patent by Kretschmer by addition of the lithiated ligand (Li-NC(N(Xyl)CH$_2$)$_2$) to Cp*TiCl$_3$.[10] Complex **3** had previously only been characterised by ^{1}H NMR spectroscopy in $CDCl_3$ and so remaking the compound allowed full characterisation by NMR spectroscopy, IR spectroscopy, EI mass spectrometry and elemental analysis. Complex **3** was also characterised by X-ray crystallography (*vide infra*), and isolated in a yield of 77%. Complex **3** is not only useful for comparison of crystallographical parameters in this Section but will also act as a good comparison for DFT and reactivity studies (Chapters **3** and **4**), *vide infra*. The ^{1}H NMR spectrum displays a single Cp* resonance at 1.85 ppm, a single C$_6$H$_3$Me$_2$ environment at 2.44 ppm and a single NC(N(Xyl)CH$_2$)$_2$ signal at 3.09 ppm. There is also a single C$_6$H$_3$Me$_2$ resonance (7.06 ppm) which is a consequence of rapid rotation about the N-C$_{ipso}$ bond at room temperature. This complex therefore has C_s symmetry in solution on the NMR timescale.

2.3.6 Crystal structure of Cp*Ti{NC(N(Xyl)CH$_2$)$_2$}Cl$_2$ (3)

Diffraction-quality crystals of **3** were grown from a saturated CH_2Cl_2 solution at room temperature. The molecular structure of **3** is displayed in Figure 2.4 and the selected bond length and angles are detailed in Table 2.3.

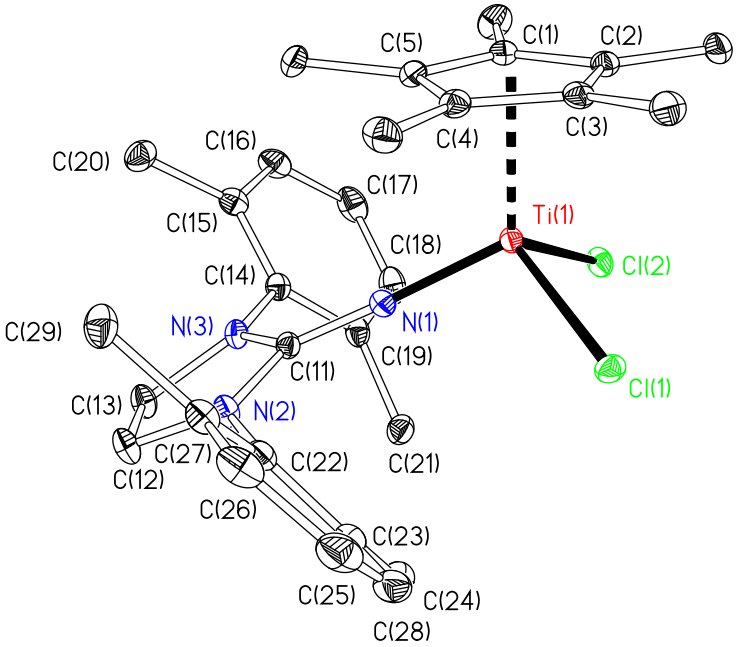

Figure 2.4 Displacement ellipsoid plot (20% probability) of Cp*Ti{NC(N(Xyl)CH)$_2$}Cl$_2$ (**3**). H atoms omitted for clarity.

Table 2.3 Selected bond lengths (Å) and angles (°) for Cp*Ti{NC(N(Xyl)CH$_2$)$_2$}Cl$_2$ (**3**). Cp$_{cent}$ is the computed Cp* ring carbon centroid.

Ti(1)-Cp$_{cent}$	2.05	Cp$_{cent}$-Ti(1)-Cl(1)	114.3
Ti(1)-Cl(1)	2.3091(8)	Cp$_{cent}$-Ti(1)-Cl(2)	114.2
Ti(1)-Cl(2)	2.3280(8)	Cp$_{cent}$-Ti(1)-N(1)	117.6
Ti(1)-N(1)	1.788(2)	Ti(1)-N(1)-C(11)	176.4(2)
N(1)-C(11)	1.302(4)	N(1)-Ti(1)-Cl(1)	104.43(8)
N(2)-C(11)	1.359(4)	N(1)-Ti(1)-Cl(2)	104.15(8)
N(3)-C(11)	1.361(4)	Cl(1)-Ti(1)-Cl(2)	100.16(3)

The molecular structure of **3** is consistent with the solution NMR data discussed beforehand and exhibits a three-legged piano stool arrangement with a *pseudo*-tetrahedral coordinated sphere. The most important bond lengths of **3** (Ti(1)-N(1) = 1.778(2) Å, N(1)-C(11) = 1.302(4) Å, N(2)-C(11) = 1.359(4) Å, N(3)-C(11) = 1.361(4) Å), as determined from crystallography, are similar to the non-cyclic analogues **1** (Ti(1)-N(1) = 1.782(3) Å, N(1)-C(11) = 1.324(5) Å, N(2)-C(11) = 1.361(5) Å, N(3)-C(11) = 1.357(5) Å) and **2** (Ti(1)-N(1) = 1.781(3) Å, N(1)-C(11) = 1.324(4) Å, N(2)-C(11) = 1.363(4) Å, N(3)-C(11) = 1.361(4) Å) showing that linking the distal alkyl groups as well as increasing the steric bulk of the ligand makes little difference to the ligand to metal bonding in this case. There is no difference at all

between the Ti(1)-N(1) bond lengths in **1**, **2** and **3** within error. However, there is a small but significant shortening of the N(1)-C(11) distance going from complexes **1** or **2** to complex **3** which is indicative of less conjugation between the amino nitrogen with the π_{CN} system in **3**. The Ti(1)-N(1)-C(11) angle (176.4(2)°) is also linear, again indicative of a pπ-dπ contribution to the bonding. The previously reported Cp derivative of **3**, $CpTi\{NC(N(Xyl)CH_2)_2\}Cl_2$ (**2.7**), has, within error, identical Ti(1)-N(1) (1.7860(15) Å), N(1)-C(11) (1.308(3) Å), N(2)-C(11) (1.353(3) Å) and N(3)-C(11) (1.362(3) Å) bond lengths.[11] However, joining the ligand's distal R-groups together has significantly decreased the distortion from planarity of the amino groups. The average distal dihedral is now 5.0° and proximal dihedral 5.4° compared to 35.2° and 8.5° in **1**.

2.4 Alkylation of dichloride compounds

The alkyl abstraction agent TBF_{20} ($[Ph_3C][B(C_6F_5)_4]$) was used to activate the dialkyl precatalysts (*vide infra*) requiring alkylation of the chloride complexes **1**, **2** and **3**. This was achieved by the treatment of the corresponding dichloride complex with the appropriate alkyl lithium reagent. The dialkyl complexes were also subsequently used for polymerisation testing by Lanxess Elastomers, see Section 4.4. In all cases the complexes have been dimethylated other than **1** which was both dimethylated and dibenzylated (*vide infra*); dibenzylation of **1** allowed access to certain aspects of chemistry for this particular complex which are described in Chapters 3 and 4.

2.4.1 Synthesis and characterisation of $Cp^*Ti\{NC(NMe_2)_2\}R_2$ (R = Me (4) or Bn (5))

The dialkyl compounds $Cp^*Ti\{NC(NMe_2)_2\}Me_2$ (**4**) and $Cp^*Ti\{NC(NMe_2)_2\}Bn_2$ (**5**) were prepared by the reaction of **1** with 2 equivs of MeLi or BnMgCl, respectively. The former was isolated as a yellow crystalline solid in 79% yield and the latter as an orange solid in 40% yield. Both complexes were characterised by NMR spectroscopy, IR spectroscopy, EI-mass spectrometry and elemental analysis.

The ^1H NMR spectrum of **4** is analogous to that of **1** with the exception of an additional singlet for the two titanium-methyl groups. The Cp*, NMe_2 and Ti-Me resonances are observed at 1.98, 2.47 and 0.52 ppm, respectively. As in **1** there is fast rotation about the N-C(sp^2) as evidenced by a single N$\underline{Me}_2$ resonance. Compound **5** also has an equivalent spectrum to **1**, but this time with the addition of the benzyl

methylene protons as doublets at 2.38 and 1.99 ppm (^2J = 10.2 Hz) and the corresponding aromatic signals. The reason that the CH_2 resonances appear as doublets in **5** is because they are diastereotopic.

2.4.2 Crystal structure of Cp*Ti{NC(NMe$_2$)$_2$}Bn$_2$ (5)

Diffraction-quality crystals of **5** were grown from a saturated pentane solution at 0 °C. The molecular structure is displayed in Figure 2.5 and is consistent with NMR data; selected bond lengths and angles are detailed in Table 2.4. The Ti(1)-N(1) bond in **5** is longer than **1** (1.8077(18) Å *vs.* 1.782(3) Å) because the benzyl groups act as better donors than chloride. This also manifests itself in an decreased N(1)-C(11) bond length from 1.324(5) Å (**1**) to 1.298(3) Å (**5**). Since the benzyl ligands are better donors the N→Ti donation is lower which results in reduced Me_2N→CN(π*) donation and thus a shorter N(1)-C(11) bond. The ligand based NMe_2 groups are rotated and slightly pyramidalised just as in **1**.

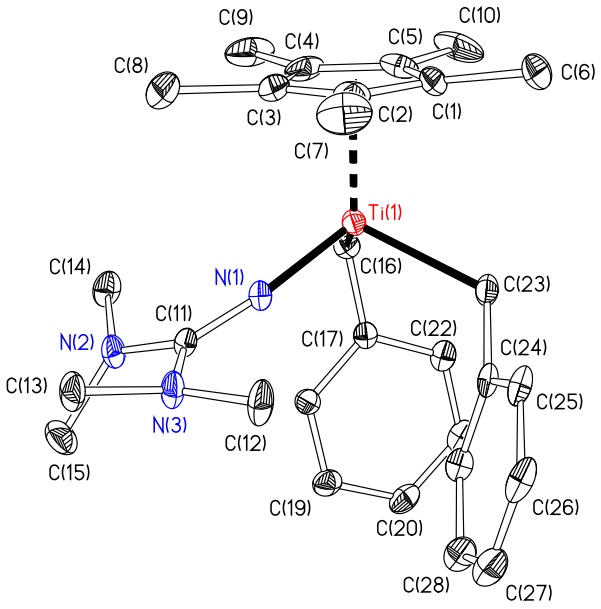

Figure 2.5 Displacement ellipsoid plot (20% probability) of Cp*Ti{NC(NMe$_2$)$_2$}Bn$_2$ (**5**). H atoms omitted for clarity.

Table 2.4 Selected bond lengths (Å) and angles (°) for Cp*Ti{NC(NMe$_2$)$_2$}Bn$_2$ (**5**) Cp$_{cent}$ is the computed Cp* ring carbon centroid.

Ti(1)-Cp$_{cent}$	2.11	Cp$_{cent}$-Ti(1)-C(16)	114.6
Ti(1)-C(16)	2.178(2)	Cp$_{cent}$-Ti(1)-C(23)	113.2
Ti(1)-C(23)	2.177(2)	Cp$_{cent}$-Ti(1)-N(1)	118.1
Ti(1)-N(1)	1.8077(18)	Ti(1)-N(1)-C(11)	174.07(16)
N(1)-C(11)	1.298(3)	N(1)-Ti(1)-C(16)	100.42(9)
N(2)-C(11)	1.369(3)	N(1)-Ti(1)-C(23)	108.63(9)
N(3)-C(11)	1.367(3)	C(16)-Ti(1)-C(23)	99.79(9)

2.4.3 Synthesis and characterisation of Cp*Ti{NC(N^{i}BuMe)$_2$}Me$_2$ (6)

The reaction of **2** with two equivs of MeLi gave Cp*Ti{NC(N^{i}BuMe)$_2$}Me$_2$ (**6**), isolated as a yellow solid in 76% yield. Complex **6** was characterised by NMR spectroscopy, IR spectroscopy and elemental analysis. The ^{1}H NMR spectrum of complex **6** contains resonances for NCH$_2$ (2.95 ppm), NMe (2.54 ppm), Cp* (2.00 ppm), C<u>H</u>Me$_2$ (1.73 ppm), CHMe$_2$ (0.85 ppm) and TiMe (0.45 ppm) which are consistent with C_s symmetry in solution.

2.4.4 Synthesis and characterisation of Cp*Ti{NC(N(Xyl)CH$_2$)$_2$}Me$_2$ (7)

The reaction of **3** with two equivs of MeLi gave Cp*Ti{NC(N(Xyl)CH$_2$)$_2$}Me$_2$ (**7**), isolated as an off-white solid in 64% yield. Complex **7** was characterised by NMR spectroscopy, IR spectroscopy and elemental analysis. Spectral features in the ^{1}H NMR spectrum are, as expected, akin to **3** with the addition of a singlet methyl resonance. The chemical shifts of C$_6$<u>H</u>$_3$Me$_2$, CH$_2$, C$_6$H$_3$<u>Me</u>$_2$, Cp* and Ti-Me are located at 6.98, 3.26, 2.47, 1.74 and 0.00 ppm, respectively and are consistent with a C_s symmetrical structure in solution.

2.4.5 Crystal structure of Cp*Ti{NC(N(Xyl)CH$_2$)$_2$}Me$_2$ (7)

Diffraction-quality crystals of **7** were grown from a saturated pentane solution at -30 °C. The molecular structure of **7** is displayed in Figure 2.6 and selected bond lengths and angles are listed in Table 2.5.

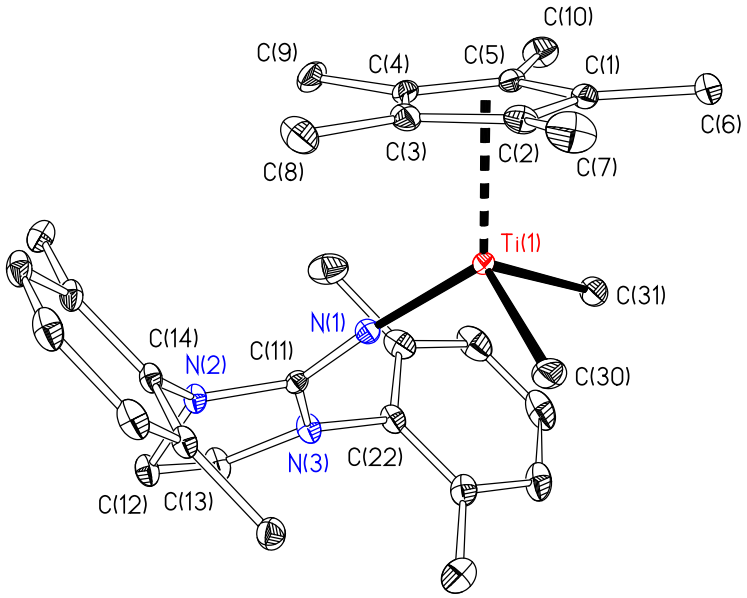

Figure 2.6 Displacement ellipsoid plot (20% probability) of Cp*Ti{NC(N(Xyl)CH_2)$_2$}Me_2 (**7**). H atoms omitted for clarity.

Table 2.5 Selected bond lengths (Å) and angles (°) for Cp*Ti{NC(N(Xyl)CH_2)$_2$}Me_2 (**7**). Cp_{cent} is the computed Cp* ring carbon centroid.

Ti(1)-Cp_{cent}	2.07	Cp_{cent}-Ti(1)-C(30)	112.5
Ti(1)-C(30)	2.1186(11)	Cp_{cent}-Ti(1)-C(31)	111.5
Ti(1)-C(31)	2.1307(10)	Cp_{cent}-Ti(1)-N(1)	124.3
Ti(1)-N(1)	1.8335(8)	Ti(1)-N(1)-C(11)	174.27(7)
N(1)-C(11)	1.2813(13)	N(1)-Ti(1)-C(30)	104.31(4)
N(2)-C(11)	1.3745(12)	N(1)-Ti(1)-C(31)	102.34(4)
N(3)-C(11)	1.3743(11)	C(30)-Ti(1)-C(31)	98.46(5)

The molecular structure of **7** shows the expected *pseudo*-tetrahedral coordination around the titanium centre similar to those discussed previously. The complex also has approximate C_s symmetry which is consistent with NMR data. The nearly linear Ti(1)-N(1)-C(11) bond angle of 174.27(7)°, as discussed previously, is indicative of a pπ-dπ contribution to the bonding. The ligand shows, in a similar fashion to **3**, a reasonably planar arrangement of the NR_2 groups to the π_{CN} system with a summed CNC angle of 357.3°. The average dihedral angles of the distal and proximal R-groups are also close to 0° (7.8° and 9.8°). The Ti(1)-N(1) bond length in **7** is significantly longer than in its dichloride analogue **3** (1.8335(8) Å *vs.* 1.788(2) Å) which is due to the increased electron donation from the methyl groups as compared to chloride. This

is consistent with a decrease in N(1)-C(11) distance going from **3** to **7** (1.302(4) to 1.2813(13) Å).

2.5 DFT calculations

DFT calculations have been performed by the author at the University of Oxford using ADF 2013[12-15] in order to understand the bonding and electronic structure of various κ^1-bound N-donor ligands. This Section aims to probe the differences and similarities in the bonding of a number of metallocene and post-metallocene titanium complexes. The DFT method and basis set used for this study were BP86 and TZ2P, respectively, chosen as a proven method for the analysis of Ti-N bonding.[16] This Section begins by looking at the frontier molecular orbitals of dicationic molecules of the type $[L_2Ti]^{2+}$ and then moves onto further analysis to establish the nature of the Ti-N bonding in a variety of titanium complexes.

2.5.1 Frontier molecular orbitals of dications $[Cp^*Ti(L)]^{2+}$

The isolobal analogy can be a useful tool used in the design of post-metallocene complexes as previously discussed in this Thesis. This provided incentive to computationally investigate the effect of different ligands, which are considered to be isolobal, on the electronic structure of the rest of the complex. The calculations in these Sections were performed on a series of half-sandwich dications of the type $[Cp^*(L)Ti]^{2+}$ where L is a monoanionic $\sigma+n\pi$ donor (n = 1 or 2, Figure 2.7). L was varied to investigate a range of different electron donors either directly relevant to supporting ligands synthesised in this Thesis (**III**) or as benchmark compounds (**I**, **II**, **IV**, **V**, **VI**). Ligands **I**-**IV** were selected as κ^1-imide-related donors with the potential to form a $\sigma+2\pi$ interaction with the metal whereas NMe_2 (**V**) was selected as an example of a κ^1-bound nitrogen $\sigma+1\pi$ donor; Cp was also included as an example of a conventional carbon based $\sigma+2\pi$ donor ligand.[17-21]

The dimethyl compounds were initially optimised to give the lowest energy structures. Although there are no corresponding crystal structures to compare to $Cp^*Ti(L^{I\text{-}VI})Me_2$ the structure of $Cp^*Ti\{NC(N^iPr_2)Ph\}Me_2$ (**2.4Q**, i.e. $Cp^*Ti(L^{XIII})Me_2$) was calculated for analysis in Section 2.5.2.4 and showed good agreement to the crystallographically determined bonding parameters[2] for example: Ti(1)-N(1) 1.8452(15) Å (DFT, 1.87 Å), N(1)-C(11) 1.290(2) Å (DFT, 1.29 Å), C(11)-N(2) 1.363(2) (DFT, 1.38 Å), Ti(1)-C(24) 2.1227(18) Å (DFT, 2.14 Å) and Ti(1)-C(24) 2.1326(19) Å (DFT, 2.15 Å). It is

also shown in Section 2.5.2.5 that this DFT method well describes the trends in the Ti-N bond lengths when compared to the X-ray structures of relevant dichloride compounds.

Following this optimisation the methyl groups were removed and the electronic structures of the remaining dicationic fragments were recalculated using a single point energy calculation (no geometry optimisation). This method allowed the frontier orbitals of the fragments to be calculated with the ligands in the same position as they would be in the neutral compounds. For this analysis the important orbitals to consider are the three lowest unoccupied molecular orbitals (LUMO, LUMO+1, LUMO+2) which are displayed for L = **I**, **III**, **IV** and **IV** in Figure 2.8. The energies of these orbitals are shown in Table 2.6.

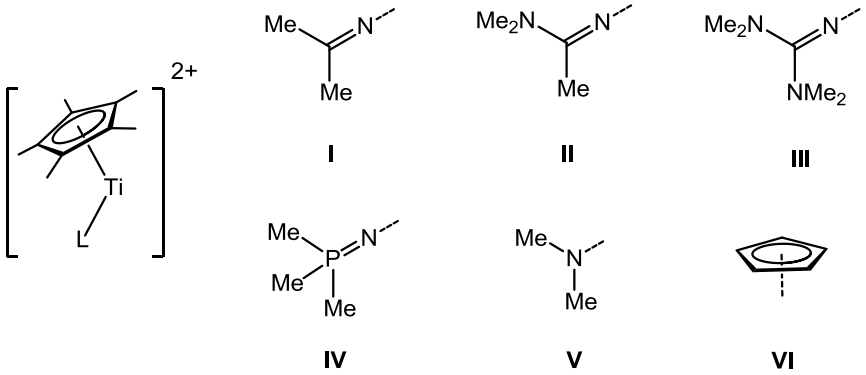

Figure 2.7 Supporting ligands, L, used in the DFT study of the bonding in titanium complexes supported by κ^1-bound N-donor ligands.

Since all the structures were formed by removing two methyl ligands from a minimised tetrahedral structure the remaining dications have a 'bent' arrangement equivalent to the C_{2v} $[Cp_2Ti]^{2+}$ dication calculated using EHT (Extended Hückel Thoery) by Lauher and Hoffman in 1975.[18] The non-linear arrangement of the two cyclopentadienyl ligands around the metal centre causes the formation of three frontier orbitals which are directed mainly in the *yz* plane (coordinate system displayed in Figure 2.8). These are the orbitals which are the most important in the coordination of further ligands and are similar to those calculated by EHT (Extended Hückel Theory)[18] and DFT[17, 22] for $[Cp_2Ti]^{2+}$. They are also analogous to the orbitals calculated by Eric Clot for the isolobal imido dication $[Ti(N^tBu)(Me_3[9]aneN_3)]^{2+}$.[22]

The LUMO+1 of $[Cp_2Ti]^{2+}$ is primarily made up of $3d_{yz}$ and the LUMO and LUMO+2 are made up of contributions from $3p_z$, $3d_{z^2-y^2}$ and $3d_{z^2}$.[18] The LUMO is strongly

directed along the *y*-axis and is best described as a $3d_{y^2}$ orbital, made largely up of $3d_{z^2-y^2}$. The higher energy LUMO+2, which is polarised along the z-axis, is made up from contributions of $3p_z$, $3d_{z^2}$ and $3d_{z^2-x^2}$. Although the LUMO, LUMO+1 and LUMO+2 are all spatially similar to each other across the different compounds, there are differences in the energies of the orbitals (Table 2.6). The average energies of the LUMO, LUMO+1 and LUMO+2 for **I**, **V** and **VI** are all reasonably similar to one another. However, the average orbital energy for the κ^1-bound iminato type ligands **II**, **III** and **IV** are all found approximately 1 eV higher. This is most likely a consequence of the ability of these ligands to act as better donors than the other systems (see Section 2.5.2).

This change in electronics means that complexes containing ligands similar to **II**, **III** and **IV** such as those reported earlier in this Chapter are more stable to reduction than complexes containing ligands **I**, **V** and **VI**. This is important since alkyl aluminium species present during the polymerisation process have the potential to reduce the active species.[23-25] A higher tolerance to reduction by alkyl aluminium species also means that polymerisations can be run at higher temperature which is important in the production of EPDM in this case which is made in solution at 90 °C, but also in general commercial polyolefin production where typically polymerisation temperatures range between 70 and 160 °C.[26]

Table 2.6 Energies (eV) of the three lowest unoccupied molecular orbitals for dications $[Cp^*Ti(L)]^{2+}$, L= $NCMe_2$ (**I**), $NC(NMe_2)Me$ (**II**), $NC(NMe_2)_2$, (**III**), $NPMe_3$ (**IV**), NMe_2 (**V**) and Cp (**VI**).

Ligand	**I**	**II**	**III**	**IV**	**V**	**VI**
LUMO+2	-11.5	-10.8	-10.6	-10.7	-11.3	-11.3
LUMO+1	-11.6	-11.2	-11.1	-11.4	-12.5	-12.3
LUMO	-12.0	-11.5	-11.4	-11.6	-12.7	-12.5
Average	-11.7	-11.2	-11.0	-11.2	-12.2	-12.0

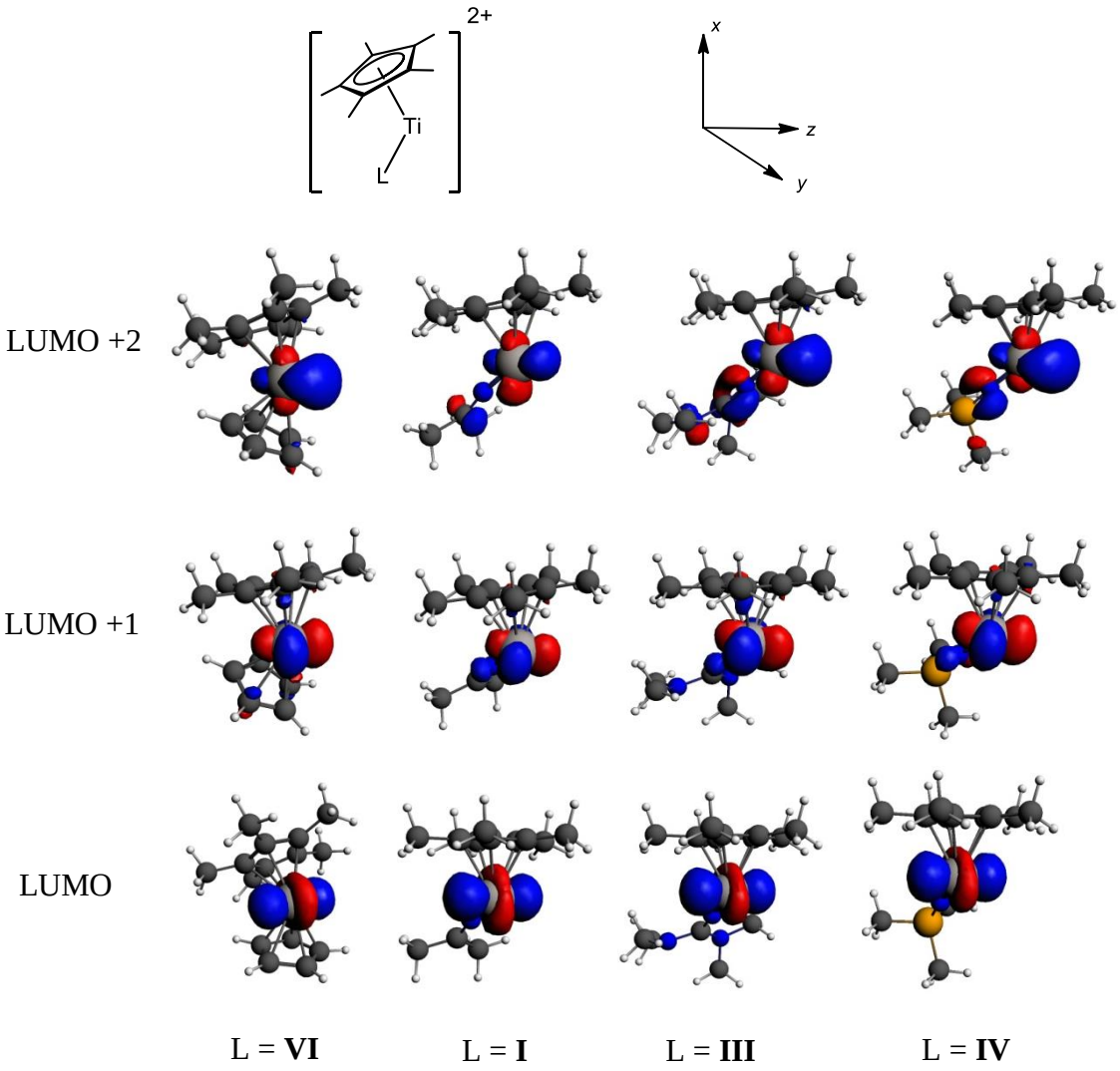

Figure 2.8 Isosurfaces of the three lowest unoccupied molecules orbitals for $[Cp^*CpTi]^{2+}$ (L = **VI**), $[Cp^*Ti(NCMe_2)]^{2+}$ (L = **I**), $[Cp^*Ti\{NC(NMe_2)_2\}]^{2+}$ (L =**III**) and $[Cp^*Ti(NPMe_3)]^{2+}$ (L = **IV**) (left to right).

2.5.2 Ti-N in bonding in κ^1-bound N-donor ligands

This Section discusses DFT investigations that have been carried out by the author in order to investigate the nature of the Ti-N bonding in a range of titanium complexes. The previous Section focused on the effect of the ligand on the metal centre orbital energies. This Section focuses on the nature of the Ti-N bond itself. The goal of this study is to investigate the nature of the metal-ligand bonding, and to what extent the ligands act as efficient electron donors to the metal centre. This involves looking at the varying degrees of σ- and π-bonding between the ligand and the metal. For example a σ+2π bonding interaction can yield in theory a maximum donation of 2σ and 4π electrons but in reality the actually figure is significantly less than this and depends on

the ligand involved. The varying extents of electron donation of σ+2π ligands has been demonstrated in previous DFT studies on imido complexes by Mountford, Green *et al*. This study showed that the σ+2π imido ligands in $Ti(NR)\{HC(pz)_3\}Cl_2$ (pz = pyrazolyl; R = Me, Ph) have quite different electron donating abilities. For example the methylimido ligand donates 0.41 σ-electrons and 1.34 π-electrons whereas the phenylimido ligand, as expected, donates significantly fewer electrons to the metal centre (σ, 0.26; π, 1.19).[16] In the author's investigation of Ti-N bonding, real systems have been studied as well as a series of model compounds. The compounds containing ligands **I**-**XII** allowed a systematic comparison of Ti-N bonding in molecules in which the ligand has methodically changing steric and electronic properties; the ligands used for this study are those used in Section 2.5.1, Figure 2.7 as well as additional systems (**VII**-**XII**) shown in Figure 2.9.

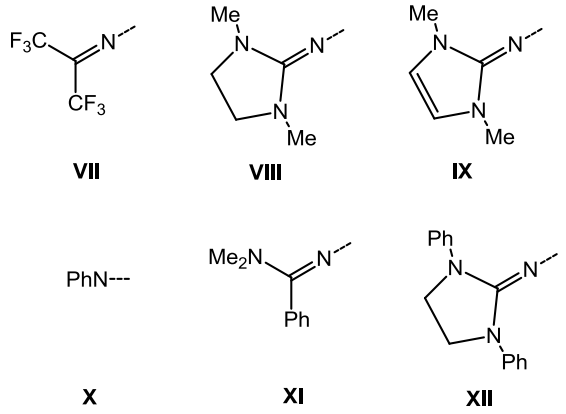

Figure 2.9 Additional ligands (**VII**-**XI**) used in the DFT study of Ti-N bonding.

The DFT calculations were carried out at the GGA:BP86/TZ2P level in ADF 2013 as a proven method for the analysis of Ti-N bonding.[16] Fragment analysis, the Mulliken populations of orbitals, overlap populations, bonding energies and Mayer bond orders[27] were utilised in order to understand the bonding between titanium and nitrogen. During fragment analyses the ligands, L, were treated as monoanionic and the $[Cp^*TiMe_2]^+$ fragments as monocationic (Ti(+4), d^0). Fragment analysis requires closed-shell fragments. This also stops problems with α and β spins during analysis. The complexes were analysed in two different geometries, the first is fully optimised whereas the second is to optimise all the atoms around a constrained Ti-N bond. The Ti-N bond in the latter case was constrained to the average Ti-N bond length of the fully optimised complexes (1.860 Å). Fixing the bond length in this way avoids any overlap/bonding variations that may occur due to the changing of the Ti-N distance.

The bonding parameters determined by DFT for all complexes can be found in Table 2.7 for systems with a constrained Ti-N bond length and Table 2.8 for systems with no constraints.

As a starting point for this analysis it is pertinent to discuss the fragment molecular orbital interaction diagram for the ketimide complex $Cp^*Ti(L^I)Me_2$ (Figure 2.12). This is formed by the combination of fragments $[NCMe_2]^-$ (**I**$^-$) and $[Cp^*TiMe_2]^+$. In the approximate C_s symmetry of the complex the principal frontier orbital bonding contributions from the ligand consist of σ (1a′), π_v (2a′), π_h (1a″) and π_v^* (3a′) (Figure 2.10). The π_v orbital is N-C π-bonding in nature whereas π_h is essentially a nitrogen based lone pair. Since π_v (HOMO-1, -0.60 eV) contains a bonding π_{CN} interaction it is lower in energy than π_h (HOMO, 2.58 eV). The lowest in energy of these frontier orbitals is, as expected, the σ orbital (HOMO-2, -1.08 eV). The π_v^* (LUMO) contains an antibonding π_{CN} interaction and so is the highest in energy of these frontier orbitals.

The structure of the $[CpTiMe_2]^+$ fragment has approximate C_s symmetry. This means there are four titanium-based orbitals frontier molecular orbitals (1a′, 2a′, 3a′ and 1a″) which are available for bonding with another ligand. Since the $[CpTiMe_2]^+$ fragment is cationic, i.e. Ti d^0, these orbitals are unoccupied.

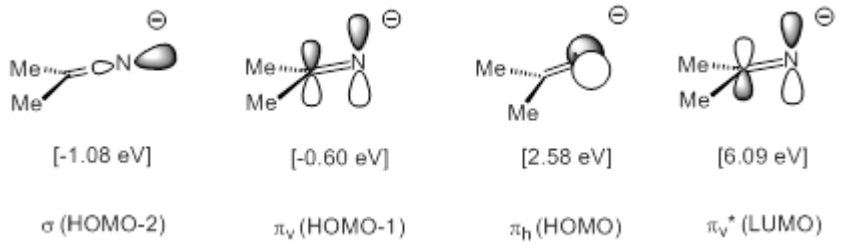

Figure 2.10 LUMO, HOMO, HOMO-1 and HOMO-2 for $[NCMe_2]^-$ (**I**$^-$).

The fragment orbital interaction diagram with ligand anion **I**$^-$ (Figure 2.12) shows the principal interactions when the anionic ligand and cationic titanium fragments are brought together. The main interactions involve the 1a′, 2a′, 3a′ and 1a″ on each fragment and the frontier molecular orbitals of the complex can be seen in Figure 2.11. The 1a′ MO of the complex is the principal σ-bonding interaction between the ligand and metal formed from the corresponding symmetry orbitals on the fragments. As well as the contribution of ligand fragment molecular orbital 1a′ to complex orbital 1a′ there is also some orbital mixing contribution from a lower energy ligand based σ-orbital, although not shown in Figure 2.10 this can be seen in the appearance of some CH

contribution in the 1a′ MO in Figure 2.11. MOs 2a′, 1a″ and 3a′ represent the principal π-interactions between ligand and metal. The 2a′ MO of complex involves the π_v(2a′) of the ligand (Figure 2.11) and the 1a′ of the metal based fragment**.** Both of these fragment orbitals also contribute to MO 3a′ although primarily this MO consists of the $[Cp^*TiMe_2]^+$ 3a′ orbital and ligand π_v^* (3a′). This π-back-bonding keeps 3a′ lower than expected giving two low energy d-type MOs whereas only one would be expected for a σ+2π imido-type ligand.

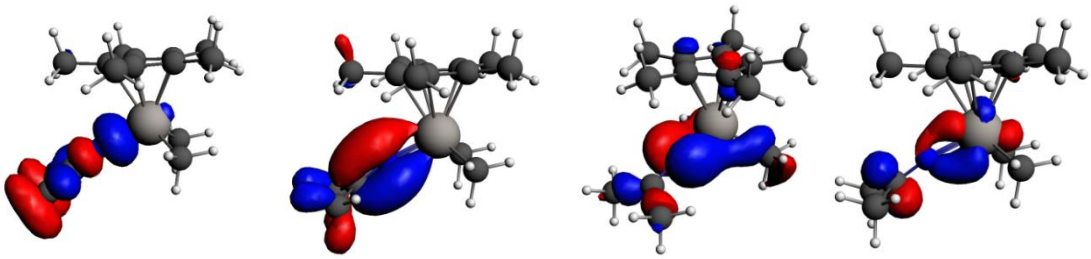

1a′	**2a′**	**1a″**	**3a′**
[-9.09 eV]	[-7.31 eV]	[-4.91 eV]	[-2.26 eV]

Figure 2.11 Principal frontier MOs of $Cp^*Ti(NCMe_2)Me_2$ (L = **I**)

The 1a″ complex MO constitutes the other metal-ligand π-interaction which is orthogonal to complex orbital 2a′. The $[Cp^*TiMe_2]^+$ 2a′ fragment orbital has approximate δ-symmetry with respect to the Ti-N vector and so does not interact significantly with the ligand. As such it remains non-bonding. Overall the bonding mode of the ligand to the metal centre is σ+2π by inspection of the MOs, consistent with expectations.

In order to gain a quantitative understanding of the bonding between the ligand and the metal, the Mulliken orbital population of the frontier orbitals on the ligand were examined using fragment analysis (Table 2.7 and Table 2.8). This type of analysis gives information of the formal donation efficiency of the ligand σ- and π-orbitals. When the ligand is not interacting with the metal 2 electrons can be assigned to each orbital and then when the two fragments are brought together the number of those electrons remaining on the ligand based orbitals indicates how many have been donated to the metal. For example if the Mulliken population of a ligand based orbital in the complex is 1.70 then 0.30 electrons have been formally donated by this orbital to the metal. The number of electrons that have been donated by each ligand frontier orbital (2 - orbital Mulliken population) is the quantity of interest for the following discussion.

With $\mathbf{I}^-$ (constrained Ti-N bond length) the number of electrons formally donated by the σ-orbital is 0.33, for π_v is 0.11 and for π_h is 0.48. The number of electrons donated by the π_h is higher than π_v. In order to confirm that this is primarily as a result of the donating ability of the ligand rather than the accepting properties of the metal based d-orbitals, an amide ligand ($[NMe_2]^-$, $\mathbf{V}^-$) was utilised as a probe. $[NMe_2]^-$ has only a single p-orbital that can act as a π-donor to the metal. When the complex is optimised with a fixed Ti-N bond length (1.860 Å) the π_v orbital donates 0.44 electrons to the metal (similar to π_h in $\mathbf{I}^-$) and when the ligand is rotated by 90° ($\mathbf{Vb}^-$), effectively the same number of π-electrons (0.43) are donated. This shows that in $Cp^*Ti(L^I)Me_2$ the reason for the difference in electron donation between π_v and π_h is due to a difference in the donor and not the acceptor orbitals; since S (the orbital overlap) will be approximately the same for the different ligands the difference is due to the energy difference between the interacting orbitals ($E_{stab} \propto -S^2/\Delta E$). Since π_v is lower in energy than π_h it has a poorer energy match and so less good interaction with the higher energy metal based orbitals; this results in a poorer electron donation from π_v.

This effect can be further illustrated by investigation of the hypothetical $[NC(CF_3)_2]^-$ ($\mathbf{VII}^-$) which is analogous to $\mathbf{I}^-$ but with the replacement of the methyl hydrogens with fluorine atoms. This decreases the energy of the surrounding orbitals due to their higher electronegativity. Compared to the non-fluorinated analogue ($\mathbf{I}^-$) π_v has decreased from -0.60 eV to -2.57 eV and the π_h from 2.58 to 1.09 eV. Since the CF_3 groups are bonded to CN which has a p-orbital which contributes to π_v but not π_h, π_v is effected more by the presence of the fluorine atoms. Accordingly the fluorine orbitals have a higher percentage contribution to π_v than π_h. The electron donation has also decreased in π_v from 0.11 to 0.07 and π_h from 0.48 to 0.32. This illustrates the effect of ligand frontier orbital energy on its donation ability. It also shows that although this ligand binds in a σ+2π mode there is a large difference between the donation ability of the two π-orbitals. This shows the importance of not only determining the σ+nπ (n = 1 or 2) binding mode but also the number of electrons that can be donated from these orbitals to the metal centre.

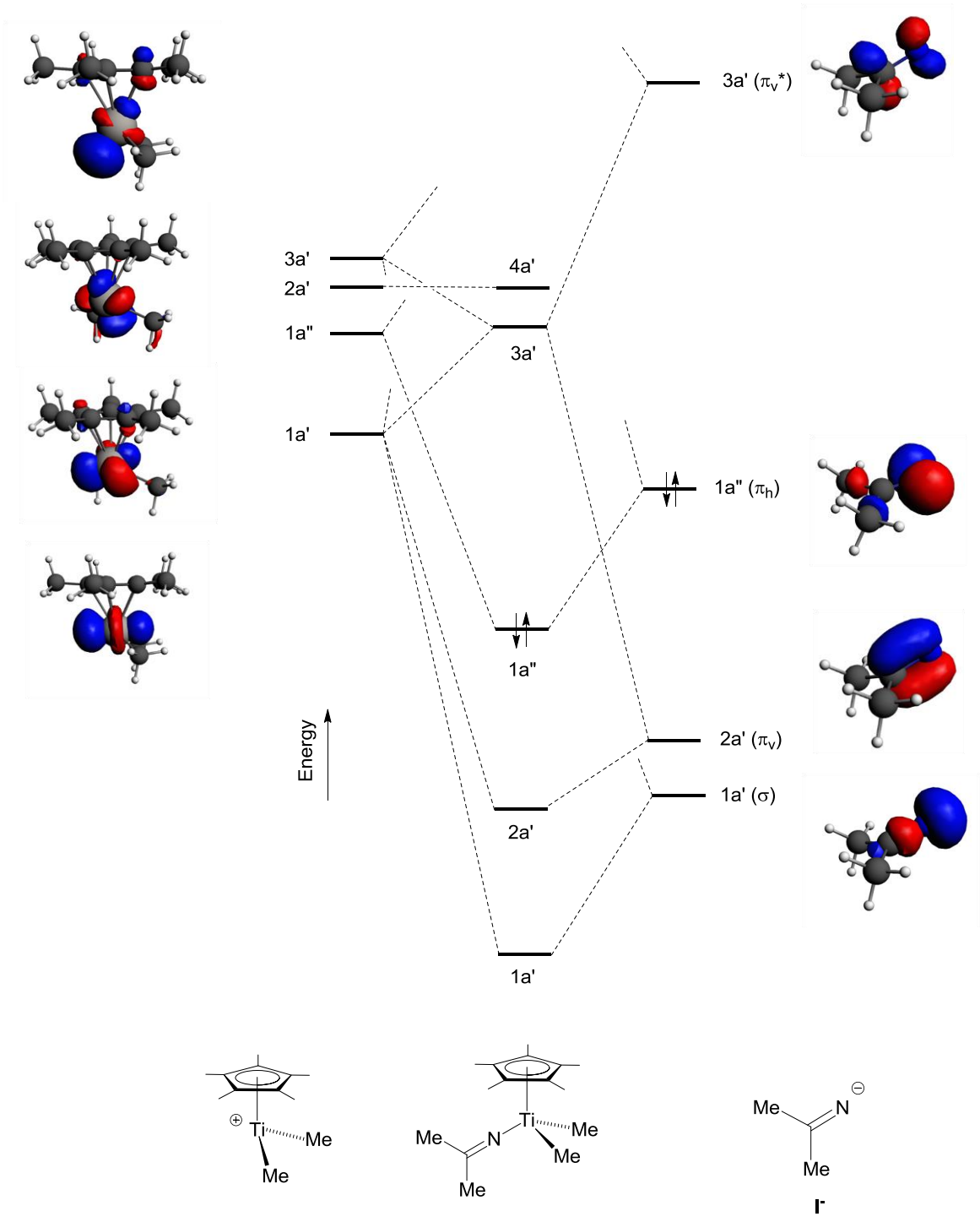

Figure 2.12 Fragment orbital interaction diagram for Cp*Ti(NCMe$_2$)Me$_2$ (L = **I**) constructed from charged fragments **I**$^-$ and [Cp*TiMe$_2$]$^+$, with Mulliken symbols appropriate for the approximate C_s symmetry of the complex.

Table 2.7 Extent of ligand σ- and π- donation for anionic ligands (electrons), Ti-N Mulliken overlap populations, Mayer bond order and ligand orbital energies (eV) for Cp*Ti(L)Me_2 where L = **I**, **II**, **III**, **IIIa**, **IIIb**, **IV**, **V**, **Vb**, **VII**, **VIII**, **IX**, **XI** and **XII** and the Ti-N bond length is fixed to 1.860 Å.

Ligand	σ-donation	π_h-donation	π_v-donation	Total π-donation	Ti-N overlap population	Mayer bond order	Ligand anion orbital energies /eV			
							π_h	π_v	σ_1	σ_2
I	0.34	0.48	0.11	0.59	0.29	1.11	2.58	-0.60	-1.08	-
II	0.33	0.44	0.22	0.66	0.30	1.15	2.45	0.97	-0.96	-
III	0.33	0.40	0.25	0.65	0.30	1.14	2.47	0.89	-1.18	-0.16
IIIa	0.33	0.38	0.31	0.69	0.32	1.20	2.50	1.50	-0.79	-
IIIb	0.36	0.47	0.11	0.58	0.31	1.11	2.60	-1.00	-1.76	0.06
IV	0.38	0.31	0.31	0.62	0.33	1.19	1.76	1.74	-0.22	-
V	0.35	-	0.44	0.44	0.26	1.04	-	2.97	1.30	-
Vb	0.35	-	0.43	0.43	0.25	1.00	-	2.97	1.30	-
VII	0.33	0.32	0.07	0.39	0.25	0.94	1.09	-2.57	-2.42	-
VIII	0.33	0.38	0.27	0.65	0.30	1.14	2.24	1.15	-0.92	-
IX	0.32	0.35	0.33	0.68	0.30	1.15	2.12	1.71	-0.96	-
XI	0.33	0.46	0.21	0.67	0.29	1.10	1.58	0.09	-1.64	-2.11
XII	0.28	0.37	0.26	0.63	0.25	1.03	0.98	-0.27	-2.23	-

Table 2.8 Extent of ligand σ- and π- donation for anionic ligands (electrons), Ti-N Mulliken overlap populations, Mayer bond order and ligand orbital energies (eV) for Cp*Ti(L)Me_2 where L = **I**, **II**, **III**, **IV**, **V**, **VIII**, **IX**, **X**, **XI** and **XII** and the Ti-N bond in the structures are not constrained.

Ligand	σ-donation	π_h-donation	π_v-donation	Total π-donation	Ti-N overlap population	Mayer bond order	Calculated Ti-N bond length/ Å
I	0.33	0.48	0.11	0.59	0.28	1.08	1.881
II	0.33	0.45	0.22	0.67	0.30	1.15	1.854
III	0.34	0.40	0.25	0.65	0.30	1.15	1.852
IV	0.38	0.31	0.31	0.62	0.33	1.20	1.848
V	0.34	-	0.42	0.42	0.26	1.01	1.926
VIII	0.33	0.38	0.27	0.65	0.30	1.15	1.850
IX	0.33	0.35	0.33	0.68	0.30	1.14	1.842
X	0.38	0.63	0.51	1.14	0.41	1.61	1.742
XI	0.33	0.46	0.21	0.67	0.28	1.10	1.862
XII	0.27	0.36	0.26	0.62	0.25	1.01	1.881

2.5.2.1 Comparison of the bonding of $[Cp^*TiMe_2]^+$ with anionic ligands $\mathbf{I}^-$, $\mathbf{II}^-$ and $\mathbf{III}^-$

Since the bonding in the ketimide complex is now understood the effect of adding one or two amino nitrogen donors can be discussed (forming amidinates and guanidinates, respectively). Analysis of the bonding between the ketimide ($\mathbf{I}^-$), amidinate ($\mathbf{II}^-$) and guanidinate ($\mathbf{III}^-$) ligands with $[Cp^*TiMe_2]^+$ reveals the differences between their donation abilities. Initially the fixed bond length (Ti-N = 1.860 Å) series will be discussed (Table 2.7).

As one examines this series of ligands there is little to no change in amount of σ-donation from the ligand to the metal centre (range 0.33-0.34 electrons). If the π-bonding is examined, however, there are noticeable variations in the donating ability of the ligand depending on the number of additional amino nitrogen donor atoms contained within it. In all cases π_h donates more electrons than π_v, *vide supra*. Going from ketimide $\mathbf{I}^-$ to the amidinate $\mathbf{II}^-$ the total amount of π-donation has increased from 0.59 to 0.67 electrons. The average energy of the π-donor orbitals for $\mathbf{I}^-$ is 0.99 eV and for $\mathbf{II}^-$ is 1.71 eV; the higher energy in $\mathbf{II}^-$ results in a better energy match with the metal d-orbitals, as mentioned previously, and hence a stronger π-bonding contribution from the amidinate ligand compared to the ketimide. The contribution of π_v is higher in $\mathbf{II}^-$ than $\mathbf{I}^-$ but the reverse is true for π_h. π_v has a higher energy in $\mathbf{II}^-$ than $\mathbf{I}^-$ and this is because of the presence of an antibonding interaction of the π_{CN} with the amino nitrogen 2p AO (Figure 2.13). This out of phase interaction explains in molecular orbital terms why the addition of amino nitrogen donors can increase π-bonding between metal and ligand.

π_h is lower in energy in the amidinate than the ketimide (and hence a poorer π-donor). This difference is due to the presence of the amino nitrogen in the amidinate rather than the carbon in the ketimide; the increased electronegativity of the amino nitrogen atom compared to carbon lowers the energy of π_h through inductive effects and thus its donating ability. The overall increase in π-bonding ability of the amidinate ligand leads to an increase in the Ti-N bond order. This bond order can be measured in a variety of ways using parameters such as the Mayer bond orders[27] and the Ti-N Mulliken atomic overlap populations. Both of these measures of bond order increase on going from **I** to **II**. The Mayer bond order increases from 1.11 to 1.15 and the overlap population increases from 0.29 to 0.30. In the fully optimised structures almost identical

parameters are determined, and accordingly, since the Ti-N bond is allowed to relax, the increased donation ability of the ligand is mirrored in the shorter Ti-N bond with **II** compared to **I** (1.854 Å *vs.* 1.881 Å). This MO analysis matches what would be expected from analysis of the bonding using resonance arguments.

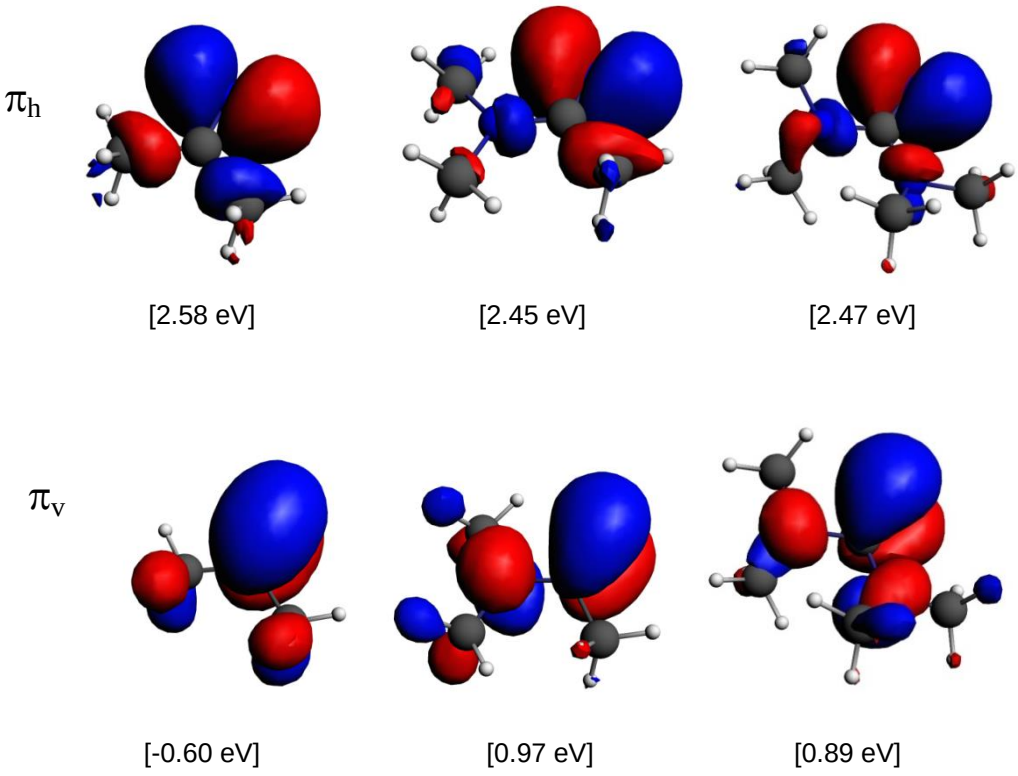

Figure 2.13 π_v and π_h of $[NCMe_2]^-$ (**I**$^-$, left), $[NC(NMe_2)Me]^-$ (**II**$^-$, centre) and $[NC(NMe_2)_2]$ (**III**$^-$, right)

Adding another amino nitrogen to **II**$^-$ yields the guanidinate ligand anion $[NC(NMe_2)_2]^-$ (**III**$^-$). From resonance arguments, discussed previously, it might be expected that **III**$^-$ should be a better π-donor than **II**$^-$. Looking at the fixed Ti-N bond length data the anionic guanidinate ligand (**III**$^-$) appears, however, to donate the same number of total π-electrons as **II**$^-$ (0.65 and 0.66, respectively). This is as a result of a combination of factors. π_v in **III**$^-$ has two amino 2p AOs that have an anti-bonding interaction with the π_{CN} bonding orbital (Figure 2.13) which one would expect to raise the energy of π_v in **III**$^-$ above that of **II**$^-$ significantly. However the contribution of these amino 2p AOs to the overall π_v in **III**$^-$ is only 24% whereas in **II**$^-$ it is 34%. There is also a rotation of the NMe_2 groups of the ligand from the plane of the π_{CN} system, also seen in the crystal structure of **1**, which prevents maximum overlap of the amino

2p AOs with the π_{CN} system (Figure 2.14). Also seen in both the DFT and molecular structures containing this ligand there is a slight pyramidalisation of the amino nitrogens indicative of some sp^3 character which is not seen in **II**; less *p*-character to the amino lone pairs again prevents the most efficient overlap with the π_{CN} system. These factors mean overall the energy of the π_v orbital is only slightly higher in **III**$^-$ than in **II**$^-$ (0.97 and 0.89 eV, respectively); **III**$^-$ donates 0.25 π_v-electrons and **II**$^-$ donates 0.22 π_v-electrons. The extra amino nitrogen in **III**$^-$ decreases the energy of π_h compared to **II**$^-$ due to the introduction of another electronegative nitrogen atom and this means the guanidinate is a less good π_h donor. Overall the slight increase in π_v donation and slight decrease in π_h donation are approximately balanced. The similarity in π-donation ability is mirrored in the Ti-N bond order. The Ti-N Mayer bond orders with **II** and **III** are 1.15 and 1.14, respectively. The Ti-N overlap populations are 0.30 for both ligands and the Ti-N bond lengths in the fully optimised structures are effectively the same (1.852 Å *vs.* 1.854 Å).

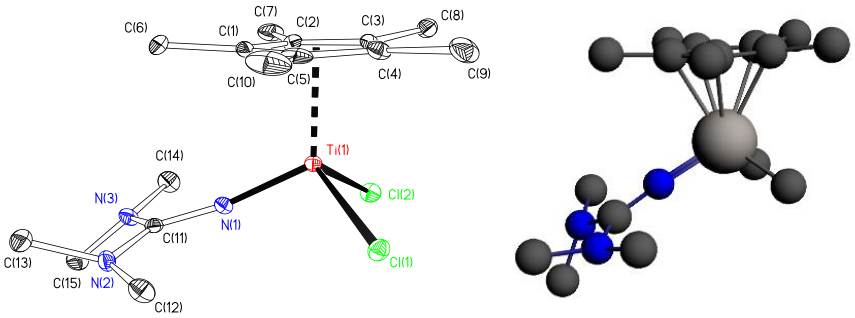

Figure 2.14 Molecular structure of Cp*Ti{NC(NMe$_2$)$_2$}Cl$_2$ (**1**) and DFT (BP86/TZ2P) calculated structure **1Q** (i.e. L = **III**) both showing rotated NMe$_2$ groups.

The effect of the NMe$_2$ group rotation in [NC(NMe$_2$)$_2$]$^-$ on the donating ability of the imine nitrogen has been further investigated by constraining the NMe$_2$ groups to both planar and orthogonal confirmations (Figure 2.15, Table 2.7). If they are constrained to planarity one would expect the π-donation ability of the ligand to increase due to the better N(2p$_\pi$)-π_{CN} overlap in π_v. Accordingly, the number of π-electrons donated does indeed increase from 0.65 to 0.69 (**IIIa**$^-$) although this will also be partially due to removing the pyramidinal conformation of the NMe$_2$ groups. The stronger antibonding interaction between the amino 2p AOs and the π_{CN} orbital increases the π_v energy (0.89 to 1.50 eV) and hence its ability to donate electrons (0.25 to 0.31). Alternatively an orthogonal NMe$_2$ geometry (**IIIb**$^-$) decreases the amino 2p AO to π_{CN} overlap causing

a decrease in energy of the π_v relative to optimised Cp*Ti{NC(NMe$_2$)$_2$}Me$_2$ (0.89 to -1.00 eV) and hence a decrease in π_v donation from 0.25 to 0.11. In this case the π_h energy is increased significantly due to the interaction of the amino 2p AOs with the imine 2p$_h$ and therefore the π_h donation increases from 0.40 to 0.47. Despite the increase in π_h donation the overall π-donation ability of **IIIb**$^-$ with orthogonal NMe$_2$ groups (0.58) is still overall less than when either the NMe$_2$ groups are constrained to planarity (0.69) or allowed to fully optimise (0.65). These effects are reflected in the Mayer bond orders for the different NMe$_2$ orientations increasing 1.11 to 1.14 to 1.20 on going from orthogonal to optimised to planar, respectively (Figure 2.15). The electronic energy of complex Cp*Ti(L^{III})Me$_2$ is -11.14 a.u. whereas as for Cp*Ti(L^{IIIa})Me$_2$ and Cp*Ti(L^{IIIb})Me$_2$ is -11.13 a.u. (an increase of 32.6 kJ mol^{-1}) and -11.08 a.u. (an increase of 114.3 kJ mol^{-1}), respectively.

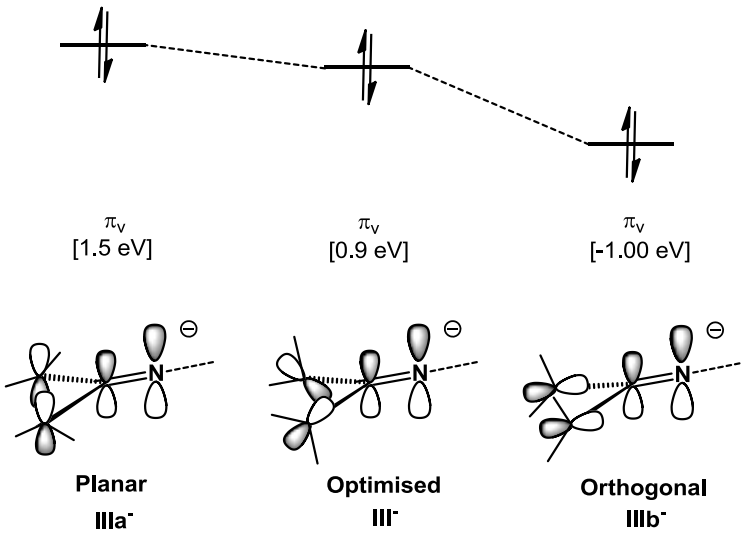

Figure 2.15 Change of π_v energy with changing amino 2p AO - π_{NC} overlap for **III**$^-$

Ligands **III**$^-$ and **VIII**$^-$ are good models for the comparison of non-cyclic guanidinates with iminoimidazolidide ligands. The DFT calculations show there is very little difference between the two types of ligand anion regarding their bonding with [Cp*TiMe$_2$]$^+$, with both donating 0.33 electrons through σ-bonding and 0.65 electrons though π-bonding. The Mayer bond orders are also 1.14 in both cases. **VIII**$^-$ donates more electrons from π_v (0.27 *vs.* 0.25) and fewer from π_h (0.38 *vs.* 0.40). This again correlates with the energy levels of the respective orbitals (π_v = 1.15 eV, π_h = 2.24 eV). Since the iminoimidazolidide is more conformationally constrained then the non-cyclic guanidinate the amino 2p AOs have a better overlap with the π_{CN} orbital, increasing the energy and the number of electrons donated from π_v. Equally the π_h contains a

smaller antibonding interaction between the amino 2p AOs and imine $2p_h$ AO so has a lower energy and therefore donates fewer electrons.

Introduction of a double bond in the backbone of ligand **VIII**$^-$ yields ligand $[NC(N(Me)CH)_2]^-$ (**IX**$^-$). These types of ligand have been utilised in titanium complexes previously to produce active precatalysts for polymerisation.[28, 29] The introduction of a double bond into the ligand backbone decreases the energy (2.24 eV to 2.12 eV) and hence the electron donation ability (0.38 to 0.35) of π_h on going from **VIII**$^-$ to **IX**$^-$. This effect is presumably due to the introduction of a sp^2 carbon adjacent to the amino nitrogen which will have a higher Z_{eff} than an sp^3 carbon. π_v however has a substantial increase in energy (1.15 eV to 1.71 eV) due to the introduction of an antibonding interaction between the amino 2p AOs and the C=C backbone π-bond (Figure 2.16). This means that π_v is now a better donor than before (0.33 *vs.* 0.27) and the number of electrons donated by each π-orbital is now nearly equal. Overall **IX**$^-$ is a more efficient π-electron donor than **VIII**$^-$ (0.68 *vs.* 0.65) and this is reflected in the increased Mayer bond order (1.15 *vs.* 1.14). The overlap population does not reflect this increase in electron donation and is 0.30 for both ligands. The bond lengths of the fully optimised complexes also mirror this with a decrease in bond length from 1.850 to 1.842 Å going from **VIII**$^-$ to **IX**$^-$. This particular ligand has been studied by DFT before (B3PW91\6-311G(d,p))[30] and the qualitative shape of the ligand's frontier orbitals and the relative energies match well to those determined in this study.

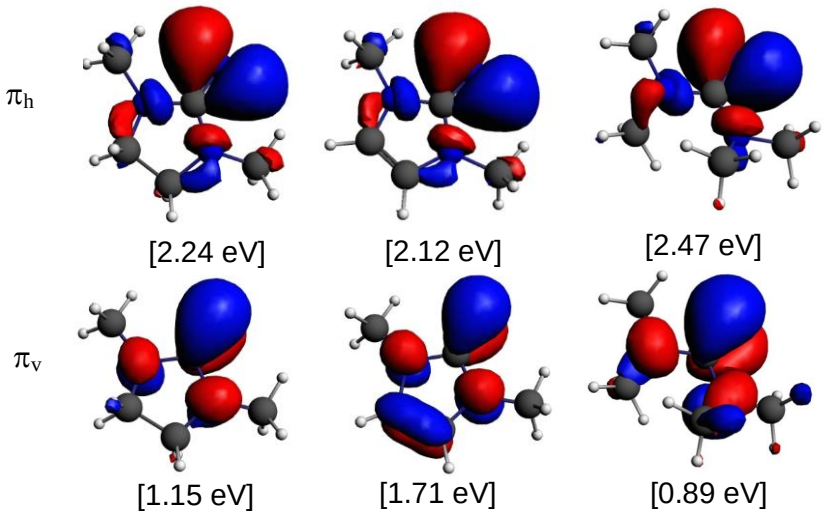

Figure 2.16 π_v and π_h of $[NC(N(Me)CH_2)]^-$ (**VIII**$^-$, left), $[NC(N(Me)CH)]^-$ (**IX**$^-$, centre) and $[NC(NMe_2)_2]^-$ (**III**$^-$, right).

2.5.2.2 Ti-N bonding analysis with phosphinimides, imides and amides

As a comparison with ligands **I**$^-$, **II**$^-$ and **III**$^-$ phosphinimide ligand $[NPMe_3]^-$ (**IV**$^-$) was also studied by DFT. These phosphinimide compounds have been widely used in the synthesis of Group 4 post-metallocene complexes and their derivatives as discussed previously. This type of ligand is known to act as a potential 5 electron donor due to the R_3P^+-N^- resonance form in the neutral ligand; this is therefore a good benchmark compound for investigating Ti-N multiple bonding in our systems. As before, complex $Cp^*Ti(L^{IV})Me_2$ was optimised with constrained and unconstrained Ti-N bond lengths. There is no significant difference in the bonding parameters between the two but for consistency the constrained version will be discussed. In contrast to **I-III**$^-$ the phosphinimide ligand shows an equal amount of electron donation from both the π_v and π_h orbitals. This is due to the local approximate C_{3v} symmetry of the ligand which results in effectively degenerate π_v and π_h orbitals (Figure 2.17).

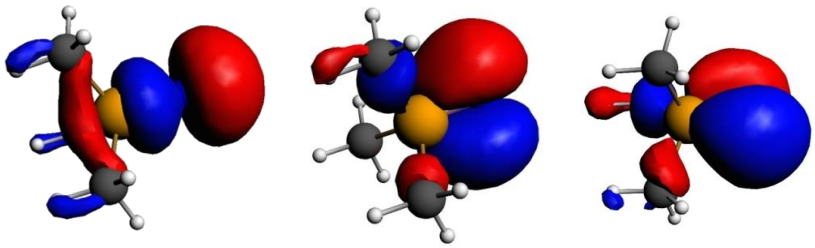

[-0.22 eV] [1.74 eV] [1.76 eV]

Figure 2.17 σ (left), π_v (centre) and (right) π_h of $[NPMe_3]^-$ (**IV**$^-$)

Compared to **IX**$^-$, the best electron donor of the "iminato" type ligands, the overall π-donation of **IV**$^-$ is less (0.62 vs 0.68) but the σ donating ability is higher (0.38 vs. 0.32). The increased σ-bond donation is a result of the higher energy of the σ-orbital (Figure 2.17) due to the lower electronegativity of phosphorus compared to carbon.[31] The phosphinimide is a marginally better overall donor and this is reflected in a higher Mayer bond order value of 1.19 as opposed to 1.15 found with **IX**. Accordingly the Ti-N overlap population for L = **IV** and **IX** are also 0.33 and 0.30 respectively.

The imido ligand $[NPh]^{2-}$ (**X**$^{2-}$) is another good example for comparison when considering Ti-N multiple bonding. This could only be studied as a fully minimised structure with no bond length constraints (introduction of the constraints led to an unstable structure in which SCF could not converge). This is not a problem, however, as it has already been established that fixing the bond length seems to make little

difference to the trends in determined bonding parameters. Imido compounds are known as excellent σ+2π donors and been studied computationally before.[16, 32-41] This imido system shows a preference of π_h donation over π_v although to a lesser extent than the monoanionic iminato-type ligands. The main difference is the extent to which these π-orbitals donate. The π_h and π_v donate 0.63 and 0.51 electrons (1.52 total), respectively *cf.* **IV**$^-$ 0.31/0.31 and **II**$^-$ 0.44/0.22. This significant amount of electron donation is why the imido ligand is assigned as an efficient σ+2π donor. The π_v and π_h orbitals of the imido ligand are both close to pure p-orbitals as opposed to the previously discussed compounds in which the π_v is C=N bonding. The Ti-N bond length for the fully optimised complex **X**$^{2-}$ is 1.742 Å. The overall donor effect is amplified by the dianionic nature of the ligand which lowers Z_{eff} of the imide nitrogen as well as increasing the electronic-electron repulsion in the frontier orbitals.

The Ti-N bond order is significantly higher with **X**$^{2-}$ than **IV**$^-$ mainly due to the N-P back bonding present in NPR_3 which takes electron density away from the Ti-N bond and contributes to the $Me_3P{=}N^-$ resonance form (*cf.* R_3P^+-N^{2-}). It has been shown that the reason for the phosphorus-heteroatom π-character in hypervalent phosphorus systems is primarily due to negative hyperconjugation from the heteroatom lone pair into the σ*-orbitals of the other substituents (π→σ*), whilst the π→d_π interaction is a secondary contribution. The d-orbitals do, however, help polarise the σ*-orbitals which leads to stronger π-bonding in the system.[42] Similar analysis has been carried out on metal bound phosphines and again reveals the importance of σ*-orbitals in hypervalent phosphorous multiple bonding.[43, 44] If the molecular orbitals of **IV**$^-$ are examined a large contribution of the P-C σ*orbitals to π_h and π_v can be seen (Figure 2.17). This N→σ* π-interaction helps prevent the efficient Ti-N π-bonding seen with **X** occurring as well with ligand **IV**. This effect of negative hyperconjugation can also be seen in the electron donation ability of π_v (0.31) and π_h (0.31) from **IV**$^-$ to titanium which are both worse donors than π_h in **I**$^-$ (0.48). This is because π_h in **I**$^-$ is essentially nitrogen lone pair whereas in **IV**$^-$ both π_h and π_v, although in theory could exist as pure lone pairs, have a significant back-donation into the P-C σ*-orbitals.

As a benchmark for a σ+1π donor, the complex $Cp^*Ti(NMe_2)Me_2$ (L = **V**) was calculated as mentioned above. Since **V**$^-$ contains only one non-bonding p-orbital it is only possible to have one π-interaction. The bond length was again constrained (1.860 Å). The number of σ-bonding electrons donated by the ligand is 0.35 which is

comparable to **I**$^-$, **II**$^-$, **III**$^-$, **VII**$^-$, **VIII**$^-$ and **IX**$^-$ (range, 0.32-0.34). The overall π-bonding, which consists exclusively of a π_v contribution, is 0.44. This is comparable to the π_h-donation from anionic ligands **I**$^-$ (0.48), **II**$^-$ (0.44) and **III**$^-$ (0.40). The lower net π-bonding contribution is reflected in the low overall Mayer bond order of 1.04 and overlap population of 0.26. As mentioned previously rotating 90° around the Ti-N bond (**Vb**$^-$) shows that Ti(π_v) and Ti(π_h) orbitals accept electrons equally from the amide 2p AO in both orientations i.e. both have the capability to accept electrons in an equal amount (shown also for **IV**$^-$). Accordingly if the structure is minimised in its entirety the Ti-N bond length increases significantly to 1.926 Å.

2.5.2.3 Effect of phenyl substituents on ligand electron donation

Ligand **XI** replaces the sp^2 carbon bound methyl group on **II** with a phenyl moiety. Optimisation of the complex with a restrained Ti-N bond length (1.860 Å) results in a complex in which the ligand phenyl group is rotated out of the π_{CN} plane whilst the amino 2p AO stays approximately co-planar to maintain conjugation. This is consistent with the molecular structure determined for Cp*Ti{NC(N^{i}Pr$_2$)Ph}Me$_2$ (**2.4**).[2] Since the sp^2 carbon of a phenyl group has a higher effective Z_{eff} than that of methyl (sp^3) and phenyl can generally be considered as an electron withdrawing groups due to resonance effects, both π_h and π_v have a lower energy in **XI**$^-$ than **II**$^-$ which results in a smaller donation of electrons from ligand to metal. The decrease in donor ability when adding a phenyl group is reflected in the Mayer bond order values of 1.10 and 1.15, and the overlap populations of 0.29 and 0.30 for **XI** and **II**, respectively, at fixed Ti-N distances. This is also reflected in the increase in bond length in the fully optimised structures going from 1.854 Å in **II** to 1.862 Å in **XI**. The Mulliken populations of the orbitals do not seem to describe this change well as they maintain roughly the same populations as in **II**. Due to the decrease in bond order seen in **XI** as a result of the introduction of a phenyl ring the guanidinate system **III** now has a higher bond order than the amidinate **XI**.

The model system **XII** is the iminoimidazolidide **VIII** but with the introduction of flanking phenyl groups rather than methyl groups. As above the introduction of a phenyl group seems to diminish the π-donating ability of the ligand. Correlating the energies of π_v and π_h in the fixed Ti-N systems shows that this can be linked to a decrease in energy of the orbitals on going from Me to Ph flanking groups (π_v 1.15 to -0.27 eV; π_h 2.24 to 0.98 eV). This is replicated in the Mayer bond order and

overlap population which decrease from 1.14 to 1.03 and 0.30 to 0.25, respectively, as well as the Ti-N bond lengths in the fully optimised structures (1.850 Å and 1.881 Å).

2.5.2.4 DFT calculations on experimentally observed systems

As well as the previously discussed systems it is important to consider the electronic structure of all the experimentally determined systems. This Section will compare the calculated versions of real systems to each other and to the appropriate model systems to see if the trends determined previously apply to experimentally determined systems. The structures were fully optimised with no constraints. The important bonding parameters are shown in Table 2.9. The only model compound that has also been synthesised and characterised is Cp*Ti{$NC(NMe_2)_2$}Me_2 (**4**, i.e. L = **III**).

Table 2.9 σ, π and total electron contributions, Ti-N overlap population, Mayer bond order and calculated Ti-N bond length determined by DFT (BP86/TZ2P) for fully optimised systems containing ligands **III**, **XI**, **XIII**, **XIV**, **XV**.

Ligand		σ	π	Total	Ti-N Overlap Population	Mayer Bond Order	Ti-N bond length (Å)
$NC(NMe_2)_2$	**III**	0.34	0.66	1.00	0.30	1.15	1.852
$NC(NMe_2)Ph$	**XI**	0.33	0.67	1.00	0.28	1.10	1.862
$NC(N^iPr_2)Ph$	**XIII**	0.30	0.68	0.98	0.28	1.10	1.870
$NC(N^iPr_2)Ar^{F_2}$	**XIV**	0.30	0.64	0.94	0.28	1.06	1.880
$NC(N(Xyl)CH_2)_2$	**XV**	0.29	0.66	1.00	0.30	1.15	1.869

Ligand **XIII** is effectively model species **XI** but with an N^iPr_2 group rather than NMe_2. There are few differences in the bonding between the two systems which have identical Ti-N overlap populations (0.28) and Mayer bond orders (1.10). The bond length does increase on going from **XI** (1.862 Å) to **XIII** (1.870 Å) but presumably this is a result of the increased steric bulk of **XIII**. Introduction of *ortho*-fluorine atoms onto the phenyl ring of **XIII** gives **XIV**. As seen with **II**$^-$ and **VII**$^-$ the introduction of these highly electronegative elements lowers the energy of the donor orbitals; this is also seen here. It has already been shown that introduction of a phenyl ring in **XI** decreases the bond order of the amidinate such that the guanidinate **III** is a superior

donor. This is no different for the comparison of **III** and **XIII**. The guanidinate **III** has a higher bond order with titanium than in the corresponding amidinate **XIII**.

The iminoimidazolidide ligand **XV** can be considered as a variation of **XII**. It has been shown in the comparison of **III** and **VIII** that the introduction of a cyclic moiety does not change the bonding of the ligand to the metal significantly. It has also been shown by the comparison of **VIII** and **XII** that introduction of Ph groups onto the iminoimidazolidide decreases the donating ability of the ligand. However ligand **XV** however shows similar donating abilities to **III**. The energies of the π_v and π_h for **XV**$^-$ are 0.33 and 1.59 eV, respectively (*cf.* **XII**$^-$, π_v -0.27 eV, π_h 0.98 eV). **XV**$^-$ has *ortho*-methyl groups which can act as electron donors into the ring which would cause an increase in donation ability of the ligand compared to **XII**. As a consequence of the increased π_h and π_v orbital energies the Mayer bond order with **XV** is 1.15 compared to 1.03 with **XII** and is the same as **III**.

2.5.2.5 Comparison of DFT structures with structurally characterised systems

Although all the calculated data are self-consistent, a comparison with crystallographically determined bond parameters must be made. This has been carried out briefly for some systems towards the start of the Chapter but this Section aims to give a broad overview of various compounds including some literature compounds in order to compare this to the DFT results. Since there is not a comprehensive list of relevant crystallographically characterised dimethyl complexes, dichloride complexes have been used for this comparison.

The complexes used for this comparison are: ketimide-supported system Cp*Ti(NC^{t}Bu$_2$)Cl$_2$ (**2.8**),[45] amidinate-supported system Cp*Ti{NC(N^{i}Pr$_2$)Ph}Cl$_2$ (**2.3**),[2] guanidinate-supported system Cp*Ti{NC(NMe$_2$)$_2$}Cl$_2$ (**1**), iminoimidazolidide-supported system Cp*Ti{NC(N(Xyl)CH$_2$)$_2$}Cl$_2$ (**3**), phosphinimide-supported system Cp*Ti(NP^{i}Pr$_3$)Cl$_2$ (**2.9**)[46] and imido-supported system Cp*Ti(NXyl){MeC(N^{i}Pr)$_2$} (**2.10**).[47] The important bond length and angle data for the selected systems are listed in Table 2.10.

Table 2.10 Selected bond lengths (Å) and angles (°) for Cp*Ti(NC^{t}Bu$_2$)Cl$_2$ (**2.8**), Cp*Ti{NC(N^{i}Pr$_2$)Ph}Cl$_2$ (**2.3**), Cp*Ti{NC(NMe$_2$)$_2$}Cl$_2$ (**1**), Cp*Ti{NC(N(Xyl)-CH$_2$)$_2$}Cl$_2$ (**3**), Cp*Ti(NP^{i}Pr$_3$)Cl$_2$ (**2.9**) and Cp*Ti(NXyl){MeC(N^{i}Pr)$_2$} (**2.10**). C(11) is the carbon directly bonded N(1) in each case.

	2.8	**2.3**	**1**	**3**	**2.9**	**2.10**
Ti(1)-N(1)	1.844(7)	1.800(3)	1.782(3)	1.788(2)	1.759(4)	1.738(2)
N(1)-C(11)	1.266(11)	1.310(4)	1.324(5)	1.302(4)	-	1.382(4)
N(2)-C(11)	-	1.340(4)	1.362(5)	1.359(4)	-	-
N(3)-C(11)	-	-	1.357(5)	1.361(4)	-	-
Ti(1)-N(1)-C(11)	166.4(7)	165.2(3)	170.3(3)	176.4(2)	-	168.9(2)

Amidinate complex **2.3** has a significantly shorter Ti-N bond than ketimide complex **2.8** (1.844(7) Å *vs.* 1.800(3) Å) and a longer N(1)-C(11) distance (1.266(11) Å *vs.* 1.310(4) Å). These significant changes are in agreement with those found in the DFT studies and are as a result of the introduction of the additional amino group. Going from **2.3** to guanidinate complex **1** there is a small but significant decrease in the Ti-N bond distance (1.800(3) Å to 1.782(3) Å) which again matches with the DFT calculated results. This difference is mainly due to the presence of the phenyl ring in **2.3** which is known to decrease the Ti-N bond order. The cyclic guanidinate **3** has the same Ti-N bond length as the non-cyclic analogue **1** as also found in the above investigation. The xylyl rings do not have the same effect as the phenyl rings in **2.3** because, as discussed previously, they have donating *ortho*-methyl groups which help balance the electron withdrawing effect of the aryl ring. The phosphinimide **2.9** has a Ti-N bond length (1.759(4) Å) significantly shorter than the previously mentioned compounds (**2.8**, **2.3**, **1**, **3** and **2.9**) and this is because of a very strong σ-bonding component to the metal centre as shown by DFT. The imido compound **2.10** synthesised by Mountford *et al.* has the shortest Ti-N bond length of them all (1.738(2) Å) because, as discussed, it is a highly efficient σ+2π donor.

2.6 Summary

This Chapter has described the synthesis and characterisation of several half-sandwich dichloride and dialkyl precatalysts. The X-ray crystal structures of some of these compounds have also been presented and compared. DFT studies were then described which investigated the influence of various ligands (L) on the frontier orbitals of [Cp(L)Ti]$^{2+}$. Following this, DFT studies of the Ti-N bonding mode and the electron

donation efficiency of the ligand, L, were detailed for a selection of κ^1-bound N-donors. Overall this Section showed that although all the ligands (other than NMe_2) bind in a $\sigma+2\pi$ mode the electron donating efficiency of the π-orbitals in these different ligands can vary significantly depending largely on the donor orbital energy and therefore the energy match between it and the metal acceptor orbitals. Overall the DFT results compared well to that determined experimentally.

2.7 References

1. E. G. Ijpeij, P. J. H. Windmuller, H. J. Arts, F. Van der Burgt, G. H. J. Van Doremaele and M. A. Zuideveld, *LANXESS ELASTOMERS, WO/2005/090418*, 2005.
2. R. Scott, *DPhil Thesis, University of Oxford*, 2013.
3. E. G. Ijpeij, B. Coussens, M. A. Zuideveld, G. H. J. van Doremaele, P. Mountford, M. Lutz and A. L. Spek, *Chem. Commun.*, 2010, **46**, 3339-3341.
4. G. H. J. van Doremaele, M. A. Zuideveld, N. V. F. Quiroga and A. Leblanc, *LANXESS Elastomers, WO2011054927A1*, 2011.
5. D. H. R. Barton, J. D. Elliott and S. D. Gero, *J. Chem. Soc., Perkin Trans. 1*, 1982, 2085-2090.
6. J. Zhang, F. Han, Y. Han, Z. Chen and X. Zhou, *Dalton Trans.*, 2009, 1806-1811.
7. F. Allen, *Acta Crystallogr., Sect. B: Struct. Sci.*, 2002, **58**, 380-388.
8. F. H. Allen, O. Kennard, J. J. Galloy, O. Johnson and D. G. Watson, *Chem. Des. Autom. News*, 1993, **8**, 1 & 31.
9. D. A. Fletcher, R. F. McMeeking and D. Parkin, *J. Chem. Inf. Comput. Sci.*, 1996, **36**, 746-749.
10. W. P. Kretschmer, *Stichting Dutch Polymer Institute, US20040192541A1*, 2004.
11. K. Nomura, H. Fukuda, S. Katao, M. Fujiki, H. J. Kim, D.-H. Kim and S. Zhang, *Dalton Trans.*, 2011, **40**, 7842-7849.
12. G. te Velde, F. M. Bickelhaupt, E. J. Baerends, C. Fonseca Guerra, S. J. A. van Gisbergen, J. G. Snijders and T. Ziegler, *J. Comput. Chem.*, 2001, **22**, 931-967.
13. C. Fonseca Guerra, J. G. Snijders, G. te Velde and E. J. Baerends, *Theor. Chem. Acc.*, 1998, **99**, 391-403.

14. *ADF2013, SCM, Theoretical Chemistry, Vrije Universiteit, Amsterdam, The Netherlands*, 2013.
15. E. Van Lenthe and E. J. Baerends, *J. Comput. Chem.*, 2003, **24**, 1142-1156.
16. T. B. Parsons, N. Hazari, A. R. Cowley, J. C. Green and P. Mountford, *Inorg. Chem.*, 2005, **44**, 8442-8458.
17. J. C. Green, *Chem. Soc. Rev.*, 1998, **27**, 263-272.
18. J. W. Lauher and R. Hoffmann, *J. Am. Chem. Soc.*, 1976, **98**, 1729-1742.
19. G. Wilkinson, M. Rosenblum, M. C. Whiting and R. B. Woodward, *J. Am. Chem. Soc.*, 1952, **74**, 2125-2126.
20. G. Wilkinson, P. L. Pauson, J. M. Birmingham and F. A. Cotton, *J. Am. Chem. Soc.*, 1953, **75**, 1011-1012.
21. C. Elschenbroich, *Organometallics*, 3rd edn., Wiley-VCH, 2006, 484-527.
22. P. D. Bolton, E. Clot, N. Adams, S. R. Dubberley, A. R. Cowley and P. Mountford, *Organometallics*, 2006, **25**, 2806-2825.
23. F. Zhu, Q. Huang and S. Lin, *J. Polym. Sci., Part A: Polym. Chem.*, 1999, **37**, 4497-4501.
24. J. C. W. Chien, Z. Salajka and S. Dong, *Macromolecules*, 1992, **25**, 3199-3203.
25. F. Zhu, Y. Huang, Y. Yang and S. Lin, *J. Polym. Sci., Part A: Polym. Chem.*, 2000, **38**, 4258-4263.
26. D. W. Stephan, *Organometallics*, 2005, **24**, 2548-2560.
27. A. J. Bridgeman, G. Cavigliasso, L. R. Ireland and J. Rothery, *J. Chem. Soc., Dalton Trans.*, 2001, 2095-2108.
28. M. Tamm, S. Randoll, T. Bannenberg and E. Herdtweck, *Chem. Commun.*, 2004, 876-877.
29. M. Tamm, S. Randoll, E. Herdtweck, N. Kleigrewe, G. Kehr, G. Erker and B. Rieger, *Dalton Trans.*, 2006, 459-467.
30. X. Wu and M. Tamm, *Coord. Chem. Rev.*, 2014, **260**, 116-138.
31. K. Li and D. Xue, *J. Phys. Chem. A*, 2006, **110**, 11332-11337.
32. A. D. Schwarz, A. J. Nielson, N. Kaltsoyannis and P. Mountford, *Chem. Sci.*, 2012, **3**, 819-824.
33. B. D. Ward, G. Orde, E. Clot, A. R. Cowley, L. H. Gade and P. Mountford, *Organometallics*, 2004, **23**, 4444-4461.
34. J. D. Selby, C. D. Manley, A. D. Schwarz, E. Clot and P. Mountford, *Organometallics*, 2008, **27**, 6479-6494.

35. P. Mountford and D. Swallow, *J. Chem. Soc., Chem. Commun.*, 1995, 2357-2359.
36. D. S. Williams, M. H. Schofield, J. T. Anhaus and R. R. Schrock, *J. Am. Chem. Soc.*, 1990, **112**, 6728-6729.
37. D. S. Williams, M. H. Schofield and R. R. Schrock, *Organometallics*, 1993, **12**, 4560-4571.
38. J. T. Anhaus, T. P. Kee, M. H. Schofield and R. R. Schrock, *J. Am. Chem. Soc.*, 1990, **112**, 1642-1643.
39. D. L. Morrison and D. E. Wigley, *Inorg. Chem.*, 1995, **34**, 2610-2616.
40. M. T. Benson, J. C. Bryan, A. K. Burrell and T. R. Cundari, *Inorg. Chem.*, 1995, **34**, 2348-2355.
41. M. T. Benson, T. R. Cundari and E. W. Moody, *J. Organomet. Chem.*, 1995, **504**, 1-13.
42. A. E. Reed and P. v. R. Schleyer, *J. Am. Chem. Soc.*, 1990, **112**, 1434-1445.
43. T. Leyssens, D. Peeters, A. G. Orpen and J. N. Harvey, *Organometallics*, 2007, **26**, 2637-2645.
44. P. D. Lyne and D. M. P. Mingos, *J. Organomet. Chem.*, 1994, **478**, 141-151.
45. A. R. Dias, M. T. Duarte, A. C. Fernandes, S. Fernandes, M. M. Marques, A. M. Martins, S. J. F. da and S. S. Rodrigues, *J. Organomet. Chem.*, 2004, **689**, 203-213.
46. D. W. Stephan, J. C. Stewart, F. Guerin, S. Courtenay, J. Kickham, E. Hollink, C. Beddie, A. Hoskin, T. Graham, P. Wei, R. E. v. H. Spence, W. Xu, L. Koch, X. Gao and D. G. Harrison, *Organometallics*, 2003, **22**, 1937-1947.
47. A. E. Guiducci, C. L. Boyd and P. Mountford, *Organometallics*, 2006, **25**, 1167-1187.

Chapter 3

Base-free titanium alkyl cations, bimetallic cations, and Lewis base adducts

3.1 Overview

It is well accepted that the active species in Group 4 homogenous olefin polymerisation is an electron deficient monoalkyl cation $[L_nMR]^+$ (L = ligand(s) , M = Group 4 metal, R = alkyl). This Chapter begins by discussing previous studies of half-sandwich monomethyl cations before going on to discuss the synthesis and characterisation of base-free cations supported by κ^1-guanidinate or κ^1-amidinate ligands. The synthesis and characterisation of the corresponding Lewis base adducts of the cations is also described.

DFT calculations have also been carried out in order to probe both the electronic characteristics and dimerisation processes of these cations. The Chapter ends with the synthesis and discussion of bimetallic monomethyl-bridged monocations and alkyl aluminium adducts.

3.2 Post-metallocene base-free cations

Following on from Section 1.6.6 which gave a general introduction into the activation and solution behaviour of dialkyl base-free cations, this Section will focus on the previously reported activation chemistry of dimethyl post-metallocene half-sandwich complexes looking solely at the stoichiometric treatment of dimethyl complexes with activating agent; the chemistry of monomethyl-bridged monocations, formed by treatment of the neutral dimethyl complexes with 0.5 equivs of activator, will be discussed later in this Chapter in Section 3.3.

In 2000 Piers *et al*. showed that treatment of the ketimide complexes $Cp^RTi(NC^tBu_2)Me_2$ (Cp^R = Cp, Cp*, $C_5Me_4SiMe_3$) with BF_{15} ($B(C_6F_5)_3$) produced the zwitterionic species $[Cp^RTi(NC^tBu_2)(\mu\text{-}Me)BF_{15}]$ as seen with the metallocene systems; these compounds decompose over *ca.* 24 h producing methane and $Cp^RTi(NC^tBu_2)(C_6F_5)(\mu\text{-}CH_2B(C_6F_5)_2)$ containing a methylene bridge.[1] TBF_{20} ($[Ph_3C][B(C_6F_5)_4]$) can also be used to activate the ketimide dimethyl complexes although the reaction requires heating to go to completion (Equation 3.1). With Cp^R = Cp* or $C_5Me_4SiMe_3$ this produces single clean monomeric cationic species by ^1H NMR (Equation 3.1) whereas with Cp a complex mixture is produced.[2]

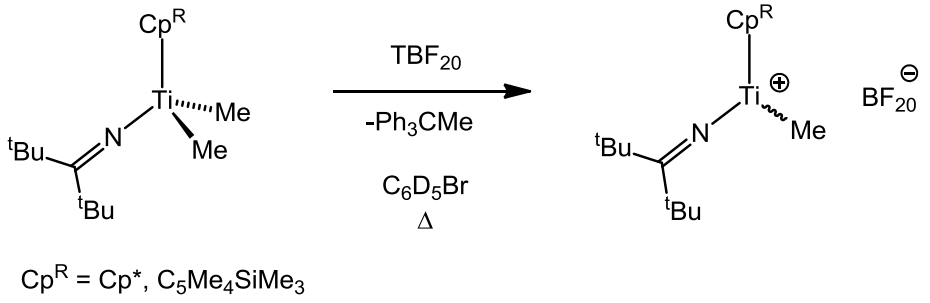

Equation 3.1 Activation of $Cp^{R}Ti(NC^{t}Bu_2)Me_2$ with TBF_{20}.

Complexes containing the phosphinimide supporting ligand has also had its activation chemistry studied with both BF_{15} and TBF_{20} by Stephan and Piers, respectively.[3, 4] The activation of dimethyl compounds $Cp^{R}Ti(NP^{t}Bu_3)Me_2$ (Cp^{R} = Cp* or Cp) with TBF_{20} produces a single clean species at room temperature which can be fully characterised by NMR spectroscopy. However, the species is unstable in solution over a longer period of time (*ca.* 12 h). The phosphinimide compounds when activated with BF_{15} form the expected zwitterionic species $CpTi(NP^{t}Bu_3)Me(\mu\text{-}Me)BF_{15}$ which was subsequently structurally characterised.

The activation of aryloxide-supported half-sandwich complexes has also been investigated. Treatment of aryloxide dimethyl complex $CpTi(O\text{-}2\text{-}Np\text{-}4,6\text{-}C_6H_2{}^{t}Bu)Me_2$ with BF_{15} produces the usual contact ion pair which was characterised by ^{1}H NMR spectroscopy. However, over time, this species decomposed with the elimination of methane to form a $Ti(\mu\text{-}CH_2)B$ containing compound.[5] Other less sterically hindered compounds such as $CpTi(O\text{-}2,6\text{-}C_6H_3Me_2)Me_2$, even at -70 °C, form a mixture of decomposition products with observation of the transient zwitterionic compound. Activation of $CpTi(O\text{-}2,6\text{-}C_6H_3Me_2)Me_2$ with TBF_{20} at -70 °C gave the corresponding cationic complex which decomposed even at -30 °C. [6-10]

Activation chemistry with BF_{15} has also been demonstrated by Marks *et al*. with the dimethyl CGC catalyst family showing similar characteristics to those previously mentioned for ketimide, aryloxide and phosphinimide supported systems.[11, 12] The synthesis of CGC cation $[(C_5Me_4SiMe_2N^{t}Bu)ZrMe][BF_{20}]$ has been detailed and the compound was isolated and characterised by elemental analysis.[13] Prior to the report of the crystallographically characterised species $\mathbf{1.26_{dim}}^{2+}$ by Lanxess Elastomers and Mountford in 2010,[14] the only crystallograpically-characterised base-free cation was the dimeric half-sandwich κ^2-amidinate compound $[Cp^{*}{}_2Zr_2(\mu\text{-}Me)_2\{N^{t}BuC(Me)\text{-}NEt\}_2][BF_{20}]_2$. This was formed by the activation of the dimethyl complex

$Cp^*Zr\{N^tBuC(Me)NEt\}Me_2$ with $[PhNMe_2H][BF_{20}]$.[15] To the author's knowledge there are no reports on the stoichiometric activation of dimethyl imidoimidazolidide or non-*ansa* amide-supported Group 4 catalysts in which the active species has been characterised.

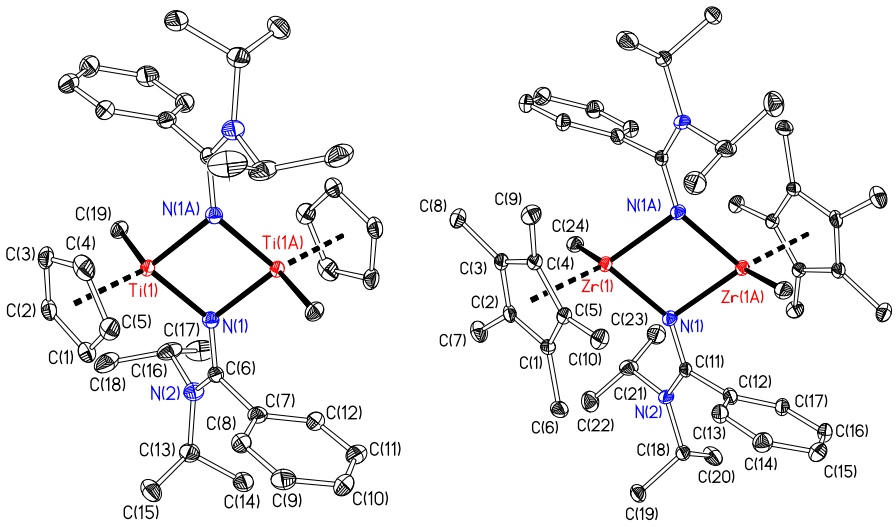

Figure 3.1 Molecular structures of $[Cp_2Ti_2\{\mu\text{-}NC(N^iPr_2)Ph\}_2Me_2]^{2+}$ (**3.4**) and $[Cp^*_2Zr\{\mu\text{-}NC(N^iPr_2)Ph\}_2Me_2]^{2+}$ (**3.5**)

Work carried out in the Mountford group concurrently with the work reported in this Thesis recently showed that reaction of amidinate supported complexes $CpTi\{NC(N^iPr_2)Ph\}Me_2$ (**3.1**), $Cp^*Zr\{NC(N^iPr_2)Ph\}Me_2$ (**3.2**) and $Cp^*Hf\{NC(N^iPr_2)Ph\}Me_2$ (**3.3**) (the Cp, Zr and Hf analogues of **2.4**, respectively) with TBF_{20} led to the immediate crystallisation of the structurally characterised nitrogen-bridged dimeric dications $[Cp_2Ti_2\{\mu\text{-}NC(N^iPr_2)Ph\}_2Me_2]^{2+}$ (**3.4**), $[Cp^*_2Zr\{\mu\text{-}NC(N^iPr_2)Ph\}_2Me_2]^{2+}$ (**3.5**) and $[Cp^*_2Hf_2\{\mu\text{-}NC(N^iPr_2)Ph\}_2Me_2]^{2+}$ (**3.6**);[16] this is in contrast to $\mathbf{1.26}^+$ which is soluble in halobenzene solvents for a short amount of time before slowly forming the crystalline dimethyl-bridged dication $\mathbf{1.26_{dim}}^{2+}$.[14] The molecular structures of **3.4** and **3.5** are shown in Figure 3.1. Due to the rapid crystallisation of **3.4**, **3.5** and **3.6** no NMR data were obtained. This result highlights that heteroatomic bridges are possible in these types of systems and could play an important role in the polymerisation process.

3.2.1 Synthesis of base-free cations

The synthesis and study of base-free cations was the logical initial step in studying the active polymerisation species. Synthesis of these cations involved abstraction of a

single methyl group from various dimethyl complexes (Section 1.6.2.3) using cocatalyst TBF_{20} (Equation 3.2); the nature of the active species is shown as a monomeric base-free alkyl cation but it must be noted, as discussed in Chapter 1, that the solution behaviour can be more complicated. The solvents used for these reactions are either C_6D_5Br if carried out on the NMR tube scale or C_6H_5F if carried out using Schlenk line techniques. C_6H_5F was used on scale-up because it has a lower boiling point than C_6H_5Br and so could be removed under vacuum more easily. These solvents are also less likely to coordinate to the produced cations though lone-pair donation. Less polar solvents such as C_6D_6 resulted in poor solubility of the ionic species and resulted in the formation of oils.

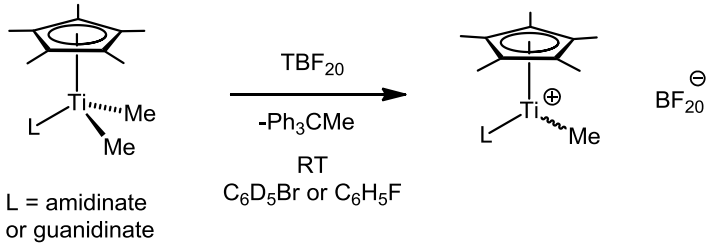

Equation 3.2

3.2.2 Diffusion measurement by NMR spectroscopy

This Chapter also details research carried out in collaboration with Dr Timothy Claridge, in the Oxford chemistry department, on determining the diffusion coefficients (D) of various cations in solution using a technique known as Diffusion Ordered Spectroscopy (DOSY) or Pulsed Gradient Spin Echo (PGSE) NMR. For a more in-depth discussion of DOSY and how the diffusion coefficient is determined the reader is referred to the relevant literature.[17] The technique has been successfully used on metallocenium complexes to determine whether the ionic active species exists as single ion pairs or as higher aggregates such as ionic quadruples.[18-21] If one assumes a spherical molecular shape the diffusion constant of a compound is inversely proportional to the cube root of the volume according to the Stoke-Einstein equation (Equation 3.3, D is the diffusion coefficient, k is Boltzmann's constant, T is temperature, η is viscosity, r is the hydrodynamic radius, V is volume and c is a numerical factor that depends on the size and shape of the solute and the hydrodynamic behaviour of the solute-solvent system).[19]

$$D = \frac{kT}{c\pi r\eta} = \frac{kT}{c\pi\eta\left(\frac{3V}{4\pi}\right)^{\frac{1}{3}}}$$

Equation 3.3

Thus if the ratio of the diffusion coefficients is known then the ratio of volumes can be determined by simply cubing the ratio D_2/D_1. Using the volumes rather than D or r gives a more tangible comparison of molecular size. In this Thesis the ratio of volumes and diffusion coefficients will be used to compare species present in each NMR tube experiment; using this approach negates any significant variations in the viscosity of the solvent and the numerical factor c that occurs, for example due to the presence of different species in solution. The ratios of diffusion coefficients have been used in reported studies to compare the size of different species previously as well as the association of anions and cations.[22-26]

A theoretical ratio of volumes will also be calculated for the species in question by using either directly determined crystallographical volumes or by using the well established rule (in the absence of X-ray structures) that the average volume required for a molecule in a crystal structure is *ca.*18 Å^3 per non-hydrogen atom.[27] The validity of this rule can be shown in these systems by the reasonable agreement between the crystallographically determined volume (2924.53(13) Å^3) and that determined using the "18 Å^3 rule" (2664 Å^3) for the molecular structure of **1.26$_{dim}$-[BF$_{20}$]$_2$**. The production of the cations leads to the formation of the side-product Ph_3CMe which was used in each case as an internal standard for the diffusion coefficient (D = 5.00 x 10^{-10} m^2 s^{-1}). Samples were prepared with a concentration of 0.1 M for each species in C_6D_5Br.

3.2.3 Base-free [Cp*Ti{NC(N^{i}Pr$_2$)Ar^{F_2}}Me][BF$_{20}$] (1.26-[BF$_{20}$])

As already discussed, preliminary work for this project was carried out by Lanxess Elastomers using the κ^1-amidinate-supported complex Cp*Ti{NC(N^{i}Pr$_2$)Ar^{F_2}}Me$_2$ (Ar^{F_2} = 2,6-$C_6H_3F_2$) (**1.49**) in collaboration with Mountford. Treatment of **1.49** with 1 equiv of TBF_{20} at room temperature leads to the quantitative and immediate formation of the monoalkyl cation (**1.26$^+$**) as judged by ^{1}H NMR spectroscopy.[14] This was characterised by ^{1}H and ^{19}F NMR spectroscopy at the time, but due to rapid crystallisation could not be characterised by ^{13}C NMR spectroscopy.

Although the dimer **1.26$_{dim}$-[BF$_{20}$]$_2$** was structurally characterised in the solid state, it was thought appropriate to use solution based techniques such as DOSY NMR to investigate whether it was also dimeric in solution. It was expected in the absence of DOSY results that the species in solution is probably monomeric since **1.26$_{dim}$-[BF$_{20}$]$_2$** cannot be redissolved in C_6D_5Br. The ^1H NMR spectrum of **1.26$^+$** in C_6D_5Br shows the formation of a single cationic product (*cf.* Cp*Ti(NC^{t}Bu$_2$)Me$_2$, *vide supra*[2]). DOSY NMR was performed on the base-free cation [Cp*Ti{NC(N^{i}Pr$_2$)Ar^{F_2}}Me]$^+$, as well as the anion [BF$_{20}$]$^-$, in C_6D_5Br using both ^1H and ^{19}F resonances. This allowed measurement and comparison of both the cationic (**1.26$^+$**) and anionic (**[BF$_{20}$]$^-$**) components of the compound. The diffusion coefficient (D) for the cation as measured by ^1H NMR was 2.75(3) x 10^{-10} m^2 s^{-1} and the anion measured by ^{19}F NMR was 2.77(3) x 10^{-10} m^2 s^{-1}. Since both components have effectively the same diffusion coefficients these experiments show that despite being a weakly coordinating anion [BF$_{20}$]$^-$ still has a strong enough association with the cation in this solvent system to diffuse along at the same rate.

To seek evidence for monomeric **1.26$_{mono}$$^+$** in solution a ^1H DOSY experiment was run with **1.26-[BF$_{20}$]** dissolved in C_6D_5Br together with the same concentration of the triphenylphosphine oxide adduct [Cp*Ti{NC(N^{i}Pr$_2$)Ar^{F_2}}(OPPh$_3$)Me][BF$_{20}$] (**1.51-[BF$_{20}$]**).[14] This adduct was chosen because it is larger than the monomeric cation but smaller than the dimer. Compound **1.51-[BF$_{20}$]** had also been reported before and is stable and soluble in solution over long periods of time.[14] The diffusion coefficient for **1.26-[BF$_{20}$]** was 2.84(3) x 10^{-10} m^2 s^{-1} compared to 2.69(3) x 10^{-10} m^2 s^{-1} for **1.51-[BF$_{20}$]**. Since **1.26-[BF$_{20}$]** has the higher diffusion coefficient it must be smaller overall than the OPPh$_3$ adduct and therefore the cation is monomeric in solution i.e. **1.26$_{mono}$-[BF$_{20}$]** not **1.26$_{dim}$-[BF$_{20}$]$_2$** (Figure 3.2). The ratio of diffusion coefficients in this case is 1.06 and the ratio of volumes is 1.18. This matches well with the calculated ratio of volumes of 1.16, derived including the [BF$_{20}$]$^-$ counterion.

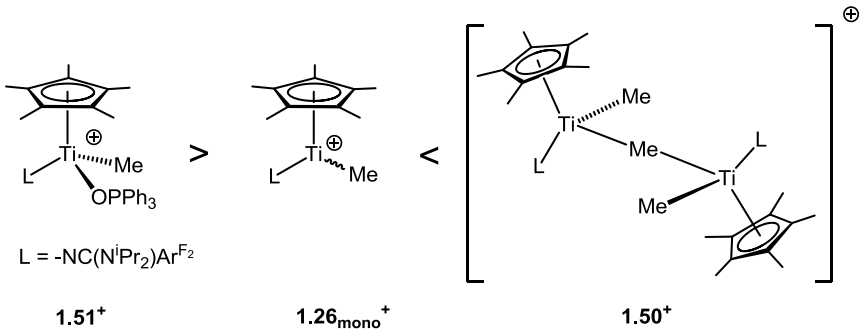

Figure 3.2 Size comparison of cation $\mathbf{1.26_{mono}}^+$ with $OPPh_3$ adduct $\mathbf{1.51}^+$ and monomethyl-bridged monocation $\mathbf{1.50}^+$ from DOSY experiments.

As another comparison, **1.26_{mono}-[BF_{20}]** was also tested against the monomethyl-bridged monocation $[Cp^*_2Ti_2\{NC(N^iPr_2)Ar^{F_2}\}_2Me_2(\mu\text{-}Me)][BF_{20}]$ (**1.50-[BF_{20}]**), synthesised by the addition of 0.5 equivs of TBF_{20} to **1.49** (see Section 3.3).[14] The diffusion constant for **1.26_{mono}-[BF_{20}]** was 2.73(4) x 10^{-10} $m^2\,s^{-1}$ compared to 2.51(3) x 10^{-10} $m^2\,s^{-1}$ for **1.50-[BF_{20}]**. The ratio of volumes is 1.29 which matches the calculated ratio of 1.28 for the ion pair. This once more confirms that $\mathbf{1.26_{mono}}^+$ is monomeric in solution (Figure 3.2). Further evidence and insight on this topic is found in Section 3.2.16.

3.2.4 [Cp*Ti{NC(N^{i}Pr$_2$)Ar^{F_2}}(L)Me][BF_{20}] (L = py (8-[BF_{20}]) or THF (9-[BF_{20}]))

As mentioned above, the cation $\mathbf{1.26}^+$ has previously been trapped with $OPPh_3$ (forming $\mathbf{1.51}^+$)[14] and indeed many of the early examples of alkyl cations were obtained as Lewis base adducts (Section 1.6.1).[28-30] Lewis bases in this Thesis are used to help probe the nature of the cations as well as to allow the formation of isolable complexes. They also add to the general underlying chemistry of these post-metallocene cations. The Lewis bases which have been utilised in this work are $OPPh_3$, py and THF which form stable cations according to Equation 3.4

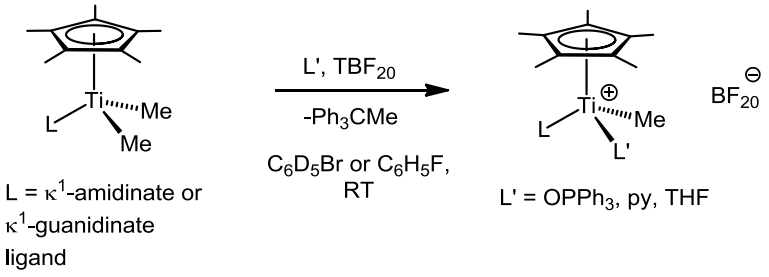

Equation 3.4

Reaction of **1.49** with TBF_{20} in the presence of pyridine yields the immediate, quantitative formation of the C_1 symmetric Lewis base-stabilised species [Cp*Ti-{NC(N^{i}Pr$_2$)Ar^{F_2}}(py)Me][BF_{20}] (**8-[BF_{20}]**) as judged by ^{1}H NMR spectroscopy. Compound **8-[BF_{20}]** was isolated in a 77% yield and characterised by NMR spectroscopy, IR spectroscopy and elemental analysis. The room temperature ^{1}H NMR spectrum showed the expected features, with resonances for Cp* at 1.50 ppm, Ti-Me at 0.78 ppm (^{13}C, 63.9 ppm) and pyridine between 6.50 and 7.50 ppm. The ^{1}H NMR spectrum also features characteristic resonances for the *iso*propyl groups with two septets at 3.36 and 3.79 ppm (C<u>H</u>Me$_2$) and doublets (CH<u>Me$_2$</u>) at 0.79, 1.06, 1.10 and 1.14 ppm. Complex **1.49** displays only two doublets due to its C_s symmetry whereas **8**$^+$ displays four since it has C_1 symmetry. This was also the case for the previously characterised **1.51**$^+$.[14] Over the period of 16 h this compound undergoes decomposition in solution to form a mixture of products. Previously, pyridine adducts of monomethyl cations have been shown to form an orthometallated species over time. For example, previous work by Mountford *et al.* showed that adduct [Ti(N^{t}Bu)(Me$_3$[9]aneN$_3$)(py)Me]$^+$ formed [Ti(N^{t}Bu)(Me$_3$[9]aneN$_3$)(η^2-NC$_5$H$_4$)]$^+$ over two days in solution.[31] Metallation was also seen by Jordan *et al.* in the reaction of [Cp$_2$Zr(THF)Me]$^+$ with pyridine yielding [Cp$_2$Zr(L)(η^2-NC$_5$H$_4$)]$^+$ (L = THF, py).[32] However there is no evidence for the formation of such metallated species amongst the decomposition products of **8**$^+$.

When **1.49** is activated by TBF_{20} in presence of THF the base stabilised species [Cp*Ti{NC(N^{i}Pr$_2$)Ar^{F_2}}(THF)Me][BF_{20}] (**9-[BF_{20}]**) is formed immediately and is quantitative as judged by ^{1}H NMR spectroscopy. Compound **9-[BF_{20}]** was isolated in 85% yield and was characterised by NMR spectroscopy, IR spectroscopy and elemental analysis. The ^{1}H NMR spectrum shows resonances consistent with a C_1 symmetric base stabilised cation; noteworthy signals include Cp* (1.58 ppm) and Ti-Me (0.52 ppm). Another important spectral feature is the splitting of the diastereotopic OCH_2 THF methylene protons into two multiplets (3.40 and 3.26 ppm) as a result of tight binding of the THF to titanium. The $OCH_2C\underline{H}_2$ protons appear as a single multiplet at 1.43 ppm. The ^{13}C-{^{1}H} NMR spectrum contains a Ti-Me signal at 63.6 ppm alongside the other expected resonances. The analogous titanocenium compound was prepared by Bochmann by the oxidation of Cp*$_2$TiMe with $AgBPh_4$; the ^{1}H NMR spectrum was recorded in C_6D_5N and so is difficult to directly compare with the

aforementioned compound **9-[BF_{20}]**.[33] On standing over 16 h $\mathbf{9}^+$ decomposes with additional O-C$\underline{H}_2$ resonances appearing, possibly due to ring opening of the bound THF.

3.2.5 Base-free [Cp*Ti{NC(N^{i}Pr$_2$)Ph}Me][BF_{20}] (10-BF_{20})

In order to study the effects of changing the electronic properties of the amidinate ligand on the subsequent base-free behaviour, the activation of Cp*Ti{NC(N^{i}Pr$_2$)Ph}Me_2 (**2.4**) was investigated. Treatment of the neutral dimethyl complex **2.4** with 1 equiv of TBF_{20} in C_6D_5Br yields a mixture of three products ($\mathbf{10a}^+$, $\mathbf{10b}^+$ and $\mathbf{10c}^+$) which can be identified by the multiple Cp* resonances, amongst others, in the ^{1}H NMR spectrum in a ratio of 2:1:1 ($\mathbf{10a}^+$:$\mathbf{10b}^+$:$\mathbf{10c}^+$). None of these signals correspond to the monomethyl monocation ($\mathbf{29}^+$, Section 3.3), which as discussed Section 3.3 can result from incomplete activation.

The major product ($\mathbf{10a}^+$) has a Cp* resonance at 1.49 with two other minor products with Cp* signals at 1.55 ($\mathbf{10b}^+$) and 1.73 ($\mathbf{10c}^+$) ppm. Signals in the ^{1}H NMR spectrum which correspond to the major product ($\mathbf{10a}^+$) can be assigned to Cp* at 1.49, Ti-Me at 0.74 and isopropyl resonances at 3.45 (C$\underline{H}$Me_2), 1.20 (CH$\underline{Me}_2$) and 0.73 (CH$\underline{Me}_2$) ppm. The position of the Ti-Me signal (^{1}H, 0.74 ppm; ^{13}C, 68.3 ppm) is very similar to that observed for monomeric species $\mathbf{1.26_{mono}}^+$ and as such suggests that the major species in this mixture is also the monomeric cation ($\mathbf{10a}^+$). The presence of only two CH$\underline{Me}_2$ doublets also is consistent with C_s time averaged symmetry which would be expected of a monomeric cation. DOSY NMR performed on the mixture yields a diffusion coefficient of 2.72(4) x 10^{-10} m^2 s^{-1} for $\mathbf{10a}^+$, which is similar to the diffusion coefficient for monomeric cation $\mathbf{1.26_{mono}}^+$.

The species ($\mathbf{10b}^+$) which corresponds to the Cp* resonance at 1.55 ppm has a diffusion coefficient of 2.12(4) x 10^{-10} m^2 s^{-1}; this corresponds to a ratio of volumes with the major product of 2.1 i.e. *ca.* double the size of $\mathbf{10a}^+$. This is consistent with the existence of a dimeric species in solution, whether this is as a result of cation dimerisation or from the existence of solution quadruples as seen by Brintzinger *et al.* with zirconocene systems is unknown.[18] Finally the third species (Cp*, 1.73 ppm, $\mathbf{10c}^+$) has a diffusion constant of 2.63(3) x 10^{-10} m^2 s^{-1} similar to $\mathbf{10a}^+$ which suggests that this species is perhaps a monomeric solvent stabilised species such as [Cp*Ti{NC(N^{i}Pr$_2$)Ph}(C_6D_5Br)Me][BF_{20}] similar to those seen by Baird and

Budzelaar *et al.* with titanocene in CD_2Cl_2.[34] The corresponding Ti-Me signals for **10b**$^+$ and **10c**$^+$are found between -1.0 and 0.5 ppm and are observed as multiple resonances.

An important consideration in these studies is to confirm whether these various species arise from equilibria between the expected monoalkyl cation in various forms or whether it was actually a result of decomposition. This is can be established by derivatising the mixture with a Lewis base, *vide infra*.

3.2.6 [Cp*Ti{NC(N^{i}Pr$_2$)Ph}(L)Me][BF$_{20}$] (L = OPPh$_3$ (11-[BF$_{20}$]), py (12-[BF$_{20}$]) or THF (13-[BF$_{20}$]))

Treatment of the mixture of cationic products (**10a**$^+$, **10b**$^+$ and **10c**$^+$, *vide supra*) with $OPPh_3$ or transient formation of the base-free cation in the presence of $OPPh_3$ results in the immediate and quantitative formation of the same single product, namely [Cp*Ti{NC(N^{i}Pr$_2$)Ph}(OPPh$_3$)Me][BF$_{20}$] (**11-[BF$_{20}$]**). This compound was isolated as a yellow powder in 53% yield and characterised by NMR spectroscopy, IR spectroscopy and elemental analysis.

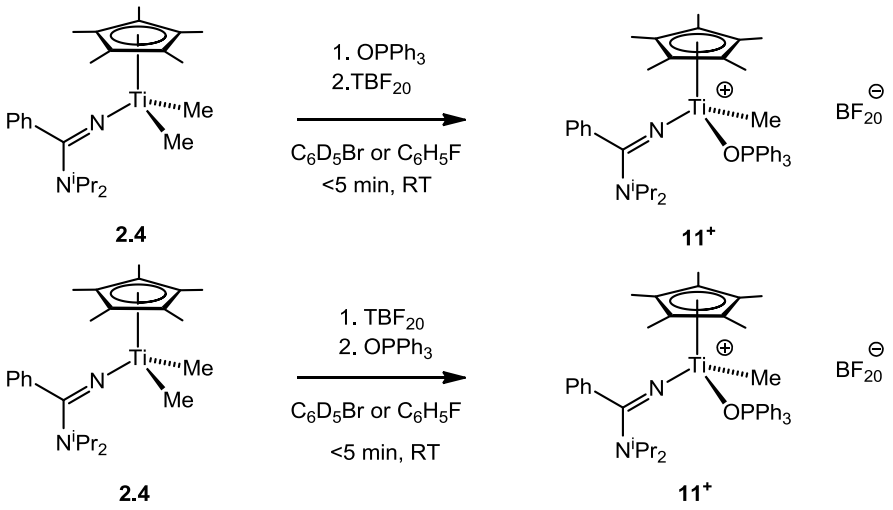

Scheme 3.1 Two alternative reactions to generate **11-[BF$_{20}$]**.

This evidence not only confirmed that the aforementioned mixture of products is not the result of decomposition but also allowed the isolation of a base-stabilised form of the cation. The ^{1}H NMR spectrum (Figure 3.3) of **11**$^+$ is consistent with C_1 symmetry in solution like **1.51**$^+$. The spectrum contains singlet Cp* and Ti-Me resonances at 1.60 ppm and 0.50 ppm, respectively. Other resonances in the spectrum are ligand based and consist of aromatic protons as well as two septets (C<u>H</u>Me$_2$) and four doublets

(CH<u>Me</u>$_2$) for the N^{i}Pr$_2$ moiety. As opposed to the neutral complex (**2.4**)[16] these are sharp at room temperature, presumably due to an increase in steric crowding around the metal centre on the addition of the large OPPh$_3$ molecule; in fact **2.4** shows only two doublets even at 223 K. In the ^{13}C-{^{1}H} NMR spectrum the Ti-Me resonance has a chemical shift of 49.3 ppm and in the ^{31}P-{^{1}H} NMR spectrum O<u>P</u>Ph$_3$ is located at 49.6 ppm. In order to check if there is any possible exchange of bound and free OPPh$_3$ on the NMR timescale a second equivalent of the phosphine oxide was added to **11**$^+$. This resulted in two resonances in ^{31}P-{^{1}H} NMR spectrum which were consistent with bound and free OPPh$_3$ showing there is no ligand exchange on this timescale.

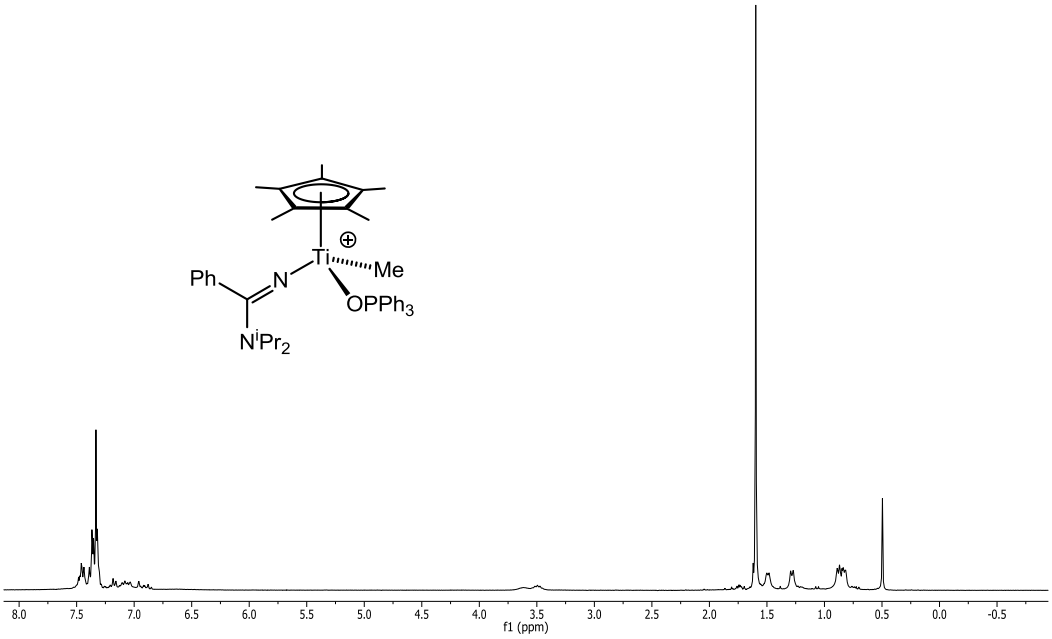

Figure 3.3 ^{1}H NMR spectrum (299.9 MHz, 293K, C_6D_5Br) of **11**$^+$ after isolation.

The pyridine and THF adducts of **10**$^+$ could also be prepared by treatment of **2.4** with TBF$_{20}$ in the presence of the respective Lewis bases to form [Cp*Ti{NC(N^{i}Pr$_2$)Ph}(py)Me][BF$_{20}$] **(12-[BF$_{20}$])** and [Cp*Ti{NC(N^{i}Pr$_2$)Ph}-(THF)Me][BF$_{20}$] (**13-[BF$_{20}$]**) which were isolated in yields of 77% and 85%, respectively. These compounds were characterised by NMR spectroscopy, IR spectroscopy and elemental analysis. The NMR spectra were almost identical to that of **8-[BF$_{20}$]** and **9-[BF$_{20}$]** and decomposition of the two species also takes place akin to **8-[BF$_{20}$]** and **9-[BF$_{20}$]**. The reactivity of these base-stabilised adducts is discussed in Chapter 4.

3.2.7 Base-free [Cp*Ti{NC(NMe$_2$)$_2$}Me][BF$_{20}$] (14-[BF$_{20}$])

Treatment of Cp*Ti{NC(NMe$_2$)$_2$}Me$_2$ (**4**) with 1 equiv of TBF$_{20}$ results in the immediate formation of an insoluble red microcrystalline solid in C_6D_5Br which was isolated in 75% yield. The insolubility of this species prevented obtaining NMR data and therefore **14-[BF$_{20}$]** was characterised by IR spectroscopy and elemental analysis; both were consistent with the expected composition. The insolubility of the cationic species perhaps suggests, based on the solubility of other dimeric species such as **1.26$_{dim}^{2+}$-[BF$_{20}$]$_2$**, that the cation dimerises rapidly to form **14$_{dim}$-[BF$_{20}$]$_2$**.

Leaving the solid to stand in C_6D_5Br for 2 weeks gave rise to the formation of a teal crystalline solid isolated in a yield of 26% and subsequently characterised by elemental analysis, IR spectroscopy and X-ray crystallography consistent with the formation of monocationic dimer [Cp*$_2$Ti$_2$Me$_2${μ-NC(NMe$_2$)$_2$}$_2$][BF$_{20}$] (**15-[BF$_{20}$]**) with approximate C_i symmetry (Figure 3.4). The formation of this nitrogen bridged dimer suggests that the species **14$_{dim}$-[BF$_{20}$]$_2$** is potentially N-bridged (explored using DFT in Section 3.2.19). Compound **15-[BF$_{20}$]** is paramagnetic due to the presence of an unpaired electron so was also characterised by EPR spectroscopy, *vide infra*. The molecular structure of **15$^+$** is shown in Figure 3.4 and selected bond distances and angles are listed in Table 3.1.

This molecule formally contains two *pseudo*-tetrahedral titanium centres, each bonded to a Cp* ligand and terminal methyl group, that are bridged by two tetramethyl-guanidinate ligands. The molecule is formally mixed valence and contains a Ti(III) and a Ti(IV) centre. A similar isoelectronic compound was reported by Mashima *et al.* in 2011 which was synthesised by a one electron reduction of the binuclear imido bridged species [Cp$_2$Ti$_2$Cl$_2${μ-NAr}$_2$] (Ar = 3,5-C$_6$H$_3$(CF$_3$)$_2$) by Cp$_2$Co to yield [Cp$_2$Ti$_2$Cl$_2${μ-NAr}$_2$]$^-$ (**3.7**).[35]

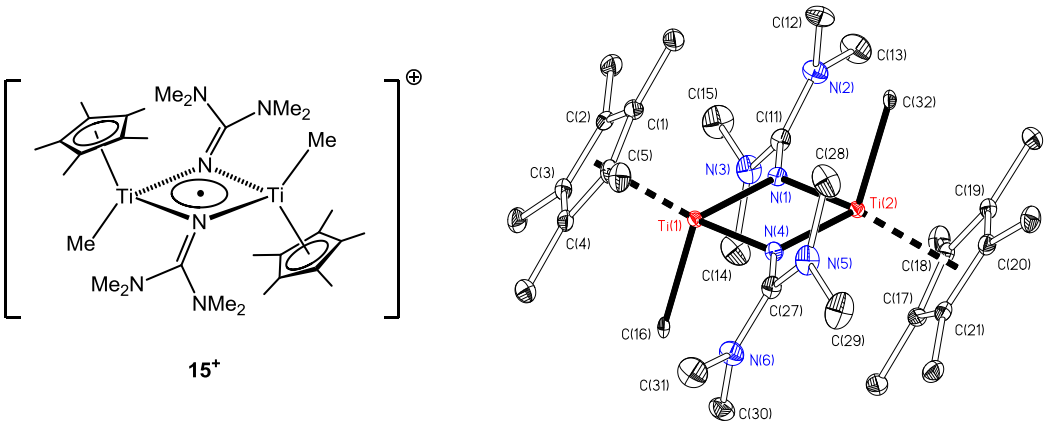

Figure 3.4 Lewis structure (left) and displacement ellipsoid plot (right, 20% probability) of $[Cp^*_2Ti_2Me_2\{\mu\text{-}NC(NMe_2)_2\}_2]^+$ **(15$^+$)**. H atoms omitted for clarity.

Table 3.1 Selected bond lengths (Å) and angles (°) for $[Cp^*_2Ti_2Me_2\{\mu\text{-}NC(NMe_2)_2\}_2]^+$ **(15$^+$)**. $Cp_{cent}(1)$ and $Cp_{cent}(2)$ are the computed Cp* ring carbon centroids.

Ti(1)-$Cp_{cent}(1)$	2.08	$Cp_{cent}(1)$-Ti(1)-C(16)	108.0
Ti(1)-Ti(2)	2.848(1)	$Cp_{cent}(1)$-Ti(1)-N(1)	124.5
Ti(1)-C(16)	2.235(2)	$Cp_{cent}(1)$-Ti(1)-N(4)	124.2
Ti(1)-N(1)	2.0083(19)	Ti(1)-N(1)-C(11)	136.22(17)
Ti(1)-N(4)	2.013(2)	N(1)-Ti(1)-C(16)	102.95(8)
N(1)-C(11)	1.345(3)	N(1)-Ti(1)-N(4)	90.15(8)
N(2)-C(11)	1.358(3)	N(4)-Ti(1)-C(16)	103.71(8)
N(3)-C(11)	1.356(3)	$Cp_{cent}(2)$-Ti(2)-C(32)	107.7
Ti(2)-$Cp_{cent}(2)$	2.08	$Cp_{cent}(2)$-Ti(2)-N(4)	124.2
Ti(2)-C(32)	2.234(2)	$Cp_{cent}(2)$-Ti(2)-N(1)	124.8
Ti(2)-N(1)	2.0174(19)	Ti(2)-N(4)-C(27)	135.62(17)
Ti(2)-N(4)	2.0158(19)	N(4)-Ti(2)-C(32)	104.41(8)
N(4)-C(27)	1.345(3)	N(1)-Ti(2)-C(32)	102.70(8)
N(5)-C(27)	1.354(3)	N(4)-Ti(2)-N(1)	89.80(8)
N(6)-C(27)	1.368(4)	Ti(1)-N(1)-Ti(2)	90.06(7)
Ti(1)-Ti(2)	2.8482(6)	Ti(1)-N(4)-Ti(2)	89.99(8)

The central $[Ti(\mu\text{-}N)_2Ti]$ unit of **15$^+$** contains four Ti-N bonds (Ti(1)-N(1), Ti(1)-N(4), Ti(2)-N(1), Ti(2)-N(4)) which are identical within error (av. 2.014(1) Å); complex **3.7** has a comparable but slightly shorter average Ti-N distance of 1.936(5) Å. The symmetry of this central unit means that the compound is best described as containing

a formally Ti(3.5)-Ti(3.5) delocalised moiety as opposed to the a valence-trapped description; this is also supported by EPR studies (*vide infra*). The Ti-N bonds are longer (av. 2.014(1) Å) than when the ligands are terminally bound (Ti-N, $\mathbf{1.26_{dim}}^{2+}$ = 1.7913(13) Å[14], **5** = 1.8077(18) Å) reflecting the bridging coordination mode of the ligands as well as Coulombic repulsion between the two formally positive titanium centres. The Ti-N bond lengths in $\mathbf{15}^{+}$ are similar to those in the dicationic μ-N amidinate species **3.4** (1.951(3)Å and 2.016(3) Å), introduced in Section 3.2, showing that the addition of the single radical electron does not perturb the bond length to any significant extent.[16]

The Ti(1)-Ti(2) distance in **3.7** was reported to be 2.761(2) Å and was said to be indicative of a Ti-Ti interaction.[35] In $\mathbf{15}^{+}$ the Ti(1)-Ti(2) distance is even longer (2.848(1) Å) which shows that the presence of a Ti-Ti interaction is less likely. The Ti-Ti distance in related Ti(III)-Ti(III) nitrogen-bridged species is 2.60-2.67 Å which is significantly shorter than that in $\mathbf{15}^{+}$.[36-39]AIM analysis performed on the optimised structure $\mathbf{15Q}^{+}$ (see Section 3.2.19) also showed no evidence of bond path or bond critical point.

Complex $\mathbf{15}^{+}$ is paramagnetic so could be characterised by EPR spectroscopy in CD_2Cl_2. This was carried out by Dr Jeffery Harmer at the University of Oxford. The experimental spectrum alongside its simulated spectrum is shown in Figure 3.5. Both experimental and simulated spectra show a very clear five-lined pattern due to hyperfine coupling of the single electron to two nitrogen atoms (^{14}N, I = 1, natural abundance = 99.64%) and also two titanium atoms (^{47}Ti, I = 5/2, natural abundance = 7.28%; ^{49}Ti, I = 7/2, natural abundance = 5.51%). This confirms the unpaired electron is in fact delocalised around the central Ti(μ-N)$_2$Ti unit. This is similar to **3.7** which has a visually identical EPR spectrum.[35] Simulations show the experimental values for g = 1.98, $A_{iso}(^{47}Ti)$ = 13.6 MHz, $A_{iso}(^{14}N)$ = 8.7 MHz. The simulated spectrum shows the total spin density on nitrogen is calculated to be less than 3%. The SOMO (Figure 3.5) of $\mathbf{15Q}^{+}$ was calculated by Betty Coussens, DSM, using DFT methods (B3LYP) on the structure obtained using the M06 level of theory (Section 3.2.19).

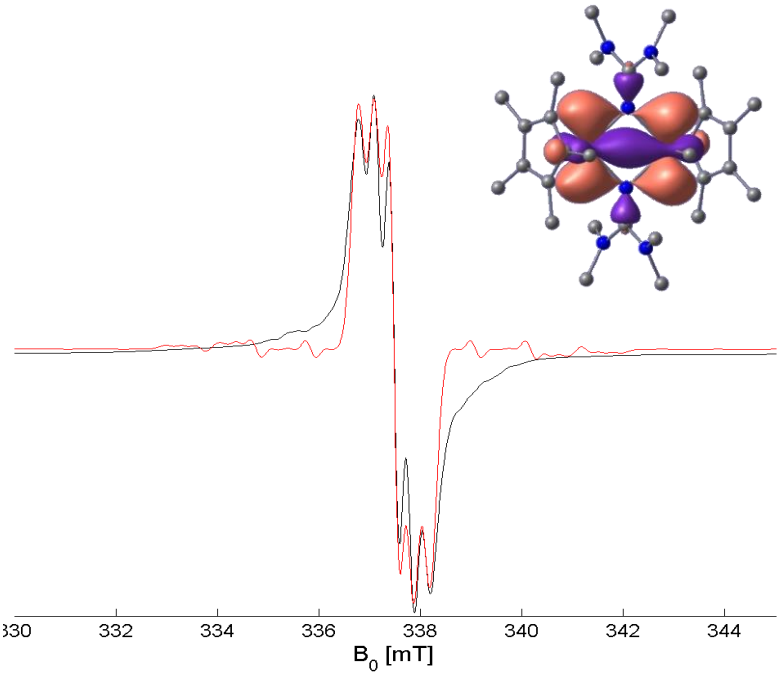

Figure 3.5 EPR spectrum (293 K) of $[Cp^*_2Ti_2\{NC(NMe_2)_2\}\}_2(\mu\text{-}Me)_2]^+$, experimental (black) and simulated (red). The simulations employed the following parameters: g = 1.98, $A(^{47}Ti)$ = 13.6 MHz, $A_\perp(^{14}N)$ = 8.3±0.2 MHz, $A_\parallel(^{14}N)$ = 9.5±2 MHz, with a Gaussian linewidth (f.w.h.h.) of $LW_\perp$ = 7 MHz, $Lw_\parallel$ = 33 MHz. Inset: isosurface of the SOMO for **15Q**$^+$.

The isosurface of the SOMO (Figure 3.5) confirms that the location of the spin density is the Ti(μ-N)$_2$Ti unit; this density is primarily on the titanium atoms with only a small amount found on the nitrogen atoms. The g-value is calculated (B3LYP) to be 1.92 and the hyperfine coupling constants are found to be 10.8 and 7.9 MHz for $A_{iso}(^{47}Ti)$ and $A_{iso}(^{14}N)$ = 8.7 MHz, respectively, in good agreement with the experimental values reported, *vide supra*.

3.2.8 NMR tube scale synthesis of [Cp*Ti{NC(NMe$_2$)$_2$}Me][MeBF$_{15}$] (14-[MeBF$_{15}$])

Since the species **14$_{mono}$-[BF$_{20}$]** seems to rapidly dimerises to form **14$_{dim}$-[BF$_{20}$]$_2$** which is insoluble, NMR data of either compound could not be obtained. In order to acquire NMR data on a related species BF_{15} was used to activate **4**. As discussed previously the anion $[MeBF_{15}]^-$ can have a close interaction with the cation and in this case had the potential to prevent dimerisation and hence rapid precipitation of the cation. Treatment of **4** with 1 equiv BF_{15} in C_6D_5Br gave an immediate colour change from yellow to red. After *ca.* 10 min a red oil formed. However, prior to this, the ^1H

and ^{19}F NMR spectra of **14-[MeBF$_{15}$]** were acquired. The ^{1}H NMR spectrum of **14-[MeBF$_{15}$]** although broad, presumably due to precipitation beginning to occur, showed the expected resonances for NMe_2, Cp*, Ti-Me and [MeBF$_{15}$]$^-$ at 2.47, 1.62, 1.46 and 0.90 ppm, respectively. Horton showed in 1996 that the separation ($\Delta(m,p)$) of the *meta*- and *para*-fluorine ^{19}F chemical shift of [MeBF$_{15}$]$^-$ gives a good indication of the degree of association of the anion.[40] A value of between 3 and 6 implies coordination and less than 3 indicates "non-coordination".

The ^{19}F NMR shifts of **14-[MeBF$_{15}$]** are -132.1 (*o*-C_6F_5), -160.0 (*p*-C_6F_5) and -164.4 (*m*-C_6F_5) ppm. This gives $\Delta(m,p)$ = 4.4 which indicates coordination of [MeBF$_{15}$]$^-$ to the cation. Treatment of **14-[MeBF$_{15}$]** with di*iso*propylcarbodiimide leads to the formation of **43-[MeBF$_{15}$]** in which the insertion of the di*iso*propylcarbodiimide into the Ti-C bond results in the formation of a κ^2-amidinate supported species (discussed further in Section 4.2.3.1) and therefore no vacant site for the anion to bind. Consistent with this $\Delta(m,p)$ for this species is reduced to 2.4 which indicates no coordination of the anion. Thus although **14$_{mono}$-[BF$_{20}$]** could not be characterised by NMR the coordination of the anion in this case allows NMR spectra of a closely related species to be acquired.

3.2.9 [Cp*Ti{NC(NMe$_2$)$_2$}(L)Me][BF$_{20}$] (L = OPPh$_3$ (16-[BF$_{20}$]), py (17-[BF$_{20}$]) or THF (18-[BF$_{20}$]))

In the absence of direct evidence of the base-free alkyl cation **14-[BF$_{20}$]**, several Lewis-base adducts have been synthesised and characterised. In all cases the dimethyl complex must be activated in the presence of the Lewis base as the insoluble base-free form produced immediately on the addition of TBF_{20} is insoluble preventing further reaction.

Reaction of **4** with 1 equiv TBF_{20} in the presence of $OPPh_3$ resulted in the formation of a yellow solution from which [Cp*Ti{NC(NMe_2)$_2$}($OPPh_3$)Me][BF_{20}] (**16-[BF$_{20}$]**) could be isolated in a 72% yield. Compound **16-[BF$_{20}$]** was characterised by NMR spectroscopy, IR spectroscopy, and elemental analysis. The Cp*, NMe_2 and Ti-Me resonances are present as singlets in the ^{1}H spectrum at 1.65, 2.28 and 0.22 ppm, respectively. The Ti-Me resonance in this case is found in the ^{13}C-{^{1}H} NMR spectrum at 48.1 ppm analogous to **11**$^+$ and **1.51**$^+$. The singlet NMe_2 signal is consistent with rapid rotation about the C(sp^2)-NMe_2 and rapid rotation about the Ti-N

bond at room temperature on the NMR timescale. This happens even in the presence of the sterically demanding $OPPh_3$ ligand (^{31}P, 49.4 ppm).

The pyridine adduct [Cp*Ti{NC(NMe_2)$_2$}(py)Me][BF_{20}] (**17-[BF_{20}]**) was prepared in an identical fashion to the $OPPh_3$ adduct and isolated as an orange powder in 78% yield. **17-[BF_{20}]** was characterised by NMR spectroscopy, IR spectroscopy and elemental analysis. The THF adduct **18-[BF_{20}]** was also prepared according to the same procedure and isolated as a yellow powder in 80% yield. Compound **18-[BF_{20}]** was characterised by NMR spectroscopy, IR spectroscopy and elemental analysis. The ^{1}H NMR spectra for **17-[BF_{20}]** and **18-[BF_{20}]** contain analogous resonances for Cp* (1.55 and 1.60 ppm, respectively), NMe_2 (2.43 and 2.37 ppm, respectively) and Ti-Me (0.63 and 0.40 ppm, respectively). The Ti-Me resonances in the ^{13}C-{^{1}H} NMR spectrum for **17-[BF_{20}]** and **18-[BF_{20}]** are 58.1 and 54.5 ppm, respectively. In a similar vein to $\mathbf{9}^+$ and $\mathbf{13}^+$ the proximal THF methylene protons are split into two multiplets (3.69 ppm and 3.48 ppm). Both THF and py adducts decompose akin to those previously detailed. The reactivity of these adducts will be discussed in Chapter 5.

3.2.10 Base-free [Cp*Ti{NC(NMe_2)$_2$}Bn][BF_{20}] (19-[BF_{20}])

The insoluble nature of **14-[BF_{20}]** is likely due to rapid dimerisation of the cation complex to form **14_{dim}-[BF_{20}]$_2$**. Thus to circumvent, this the activation chemistry of the closely related Cp*Ti{NC(NMe_2)$_2$}Bn_2 (**5**) was investigated with TBF_{20} in the hope that when treated with TBF_{20} there was the possibility that the cations would be stabilised by an Ti···C_{ipso} interaction (as discussed in Section 1.6.5 *vide supra*) with the remaining benzyl ligand and therefore stay in solution long enough to be studied by NMR spectroscopy.

The use of the benzyl ligand has precedence in metallocene and post-metallocene chemistry; some examples include the formation of [($C_5Me_4SiMe_2N^tBu$)MBn]$^+$ (M = Ti, Zr),[12, 41] [$Cp_2ZrBn(C_6H_5Cl)$]$^+$,[42] [{$Me_3SiN(CH_2CH_2NSiMe_3)_2$}ZrBn]$^+$ [43] and [CpTi(NMe_2)Bn]$^+$ [44] *via* activation with either TBF_{20} or BF_{15}. These compounds are all stabilised by an η^2-coordination of the benzyl ligand (*ipso*-interaction) as evident by the larger $^{1}J_{CH}$ coupling constants and upfield ^{13}C chemical shift of the benzyl methylene group compared to a non-interacting benzyl ligand (e.g. **5**).

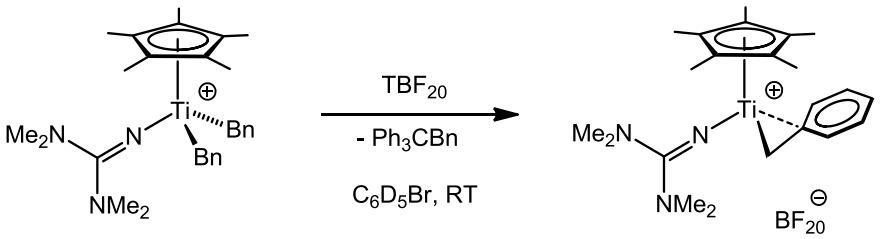

5 **19-[BF_{20}]**

Equation 3.5

Treatment of **5** with TBF_{20} resulted in the quantitative formation of a soluble alkyl cation, [Cp*Ti{$NC(NMe_2)_2$}Bn][BF_{20}] (**19-[BF_{20}]**, Equation 3.5), which was studied and characterised by ^1H , ^{13}C-{^1H}, ^{19}F and ^{11}B NMR spectroscopy in C_6D_5Br. In this case only a single product is formed in quantitative yield by ^1H NMR spectroscopy (Figure 3.6). Unfortunately this product could not be isolated on a preparative scale. There is a single Cp* signal found at 1.58 ppm and a single NMe_2 environment at 2.30 ppm; the single NMe_2 signal is indicative of fast rotation around the amino C(sp^2)-N and Ti-N bonds. The benzyl CH_2 resonance is observed as a singlet at 2.91 ppm, indicative of rapid inversion of stereochemistry at the titanium centre to prevent the methylene protons becoming inequivalent.

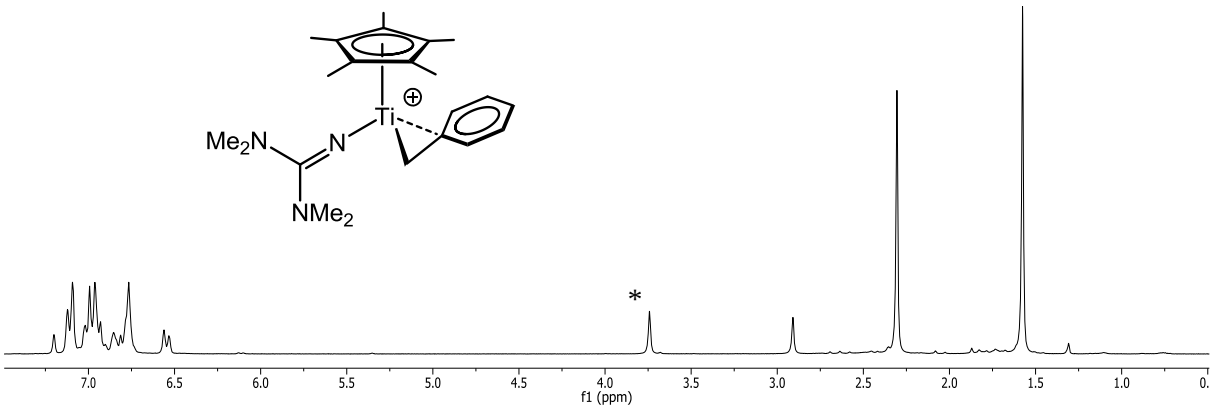

Figure 3.6 ^1H NMR spectrum (299.9 MHz, 293K, C_6D_5Br) of **19**$^+$. $Ph_3CC\underline{H}_2Ph$ labelled '*'.

The presence of an *ipso*-interaction between the benzyl phenyl group and the cationic titanium centre can be established by extraction of the $^1J_{CH}$ methylene coupling constant from the ^1H-coupled ^{13}C-NMR spectrum and as well by the chemical shift of the *ipso*-carbon.[43, 45, 46] The $^1J_{CH}$ for **19**$^+$ is 144.8 Hz (142 Hz in **1.27**) consistent with η^2-coordination of the benzyl ligand; this is reinforced by the upfield shift of 138.7

ppm for the *ipso*-carbon (137.5 ppm in **1.27**). DOSY NMR was carried out on the base-free cation alongside its $OPPh_3$ adduct $[Cp^*Ti\{NC(NMe_2)_2\}Bn\text{-}(OPPh_3)][BF_{20}]$ (**20-[BF$_{20}$]**, *vide infra*) as a standard. The diffusion constant was determined to be higher for **19-[BF$_{20}$]** than **20-[BF$_{20}$]** (2.89(4) x 10^{-10} m^2 s^{-1} and 2.70(3) x 10^{-10} m^2 s^{-1}). Since the diffusion constant is lower for **20-[BF$_{20}$]** the data is consistent with **19**$^+$ being monomeric in solution as expected. The ratio of diffusion constants and volumes are 1.07 and 1.24, respectively, in good agreement with the calculated ratio of volumes which is calculated as 1.28 for the ion pairs. The DFT structure of **19**$^+$ (**19Q**$^+$) has been calculated and is discussed in Section 3.2.18 below.

3.2.11 NMR tube scale synthesis of $[Cp^*Ti\{NC(NMe_2)_2\}Bn(OPPh_3)][BF_{20}]$ (20-[BF$_{20}$])

Activation of **5** in presence of $OPPh_3$ results in the formation of $[Cp^*Ti\{NC(NMe_2)_2\}\text{-}Bn(OPPh_3)][BF_{20}]$ (**20-[BF$_{20}$]**) quantitatively as judged by ^{1}H NMR spectroscopy. Unfortunately this compound decomposed significantly after *ca.* 30 mins and could not be isolated on a preparative scale. The ^{1}H NMR spectrum of **20**$^+$ contains resonances for Cp* (1.68 ppm), NMe_2 (2.37) and CH_2 (2.41 and 1.99 ppm) together with the expected aryl signals (7.45-6.45 ppm).

3.2.12 Base-free $[Cp^*Ti\{NC(N^iBuMe)_2\}Me][BF_{20}]$ (21-[BF$_{20}$])

Treatment of the dimethyl complex $Cp^*Ti\{NC(N^iBuMe)_2\}Me_2$ (**6**) with TBF_{20} in C_6D_5Br leads, in a similar way to **2.4**, to the formation of multiple species in solution (**21a-[BF$_{20}$]**, **21b-[BF$_{20}$]** and **21c-[BF$_{20}$]**), none of which coincide with the monomethyl-bridged monocation **31-[BF$_{20}$]** (see Section 3.3).

After *ca.* 10 min there is near-quantitative formation of a dark red crystalline solid preventing the recording of a ^{13}C-{^{1}H} NMR spectrum. This limited time frame also meant that DOSY data could not be for the sample to determine the relative sizes of the species in solution. It is likely, however, that a similar situation is present as in the previously discussed **10**$^+$. There are three species **21a**$^+$, **21b**$^+$ and **21c**$^+$ in a ratio of 7:5:1.

The ^{1}H NMR spectrum resonances for the major species (**21a**$^+$) can be assigned as $NC\underline{H}_2CH(Me)_2$ (2.71 ppm), $N\underline{Me}$ (2.36 ppm), Cp* (1.69 ppm), $NCH_2C\underline{H}(Me)_2$ (1.47 ppm), Ti-$\underline{Me}$ (0.62 ppm) and $NCH_2CH(\underline{Me})_2$ (0.56 ppm). By analogy with **10a**$^+$ it is likely that **21a**$^+$ is also monomeric. The resonances of **21a**$^+$ are also consistent with C_s

symmetry which is also suggestive of a monomeric species. The other two related species **21b**$^+$ and **21c**$^+$ have Cp* resonances at 1.18 and 1.72 ppm, respectively but could not be fully assigned due to the fast precipitation of the dark red crystalline solid. As with **10**$^+$ there are multiple small Ti-Me resonances between -0.5 and 0.3 ppm.

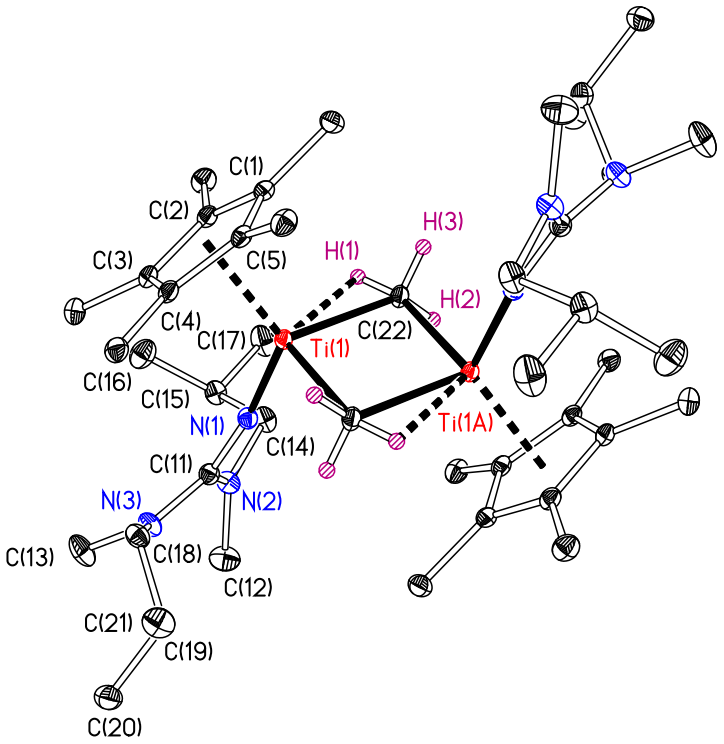

Figure 3.7 Displacement ellipsoid plot (20% probability) of $[Cp^*_2Ti_2\{NC(N^iBuMe)_2\}_2(\mu\text{–}Me)_2]^{2+}$ (**21$_{dim}$**$^{2+}$). H atoms other than those of the Ti(μ–Me)$_2$Ti omitted for clarity. Atoms carrying the suffix 'A' are related to their counterparts by the symmetry operator [1-*x*, 1-*y*, 1-*z*].

Table 3.2 Selected bond lengths (Å) and angles (°) for $[Cp^*_2Ti_2\{NC(N^iBuMe)_2\}_2(\mu\text{–}Me)_2]^{2+}$ (**21$_{dim}$**$^{2+}$). Cp_{cent} is the computed Cp* ring carbon centroid.

Ti(1)-Cp_{cent}	2.05	Cp_{cent}-Ti(1)-C(22)	114.9
Ti(1)-C(22)	2.2574(18)	Cp_{cent}-Ti(1)-C(22A)	114.6
Ti(1)-C(22A)	2.2576(19)	Cp_{cent}-Ti(1)-N(1)	122.8
Ti(1)-N(1)	1.7794(16)	Ti(1)-N(1)-C(11)	169.62(14)
N(1)-C(11)	1.334(2)	N(1)-Ti(1)-C(22)	101.83(7)
N(2)-C(11)	1.353(2)	N(1)-Ti(1)-C(22A)	102.15(7)
N(3)-C(11)	1.355(2)	C(22)-Ti(1)-C(22A)	96.77(6)
Ti(1)···H(1)	2.17(3)	Ti(1)-C(22)-Ti(1A)	83.23(6)

The crystallised species was structurally characterised and revealed the formation of a dimethyl-bridged dication with crystallographic C_i symmetry (**21**$_{dim}^{2+}$). The molecular structure of the cation can be seen in Figure 3.7 and selected bond distances and angles are listed in Table 3.2. The structure of **21**$_{dim}^{2+}$ is consistent with NMR data for **21a**$^{+}$ and the structure has many similarities with that of **1.26**$_{dim}^{2+}$.[14] The Cp*$_{cent}$-Ti(1) distance in the structures of **1.26**$_{dim}^{2+}$ (2.04 Å) and **21**$_{dim}^{2+}$ (2.05 Å) are comparable as are the Ti(1)-N(1) distances (1.791(1) Å and 1.779(2) Å, respectively). It might be expected on face value that the guanidinate supported dimer should have a shorter Ti-N distance but as discussed in Section 2.5, DFT calculations show that the difference should be insignificant. The Ti-Me distances are also similar in both structures: 2.2575(15) and 2.2838(15) Å in **1.26**$_{dim}^{2+}$ and 2.2574(18) and 2.2576(19) Å in **21**$_{dim}^{2+}$. For H(1), H(2) and H(3) located on the bridging methyl group C(22) were located from a Fourier difference map and positionally and isotropically refined. The bridging pentacoordinate methyl groups in **21**$_{dim}^{2+}$ each have a single α-agostic interaction with only one titanium centre. This type of bonding can be described as distorted trigonal bipyramidal (TBP, Figure 3.8) in which one of metal atoms (M) and one of the hydrogens (H_{ax}) occupy the formal axial positions and the other metal and the other two hydrogens (H_{eq}) occupy the formal equatorial positions.

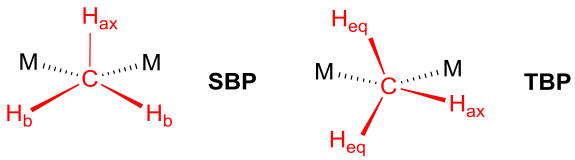

Figure 3.8 Geometries in pentacoordinate bridging methyl groups.

In contrast, **1.26**$_{dim}^{2+}$ contains bridging pentacoordinate methyl groups which have a distorted square base pyramidal (SBP) geometry in which both metal atoms and two hydrogens (2 x H_b) form the base and single hydrogen atom occupies the formal axial site (H_{ax}). These methyl groups each have two α-agostic interactions, one to each titanium centre. The structure of dimeric **21**$_{dim}^{2+}$ was calculated by DFT (as **21Q**$_{dim}^{2+}$) at the M06 level (Dr Betty Coussens) and the methyl groups possessed a SBP geometry similar to that in **1.26**$_{dim}^{2+}$. However, the energy of rotation of the methyl groups to the TBP conformation seen in the X-ray structure was also calculated resulting in only a small increase in energy by 3.8 kJ mol^{-1} showing that the orientation of the methyl groups is reasonably flexible. The Ti(1)···H(1) distance in the X-ray

structure is 2.17(3) Å which is in the correct range for an α-agostic interaction.[14, 47-55] The ^{i}Bu groups are, similar to in **2**, proximal to the metal centre to avoid the steric clash that would take place if they were distal.

3.2.13 [Cp*Ti{NC(N^{i}BuMe)$_2$}(L)Me][BF$_{20}$] (L = OPPh$_3$ (22-[BF$_{20}$]), py (23-[BF$_{20}$]) or THF (24-[BF$_{20}$]))

Even though the dimeric dication $\mathbf{21_{dim}}^{2+}$ could be characterised by X-ray crystallography the full NMR data of the solution species could not be obtained before crystallisation occurred. Equally, as with $\mathbf{10}^{+}$, the mixture had to be tested to see if it contained an assortment of species directly related to the monomethyl cation or whether decomposition of the monoalkyl cation had occurred. Addition of $OPPh_3$ to the mixture of species produced on activation, or activation of **6** in the presence of $OPPh_3$, produced [Cp*Ti{NC(N^{i}BuMe)$_2$}(OPPh$_3$)Me][BF$_{20}$] (**22-[BF$_{20}$]**) which was isolated as a yellow powder in a 64% yield. Compound **22-[BF$_{20}$]** was characterised by NMR spectroscopy, IR spectroscopy and elemental analysis. This evidence shows that the mixture seen on treatment of **6** with TBF_{20} is therefore not a result of decomposition.

The ^{1}H NMR spectrum of $\mathbf{22}^{+}$ shows the expected signals. The Cp* and Ti-Me resonances appear at 1.65 and 0.24 ppm respectively. The introduction of the $OPPh_3$ ligand, and thus C_1 symmetry, results in diastereotopic methylene and methine environments which results in two CH<u>Me</u>$_2$ doublets (0.58, 0.54 ppm), C<u>H</u>Me$_2$ multiplets (1.47 ppm) and two mutually coupled methylene resonances at 2.89 and 2.21 ppm (^{2}J = 12.3 Hz). The based NMe resonance (2.40 ppm) is, however, still a single resonance consistent with rapid rotation about the Ti-N on the NMR timescale. The ^{31}P shift of 48.7 ppm is consistent with bound $OPPh_3$.

The py and THF adducts [Cp*Ti{NC(N^{i}BuMe)$_2$}(py)Me][BF$_{20}$] (**23-[BF$_{20}$]**) and [Cp*Ti{NC(N^{i}BuMe)$_2$}(THF)Me][BF$_{20}$] (**24-[BF$_{20}$]**), respectively, were also synthesised and isolated in yields of 66% and 75%, respectively. The Ti-Me and Cp* resonances for **23-[BF$_{20}$]** are located at 0.67 ppm and 1.59 ppm and are comparable to those for $\mathbf{8}^{+}$, $\mathbf{12}^{+}$, and $\mathbf{17}^{+}$. The NC(N^{i}BuMe)$_2$ signals are analogous for $\mathbf{22}^{+}$ above. Ti-Me (0.43 ppm) and Cp* (1.64 ppm) resonances are also present in the ^{1}H NMR spectrum for $\mathbf{24}^{+}$ in the expected positions. These are equivalent to those discussed in previous Sections for $\mathbf{9}^{+}$, $\mathbf{13}^{+}$ and $\mathbf{18}^{+}$.

3.2.14 Base-free [Cp*Ti{NC(N(Xyl)CH$_2$)$_2$}Me][BF$_{20}$] (25-[BF$_{20}$])

As a well studied κ^1-bound N-donor ligand the base-free cation behaviour of the iminoimimidazolidide dimethyl complex **7** was also investigated to allow comparison to the non-cyclic guanidinate systems. Surprisingly, this type of study has not been reported for these compounds. Treatment of **7** with 1 equiv of TBF$_{20}$ in C_6D_5Br produced a single base-free cation (**25**$^+$) as determined by ^{1}H NMR spectroscopy (Figure 3.9).

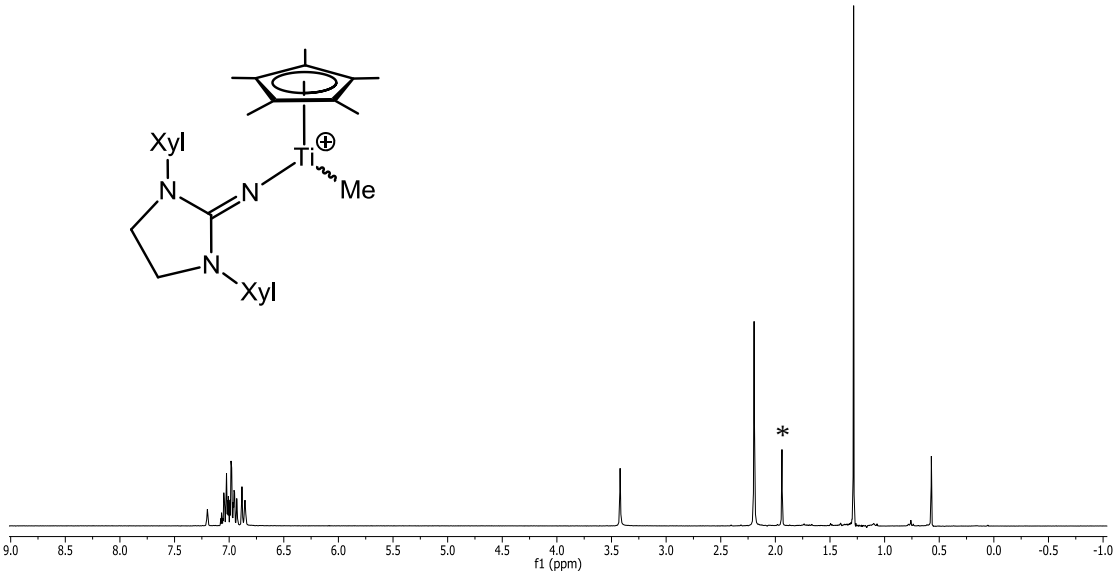

Figure 3.9 ^{1}H NMR spectrum (299.9 MHz, 293K, C_6D_5Br) of X. $Ph_3C\underline{Me}$ labelled '*'.

At room temperature there is fast rotation about the N-C_{ipso} bonds making the $C_6H_3\underline{Me}_2$ groups equivalent on the NMR timescale (2.20 ppm). There is a single Cp* environment at 1.28 ppm and the backbone CH_2 protons are equivalent and situated at 3.41 ppm. The Ti-Me is found at 0.57 ppm and the corresponding ^{13}C-{^{1}H} NMR resonance appears at 68.6 ppm. DOSY NMR experiments were carried out on this cation to determine whether it is monomeric or dimeric in solution. Initially the experiment was performed alongside the $OPPh_3$ adduct (**26-[BF$_{20}$]**) as a benchmark as before. The diffusion coefficient for the base-free cation (**25-[BF$_{20}$]**) is 2.55(3) x 10^{-10} $m^2\,s^{-1}$ and for the $OPPh_3$ adduct (**26-[BF$_{20}$]**) is 2.42(3) x 10^{-10} $m^2\,s^{-1}$. This result shows that the single species in solution when the dimethyl complex and TBF$_{20}$ are mixed stoichiometrically is smaller than the $OPPh_3$ adduct and therefore monomeric. The experimental ratio of volumes in this case is 1.17 (calcd. 1.25).

In the same vein as for **1.26$_{mono}$-[BF$_{20}$]** the monomethyl-bridged monocation (**32-[BF$_{20}$]**, Section 3.3) was also used as a benchmark for relative size. The diffusion constant for **25-[BF$_{20}$]** in this measurement was 2.66(4) x 10^{-10} and for **32-[BF$_{20}$]** was 2.48(2) x 10^{-10} m^2 s^{-1}; the ratio of experimental volumes is 1.23 (calcd. 1.25). This once more supports the existence of a monomeric cation in solution (i.e. **25$_{mono}^+$**).

3.2.15 [Cp*Ti{NC(N(Xyl)CH$_2$)$_2$}(L)Me][BF$_{20}$] (L = OPPh$_3$ (26-[BF$_{20}$]), py (27-[BF$_{20}$]) or THF (28-[BF$_{20}$]))

[Cp*Ti{NC(N(Xyl)CH$_2$)$_2$}(OPPh$_3$)Me][BF$_{20}$] (**26-[BF$_{20}$]**) was prepared by activation of **7** with TBF$_{20}$ in the presence of OPPh$_3$ and was isolated as a yellow powder in a 64% yield. Compound **26-[BF$_{20}$]** was characterised by NMR spectroscopy, IR spectroscopy and elemental analysis. The ^{1}H NMR spectrum contains similar resonances to the base-free cation **25$_{mono}^+$**. There are two resonances for C$_6$H$_3$<u>Me</u>$_2$ due to the introduction of C_1 symmetry in this molecule (2.61 ppm and 2.24 ppm). The backbone CH$_2$ protons, despite being diastereotopic also appear as a single resonance. The coincidence in chemical shift of the CH$_2$ environments is because of their distance from the chiral metal centre. The Ti-Me chemical shift is 0.11 ppm in the ^{1}H NMR spectrum (^{13}C, 49.0 ppm) and the ^{31}P shift for **26$^+$** (O<u>P</u>Ph$_3$) is 48.0 ppm consistent with bound OPPh$_3$.

The py adduct [Cp*Ti{NC(N(Xyl)CH$_2$)$_2$}(py)Me][BF$_{20}$] (**27-[BF$_{20}$]**) was prepared by the activation of **7** with TBF$_{20}$ in presence of py. This reaction was quantitative by ^{1}H NMR spectroscopy and the compound was isolated as a yellow powder in a 60% yield. The Cp* and Ti-Me resonances are found at 1.27 and 0.40 (^{13}C, 62.4 ppm), respectively, in the ^{1}H NMR spectrum. The C$_6$H$_3$<u>Me</u>$_2$ resonances are located at 2.21 and 1.99 ppm and the CH$_2$ groups at 3.37 ppm.

The THF adduct [Cp*Ti{NC(N(Xyl)CH$_2$)$_2$}(THF)Me][BF$_{20}$] (**28-[BF$_{20}$]**) was also prepared by the same route and isolated in 60% yield. The Cp* and Ti-Me resonances are located in the ^{1}H NMR spectrum at 1.37 and 0.21 ppm (^{13}C, 61.8 ppm), respectively. The OCH$_2$ THF signals are split into two multiplets (2.53 and 2.75 ppm) just as in **9**, **13**, **18** and **24**. The C$_6$H$_3$<u>Me</u>$_2$ resonances appear as two singlets at 2.18 and 2.10 ppm again due to the C_1 symmetry of **28$^+$** on the NMR timescale. The methylene backbone of the ligand is present in the ^{1}H NMR spectrum as a singlet at 3.35 ppm.

3.2.16 Cross-over and ^{13}C-labelling experiments

Since **1.26$_{mono}^{+}$** and **25$_{mono}^{+}$** are single monomeric species in solution further investigations were performed on these compounds to provide further understanding of the cations' solution behaviour. As a further probe of the monomeric nature of **1.26$_{mono}^{+}$** and **25$_{mono}^{+}$** in solution the two cations were mixed together in C_6D_5Br at room temperature. If they were to dimerise the presence of mixed dimer [**1.26**-**25**]$^{2+}$ as well as **1.26$_{dim}^{2+}$** and **25$_{dim}^{2+}$** might be expected. However, when the two were mixed the ^{1}H NMR spectrum showed only a resonances belonging to **1.26$_{mono}^{+}$** and **25$_{mono}^{+}$**, and showed no evidence of another species.

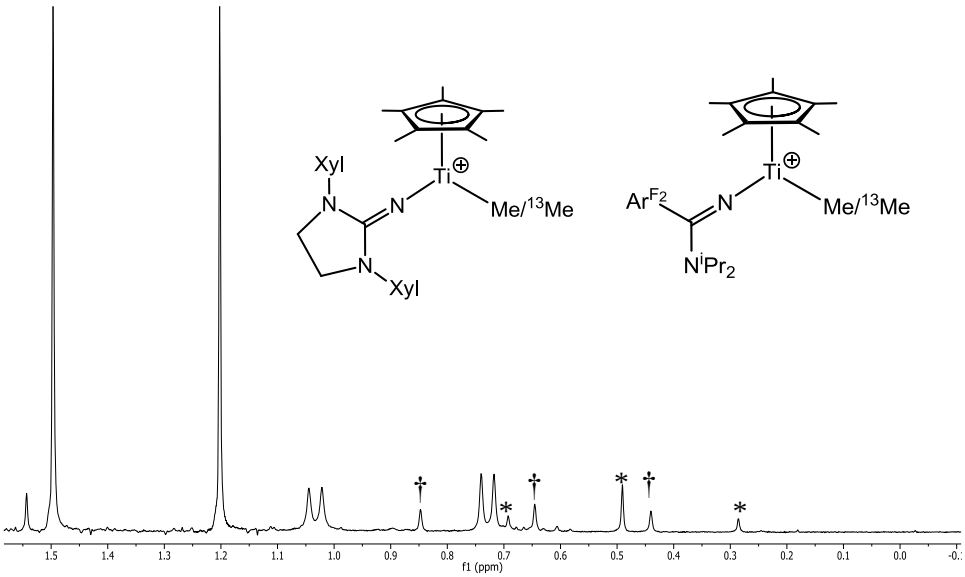

Figure 3.10 ^{1}H NMR spectrum (299.9 MHz, 293K, C_6D_5Br) of **1.26$_{mono}^{+}$**, **1.26_^{13}Me$_{mono}^{+}$**, **25$_{mono}^{+}$** and **25_^{13}Me$_{mono}^{+}$** showing a mixture of ^{13}C labelled Ti<u>Me</u> groups. Ti-<u>Me</u> groups for **25$_{mono}^{+}$** and **25_^{13}Me$_{mono}^{+}$** labelled '*' and for **1.26$_{mono}^{+}$**, and **1.26_^{13}Me$_{mono}^{+}$** labelled '†'.

To test for the possible transient formation of dimers in solution, or the existence of these dimers at low equilibrium concentrations, ^{13}C labelling experiments were carried out; in this study the Ti-<u>Me</u> groups of **1.49** were labelled (**1.49_^{13}Me$_2$**). The labelled cation **1.26_^{13}Me$_{mono}^{+}$** was mixed with non-^{13}C-labelled **25$_{mono}^{+}$** on the NMR tube scale in C_6D_5Br and monitored over time. Initially the presence of 100% ^{13}C in **1.26_^{13}Me$_{mono}^{+}$** splits the corresponding Ti-<u>Me</u> singlet into a doublet whereas in **25$_{mono}^{+}$** Ti-Me is a singlet with the normal (natural abundance) ^{13}C satellites. Over *ca.*

15 minutes the ^{13}C labelled and non-^{13}C-labelled methyl groups exchanged to form a mixture of $\mathbf{1.26_{mono}}^+$, $\mathbf{1.26\_^{13}Me_{mono}}^+$, $\mathbf{25_{mono}}^+$ and $\mathbf{25\_^{13}Me_{mono}}^+$ as observed by ^1H NMR spectroscopy (Figure 3.10). The exchange of methyl groups shows that the monomeric cations interact transiently in solution as exchange of methyl groups must occur *via* the formation of methyl bridged dimers.

3.2.17 DFT studies of base-free alkyl cations

Density functional theory (DFT) calculations were performed by Dr Betty Coussens in order to enhance the understanding of the bonding and general electronic structure in the base-free monoalkyl cations discussed in this Chapter. Group 4 metallocenium and related methyl cations have been of great interest and computational studies on these species have been carried out before.[31, 55-60] Initially the divalent dications of the form $[Cp(L)M]^{2+}$ (M = Ti, L = supporting ligand), analogous to those discussed for model systems in Section 2.5.1, will be discussed.

This Section will concentrate on the effect of the energy and shape on these frontier orbitals on the structures of the monoalkyl cations. To this end the dicationic complexes $[Cp_2Ti]^{2+}$ (**XVI**), $[Cp^*Ti\{NC(N^iPr_2)\}Ph]^{2+}$ (**XVII**) and $[Cp^*Ti\{NC(NMe_2)_2\}]^{2+}$ (**XVIII**) were calculated (B3LYP); the latter two chosen as representative examples of κ^1-amidinate and κ^1-guanidinate supported complexes, respectively.

Before analysis of the electronic structure each of the dications were geometry optimised. All systems feature a bent Cp*-Ti-N geometry as expected. Similar to the model systems detailed previously in this Thesis the frontier orbitals display the expected shapes which are in all cases qualitatively consistent with those described by Lauher and Hoffman in 1975 for bent titanocene and by Mountford, Clot *et al.* also for bent titanocene and isolobal $[Ti(N^tBu)(Me_3[9]aneN_3)]^{2+}$.[31, 61] The lowest unoccupied molecular orbitals (LUMOs) are illustrated in Figure 3.11, together with their corresponding energies. As in Section 2.5.1 the global frontier molecular orbital energy of **XVII** and **XVIII** is higher than **XVI**. The average energies of the LUMO, LUMO+1 and LUMO+2 for **XVIII** is -10.7 eV for **XVII** is -10.3 eV and for **XVI** is -12.8 eV.

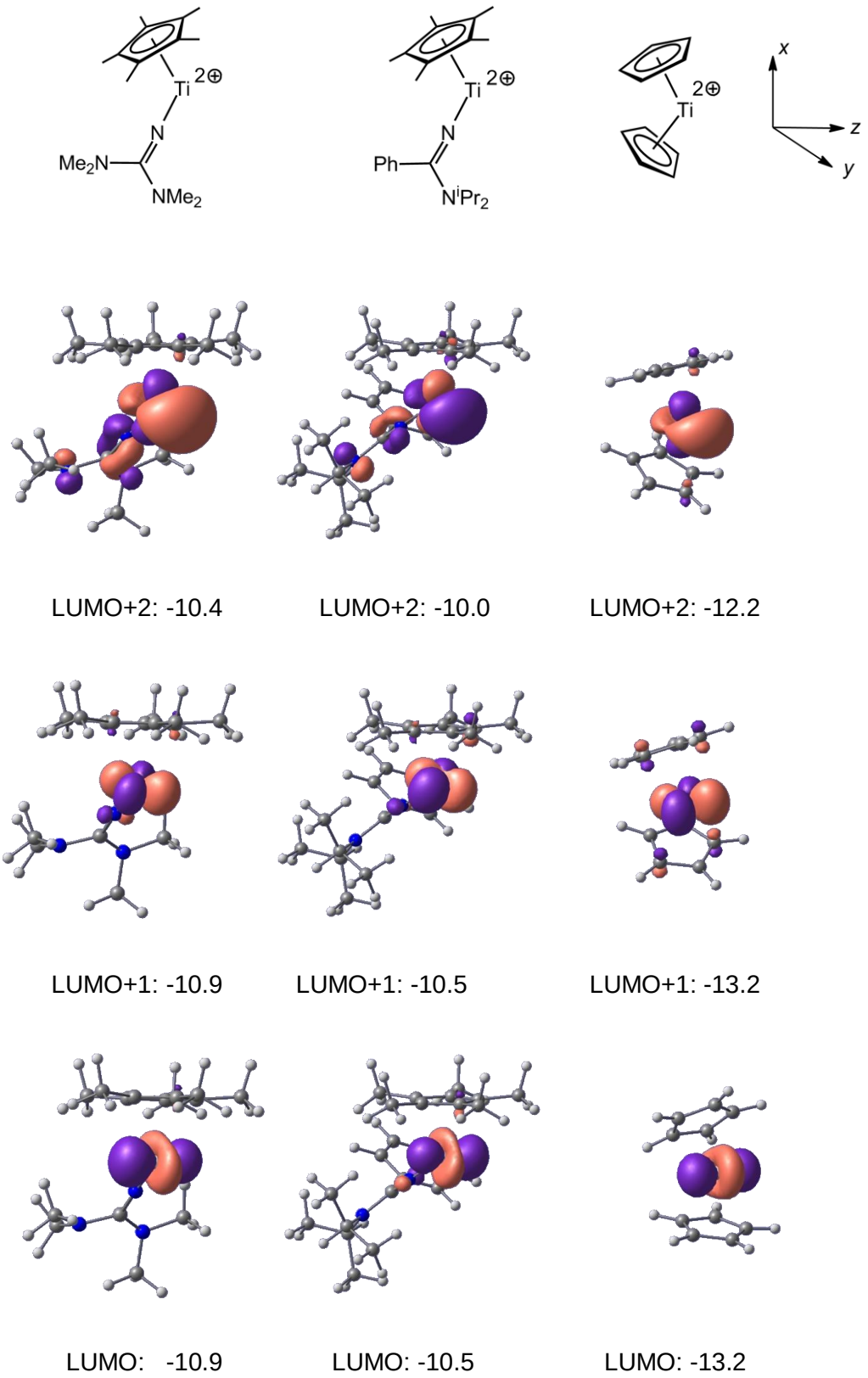

Figure 3.11 DFT calculated (B3LYP) LUMO, LUMO+1 and LUMO+2 (with energies, eV) of dicationic fragments $[Cp^*Ti\{NC(NMe_2)_2\}]^{2+}$ (**XVIII**, left) $[Cp^*Ti\{NC(N^iPr_2)Ph\}]^{2+}$ (**XVII**, centre) and $[Cp_2Ti]^{2+}$ (**XVI**, right).

3.2.18 DFT structures of monoalkyl cations

The energies and arrangement of the frontier orbitals of the dications have an effect on the structure of the monomeric monomethyl cations. Lauher and Hoffman[61] showed using EHT (Extended Hückel Theory) that in the hypothetical compound $[Cp_2TiH]^+$ (**XIX**) the Ti-H bond is not directed along the *z*-axis but is in fact *ca.* 65° off the axis (i.e. α = 65 °, Figure 3.12).

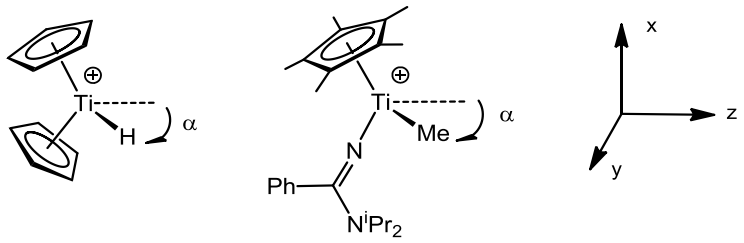

Figure 3.12 Structures of $[Cp_2TiH]^+$ (**XIX**) and $\mathbf{10Q_{mono}}^+$ illustrating the deviation of hydride and methyl groups from the *z*-axis, respectively.

The main interaction of hydride with the dicationic fragment $[Cp_2Ti]^{2+}$ would be expected to be on the *z*-axis where the 1s orbital could overlap with the LUMO+2 and less significantly with the LUMO. However, the LUMO+2 is the highest in energy and so does not interact strongly with the hydride.[61] Distortion of the hydride ligand from the *z*-axis in *yz* plane allows better overlap with both the LUMO, which is polarised along the y-axis, and especially the LUMO+1 which, before distortion, does not have the correct symmetry to interact with the hydride. This alteration of the Ti-H bond leads to an overall general stabilisation of the molecule. DFT calculations on $[Cp_2TiH]^+$ (**XIX**) and $[Ti(NMe)(H_3[9]aneN_3)H]^+$ (**3.8q**) have previously been reported by Mountford, Clot *et al.* with interesting results. **XIX**, in agreement with EHT, was found to be most stable with a distortion of hydride from the *z*-axis (α = 42°). In contrast **3.8q** was found to be most stable when the hydride did not distort at all, i.e. α = 0. The reason for the stability to distortion in **3.8q** is due to a strong polarisation of the LUMO along the *z*-axis as well as a larger energy difference between the LUMO and LUMO+1.[31]

In the aforementioned study it was also shown that in $[Cp_2TiMe]^+$ (**XX**) the distortion of the methyl group from the *z*-axis was significantly less (α = 18°) than in $[Cp_2TiH]^+$ (**XIX**). This is because in **XX** the requirement of the existence of a σ(C-H) interaction

with the LUMO+1 prevents the methyl group distorting too far whereas in **XIX** no such interaction can exist.[31]

In order to probe the structure and electronics of the monomethyl cations for systems $[Cp_2TiMe]^+$ (**XX**), $[Cp^*Ti\{NC(N^iPr_2)Ph\}Me]^+$ (**10Q$_{mono}^+$**) and $[Cp^*Ti\{NC(NMe_2)_2\}Me]^+$ (**14Q$_{mono}^+$**) and how they relate to the frontier orbitals of the dications discussed above, DFT calculations were carried out by Dr Betty Coussens at the M06 level of theory. The M06 level of theory was used in this particular study because it treats dispersion forces well.[62] In Section 3.2.19 dimerisation of these monoalkyl cations will be discussed and the treatment of dispersion forces when considering bridging methyl or N-donor groups was found to be important.[63, 64]

The DFT structure of $[Cp_2TiMe]^+$ (**XX**, Figure 3.13) was calculated (M06) and shows the expected bent metallocene structure (Cp-Ti-Cp = 140°) . The methyl group lies off the *z*-axis with α = 18° which is in excellent agreement with the previously calculated value by Clot (also α = 18°).[31] The energy difference between the LUMO and LUMO+1 in the corresponding dication **XVIII** is only 0.02 eV in this case but is 1.05 eV between the LUMO+1 and LUMO+2. The large energy gap between the LUMO+1 and LUMO+2 gives a large driving force to distort allowing better interactions with the lower energy LUMO and LUMO+1.

On top of this distortion there is also a clear α-agostic interaction in **XX** between the methyl C-H and the titanium centre. This manifests itself geometrically as a short Ti···H distance (2.07 Å) and small Ti-C-H angle (80°) as well as in the lengthening of the agostic bonding C-H compared to the other two (1.14 Å *vs.* 1.10 Å). The Ti···H distance and Ti-C-H angle are in good agreement with those determined previously by Mountford, Clot *et al.* (Ti···H = 2.25 Å and Ti-C-H = 84°).[31] The sum of the angles in CH_2Ti (i.e. not including the α-agostic C-H) group is 354.9° which is very close to the ideal sp^2 angle of 360° and thus the agostic C-H bond has a significant amount of p-character and σ_{CH3} orbital a significant amount of s-character. The s-character in the σ_{CH3} orbital results in a relatively short Ti-C bond (2.07 Å). The α-agostic interaction arises as previously discussed, mainly because of the interaction of the $\sigma_{CH3}$with the LUMO and LUMO+1; rotation of the methyl group allows a better overlap interaction with both the LUMO and LUMO+1. However there is also a bonding contribution from the σ(C-H) interaction with the metal centre. Both the σ(C-H) and σ_{CH3} interactions can be seen in the LUMO+1 and LUMO+4 (Figure 3.14). The LUMO+1 shows the

antibonding interaction of the metal LUMO with the C-H bond and also an antibonding interaction between Ti and σ_{CH3}. The LUMO+4 shows only the interaction between Ti and σ_{CH3}.

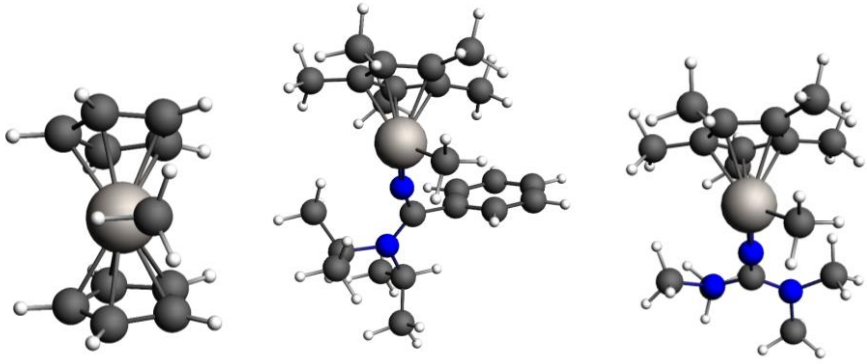

Figure 3.13 DFT (M06) calculated structures of monomeric monomethyl cations **XX** (left), $\mathbf{10Q_{mono}}^+$ (centre) and $\mathbf{14Q_{mono}}^+$ (right).

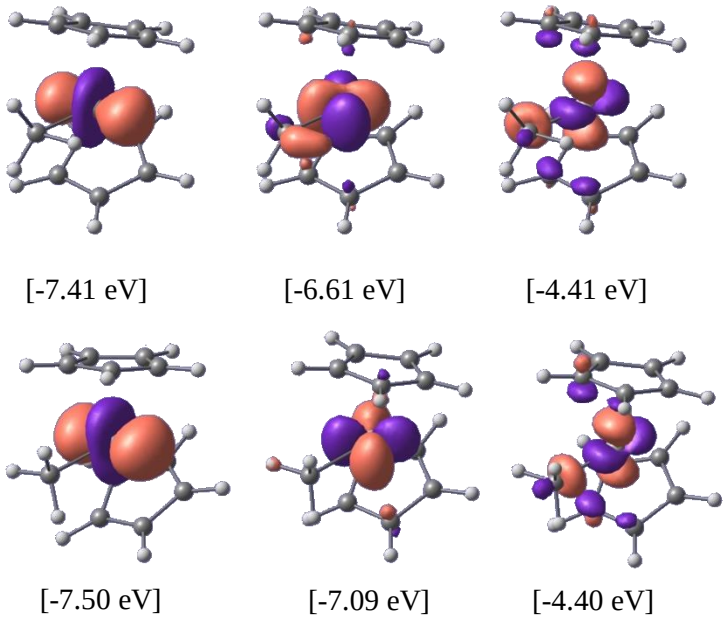

Figure 3.14 Frontier molecular orbitals (left to right: LUMO, LUMO+1 and LUMO+4) for $[Cp_2TiMe]^+$ (**XX**) fully optimised (top) and with methyl group restrained to remove α-agostic interaction (bottom).

To estimate the strength of the agostic interaction in **XX** the structure of $[Cp_2TiMe]^+$ was recalculated but with the three Ti-C-H angles fixed at 109.5° (**XX_109.5**). This led to an increase in energy by 9.7 kJ mol^{-1} which is consistent with previous findings.[31] This is only, however, an estimate of the energy of the agostic interaction since the distortion of the CH_3 group will also be included in this energy. The C-H

bonds in the structure show no lengthening of any of the C-H bonds and the Ti-C distance (2.11 Å) is longer than in **XX** which is expected due to the increased p-character in the bond. The LUMO and LUMO+4 do not change on going from **XX** to **XX_119.5** but the loss of the σ(C-H)-Ti interaction, which is C-H···Ti antibonding, means the LUMO+1 decreases in energy (-6.61 *vs.* -7.09 eV) as expected.

The monomethyl cations $[Cp^*Ti\{NC(N^iPr_2)Ph\}Me]^+$ (**10Q$_{mono}^+$**) and $[Cp^*Ti\{NC(NMe_2)_2\}Me]^+$ (**14Q$_{mono}^+$**) were also calculated using DFT methods (M06). These complexes also showed a similar distortion of the Ti-C bond away from the theoretical *z*-axis (as defined in Figure 3.12) of the molecule at angles of 40° and 42°, respectively. These angles are the optimum angles to allow the best overlap combination with the LUMO, LUMO+1 and LUMO+2 for the greatest stabilisation energy. The Cp-Ti-N angle for both **10Q$_{mono}^+$** and **14Q$_{mono}^+$** is 125°; the Ti-C distances are 2.07 and 2.08 Å, and the Ti-N distances are 1.78 and 1.77 Å, respectively.

In these two systems there is no apparent α-agostic interaction as in **XX**. Also the C-H in the equatorial plane of **10Q$_{mono}^+$** and **14Q$_{mono}^+$** is facing away from the *z*-axis as opposed to towards it as seen in **XX**. This has been seen before in $[Ti(NMe)(H_3[9]aneN_3)Me]^+$ (**3.9q**) by Mountford, Clot *et al.* which showed that because the corresponding dication $[Ti(NMe)(H_3[9]aneN_3)]^{2+}$ (**3.10q**) has globally higher energy MOs compared to $[Cp_2Ti]^{2+}$ making it less electrophilic and thus less likely to form an α-agostic interaction.[31] The global increase in frontier molecular orbital energies of $[Cp^*Ti\{NC(N^iPr_2)Ph\}]^{2+}$ (**XVII**) and $[Cp^*Ti\{NC(NMe_2)_2\}]^{2+}$ (**XVIII**) compared to $[Cp_2Ti]^{2+}$ (**XVI**) has already been demonstrated in Section 3.2.17.

To gain further insight into this the model system $[Cp^*Ti\{NC(NMe_2)Me\}Me]^+$ (**10q$_{mono}^+$**) was investigated which is the same as **10Q$_{mono}^+$** but contains Me and NMe_2 in place of Ph and N^iPr_2. Initially **10q$_{mono}^+$** was optimised and, as in **10Q$_{mono}^+$** and **14Q$_{mono}^+$**, showed no α-agostic interaction but did show a distortion from the *z*-axis (α = 31°). The Ti-N distance is 1.78 Å and the Ti-C distance is 2.07 Å. As in **10Q$_{mono}^+$** and **14Q$_{mono}^+$** the methyl groups is rotated such that the C-H in the equatorial plane is rotated *ca.* 180° from the orientation usually seen in the presence of an α-agostic interaction (**XX**). In this structure the C-H bond lengths are all the same (1.11 Å) and Ti-C bond length is 2.07 Å. Accordingly there is no evidence of the existence of an agostic interaction in the LUMO, LUMO+1 or LUMO+2 of **10q$_{mono}^+$**. The CH_3 group

was constrained to contain the same Ti···H and C-H distances as well as the same Ti-C-H angle as in $[Cp_2TiMe]^+$ so that the energy cost of forcing the α-agostic interaction in $\mathbf{10q_{mono}}^+$ could be estimated. This led to an increase in the electronic energy of 6.8 kJ mol^{-1} overall and shows that presence of an α-agostic interaction in $\mathbf{10q_{mono}}^+$ is energetically unfavourable. The presence of the α-agostic interaction is now present as an antibonding interaction in the LUMO+2 of $\mathbf{10q_{mono}}^+$ in an analogous fashion to **XX**. Thus overall it seems that in $\mathbf{10Q_{mono}}^+$, $\mathbf{14Q_{mono}}^+$ and $\mathbf{10q_{mono}}^+$ that the absence of an agostic interaction is a result of the high energy of the frontier orbitals the corresponding dications.

To check the trend observed for the dications in Section 3.2.17 is also consistent with M06 functional the dications **XVI** and **XXI** were calculated by minimising the corresponding dimethyl compounds, removing the methyl groups and running a single point energy calculation with M06. In both cases the frontier molecular orbitals (i.e. LUMO, LUMO+1 and LUMO+2) are spatially similar to those in Sections 3.2.17 and 2.5.1. If **XVI** using B3LYP and M06 are directly compared the energy levels of the LUMO (-13.0 eV), LUMO+1 (-12.9 eV) and LUMO+2 (-12.0) of using M06 are very similar to those using B3LYP (-13.2, -13.2 and -12.2 eV, respectively) with a systematic difference of *ca.* 0.2 eV between the two. As expected the frontier orbitals of **XXI** are globally higher energy and as such explains why the α-agostic interaction is not present in $\mathbf{10q_{mono}}^+$.

Table 3.3 Energy (eV) of the frontier orbitals (LUMO, LUMO+1 and LUMO+2) of cations $[Cp_2Ti]^{2+}$ (**XVI**) and $[CpTi\{NC(NMe_2)Me\}]^{2+}$ (**XXI**) using the M06 functional.

Compound	LUMO	LUMO+1	LUMO+2	Average
XVI	-13.0	-12.9	-12.0	-12.6
XXI	-10.9	-10.7	-10.4	-10.6

The model hydride species $[Cp_2TiH]^+$ (**XIX**), $[Cp^*Ti\{NC(NMe_2)_2\}H]^+$ ($\mathbf{14Q_{mono}\_H}^+$) and $[Cp^*Ti\{NC(NMe_2)Me\}H]^+$ ($\mathbf{10q_{mono}\_H}^+$) were calculated as a more simple comparison between the different ligand sets since in absence of α-agostic interactions the situation is more straightforward. Initially **XIX** was optimised to give the expected bent metallocene structure (Cp-Ti-Cp, 142°) with α = 61°. The calculated distortion of

the hydride from the *z*-axis is in excellent agreement of that determined by EHT (α = 65°).[61] As found by Mountford, Clot *et al.* this is a significantly greater distortion than for $[Cp_2TiMe]^+$ (**XX**, α = 18°) since there is no requirement in this case for the α-C-H to interact with the relevant frontier orbital. The structure of $\mathbf{14Q_{mono}\_H^+}$ has a Cp-Ti-N angle of 125° and α = 54° and the structure of $\mathbf{10q_{mono}\_H^+}$, which is very similar to $\mathbf{14Q_{mono}\_H^+}$ has a Cp-Ti-N angle of 125° and α = 52°. The larger distortion of hydride from the *z*-axis in **XIX** is consistent with the lower energy LUMO+1 in **XVI** (due to its globally lower energy frontier MOs) which allows for a better interaction with the hydride 1s orbital.

The structure of monobenzyl cation $\mathbf{19Q_{mono}^+}$ was also calculated and featured the expected Ti···C_{ipso} interaction (Figure 3.15) consistent with NMR data, *vide supra*. Benzyl ligands in general are well known to stabilise electron deficient centre *via* a M···C_{ipso} interaction as already discussed.[12, 42, 46, 65] The structure possesses an acute Ti-C-C_{ipso} angle of 78.1° and a Ti···C_{ipso} contact of only 2.34 Å.[46, 66] The Ti-C distance is 2.18 Å and the Ti-N distance is 1.78 Å.

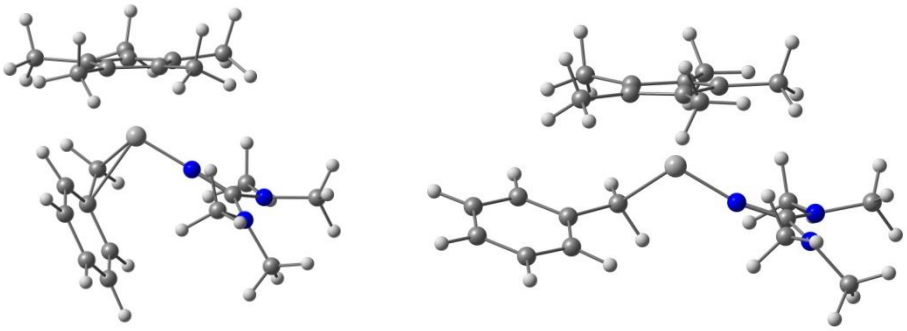

E_{rel} = 0 kJ mol^{-1} E_{rel} = +64.7 kJ mol^{-1}

Figure 3.15 DFT structure (M06) of $\mathbf{19Q^+}$ featuring a Ti···C_{ipso} interaction (left) and $\mathbf{19Q^+\_115}$ with a constrained Ti-C-C angle (right, 115°).

In order to estimate the strength of this interaction the structure was optimised again, but this time with the Ti-C-C angle constrained at 115° ($\mathbf{19Q_{mono}\_115^+}$), i.e. the angle in the crystal structure of **5**. The removal of the Ti···C_{ipso} resulted in a significant increase in electronic energy (64.7 kJ mol^{-1}) going from $\mathbf{19Q_{mono}^+}$ to $\mathbf{19Q_{mono}\_115^+}$ showing that this interaction provides important stabilisation to the benzyl cation. The Ti-N and Ti-C bond lengths in $\mathbf{19Q_{mono}\_115^+}$ are 1.78 and 2.08 Å, respectively. As expected, removal of the *ipso*-interaction causes a decrease in the Ti-C bond length to a value more similar to that seen in $\mathbf{14Q_{mono}^+}$. The energy of stabilisation caused by the

ipso-interaction is large, even when compared to that of the previously reported $[Ti(NMe)(H_3[9]aneN_3)CH_2Ph]^+$ which had a significant stabilisation energy of 25.5 kJ mol^{-1}.[67] The stabilisation energy of the *ipso*-interaction in $[Ti(NMe)(H_3[9]aneN_3)$-$CH_2Ph]^+$ is not as high as in **19Q**$^+$ because the required distortion of the Ti-C bond away from the *z*-axis, as discussed before, is not favourable.

3.2.19 DFT studies on the dimerisation of monoalkyl cations

Further density functional theory calculations were carried out in collaboration with Dr Betty Coussens at DSM. As discussed throughout this Thesis so far, the ability of monoalkyl cations to interact with solvent, anions and themselves is important in understanding their solution behaviour. In the solid state it has been shown by X-ray crystallography that the cations always form dimers. In order to gain some insight into these processes DFT calculations were carried out in order to determine thermodynamic parameters (i.e. ΔE, ΔG, ΔH and ΔS). Since methyl and nitrogen bridging is possible in these compounds the dimerisation processes for both dimethyl- and dinitrogen- bridging were calculated (Scheme 3.2).

The monomers and dimers were optimised to their lowest energy structures and the thermodynamic parameters calculated at 298.15 K. The dimerisation parameters ($\Delta H_{\mu\text{-}N}$, $\Delta H_{\mu\text{-}R}$, $\Delta E_{\mu\text{-}N}$ and $\Delta E_{\mu\text{-}R}$) were calculated by subtraction of twice the monomer from the dimer; the results are summaried in Table 3.4. $\Delta(\Delta H)$ and $\Delta(\Delta E)$ shows the relative enthalpy difference between the nitrogen- and alkyl-bridged dimers for each supporting ligand ($\Delta H_{\mu\text{-}R}$-$\Delta H_{\mu\text{-}N}$ and $\Delta E_{\mu\text{-}R}$-$\Delta E_{\mu\text{-}N}$, repectively). These calculations ignore anion and solvent interactions and so the resultant quantities are relative values and not absolute.

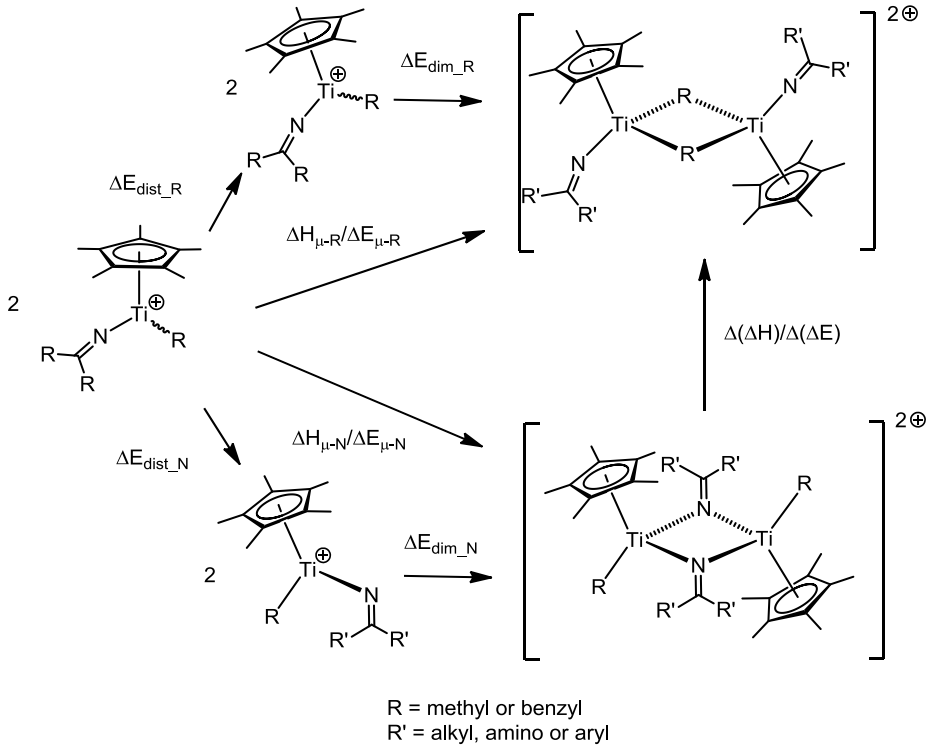

Scheme 3.2 Dimerisation of a monoalkyl cation to either a Me- or N-bridged dimer.

In all cases the entropy of dimerisation is unfavourable as expected. The average ΔS is -320 J mol^{-1} K^{-1}. Overall this entropy effect is large enough such that the ΔG of dimerisation is unfavourable to varying degrees for each system, thus suggesting that the monomeric form is the most favoured in each case. As a general trend this matches well with experimental results which show that monomers are generally the dominant or only species found in solution. Another general pattern that can be observed is that the enthalpy and electronic energy trends are also very similar. Since the calculations found no significant or systematic difference in dimerisation entropy (ΔS typically varied between *ca.* -300 and -350 J mol^{-1} K^{-1}) or in the trends displayed by enthalpy and electronic energy this discussion will focus mainly on the differences in electronic energy (i.e. ΔE).

Table 3.4 Thermodynamic parameters (ΔE, ΔH, TΔS, ΔG, Δ(ΔE) and Δ(ΔH) at 298 K) for dimerisation processes from fully optimised monomers and dimers. $\Delta(\Delta E) = \Delta E_{\mu\text{-}R} - \Delta E_{\mu\text{-}N}$ and $\Delta(\Delta H) = \Delta H_{\mu\text{-}R} - \Delta H_{\mu\text{-}N}$

Dimeric compound	$\Delta E_{\mu\text{-}N}$ or $\Delta E_{\mu\text{-}R}$	$\Delta H_{\mu\text{-}N}$ or $\Delta H_{\mu\text{-}R}$	TΔS	ΔG	Δ(ΔH)	Δ(ΔE)
	kJ mol^{-1}	kJ mol^{-1}	kJ mol^{-1}	kJ mol^{-1}	kJ mol^{-1}	kJ mol^{-1}
1.26Q$_{dim}^{2+}$_μ-Me	-44.4	-29.1	-91.1	62.3	-75.6	-71.7
1.26Q$_{dim}^{2+}$_μ-N	27.3	46.5	-97.0	143.5	0	0
10Q$_{dim}^{2+}$_μ-Me	-31.6	-13.0	-93.6	80.6	-9.8	-7.3
10Q$_{dim}^{2+}$_μ-N	-24.3	-3.2	-105.7	102.6	0	0
10q$_{dim}^{2+}$_μ-Me	-52.3	-39.2	-92.1	52.9	+61.4	+65.1
10q$_{dim}^{2+}$_μ-N	-117.4	-100.6	-110.3	9.7	0	0
14Q$_{dim}^{2+}$_μ-Me	-69.8	-53.2	-88.7	35.3	+43.1	+45.9
14Q$_{dim}^{2+}$_μ-N	-115.7	-96.3	-101.7	5.5	0	0
21Q$_{dim}^{2+}$_μ-Me	-77.6	-68.3	-76.4	8.1	-10.1	+2.3
21Q$_{dim}^{2+}$_μ-N	-79.9	-58.2	-96.3	38.2	0	0
19Q$_{dim}^{2+}$_μ-Bn	160.1	172.5	-78.2	250.8	+47.6	+52.6
19Q$_{dim}^{2+}$_μ-N	107.5	124.9	-99.7	224.5	0	0

To help explain the differences in $\Delta E_{\mu\text{-}R}$, $\Delta E_{\mu\text{-}R}$ and Δ(ΔE) the dimerisation processes can be further split into the distortion of the monomer (endothermic) to the confirmation it has in the dimer (preorganised monomer) and then subsequent dimerisation of two of these preorganised monomers to form the dimer (exothermic). This has been carried out for a selection of compounds, *vide infra*. Again to do this the electronic energies (ΔE), rather than enthalpies, will be considered. The electronic energy change on distorting the monomer into the preorganised monomer (i.e. the geometry of the monomeric fragment in the dimer) is represented by the terms ΔE_{dist_R} and ΔE_{dist_N} and the dimerisation of these fragments by ΔE_{dim_R} and ΔE_{dim_N}. These parameters are shown in Table 3.5.

The $\Delta E_{\mu\text{-}R}$ and $\Delta E_{\mu\text{-}N}$ values for the μ-Me and μ-N forms of $\mathbf{1.26Q_{dim}^{2+}}$ are -44.4 and 27.3 kJ mol^{-1}, respectively. Between the two bridging forms the μ-Me is favoured by 71.7 mol^{-1} which is consistent with the crystal structure obtained, *vide supra*.[14] ΔE_{dist_R} (187.6 kJ mol^{-1}) is significantly less than ΔE_{dist_N} (343.3 kJ mol^{-1}) which is anticipated since distortion of the N-bound ligand from a Ti-N-C angle of 164.2° in the monomer to 136.2° in the pre-organised monomer is expected to require a larger amount of energy, not only because of the distortion of the Ti-N bond but also because of the increase in sterics as the ligand approaches Cp*. This distortion to give the preorganised monomer also causes a change in the Ti-N distance from 1.79 to 2.04 Å. ΔE_{dim_N} (-316.0 kJ mol^{-1}) is larger than ΔE_{dim_R} (-232.0 kJ mol^{-1}) again as anticipated, despite the larger steric interactions involved in the nitrogen bridged dimer, since the formation of two 2c-2e electron bonds rather than a 3c-2e bond in the methyl-bridged dimer is more favourable. Despite the more favourable ΔE_{dim_N} the magnitude of ΔE_{dist_N} is sufficiently larger than ΔE_{dist_R} to make the methyl-bridged dimer most favourable overall in this case.

Removal of the *ortho*-fluorine groups from $\mathbf{1.26Q_{dim}^{2+}}$ to give $\mathbf{10Q_{dim}^{2+}}$ does not make a difference to the order of preference for the μ-Me ($\Delta E_{\mu\text{-}R}$ = -31.6 kJ mol^{-1}) and μ-N ($\Delta E_{\mu\text{-}N}$ = -24.3 kJ mol^{-1}) but it does significantly close the energy gap between the two ($\Delta(\Delta E)$) to only -7.3 kJ mol^{-1}. The removal of the two fluorine atoms is expected to make the μ-N bridged more favourable due to steric reasons. The electronic difference between the two ligands due to the introduction of electronegative fluorine atoms to the ligand is only small so should not be a large contributing factor to the dimerisation energy (see Section 2.5). ΔE_{dist_R} for $\mathbf{10Q_{dim}^{2+}}$**_μ-Me** is comparable to $\mathbf{1.26Q_{dim}^{2+}}$**_μ-Me** (184.4 *vs.* 187.6 kJ mol^{-1}). However, the ΔE_{dist_N} is *ca.* 40 kJ mol^{-1} less costly for $\mathbf{10Q_{dim}^{2+}}$**_μ-N** than $\mathbf{1.26Q_{dim}^{2+}}$**_μ-N** (303.6 *vs.* 343.3 kJ mol^{-1}) because of the lower steric bulk of the ligand NC(N^{i}Pr$_2$)Ph compared to NC(N^{i}Pr$_2$)Ar^{F_2}. The distortion of the Ti-N-C angle associated with ΔE_{dist_N} is 163.6° to 141.4° and the Ti-N bond length change is 1.79 to 2.02 Å which are both less than for $\mathbf{1.26Q_{dim}^{2+}}$**_μ-N**. Also since ΔE_{dim_N} for $\mathbf{10Q_{dim}^{2+}}$**_μ-N** is more favourable than for $\mathbf{1.26Q_{dim}^{2+}}$**_μ-N** (-327.9 *vs.* -316.0) kJ mol^{-1} and ΔE_{dim_R} is less favourable for $\mathbf{10Q_{dim}^{2+}}$**_μ-Me** than $\mathbf{1.26Q_{dim}^{2+}}$**_μ-Me** (-216.0 *vs.* -232.0 kJ mol^{-1}) overall these energy changes cause the smaller $\Delta(\Delta E)$ for $\mathbf{10Q_{dim}^{2+}}$ than $\mathbf{1.26Q_{dim}^{2+}}$. These energy values overall indicate that

the dimer that seems to be present in solution by ^{1}H NMR spectroscopy (Section 3.2.5) should be dimethyl-bridged not nitrogen-bridged.

Table 3.5 Electronic energy values for $\Delta E_{\mu-R}$ or $\Delta E_{\mu-N}$, ΔE_{dist_R}, ΔE_{dist_N}, ΔE_{dim_R} and ΔE_{dim_N} for dimerisation processes to form **1.26Q$_{dim}^{2+}$**, **10Q$_{dim}^{2+}$**, **14Q$_{dim}^{2+}$**, **21Q$_{dim}^{2+}$** and **19Q$_{dim}^{2+}$**.

Compound	ΔE_{dist_R} or ΔE_{dist_N}	ΔE_{dim_R} or ΔE_{dim_N}	$\Delta E_{\mu-R}$ or $\Delta E_{\mu-N}$
	kJ mol^{-1}	kJ mol^{-1}	kJ mol^{-1}
1.26Q$_{dim}^{2+}$_μ-Me	187.6	-232.0	-44.4
1.26Q$_{dim}^{2+}$_μ-N	343.3	-316.0	27.3
10Q$_{dim}^{2+}$_μ-Me	184.4	-216.0	-31.6
10Q$_{dim}^{2+}$_μ-N	303.6	-327.9	-24.3
14Q$_{dim}^{2+}$_μ-Me	139.6	-209.4	-69.8
14Q$_{dim}^{2+}$_μ-N	212.3	-328.0	-115.7
21Q$_{dim}^{2+}$_μ-Me	150.4	-228.0	-77.6
21Q$_{dim}^{2+}$_μ-N	284.9	-364.8	-79.9
19Q$_{dim}^{2+}$_μ-Bn	182.1	-22.1	160.1
19Q$_{dim}^{2+}$_μ-N	402.0	-294.6	107.5

To help give additional insight into the reason for the preference of the μ-Me dimer a model system, with the ligand NC(NMe$_2$)Me (**10q$_{dim}^{2+}$**) was calculated which has a lower steric bulk than either NC(N^{i}Pr$_2$)Ph or NC(N^{i}Pr$_2$)Ar^{F_2}. The effect of this transformation is a switch in preference of the μ-Me (-52.3 kJ mol^{-1}) for the μ-N (-117.4 kJ mol^{-1}) dimer; now the μ-N is favoured by 65.1 kJ mol^{-1}. Thus electronically is seems that amidinate ligands would rather bridge the two titanium centres *via* nitrogen but in the case of **10Q$_{dim}^{2+}$** and **1.26Q$_{dim}^{2+}$** this is prevented by the steric bulk of the ligand. The electronic preference for bridging nitrogen atoms over bridging methyl groups is not surprising given the former gives 2 x 2c-2e bonds whereas the latter is 3c-2e. The more stable μ-N bonding in **10q$_{dim}^{2+}$_μ-N** compared to **10Q$_{dim}^{2+}$_μ-N** and **1.26Q$_{dim}^{2+}$_μ-N** is also reflected in a shortening of the Ti-N bonds. In **10q$_{dim}^{2+}$_μ-N** the av. Ti-N distance is 1.99 Å whereas in **10Q$_{dim}^{2+}$_μ-N** and **1.26Q$_{dim}^{2+}$_μ-N** it is 2.02 and 2.04 Å, respectively.

Compound $\mathbf{14Q_{dim}^{2+}}$, similar to $\mathbf{10q_{dim}^{2+}}$, shows a considerable preference for μ-N (-115.7 kJ mol^{-1}) over μ-Me (-69.8 kJ mol^{-1}) (Δ(ΔE) = 45.9 kJ mol^{-1}). This large Δ(ΔE) shows that it is highly likely that the insoluble dimer $\mathbf{14_{dim}\text{-}[BF_{20}]}$ discussed in Section 3.2.7 is nitrogen-bridged. The small steric bulk of the ligand compared to NC(N^{i}Pr$_2$)Ph and NC(N^{i}Pr$_2$)Ar^{F_2} allows efficient Ti(μ-N)Ti bonding to occur in $\mathbf{14Q_{dim}^{2+}\_\mu\text{-}N}$ (Ti-N, 2.01 Å). ΔE_{dist_R} and ΔE_{dist_N} are, in this case, significantly lower than in $\mathbf{10Q_{dim}^{2+}}$ and $\mathbf{1.26Q_{dim}^{2+}}$, although, as before ΔE_{dist_N} is less favourable than ΔE_{dist_R} (139.6 vs. 212.3 kJ mol^{-1}). The distortion associated with ΔE_{dist_N} in this case is from a Ti-N bond length of 1.77 Å and Ti-N-C bond angle of 164.9° in the monomer to 2.01 Å and 133.2° in the preorganised monomer. The small Ti-N distance in the preorganised monomer (and hence dimer) is a result of the low steric bulk of NC(NMe$_2$)$_2$. ΔE_{dist_N}, likely due to the lower steric bulk of NC(NMe$_2$)$_2$, is appreciably lower than in $\mathbf{10Q_{dim}^{2+}\_\mu\text{-}N}$ and $\mathbf{1.26Q_{dim}^{2+}\_\mu\text{-}N}$ but ΔE_{dim_N} is comparable to $\mathbf{10Q_{dim}^{2+}\_\mu\text{-}N}$ and $\mathbf{1.26Q_{dim}^{2+}\_\mu\text{-}N}$ which makes the overall $\Delta E_{\mu\text{-}N}$ particularly favourable in this case (-115.7 kJ mol^{-1}). $\Delta E_{\mu\text{-}R}$ is this case is also more favourable in this case than in $\mathbf{10Q_{dim}^{2+}\_\mu\text{-}Me}$ and $\mathbf{1.26Q_{dim}^{2+}\_\mu\text{-}Me}$ but not as favourable as $\Delta E_{\mu\text{-}N}$.

In order to validate the DFT data against another crystallographically characterised species the electronic energy difference between the μ-N and μ-Me dimers for the mixed valence species $\mathbf{15Q^{+}}$ was calculated; this also showed a preference for the μ-N bridged by Δ(ΔE) = 69.7 kJ mol^{-1} (Δ(ΔH) = 65.2 kJ mol^{-1}) consistent with the structural data in Section 3.2.7. The larger Δ(ΔE) in this case compared to $\mathbf{14Q_{dim}^{2+}}$ can be partly traced to the energy of the α-SHOMO of the μ-N compound which is *ca.* 10 eV more stable than in the μ-Me compound. Also the slight lengthening of the Ti-N bonds (2.02 Å *vs.* 2.01 Å) in $\mathbf{15Q^{2+}\_\mu\text{-}N}$ compared to $\mathbf{14Q_{dim}^{2+}\_\mu\text{-}N}$ should result in a steric relief on the μ-N ligands more than the steric relief on the μ-Me ligands going from $\mathbf{14Q_{dim}^{2+}\_\mu\text{-}Me}$ (2.25 Å) to $\mathbf{15Q^{2+}\_\mu\text{-}N}$ (Ti-Me, 2.26).

Complex $\mathbf{21Q_{dim}^{2+}}$, with the introduction of ^{i}Bu groups on the amine nitrogens, shows a slight preference for the μ-N dimer (-79.9 kJ mol^{-1}) over the μ-Me (-77.6 kJ mol^{-1}) when considering electronic energies (Δ(ΔE) = +2.3). This small difference, *cf.* $\mathbf{14Q_{dim}^{2+}}$, is due to introduction of increased steric bulk in the ligand compared to NC(NMe$_2$)$_2$. In this case, however, when considering the enthalpy values instead the μ-Me structure is more favoured than the μ-N structure, although not by a significant amount (-10.1 kJ mol^{-1}). The crystal structure of $\mathbf{21_{dim}^{2+}}$ (Section 3.2.12) shows μ-Me

bridging which is more consistent with analysis of the enthalpy rather than electronic energy values.

ΔE_{dist_N} (284.9 kJ mol^{-1}) in this case has increased significantly from that in **14Q$_{dim}^{2+}$_μ-N** (212.3 kJ mol^{-1}) due to an increase in steric hinderance and although ΔE_{dim_N} has also become slightly more favourable the increase in ΔE_{dist_N} means that $\Delta E_{\mu-N}$ is less favourable than in **14Q$_{dim}^{2+}$_μ-N** (-79.9 *vs.* -115.7 kJ mol^{-1}). The distortion associated with ΔE_{dist_N} in this case is from a Ti-N bond length of 1.77 Å and Ti-N-C bond angle of 171.0° in the monomer to 2.02 Å and 133.5° in the preorganised monomer. ΔE_{dist_R} increases slightly on going from **14Q$_{dim}^{2+}$_μ-Me** to **21Q$_{dim}^{2+}$_μ-Me** (139.6 *vs.* 150.4 kJ mol^{-1}) but the ΔE_{dim_R} is more favourable for **21Q$_{dim}^{2+}$_μ-Me** (-228.0 vs. -209.4 kJ mol^{-1}) which overall causes $\Delta E_{\mu-R}$ to be more favourable for **21Q$_{dim}^{2+}$_μ-Me** than **14Q$_{dim}^{2+}$_μ-Me** (-77.6 *vs.* -69.8 kJ mol^{-1}). This overall decrease in $\Delta E_{\mu-R}$ and increase in $\Delta E_{\mu-N}$ gives rise to the small $\Delta(\Delta E)$ value (2.3 kJ mol^{-1}) in this case.

The dimerisation energies of **19Q$_{dim}^{2+}$** were also calculated and showed that the stabilisation of the alkyl cation by the *ipso*-interaction, *vide supra*, makes dimerisation *via* μ-N extremely unfavourable ($\Delta E_{\mu-N}$ = 107.5 kJ mol^{-1}) consistent with experimental observation. The formation of the benzyl bridged dimer ($\Delta E_{\mu-R}$ = 160.1 kJ mol^{-1}) is even more unfavourable than for the nitrogen bridged dimer. The energy difference between μ-N and μ-Bn dimer is +52.6 kJ mol^{-1} which is higher than between the μ-N and μ-Me in **14Q$_{dim}^{2+}$** (+45.9 kJ mol^{-1}). This effect is presumably due to the larger steric bulk of the benzyl ligand which would make bridging more unfavourable compared to methyl groups. Possibly for this reason existence of structurally characterised benzyl-bridged bimetallic transition metal species limited with only a few that have been structurally characterised.[68-73] Interestingly the structure of dibenzyl bridged **19Q$_{dim}^{2+}$_μ-Bn** is not bridged by symmetrical 2c-3e interactions but actually *via* two agostic interactions between the benzyl methylene groups on one monomer and the titanium centre on the other monomer. The Ti-CH_2 bond lengths are 2.20 Å for both monomers whereas the distance between the benzyl methylene carbon on one monomer and the titanium on the other monomer is significantly different (2.58 Å). The Ti···H distances are 2.13 and 2.17 Å for one monomer and 2.14 and 2.26 Å for the other consistent with agostic interactions. This type of asymmetric bridging with benzyl groups is not unprecented, for example in the structurally characterised

complex $[Mo_2Cp_2(\mu\text{-}CH_2Ph)(\mu\text{-}PCy_2)(CO)_2]$ the benzyl group is bound to one of the molybdenum atoms though a normal 2c-2e single bond whilst being involved in an agostic interaction with the other.[70]

ΔE_{dist_R} in this case is larger **$19Q_{dim}^{2+}$_μ-Bn** than **$14Q_{dim}^{2+}$_μ-Me** (182.1 *vs.* 139.6 kJ mol^{-1}) of which the breaking of the Ti···C_{ipso} interaction is likely a considerable portion. ΔE_{dist_N} (402 kJ mol^{-1}) is also significantly higher than ΔE_{dist_R} as it involves both distortion of the Ti-N-C bond angle (177.4° to 135.8°) and bond length (1.78 to 2.00 Å), as well as breaking the *ipso*-interaction. ΔE_{dist_N} is also higher than in **$14Q_{dim}^{2+}$_μ-N**. ΔE_{dim_R} for **$19Q_{dim}^{2+}$_μ-Bn** is low (-22.1 kJ mol^{-1}) because as discussed above it does not form a 2c-3e symmetrical benzyl bridged dimer. ΔE_{dim_N} (-228.0 kJ mol^{-1}) although larger than ΔE_{dim_R} is still not close to the compensating the energy of ΔE_{dist_N}. All these parameters add up to the unfavourable $\Delta E_{\mu\text{-}R}$ and $\Delta E_{\mu\text{-}N}$ values for this compound. Overall the difference between $\Delta E_{\mu\text{-}R}$ and $\Delta E_{\mu\text{-}N}$ in **$19Q_{dim}^{2+}$** and **$14Q_{dim}^{2+}$** explains why the former dimerises rapidly and precipitates whereas the latter will stay in solution as a monomer.

This set of calculations shows that for the studied compounds the steric bulk of the ligands is the most important factor when determining whether a dimer will be methyl or nitrogen bridged. This effect is consistent with previous work carried out by Mountford *et al.*; half-sandwich TACN-supported imido cations are encouraged to dimerise through the imido moiety by decreasing steric bulk on the ligands.[74-76] Also work carried out by Dr. Richard Scott in the Mountford group as previously discussed (Section 3.2) showed that when using either a larger zirconium (**3.5**) or hafnium (**3.6**) metal centre less sterically demanding Cp based ligand with titanium (**3.4**), nitrogen bridged dimers can be isolated and crystallographically characterised.[77] These calculations have also showed that entropy effects are significant in the dimerisation process and assists in explaining why monomers are the dominant species in solution.

3.3 Monomethyl-bridged bimetallic species

In 1994 Bochmann showed that reaction of Cp_2ZrMe_2 at -60 °C with TBF_{20} proceeds to form the monomethylbridged monocation (**3.10**, Figure 3.16) even in the presence of a full equivalent of TBF_{20}.[78] Warming to -40 °C does, however, allow the reaction to proceed to completion to yield the base-free cation. The stability of zirconocene monomethyl-bridged monocations was shown to be dependent on the nature of the

cyclopentadienyl ligand, for example complex $Me_2Si(Ind)_2ZrMe_2$ forms the corresponding monomethyl-bridged dimer which is stable in the presence of excess TBF_{20} even at 20 °C. The species $[(Ind)_4Ti_2Me_2(\mu\text{-}Me)]^+$ has also been observed as an intermediate in the activation of Ind_2TiMe_2 with 1 equiv $[Ph_3C]^+$ [79] and Marks *et al.* have observed the analogous thorium species $[Cp^*_4Th_2(\mu\text{-}Me)Me_2]^+$.[80] In a general sense the synthesis of monomethyl-bridged monocations can be achieved by the treatment a dialkyl complex with 0.5 equivs of activating agent. These compounds can be thought of as a base-free monoalkyl cation (Chapter 3) trapped by neutral dialkyl complex.

Work by Piers *et al.* also showed that the formation monomethyl-bridged monocations were possible using κ^1-ketimide-supported half-sandwich complexes. These decomposed over the period of 6-12 hours to release methane and led to the formation of CH_2-bridged bimetallic compounds.[2] Analogous reactivity has been reported by Bochmann *et al.* in 1994 who showed that activation of zirconocene complex $\{CpZr(CH_3)_2\}_2(\eta^5\text{:}\eta^5\text{-}C_{10}H_8)$ with 0.5 equivs of TBF_{20} at -60 °C resulted in the immediate formation of methylene bridged species **3.11** displayed in Figure 3.16. This is interesting since complex **3.10** does not show this reactivity. Monomethyl-bridged complexes like **3.9** must dissociate before catalysis can occur. However methylene bridged complexes like **3.11** have been shown to polymerise albeit with lower productivities than $[Cp_2ZrMe]^+$.[81]

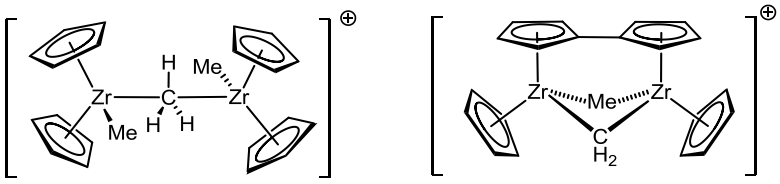

3.10 **3.11**

Figure 3.16 Homobimetallic cations.

It has already been shown by collaborative work between Lanxess Elastomers and Mountford in 2010 has shown that treatment of compound **1.49** with 0.5 equivs of TBF_{20} leads to the quantitative formation of monomethyl-bridged monocationic species $[Cp^*_2Ti_2\{NC(N^iPr_2)Ar^{F_2}\}_2(\mu\text{-}Me)Me_2][BF_{20}]$ (**1.50**$^+$, Scheme 1.4). Alternatively the same result could be achieved by addition of the neutral dimethyl complex **1.49** to cation **1.26**$_{\mathbf{mono}}^+$. This species could not be isolated but was characterised by ^{1}H NMR spectroscopy. In this case there is no evidence of separated

1.49 and $\mathbf{1.26_{mono}}^+$. In contrast to the higher symmetry metallocene monomethyl-bridged bimetallic species, cation $\mathbf{1.50}^+$ exists as diastereoisomers in solution.[14] This is also the case for the ketimide system reported by Piers *et al.*[2] In the ^{1}H and ^{13}C NMR spectra the existence of diastereoisomers can be identified when there are two resonancess for each environment. This Section will describe the formation and characterisation of these monomethyl-bridged species for the other κ^1-amidinate and κ^1-guanidinate complexes relevant to this work.

3.3.1 NMR tube scale synthesis and characterisation of $[Cp^*_2Ti_2(L)_2(\mu\text{-}Me)Me_2][BF_{20}]$ (L = $NC(N^iPr_2)Ph$ (29-$[BF_{20}]$), $NC(NMe_2)_2$ (30-BF_{20}) or $NC(N^iBuMe)_2$ (31-$[BF_{20}]$))

Treatment of **2.4** with 0.5 equivs of TBF_{20} on the NMR tube scale yields the quantitative formation of the monomethyl-bridged bimetallic species $[Cp^*_2Ti_2\{NC(N^iPr_2)Ph\}_2(\mu\text{-}Me)Me_2][BF_{20}]$ (**29-[BF_{20}]**) which exists as a mixture of diastereoisomers (Equation 3.6) in a ratio of 3:2. Although it is not possible to assign which set of signals belong to which isomer the major diastereoisomer has been labelled $\mathbf{29a}^+$ and the minor diastereoisomer $\mathbf{29b}^+$ in NMR characterisation. Compound **29-[BF_{20}]** has been characterised by ^{1}H, ^{19}F, ^{11}B and ^{13}C-{^{1}H} NMR spectroscopy but could not be isolated cleanly due to its sensitivity. Addition of a further 0.5 equivs of TBF_{20} gave complete conversion to the same product mixture of $\mathbf{10a}^+$, $\mathbf{10b}^+$ and $\mathbf{10c}^+$discussed in Section 3.2.5. Cation $\mathbf{29}^+$ was stable in C_6D_5Br at room temperature for *ca.* 1 h before decomposition became significant. Decomposition led to a mixture of products and not the clean formation of CH_2 bridged species observed in related ketimide and metallocene systems.

The ^{1}H NMR spectrum of $\mathbf{29}^+$ is consistent with the existence of two diastereoisomers $\mathbf{29a}^+$ and $\mathbf{29b}^+$ *cf.* $\mathbf{1.50}^+$. Unlike $\mathbf{1.50}^+$ the Cp* (1.54 ppm) and Ti-Me (0.35 ppm) resonances for the two diastereoisomers are overlapping. The Ti(μ-Me)Ti resonances can be distinguished for each diastereoisomer and shows that they exist in a ratio of 3:2. The terminal Ti-Me signals for $\mathbf{29a}^+$ and $\mathbf{29b}^+$ are found at -0.96 and -0.84 ppm, respectively. The $NC(N^iPr_2)Ph$ ligand shows some fluxional behaviour at room temperature which leads to slight broadening of the C<u>H</u>Me_2 (3.56) and CH<u>Me_2</u> (1.46, 1.25, 0.81). Cooling to -35°C in C_6D_5Br (close to the freezing point) does not lead to the "freezing out" of these signals. As with $\mathbf{1.50}^+$ there is no evidence of the existence of dimethyl complex **2.4** or monoalkylcation $\mathbf{10}^+$ in solution. Addition of 1 equiv

$OPPh_3$ to $\mathbf{29}^+$ results in the formation of the dimethyl complex **2.4** and $OPPh_3$ adduct $\mathbf{11}^+$.

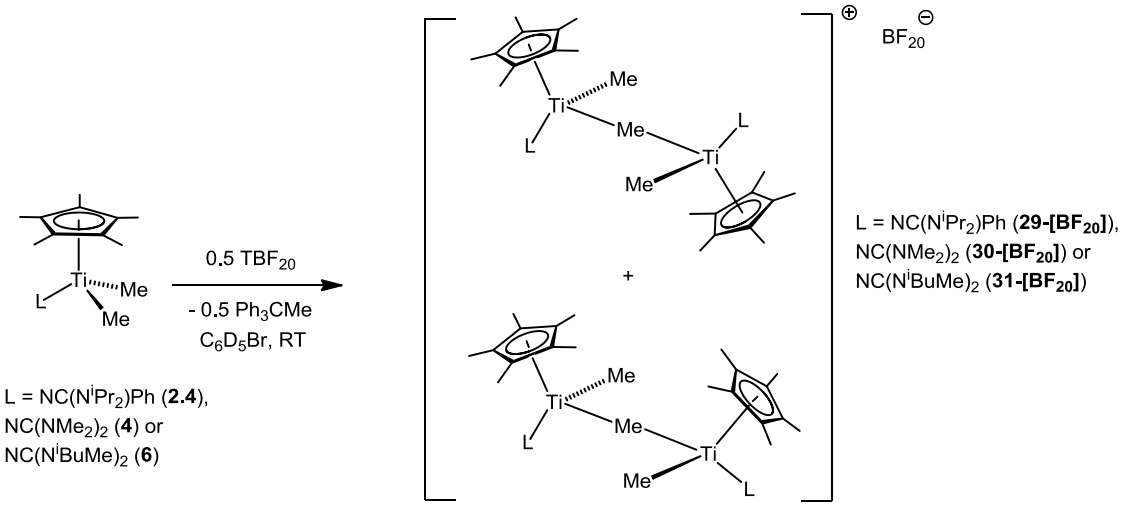

Equation 3.6

The activation of κ^1-guanidinate complexes **4** and **6** with 0.5 equivs TBF_{20} resulted in the immediate and quantitative formation of $[Cp^*_2Ti_2\{NC(NMe_2)_2\}_2(\mu\text{-}Me)Me_2][BF_{20}]$ (**30-[BF_{20}]**) and $[Cp^*_2Ti_2\{NC(N^iBuMe)_2\}_2(\mu\text{-}Me)Me_2][BF_{20}]$ (**31-[BF_{20}]**), respectively, by ^1H NMR spectroscopy (Equation 3.6). Neither **30-[BF_{20}]** or **31-[BF_{20}]** could be isolated on a preparative scale but were characterised by ^1H, ^{13}C, ^{19}F NMR spectroscopy. Both cations $\mathbf{30}^+$ and $\mathbf{31}^+$ exist as a mixture of diastereoisomers in a ratio of 3:2 just as with $\mathbf{29}^+$. The treatment of $\mathbf{30}^+$ and $\mathbf{31}^+$ with 1 equiv $OPPh_3$ led to the formation of the corresponding dimethyl complexes (**4** and **6**, respectively) and $OPPh_3$ stabilised cations ($\mathbf{16}^+$ and $\mathbf{22}^+$, respectively). As with $\mathbf{29}^+$, $\mathbf{30}^+$ and $\mathbf{31}^+$ decompose over *ca*. 1 h to form a mixture of products. Interestingly as opposed to **14-[BF_{20}]**, **30-[BF_{20}]** is soluble in C_6D_5Br showing that dicationic dimers must form before precipitation occurs. The details of the characterisation of these **30-[BF_{20}]** and **31-[BF_{20}]** will not be discussed but characterising data for each compound can be found in Chapter 5.

3.3.2 NMR tube scale synthesis and characterisation of $[Cp^*_2Ti_2\{NC(N(Xyl)CH_2)_2\}_2(\mu\text{-}Me)Me_2][BF_{20}]$ (32-$[BF_{20}]$)

Activation of **7** with 0.5 equivs TBF_{20} results in the quantitative formation of monomethyl-bridged monocation $[Cp^*_2Ti_2\{NC(N(Xyl)CH_2)_2\}_2(\mu\text{-}Me)Me_2][BF_{20}]$ (**32-[BF_{20}]**) which exists as two diastereoisomers (**32a**$^+$ and **32b**$^+$) in a ratio of 3:2 as judged by ^{1}H NMR spectroscopy. The details of the NMR spectra will not be discussed, however NMR data can be found in Chapter 5. An interesting difference between **32**$^+$ and the other analogous species discussed, *vide supra*, is the existence of an equilibrium between the monomethyl-bridged species (**32a**$^+$ and **32b**$^+$) and the corresponding neutral dimethyl complex (**7**) and monoalkyl cation (**25$_{mono}$**$^+$) in the ^{1}H NMR spectrum; these exist in a ratio of 15:1:1 respectively. In this case the dimethyl complex **7** is acting as a less strong donor to the monoalkyl cation compared to the previously discussed compounds which results in this equilibrium (Scheme 3.3). Since the electronic differences between $NC(N(Xyl)CH_2)_2$ and the other ligands already discussed should not be significant (Section 2.5) it is likely that the large steric bulk of this ligand is the main factor is shifting the equilibrium position. Treatment of the equilibrium mixture with 1 equiv $OPPh_3$ led to the quantitative formation of **7** and **26**$^+$ as expected.

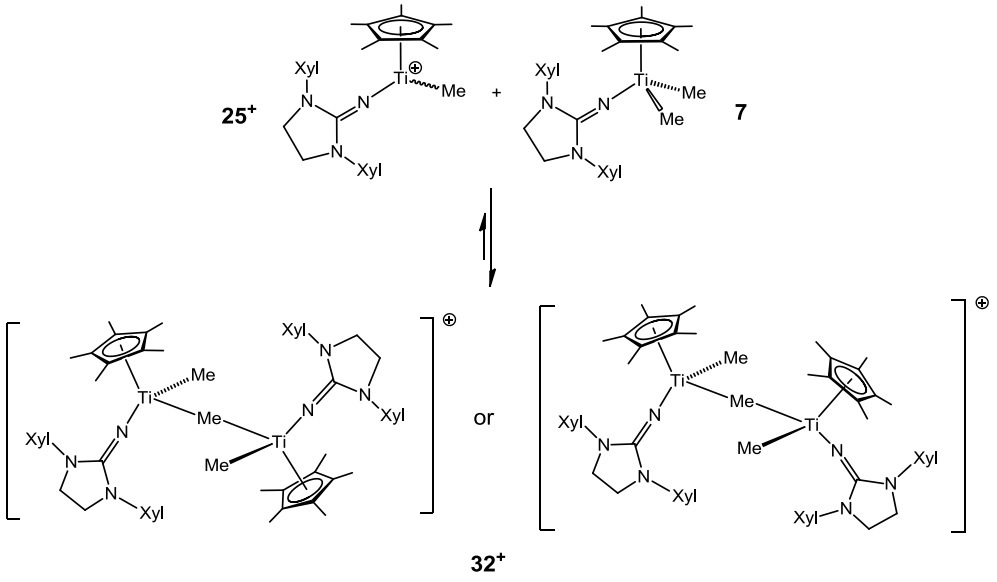

Scheme 3.3 Equilibrium between $[Cp^*_2Ti_2\{NC(N(Xyl)CH_2)_2\}_2(\mu\text{-}Me)Me_2]^+$ (**32**$^+$) and $[Cp^*Ti\{NC(N(Xyl)CH_2)_2\}Me]^+$ (**25**$^+$) and $Cp^*Ti\{NC(N(Xyl)CH_2)_2\}Me_2$ (**7**).

3.4 Aluminium-containing bimetallic species

The reactivity of monoalkyl species with alkyl aluminium species is of particular importance when considering the polymerisation process. MAO contains up to 30 wt% trimethylaluminium and aluminium alkyls are sometimes added into the polymerisation process to act as scavengers of water and oxygen. The species formed when the active monoalkyl cations are trapped with alkylaluminium inhibit the polymerisation process and can also act as chain transfer agents.[82-85]

Previous work in the Mountford group produced the first structurally characterised Group 4 cationic $AlMe_3$ adduct (**1.20**, Figure 3.17),[86] 11 years after the first report by Bochmann *et al.* who reported the first isolable species of this kind $[Cp_2Zr(\mu\text{-}Me)_2AlMe_2][BF_{20}]$ (**1.19**).[78] Both of these species contain two methyl bridges between the transition metal and aluminium i.e. a $M(\mu\text{-}Me)_2Al$ linkage (M = Ti, Zr).

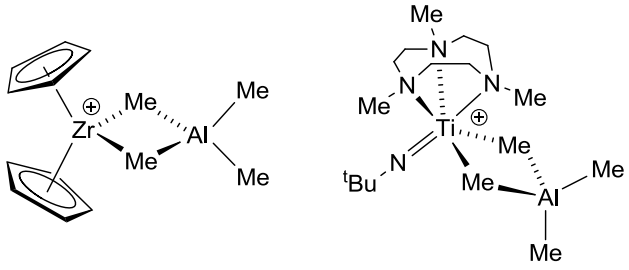

1.19 **1.20**

Figure 3.17 Examples of $AlMe_3$-trapped Group 4 cations.

Other examples of aluminium adducts have also been reported and studied, for example the reaction of $[rac\text{-}Me_2Si(2\text{-}Me\text{-}4\text{-}^tBu\text{-}C_5H_2)_2ZrMe]^+$ with $AlMe_3$ and aniline (by-product of activation) gives an unsymmetrical adduct $[rac\text{-}Me_2Si(2\text{-}Me\text{-}4\text{-}^tBu\text{-}C_5H_2)_2ZrMe(\mu\text{-}Me)AlMe_3(NMe_2Ph)]^+$ due to the steric hindrance around the metal centre.[87-92] The general preference to form $M(\mu\text{-}Me)_2Al$ (M = Group 4 metal) linkages is perhaps not surprising in metallocenium systems but in half-sandwich post-metallocene cations, which tend to be supported by heteroatom bound ligands, one could conceptually imagine the heteroatom becoming involved in the bonding with aluminium. DFT studies by Mountford *et al.* on **1.20** showed that if the imido ^{t}Bu group and triazacyclononane methyl groups were replaced by a methyl group and hydrogen atoms, respectively, that the $AlMe_3$ would rather interact with the imide nitrogen then form the locally C_2 symmetrical $M(\mu\text{-}Me)_2Al$ bonding arrangement.[74] This result showed that there is likely to be a preference for a nitrogen-bound

arrangement electronically but sterics prevents this from occurring. With phosphinimide supported systems Stephan *et al.* have observed more unusual behaviour in which multiple C-H bond activation occurs with neutral dialkyl catalysts resulting in the formation of carbide complexes similar to that seen in the formation of Tebbe's reagent.[93-95] An example of such a reaction is shown in Equation 3.6 where the reaction of 3 equivs of $AlMe_3$ with **3.12** results in the formation of carbide species **3.13** with the release of methane. Carbides can be identified by their high chemical shift in the ^{13}C spectrum, for example in **3.13** the carbide is found at 304.7 ppm.

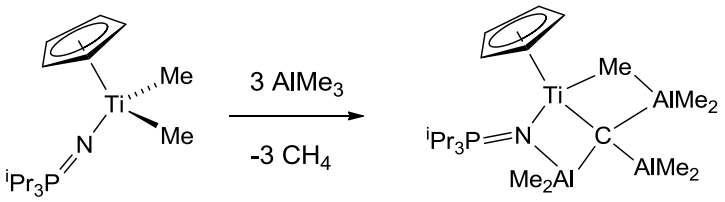

3.12 **3.13**

Equation 3.7

Kang *et al.* have also demonstrated that $AlMe_3$ can abstract ligands from neutral post-metallocene aryloxide supported complexes. Treatment of $Cp^*Ti(C_6H_5\text{-}C_6H_4\text{-}O)Cl_2$ with 1 equiv $AlMe_3$ yields $Cp^*TiMeCl_2$ and the aluminium dimer $(C_6H_5\text{-}C_6H_4\text{-}O)_2Al_2Me_4$. This was also observed with $Cp^*Ti(C_6H_5\text{-}C_6H_4\text{-}O)_2Cl$ and $Cp^*Ti(C_6H_5\text{-}C_6H_4\text{-}O)_3$.[96]

3.4.1 Synthesis and characterisation of $[Cp^*Ti\{NC(NMe_2)_2\}Me(\mu\text{-}Me)AlMe_2]\text{-}[BF_{20}]$ (33-BF_{20})

Treatment of the dimethyl complex **4** with 1 equiv TBF_{20} in the presence of 1 equiv $AlMe_3$ leads to the formation of $[Cp^*Ti\{NC(NMe_2)_2\}Me(\mu\text{-}Me)AlMe_2][BF_{20}]$ **(33-[BF_{20}]**, Equation 3.8). Compound **33-[BF_{20}]** was characterised by ^1H, ^{13}C, ^{19}F and ^{11}B NMR spectroscopy. However, this product could not be isolated on a preparative scale forming multiple unknown products on attempted isolation.

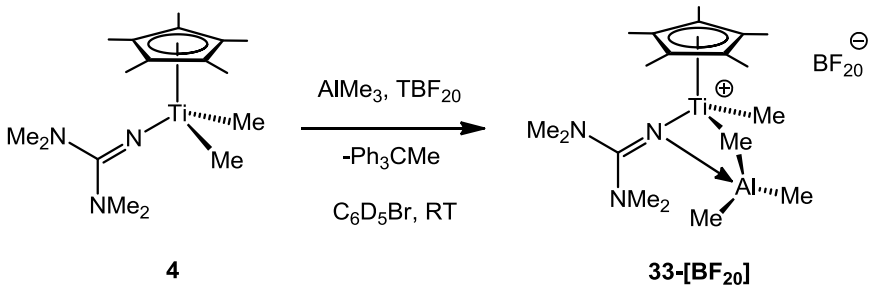

Equation 3.8

The room temperature ^{1}H NMR spectrum in C_6D_5Br (Figure 3.18) shows the familiar single NMe_2 and Cp* resonances, in this case at 2.37 and 1.59 ppm, respectively. The spectrum also contains a further two singlets at 0.66 and -0.70 ppm in a ratio of 1:1 which correspond to methyl groups bound to aluminium. At room temperature this molecule has apparent time-averaged C_s symmetry in solution. One important difference between this ^{1}H NMR spectrum and that of the imido cation **1.20** previously reported by Mountford *et al.* is the presence of only two Al-Me signals rather than three. In the imido compound there are signals for μ-Me-Al, terminal Al-Me "up" and Al-Me "down" (with respect to the face-capping ligand) in a 2:1:1 ratio; **33**$^+$ shows only two resonances in a ratio of 1:1.

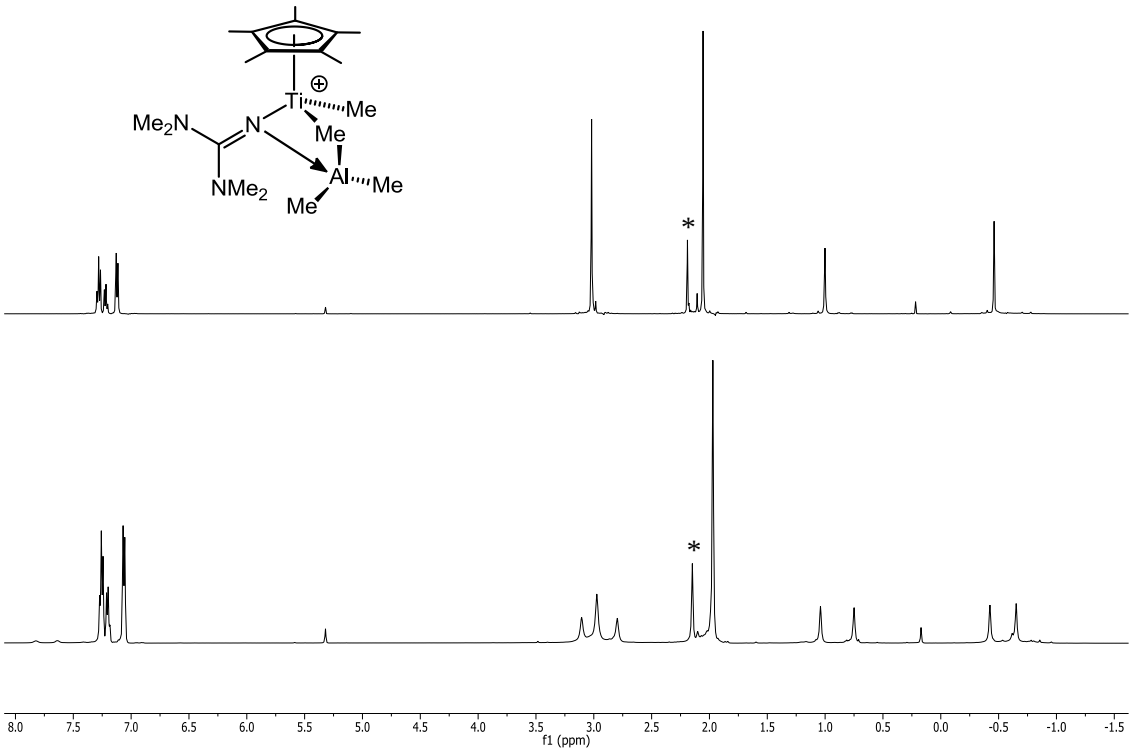

Figure 3.18 ^{1}H NMR spectra (299.9 MHz, CD_2Cl_2) of **33**$^+$. Top: 298 K Bottom: 183 K. Ph_3CMe is labelled '*'.

^{13}C-{^{1}H} NMR analysis of the compound reveals that the two M-Me (M = Al, Ti) environments are located at -8.7 ppm and 64.9 ppm, respectively. The former is usual for a terminal Al-Me environment whereas the latter is more typical of a terminal Ti-Me or bridging group. With only the information from room temperature NMR spectra it is still possible that the dialkyl bridged bimetallic species [Cp*Ti{NC(NMe$_2$)$_2$}(μ-Me)$_2$AlMe$_2$][BF$_{20}$] could be assigned as the product. For example if the "up" and "down" Al-Me groups were coincidental in both the ^{1}H and ^{13}C NMR spectra this would still fit the NMR data. However, the low temperature ^{1}H NMR spectrum of **33**$^{+}$ (183 K in CD_2Cl_2, Figure 3.18) reveals that in the low temperature limit the molecule has C_1 symmetry and has four chemically inequivalent M-Me (M = Ti or Al) environments. This is consistent with the formation of a nitrogen-bound $AlMe_3$ adduct as shown in Equation 3.8 and not with the C_s symmetric structure of [Cp*Ti{NC(NMe$_2$)$_2$}(μ-Me)$_2$AlMe$_2$][BF$_{20}$].

In the structure of **33**$^{+}$ there is one terminal Ti-Me environment, two terminal Al-Me and one Ti(μ-Me)Al environment with a 3c-2e bond. The ^{1}H NMR spectrum at 183 K contains resonances for Cp* (1.97 ppm), Ti-Me (1.04 ppm), Ti(μ-Me)Al (0.75 ppm), Al-Me (-0.43 and -0.65 ppm) which are consistent with the proposed structure of **33**$^{+}$. Interestingly, at low temperature the NMe_2 resonance of the supporting guanidinate ligand also splits in the ^{1}H NMR spectrum into three signals with a ratio of integrals of 3H:6H:3H (Figure 3.18). At this temperature the guanidinate ligand is no longer rotating freely.

The ^{13}C-{^{1}H} NMR spectrum was also recorded at low temperature (183 K). The terminal Ti-Me resonance is found at 70.6 ppm, whereas the μ-Me resonance is, as expected, situated more upfield at 57.2 ppm. The terminal Al-Me resonances are also located in their typical upfield positions (-9.1 and -9.6 ppm).[74, 78] The NC(N$\underline{Me}_2$)$_2$ resonances in the ^{13}C-{^{1}H} spectrum exist as a four singlets at 44.1, 42.4, 42.1 and 39.5 ppm.

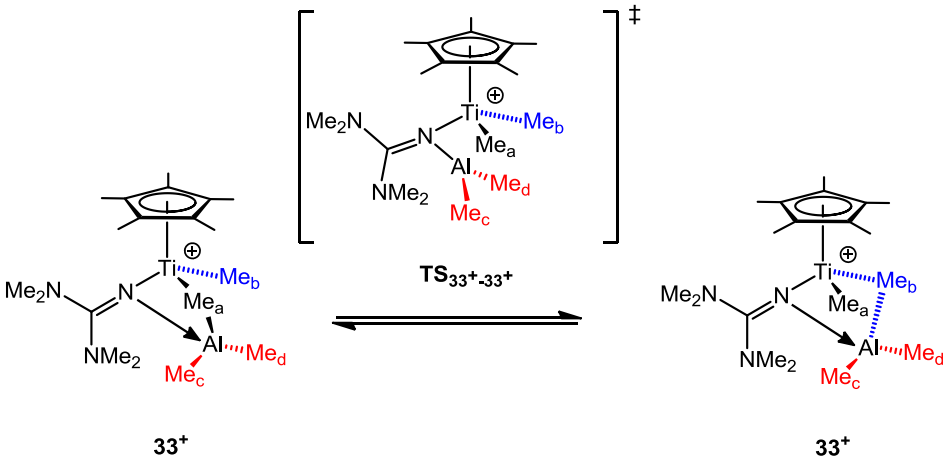

Equation 3.9

In order for the low temperature C_1 symmetric structure to become time-averaged C_s symmetric at room temperature conversion between the two enantiomers must occur to yield two sets of time-averaged methyl resonances. The conversion between these two enantiomers can occur by a "swinging" of the $AlMe_2$ unit between the two methyl groups Me_a and Me_b (Equation 3.9) *via* a C_s symmetric transition state (**TS**$_{33^+\text{-}33^+}$), discussed further in Section 3.4.3. It can also be established experimentally that the conversion takes place *via* an intramolecular process by the use of SST NMR spectroscopy. Addition of excess $AlMe_3$ to **33**$^+$ shows no exchange of bound and free $AlMe_3$ on this timescale. Saturation of the free-$AlMe_3$ signal also shows that there is no exchange with bound-$AlMe_3$. SST experiments also show that there is no exchange of Me_a/Me_b with Me_c/Me_d. The suggested intramolecular conversion between enantiomers of **33**$^+$ would give rise to a single resonance for Me_a/Me_b which is observed at room temperature. Me_c and Me_d point "up" and "down" and the motion would also give rise to exchange between them; this would again result in a single resonance for Me_c and Me_d in the fast exchange regime. Overall this motion explains the observed room temperature ^{1}H NMR spectrum.

In order to establish whether binding of $AlMe_3$ to **14**$^+$ is chemically reversible, **33**$^+$ was treated with 2 equivs of di*iso*propylcarbodiimide on the NMR tube scale. The products of this reaction were the complex **43**$^+$ (discussed in Section 4.2.3.1) and $\{MeC(N^iPr_2)_2\}AlMe_2$ formed by the insertion of the unsaturated substrate into the Ti-Me and Al-Me bonds, respectively. This reactivity demonstrates that $AlMe_3$ and cation **14**$_{\text{mono}}^+$ indeed form a reversible adduct which can be separated on a chemical timescale.

3.4.1.1 Eyring analysis of methyl exchange processes in 33^+

To obtain a better understanding of the kinetics of the conversion processes occurring with $\mathbf{33}^+$ variable temperature ^{1}H NMR spectra were recorded in CD_2Cl_2 between 181 and 209 K in 4 K intervals. Relevant activation parameters were obtained using line width analysis. In each case observed line widths ($\nu_{1/2}$(obs)) were corrected to give $\nu_{1/2}$(corr) by subtraction of the natural line widths from the observed values. $\nu_{1/2}$(obs) values were used to calculate observed rate constants k_{obs} according to the formula k = $\pi\nu_{1/2}$(corr).[97]

The analysis was carried out on the Ti-Me_a and Ti-Me_b resonances to analyse the exchange of Me_a with Me_b, and on one of the terminal Al-Me signals to analyse the exchange of Me_c with Me_d. The second Al-Me signal was not analysed as the signal was distorted by a minor impurity which prevented measuring accurate peak linewidths. Assuming that the chemical exchange rate constant k_c is equal to twice the observed rate constant k_{obs} Eyring plots can be constructed and the values of $\Delta H^{\ddagger}$, $\Delta S^{\ddagger}$ and $\Delta G^{\ddagger}$ can be determined.[98, 99] The Eyring plot for the Ti-Me resonances was constructed by plotting both sets of data for Ti-Me_a and Ti-Me_b together (Figure 3.19). The analysis of the Eyring plot for the Ti-Me resonances results in a $\Delta H^{\ddagger}$ value of 42.0(5) kJ mol^{-1} and $\Delta S^{\ddagger}$ value of -2(3) J K^{-1} mol^{-1}. Similar analysis for the Al-Me resonance yields values which are identical within error ($\Delta H^{\ddagger}$ = 41(1) kJ mol^{-1}, $\Delta S^{\ddagger}$ = -4(5) J K^{-1} mol^{-1}). The $\Delta G^{\ddagger}$(298 K) value for the Ti-Me resonances at 298 K is 43(1) kJ mol^{-1} and for the Al-Me signal is 42(2) kJ mol^{-1}.

Table 3.6 Corrected line widths ($\nu_{1/2}$(corr), Hz) and observed rate constants (k_{obs}, s^{-1}) for Ti-Me_a and Ti-Me_b exchange and Al-Me_c and Al-Me_d exchange in **33**$^+$.

Temp (K)	$Me_a \rightarrow Me_b$		$Me_b \rightarrow Me_a$		$Me_{c/d} \rightarrow Me_{d/c}$	
	$\nu_{1/2}$(corr)	k_{obs}	$\nu_{1/2}$(corr)	k_{obs}	$\nu_{1/2}$(corr)	k_{obs}
209	35.1	110.4	36.1	113.4	37.5	117.8
205	21.5	67.6	20.9	65.7	27.7	87.0
201	13.9	43.5	12.8	40.2	16.4	51.5
197	7.8	24.4	7.8	24.4	9.3	29.3
193	4.0	12.7	4.3	13.6	5.8	18.1
189	2.7	8.5	2.8	8.7	3.6	11.3
185	1.4	4.4	1.5	4.6	2.8	8.8
181	0.7	2.0	0.7	2.3	1.8	5.8

Since the activation parameters are similar for both the Ti-Me and Al-Me resonances they are likely exchanging *via* the same mechanism which is consistent with the proposed exchange process. The low entropy values are also consistent with the intramolecular exchange of the two enantiomers, consistent with SST experiments. The $\Delta G^{\ddagger}$ values obtained are also consistent with the process being able to occur readily at room temperature.

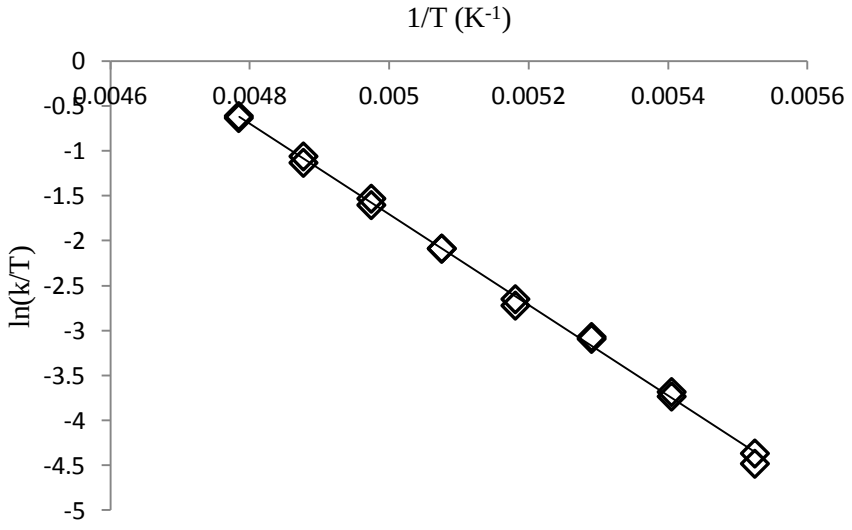

Figure 3.19 Plot of ln(k/T) *vs.* 1/T (R^2 = 0.9977): $\Delta H^{\ddagger}$ = 42.0(5) kJ mol^{-1} , $\Delta S^{\ddagger}$ = -2(3) J K^{-1} mol^{-1}, $\Delta G^{\ddagger}$(298 K)= 43(1) kJ mol^{-1} for Ti-Me_a and Ti-Me_b resonances.

3.4.2 Synthesis and characterisation of [Cp*Ti{NC(NMe$_2$)$_2$}Me(μ-Cl)AlMe$_2$]-[BF$_{20}$] (34-[BF$_{20}$])

To synthesise an isolable compound analogous to **33-[BF$_{20}$]** the complex **4** was treated with TBF$_{20}$ in presence of Me$_2$AlCl. It was also suspected that use of Me$_2$AlCl, rather than AlMe$_3$, would also introduce more asymmetry into the product cation at room temperature. The reaction (Equation 3.10) resulted in the quantitative formation of a new species [Cp*Ti{NC(NMe$_2$)$_2$}Me(μ-Cl)AlMe$_2$][BF$_{20}$] (**34-[BF$_{20}$]**) by ^{1}H NMR spectroscopy. Compound **34-[BF$_{20}$]** was isolated in a 52% yield and characterised by NMR spectroscopy, IR spectroscopy and elemental analysis.

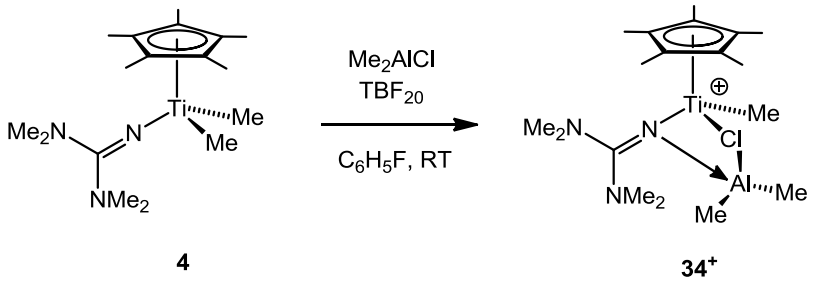

Equation 3.10 Reaction of **4** with TBF$_{20}$ in the presence of Me$_2$AlCl.

The room temperature ^{1}H NMR spectrum is consistent with a C_1 symmetric species (Figure 3.20). In a similar manner to **33**$^+$ the room temperature spectrum shows one Cp* (2.19 ppm) and one NMe$_2$ resonance (3.02 ppm). There are also two methyl resonances one at 1.70 ppm (Ti-Me) and the other at -0.40 ppm (Al-Me) in a ratio of 1:2. This ^{1}H NMR spectrum again does not have "up" Al-Me and "down" Al-Me signals as seen in the imido compound (**1.20**) at room temperature as discussed previously (Section 3.4.1); the molecular structure is then likely to be similar to **33**$^+$ (Equation 3.8). The chloride ligand is expected to be bridging rather than Me because it is able to form two 2c-2e bonds. The expected structure type is confirmed by the presence of a Ti-Me resonance in the ^{13}C-{^{1}H} NMR spectrum at 80.7 ppm, characteristic of a terminal Ti-Me environment and an Al-Me proton environment (2 x Me) found at -8.3 ppm; the chloride ligand must be bridging, as expected, by elimination.

Exchange of the two terminal Al-Me environments would occur *via* rotation about either the Al-Cl or Al-N bond *via* breaking of the Al-N or Al-Cl bonds, respectively. SST NMR experiments performed on **34**$^+$ in the presence of excess Me$_2$AlCl illustrate that there is no exchange between free and bound Me$_2$AlCl showing that this is not a

competetive route for exchange of the two Al-Me environments. Saturation of the Ti-Me resonance also shows no exchange with the Al-Me environments.

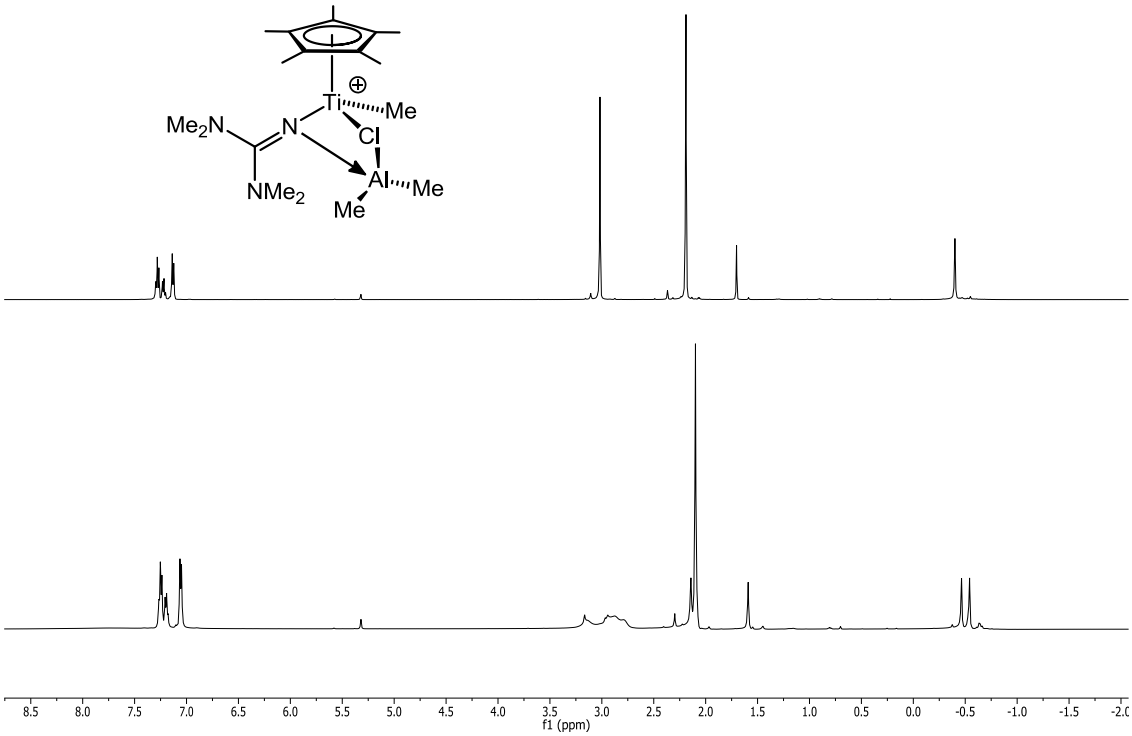

Figure 3.20 ^{1}H NMR spectra (299.9 MHz, CD_2Cl_2) of **34**$^{+}$. Top: 298 K, Bottom: 208 K

Low temperature NMR studies (208 K, Figure 3.20) of the compound show splitting of the downfield Al-Me environments into two separate singlets at -0.46 and -0.54 ppm. The Ti-Me terminal signal remains as a singlet because it is not exchanging with another environment. At low temperature the terminal Ti-Me resonance still shows a characteristic ^{13}C NMR shift of 79.9 ppm; the terminal Al-Me resonances are located at -8.5 and -9.4 ppm. At low temperature similar to **33**$^{+}$ the ligand NMe_2 signals split out, this time into four broad signals in the ^{1}H and ^{13}C NMR spectrum, one for each NMe environment. VT ^{1}H NMR experiments show that the coalescence temperature for the Al-Me resonances is 271 K which results in a $\Delta G^{\ddagger}$ value of 31.9 kJ mol^{-1}. Assuming the entropy of this process is close to 0 J K^{-1} mol^{-1}, as with conversion between enantiomers of **33Qa**$^{+}$, the $\Delta G^{\ddagger}$ value at room temperature should be similar and therefore is consistent with the ^{1}H NMR spectrum which shows that this process occurs readily at room temperature.

3.4.3 DFT studies on aluminium containing bimetallic species

DFT calculations (M06) were performed by Dr Betty Coussens (DSM) in order to develop an understanding of the bonding, thermodynamics and kinetics in systems **33**$^+$ and **34**$^+$. The optimised structures for both approximately C_1-symmteric $[Cp^*Ti\{NC(NMe_2)_2\}Me(\mu\text{-}Me)AlMe_2]^+$ (**33Qa**$^+$) and approximately C_s-symmetric $[Cp^*Ti\{NC(NMe_2)_2\}(\mu\text{-}Me)_2AlMe_2]^+$ (**33Qb**$^+$) $AlMe_3$ adducts were calculated and are shown in Figure 3.21.

The Ti-Me distances (2.218 and 2.219 Å) in **33Qb**$^+$ are shorter than those reported for the X-ray structure of **1.20** (2.344(2) and 2.335(2) Å) as are the Al-Me distances (1.956 and 1.946 Å *vs.* 1.963(3) and 1.981(3) Å) perhaps as a result of a more electron deficient titanium centre or the lack of nitrogen-trans-influence as discussed before.[74] The Ti-N bond length is 1.76 Å consistent with the expected value for this bond with a cationic titanium centre (Section 3.2.18).

The Al-N bond in **33Qa**$^+$ is 1.991 Å which is longer than a normal Al-N covalent single bond (*ca.* 1.79-1.87 Å)[100, 101] and is more consistent with a dative Al-N bond length.[101-104] The Ti-N bond length is 1.89 Å which is significantly longer than for **33Qb**$^+$. This is a consequence of the interaction of aluminium with the titanium bound nitrogen and this bond length is infact closer to an amide-titanium bond. Calculations were carried out to assess the relative thermodynamic stabilities of these species. For the overall reaction the formation of **33Qa**$^+$ from monomeric **14Q**$^+$ and 0.5 Al_2Me_6 has a ΔH of -137.2 kJ mol^{-1} whereas for **33Qb**$^+$ it is -124.6 kJ mol^{-1}. Therefore complex **33Qa**$^+$ is -12.6 kJ mol^{-1} more stable than **33Qb**$^+$, which is consistent with experimental observation. In this case it seems that the steric factors present in the system are low enough to allow the formation of a favourable Al-N interaction.

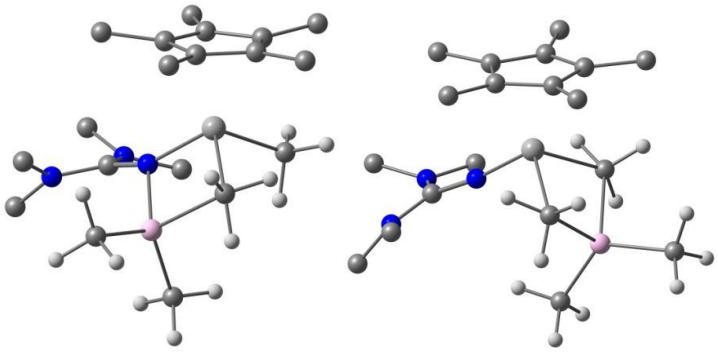

Figure 3.21 DFT calculated structures (M06) monomethyl-bridged **33Qa**$^+$ (left) and dimethyl bridged **33Qb**$^+$ (right). H atoms omitted on supporting ligands for clarity.

In an attempt to locate transition states between the two enantiomers of **33Qa**$^+$, to help explain the observed dynamics in complex **33**$^+$ by NMR spectroscopy, two different transition states were found. The first (**TS$_{33Qa^+\text{-}33Qa^+}$**) is the transition state which describes the conversion of the two enantiomers of **33Qa**$^+$ (Equation 3.8) and the second (**TS$_{33Qa^+\text{-}33Qb^+}$**) is the transition state which describes the conversion of the monomethyl-bridged species (**33Qa**$^+$) to the dimethyl-bridged species (**33Qb**$^+$), Equation 3.10.

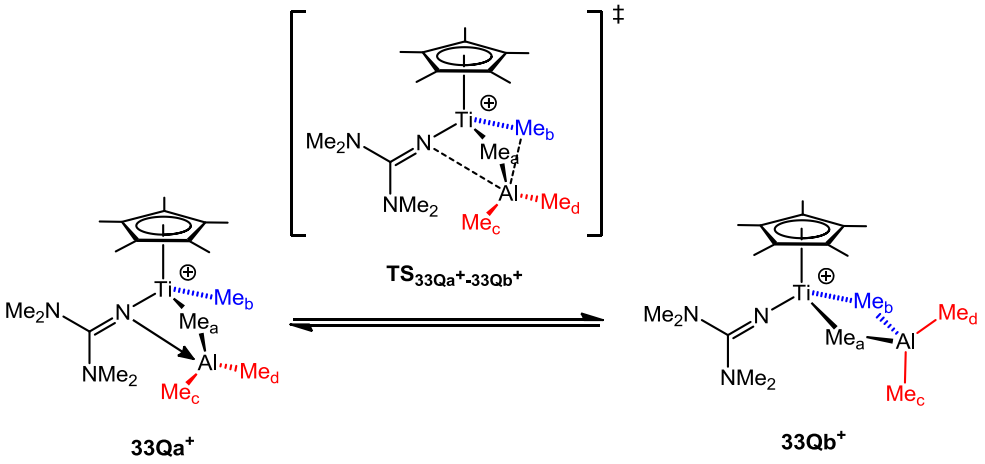

Equation 3.11

TS$_{33Qa^+\text{-}33Qa^+}$ (Equation 3.9) is approximately C_s symmetric and has a single imaginary frequency which corresponds to the swinging motion that leads to the interconversion of the two enantiomers of **33Qa**$^+$. The aluminium atom has two bonds to methyl groups and a single bond to nitrogen making it overall 3-coordinate. The Al-Me bond lengths are 1.94 and 1.93 Å and the Al-N bond length is 1.90 Å. The distances between the aluminium centre and the two Ti-Me groups are 3.47 and 3.28 Å. The calculated Ti-N bond length is 1.96 Å which is a significant increase from that in **1** (1.782(3) Å)

and is more consistent with an amide-Ti bond length. The calculated $\Delta H^{\ddagger}$ for this transition state is 55.7 kJ mol^{-1} which is in good agreement with that determined by Eyring analysis ($\Delta H^{\ddagger}$ = 42(1) kJ mol^{-1}), *vide supra*. **TS$_{\mathbf{33Qa^+\text{-}33Qb^+}}$** is C_1 symmetric and has a single imaginary frequency which corresponds to the conversion between **33Qa$^+$** and **33Qb$^+$**. In this case Me$_c$ becomes the "down" Al-Me and Me$_d$ becomes the "up" Al-Me (Equation 3.11). The Al-N distance is 2.77 Å which is consistent with no significant interaction between the two atoms. The Ti-N bond length is 1.78 Å and is also consistent with no significant interaction between the titanium bound nitrogen and aluminium. The aluminium atom has two single bonds to Me$_c$ and Me$_d$ with bond lengths of 1.95 and 1.94 Å, respectively. The Al-Me$_a$ and Al-Me$_b$ bond lengths are 2.06 and 3.00 Å, respectively, consistent with a significant interaction in the former but not in the latter. The calculated $\Delta H^{\ddagger}$ for this transition state is 70.3 kJ mol^{-1} from **33Qa$^+$**. This is significantly higher than for transition state **TS$_{\mathbf{33Qa^+\text{-}33Qa^+}}$** and is consistent with the fact that conversion of enantiomers of **33Qa$^+$** are observed experimentally but the conversion to **33Qb$^+$** is not.

As with **33Q$^+$** the possible adducts between **14Q$^+$** and Me_2AlCl (to form **34Q$^+$**) were also calculated with a range of different isomers. In this case the introduction of a chloride ligand means there are more perturbations of the structure (Figure 3.22).

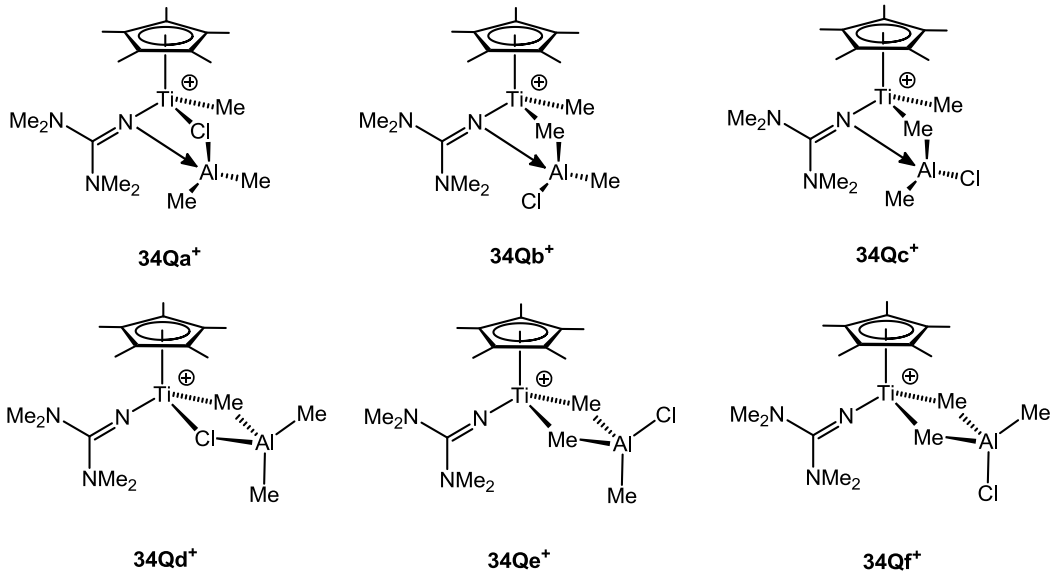

Figure 3.22 Different isomers **34Qa$^+$-34Qf$^+$** for an adduct between **4$^+$** and Me_2AlCl.

When considering the species which contain an Al-N interaction three possible structures were calculated, one where the chloride is the bridge (**34Qa$^+$**) and two in which a methyl group is bridging. When the methyl group is bridging the chloride

atoms can either be pointing "up" (**34Qb**$^+$) or "down" (**34Qc**$^+$) from the aluminium atom. The enthalpy was again calculated from the monomeric cation **14Q**$^+$ and 0.5 $Al_2Me_4Cl_4$ to the various isomers of **34Q**$^+$. The ΔH values are -147.1, -120.1 and -124.6 kJ mol^{-1} for **34Qa**$^+$, **34Qb**$^+$ and **34Qc**$^+$, respectively. This is consistent with, as expected, the chloride bridged isomer being the most stable by 26.0 and 22.5 kJ mol^{-1} compared to **34Qb**$^+$ and **34Qc**$^+$, respectively. The structure of **34Qa**$^+$ is illustrated in Figure 3.23.

The isomers of **34Q**$^+$ which contain no Al-N interaction but form a double bridged structure between aluminium and titanium also has several isomers which have been calculated. The chloride ligand can be bridging (**34Qd**$^+$) or terminal. When terminal the chloride atom can be pointing "up" (**35Qe**$^+$) or "down" (**34Qf**$^+$) relative to the aluminium. The calculated ΔH values of reaction for **34Qd**$^+$, **34Qe**$^+$ and **34Qf**$^+$ are -121.9, -101.1 and -107.6 kJmol^{-1}. In this case the chloride bridged isomer (**34Qd**$^+$) is, as expected, the most stable and is shown in Figure 3.23. The most stable of the discussed structures is **34Qa**$^+$ which is more stable than **34Qd**$^+$ by 25.1 kJ mol^{-1} and is consistent with the NMR spectra observed experimentally.

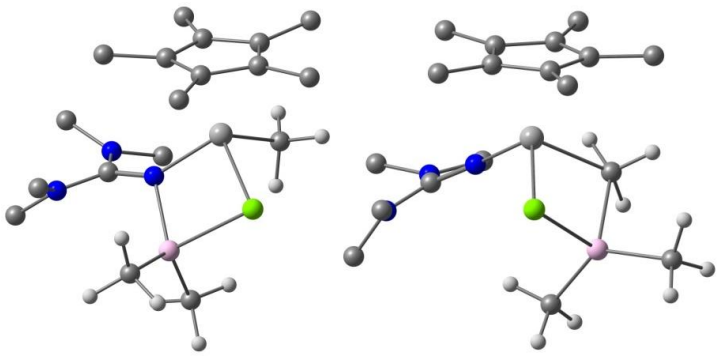

Figure 3.23 DFT calculated structure of **34Qa**$^+$with a single aluminium titanium bridge (left) or **34Qd**$^+$ with a double aluminium titanium bridge (right).

3.5 Reaction of $AlMe_3$ with other cations

Activation of complexes **1.49**, **2.4**, **6** and **7** in the presence of $AlMe_3$ led in all cases to the formation of multiple products and production of a significant amount of methane by ^{1}H NMR spectroscopy. Unfortunately the mixtures could not be purified in order to try and isolate a single product. This decomposition is important to consider since $AlMe_3$ is not only forming an adduct with the active species but is actually decomposing it. The large amount of methane release is indicative that these species

may be undergoing similar reactivity to that observed by Stephan *et al.*[94] To try help and indentify any diagnostic resonances in a ^{13}C-{^{1}H} NMR spectrum the ^{13}C-labelled **1.49_^{13}Me$_2$** was activated with 1 equiv TBF_{20} in the presence of 1 equiv $AlMe_3$ and showed the expected decomposition. The ^{13}C-{^{1}H} NMR spectrum of this compound showed a resonance at 258.2 ppm. To check this resonance was not the result of a μ-CH_2 species the ^{1}H-coupled ^{13}C spectrum was acquired which showed the signal at 258.2 ppm was a doublet ($^{1}J_{CH}$ = 129.1 Hz) which is not consistent with a μ-CH_2 group but with a methine group. The species Cp*Ti(μ-Me)(μ-NP^{i}Pr$_3$)(μ-CH)($AlMe_2$)$_2$ was reported by Stephan *et al.* from the reaction of $AlMe_3$ with Cp*Ti(NP^{i}Pr$_3$)Me_2. Cp*Ti(μ-Me)(μ-NP^{i}Pr$_3$)(μ-CH)($AlMe_2$)$_2$ contained a ^{13}C NMR signal at 241 ppm although the coupled spectrum was not reported.[94] The other signals in the ^{1}H and ^{13}C NMR spectra for the reaction of **1.49** with $AlMe_3$ and TBF_{20} could not be confidentially assigned but one of the products of this reaction likely involves the production of a methine containing species. An EPR spectrum of the decomposition mixture of **1.49** with $AlMe_3$ and TBF_{20} also showed no evidence of any significant amount of Ti(III) species being formed.

3.6 Summary

The Chapter has shown by the utilisation of various NMR experiments that the previously reported **1.26$_{dim}$-[BF$_{20}$]$_2$**, although dimeric in the solid state exists as a monomer (**1.26$_{mono}$-[BF$_{20}$]**) in C_6D_5Br.[14] This solution behaviour is also true with the iminoimidazolidide system **25-[BF$_{20}$]** determined by a similar set of experiments. Lewis base adducts (L = py and THF) starting from both **1.49** and **7** were synthesised and fully characterised. Compounds **2.4** and **6** both give a mixture of products in solution when treated with TBF_{20} which can be converted into single Lewis base products by the addition of $OPPh_3$.

DOSY NMR showed that the mixture of cations (**10a**$^{+}$, **10b**$^{+}$ and **10c**$^{+}$) seem to consist of monomers and dimers and although DOSY data could not be acquired for **21-[BF$_{20}$]** it is likely true in this case also. Crystallisation of **21$_{dimer}$-[BF$_{20}$]$_2$** from bromobenzene led to a second example of a crystallographically characterised Group 4 dimethyl-bridged dication. Activation of **4** with TBF_{20} gave an insoluble compound which could not be characterised by solution based techniques, however activation of the benzyl derivative **5** gave a monomeric cation (**19**$^{+}$) in solution when treated with TBF_{20} that could be characterised by NMR spectroscopy. Leaving **14$_{dim}$-[BF$_{20}$]$_2$** for 2 weeks in

solvent led to the formation of a mixed valence compound (**15**$^+$), bridged by two tetramethyl-guanidinate ligands, which was characterised by X-ray crystallography and EPR. The $OPPh_3$, Py and THF adducts of **14**$^+$ were also discussed.

DFT studies showed that the investigated κ^1-amidinate ligands as well as the κ^1-guanidinate ligand in **21Q**$^+$ prefer to methyl-bridge rather than nitrogen-bridge because of steric reasons. The ligand in **14Q**$^+$ is however small enough to allow nitrogen-bridging to become preferential and in this way it stands out from the other synthesised compounds. Calculations have also shown that for representative ligands of the real and model systems that the frontier orbitals of the divalent dications are qualitatively similar to $[Cp_2Ti]^{2+}$ and that in both the metallocene and the post-metallocene systems studied this results in a deviation of the Ti-Me bond from the *z*-axis for the monomethyl cations. The amidinate and guanidinate complexes, unlike, $[Cp_2TiMe]^+$, do not show an agostic interaction with the metal centre due to the frontier orbital energies being globally higher than in the titanocene analogue.

Treatment of all studied dimethyl complexes with 0.5 equiv TBF_{20} results in the formation of the corresponding monomethyl monocations which in each case exists as a mixture of two diastereoisomers. In the case of **32**$^+$ this exists in equilibrium with its corresponding dimethyl complex (**7**) and monomeric methylcation (**25$_{mono}$**$^+$). Finally the activation of **4** in the presence of 1 equiv $AlMe_3$ was shown to form a C_1 symmetric adduct (**33**$^+$) in which the imine nitrogen of the ligand is bound to aluminium. Similarly activation of **4** in the presence of Me_2AlCl gave the analogous compound (**34**$^+$) but instead with a single chloride bridge. DFT studies on **33Q**$^+$ and **34Q**$^+$ show that this nitrogen bound adduct is in fact more favourable in these systems that the more common dimethyl-bridged bimetallic species. The transition state for the conversion between enantiomers of **34Qa**$^+$ was also located with DFT and the calculated activation enthalpy is consistent with that determined by Eyring analysis.

3.7 References

1. S. Zhang, W. E. Piers, X. Gao and M. Parvez, *J. Am. Chem. Soc.*, 2000, **122**, 5499-5509.
2. S. Zhang and W. E. Piers, *Organometallics*, 2001, **20**, 2088-2092.
3. K. Ma, W. E. Piers, Y. Gao and M. Parvez, *J. Am. Chem. Soc.*, 2004, **126**, 5668-5669.

4. D. W. Stephan, J. C. Stewart, F. Guérin, R. E. v. H. Spence, W. Xu and D. G. Harrison, *Organometallics*, 1999, **18**, 1116-1118.
5. M. G. Thorn, J. S. Vilardo, P. E. Fanwick and I. P. Rothwell, *Chem. Commun.*, 1998, 2427-2428.
6. T. A. Manz, J. M. Caruthers, S. Sharma, K. Phomphrai, K. T. Thomson, W. N. Delgass and M. M. Abu-Omar, *Organometallics*, 2012, **31**, 602-618.
7. T. A. Manz, K. Phomphrai, G. Medvedev, B. B. Krishnamurthy, S. Sharma, J. Haq, K. A. Novstrup, K. T. Thomson, W. N. Delgass, J. M. Caruthers and M. M. Abu-Omar, *J. Am. Chem. Soc.*, 2007, **129**, 3776-3777.
8. T. A. Manz, S. Sharma, K. Phomphrai, K. A. Novstrup, A. E. Fenwick, P. E. Fanwick, G. A. Medvedev, M. M. Abu-Omar, W. N. Delgass, K. T. Thomson and J. M. Caruthers, *Organometallics*, 2008, **27**, 5504-5520.
9. K. Nomura, J. Liu, S. Padmanabhan and B. Kitiyanan, *J. Mol. Catal. A: Chem.*, 2007, **267**, 1-29.
10. K. Nomura and A. Fudo, *Inorg. Chim. Acta*, 2003, **345**, 37-43.
11. Y.-X. Chen, M. V. Metz, L. Li, C. L. Stern and T. J. Marks, *J. Am. Chem. Soc.*, 1998, **120**, 6287-6305.
12. Y.-X. Chen and T. J. Marks, *Organometallics*, 1997, **16**, 3649-3657.
13. L. Jia, X. Yang, C. L. Stern and T. J. Marks, *Organometallics*, 1997, **16**, 842-857.
14. E. G. Ijpeij, B. Coussens, M. A. Zuideveld, G. H. J. van Doremaele, P. Mountford, M. Lutz and A. L. Spek, *Chem. Commun.*, 2010, **46**, 3339-3341.
15. R. J. Keaton, K. C. Jayaratne, J. C. Fettinger and L. R. Sita, *J. Am. Chem. Soc.*, 2000, **122**, 12909-12910.
16. R. Scott, *DPhil Thesis, University of Oxford*, 2013.
17. T. D. W. Claridge, *High-Resolution NMR Techniques in Organic Chemistry*, Second edn., Elsevier, 2008.
18. S. Beck, A. Geyer and H.-H. Brintzinger, *Chem. Commun.*, 1999, 2477-2478.
19. C. Zuccaccia, N. G. Stahl, A. Macchioni, M.-C. Chen, J. A. Roberts and T. J. Marks, *J. Am. Chem. Soc.*, 2004, **126**, 1448-1464.
20. M. Bochmann, *J. Organomet. Chem.*, 2004, **689**, 3982-3998.
21. N. G. Stahl, C. Zuccaccia, T. R. Jensen and T. J. Marks, *J. Am. Chem. Soc.*, 2003, **125**, 5256-5257.

22. A. Moreno, P. S. Pregosin, L. F. Veiros, A. Albinati and S. Rizzato, *Chem. Eur. J.*, 2008, **14**, 5617-5629.
23. A. Moreno, P. S. Pregosin, L. F. Veiros, A. Albinati and S. Rizzato, *Chem. Eur. J.*, 2009, **15**, 6848-6862.
24. D. Sirbu, G. Consiglio, B. Milani, P. G. A. Kumar, P. S. Pregosin and S. Gischig, *J. Organomet. Chem.*, 2005, **690**, 2254-2262.
25. P. G. A. Kumar, P. S. Pregosin, M. Vallet, G. Bernardinelli, R. F. Jazzar, F. Viton and E. P. Kündig, *Organometallics*, 2004, **23**, 5410-5418.
26. A. Macchioni, *Chem. Rev.*, 2005, **105**, 2039-2074.
27. W. Clegg, *Crystal Structure determination*, Oxford University Press, 1998.
28. R. F. Jordan, C. S. Bajgur, R. Willett and B. Scott, *J. Am. Chem. Soc.*, 1986, **108**, 7410-7411.
29. M. Bochmann and L. M. Wilson, *J. Chem. Soc., Chem. Commun.*, 1986, 1610-1611.
30. M. Bochmann, L. M. Wilson, M. B. Hursthouse and R. L. Short, *Organometallics*, 1987, **6**, 2556-2563.
31. P. D. Bolton, E. Clot, N. Adams, S. R. Dubberley, A. R. Cowley and P. Mountford, *Organometallics*, 2006, **25**, 2806-2825.
32. R. F. Jordan, D. F. Taylor and N. C. Baenziger, *Organometallics*, 1990, **9**, 1546-1557.
33. M. Bochmann, A. J. Jaggar, L. M. Wilson, M. B. Hursthouse and M. Motevalli, *Polyhedron*, 1989, **8**, 1838-1843.
34. F. Sauriol, J. F. Sonnenberg, S. J. Chadder, A. F. Dunlop-Brière, M. C. Baird and P. H. M. Budzelaar, *J. Am. Chem. Soc.*, 2010, **132**, 13357-13370.
35. H. Tsurugi, H. Nagae and K. Mashima, *Chem. Commun.*, 2011, **47**, 5620-5622.
36. Jin-shan Li, F.Weller, F.Schmock and K.Dehnicke, *Z. Anorg. Allg. Chem.*, 1995, **621**, 2097.
37. T. W. Graham, J. Kickham, S. Courtenay, P. Wei and D. W. Stephan, *Organometallics*, 2004, **23**, 3309-3318.
38. G. B. Nikiforov, I. Vidyaratne, S. Gambarotta and I. Korobkov, *Angew. Chem. Int. Ed.*, 2009, **48**, 7415-7419.
39. L. Morello, P. Yu, C. D. Carmichael, B. O. Patrick and M. D. Fryzuk, *J. Am. Chem. Soc.*, 2005, **127**, 12796-12797.

40. A. D. Horton, J. de With, A. J. van der Linden and H. van de Weg, *Organometallics*, 1996, **15**, 2672-2674.
41. J. Okuda, K. Musikabhumma and P.-J. Sinnema, *Isr. J. Chem.*, 2002, **42**, 383-392.
42. F. Wu, A. K. Dash and R. F. Jordan, *J. Am. Chem. Soc.*, 2004, **126**, 15360-15361.
43. A. D. Horton, W. J. de, d. L. A. J. van and d. W. H. van, *Organometallics*, 1996, **15**, 2672-2674.
44. P.-J. Sinnema, T. P. Spaniol and J. Okuda, *J. Organomet. Chem.*, 2000, **598**, 179-181.
45. M. Bouwkamp, D. van Leusen, A. Meetsma and B. Hessen, *Organometallics*, 1998, **17**, 3645-3647.
46. X. Bei, D. C. Swenson and R. F. Jordan, *Organometallics*, 1997, **16**, 3282-3302.
47. M. Brookhart and M. L. H. Green, *J. Organomet. Chem.*, 1983, **250**, 395-408.
48. Z. Dawoodi, M. L. H. Green, V. S. B. Mtetwa and K. Prout, *J. Chem. Soc., Chem. Commun.*, 1982, 1410-1411.
49. Z. Dawoodi, M. L. H. Green, V. S. B. Mtetwa and K. Prout, *J. Chem. Soc., Chem. Commun.*, 1982, 802-803.
50. R. H. Grubbs and G. W. Coates, *Acc. Chem. Res.*, 1996, **29**, 85-93.
51. W. Scherer and G. S. McGrady, *Angew. Chem. Int. Ed.*, 2004, **43**, 1782-1806.
52. D. M. Roe, P. M. Bailey, K. Moseley and P. M. Maitlis, *J. Chem. Soc., Chem. Commun.*, 1972, 1273-1274.
53. Z. Dawoodi, M. L. H. Green, V. S. B. Mtetwa, K. Prout, A. J. Schultz, J. M. Williams and T. F. Koetzle, *J. Chem. Soc., Dalton Trans.*, 1986, 1629-1637.
54. M. Brookhart, M. L. H. Green and L.-L. Wong, *Prog. Inorg. Chem.*, 1988, **36**, 1.
55. L. Fan, D. Harrison, T. K. Woo and T. Ziegler, *Organometallics*, 1995, **14**, 2018-2026.
56. H. Kawamura-Kuribayashi, N. Koga and K. Morokuma, *J. Am. Chem. Soc.*, 1992, **114**, 8687-8694.
57. E. P. Bierwagen, J. E. Bercaw and W. A. Goddard, *J. Am. Chem. Soc.*, 1994, **116**, 1481-1489.
58. T. K. Woo, L. Fan and T. Ziegler, *Organometallics*, 1994, **13**, 2252-2261.

59. A. Pizzano, L. Sanchez, E. Gutierrez, A. Monge and E. Carmona, *Organometallics*, 1995, **14**, 14-16.
60. J. C. Green and C. N. Jardine, *J. Chem. Soc., Dalton Trans.*, 2001, 274-276.
61. J. W. Lauher and R. Hoffmann, *J. Am. Chem. Soc.*, 1976, **98**, 1729-1742.
62. Y. Zhao and D. Truhlar, *Theor. Chem. Acc.*, 2008, **120**, 215-241.
63. B. G. Willis and K. F. Jensen, *J. Phys. Chem. A*, 1998, **102**, 2613-2623.
64. U. Ryde, R. A. Mata and S. Grimme, *Dalton Trans.*, 2011, **40**, 11176-11183.
65. M. Bochmann and S. J. Lancaster, *Organometallics*, 1993, **12**, 633-640.
66. P. Bolton, *DPhil Thesis, University of Oxford*, 2006.
67. P. D. Bolton, E. Clot, N. Adams, S. R. Dubberley, A. R. Cowley and P. Mountford, *Organometallics*, 2006, **25**, 2806-2825.
68. J. Cámpora, P. Palma, C. M. Pérez, A. Rodríguez-Delgado, E. Álvarez and E. Gutiérrez-Puebla, *Organometallics*, 2010, **29**, 2960-2970.
69. C. G. Howard, G. Wilkinson, M. Thornton-Pett and M. B. Hursthouse, *J. Chem. Soc., Dalton Trans.*, 1983, 2025-2030.
70. M. E. García, A. Ramos, M. A. Ruiz, M. Lanfranchi and L. Marchio, *Organometallics*, 2007, **26**, 6197-6212.
71. C. M. Thomas, J. W. Napoline, G. T. Rowe and B. M. Foxman, *Chem. Commun.*, 2010, **46**, 5790-5792.
72. T. Shima, M. Nishiura and Z. Hou, *Organometallics*, 2011, **30**, 2513-2524.
73. T. H. Warren, R. R. Schrock and W. M. Davis, *Organometallics*, 1996, **15**, 562-569.
74. P. D. Bolton, E. Clot, A. R. Cowley and P. Mountford, *J. Am. Chem. Soc.*, 2006, **128**, 15005-15018.
75. C. T. Owen, P. D. Bolton, A. R. Cowley and P. Mountford, *Organometallics*, 2006, **26**, 83-92.
76. P. D. Bolton, N. Adams, E. Clot, A. R. Cowley, P. J. Wilson, M. Schroeder and P. Mountford, *Organometallics*, 2006, **25**, 5549-5565.
77. R. T. W. Scott and P. Mountford, in *Unpublished Results*, 2012.
78. M. Bochmann and S. J. Lancaster, *Angew. Chem. Int. Ed. Engl.*, 1994, **33**, 1634-1637.
79. M. Bochmann and S. J. Lancaster, *J. Organomet. Chem.*, 1992, **434**, C1-C5.
80. X. Yang, C. Stern and T. J. Marks, *Organometallics*, 1991, **10**, 840-842.

81. M. Bochmann, T. Cuenca and D. T. Hardy, *J. Organomet. Chem.*, 1994, **484**, c10-c12.
82. B. Rieger and C. Janiak, *Angew. Makromol. Chem.*, 1994, **215**, 35-46.
83. A. R. Barron, *Organometallics*, 1995, **14**, 3581-3583.
84. I. Tritto, M. C. Sacchi, P. Locatelli and S. X. Li, *Macromol. Chem. Phys.*, 1996, **197**, 1537-1544.
85. F. Zhu, Q. Huang and S. Lin, *J. Polym. Sci., Part A: Polym. Chem.*, 1999, **37**, 4497-4501.
86. P. D. Bolton, E. Clot, A. R. Cowley and P. Mountford, *Chem. Commun.*, 2005, 3313-3315.
87. R. A. Petros and J. R. Norton, *Organometallics*, 2004, **23**, 5105-5107.
88. I. Tritto, R. Donetti, M. C. Sacchi, P. Locatelli and G. Zannoni, *Macromolecules*, 1997, **30**, 1247-1252.
89. K. P. Bryliakov, E. P. Talsi and M. Bochmann, *Organometallics*, 2003, **23**, 149-152.
90. L. Schröder, H.-H. Brintzinger, D. E. Babushkin, D. Fischer and R. Mülhaupt, *Organometallics*, 2005, **24**, 867-871.
91. K. P. Bryliakov, D. E. Babushkin, E. P. Talsi, A. Z. Voskoboynikov, H. Gritzo, L. Schröder, H.-R. H. Damrau, U. Wieser, F. Schaper and H. H. Brintzinger, *Organometallics*, 2005, **24**, 894-904.
92. J. L. Eilertsen, J. A. Støvneng, M. Ystenes and E. Rytter, *Inorg. Chem.*, 2005, **44**, 4843-4851.
93. F. N. Tebbe, G. W. Parshall and G. S. Reddy, *J. Am. Chem. Soc.*, 1978, **100**, 3611-3613.
94. J. E. Kickham, F. Guérin, J. C. Stewart, E. Urbanska and D. W. Stephan, *Organometallics*, 2001, **20**, 1175-1182.
95. F. N. Tebbe and R. L. Harlow, *J. Am. Chem. Soc.*, 1980, **102**, 6149-6151.
96. T.-J. Kim, S.-K. Kim, B.-J. Kim, H.-J. Son, J. S. Hahn, M. Cheong, M. Mitoraj, M. Srebro, Ł. Piękoś, A. Michalak and S. O. Kang, *Chem. Eur. J.*, 2010, **16**, 5630-5644.
97. J. Sandström, *Dynamic NMR spectroscopy*, Academic Press: London, 1992.
98. M. L. H. Green, L. L. Wong and A. Sella, *Organometallics*, 1992, **11**, 2660-2668.
99. H. Eyring, *J. Chem. Phys.*, 1935, **3**, 107-115.

100. K. Knabel, I. Krossing, H. Nöth, H. Schwenk-Kircher, M. Schmidt-Amelunxen and T. Seifert, *Eur. J. Inorg. Chem.*, 1998, **1998**, 1095-1114.

101. A. D. Schwarz, Z. Chu and P. Mountford, *Organometallics*, 2010, **29**, 1246-1260.

102. J. Müller, U. Ruschewitz, O. Indris, H. Hartwig and W. Stahl, *J. Am. Chem. Soc.*, 1999, **121**, 4647-4652.

103. T. M. Ovitt and G. W. Coates, *J. Am. Chem. Soc.*, 2002, **124**, 1316-1326.

104. N. Nomura, R. Ishii, Y. Yamamoto and T. Kondo, *Chem. Eur. J.*, 2007, **13**, 4433-4451.

Chapter 4

Reactions of amidinate and guanidinate titanium cations with unsaturated substrates and polymerisation studies

4.1 Overview

This Chapter describes the reactions of various alkyl cations with a selection of unsaturated substrates. The Chapter begins by discussing the reactions of alkyl cations with polar unsaturated substrates before moving on to detailing reactions with non-polar substrates. High temperature ethylene-propylene (EP) copolymerisation experiments were performed by Lanxess Elastomers allowing a comparison to be made between the activities of the various types of complex and so the polymerisation capabilities of the various catalysts will also be discussed.

4.2 Reactions with polar unsaturated substrates.

The reactions of alkyl cations with polar unsaturated substrates to give Ti-C insertion products (discussed in Chapter 1) is well known, for example the reaction of di*iso*propylcarbodiimide with post-metallocene cation $[CpTi(NP^tBu_3)Me][MeBF_{15}]$ yields migratory insertion product $[CpTi(NP^tBu_3)\{MeC(N^iPr_2)_2)\}Me][MeBF_{15}]$ (**1.31**), as previously discussed in Section 1.6.6.1.[1] There have also been a large number of examples of [2+2] cycloaddition reactions with titanium imido compounds with carbodiimides and isocyanates.[2-5] Given the multiple bonded nature of the κ^1-amidinate or κ^1-guanidinate ligand with the titanium centre there was also a possibility that an analogous type of reactivity was possible in the discussed monoalkyl cationic complexes. Such reactivity has been previously noted by Tamm *et al.* with $Sc(\eta^8\text{-}C_8H_8)\{NC(N(Dipp)CH)_2\}$ which reacts with XylNCS to form the corresponding [2+2] cycloaddition product *via* addition of the N=C bond of the *iso*thiocyanate across the Sc-N bond.[6]

4.2.1 Reaction of amidinate-supported cations with heterocumulenes

The reaction of Group 4 alkyl cations with carbodiimides has been introduced previously (Section 1.6.6.1) but Group 4 species have also been shown to react with isocyanates to produce stable acetamido complexes, i.e. $(L_n)M\{OC(R)NR\}$, L = supporting ligand, R = alkyl. The first example of an isocyanate insertion product from a titanium alkyl cation was reported by Mountford *et al*. in 2008 by the insertion of *tert*-butyl*iso*cyanate into the Ti-C bond of $[Ti(N^tBu)(Me_3[9]aneN_3)Me]^+$ to yield $[Ti(N^tBu)(Me_3[9]aneN_3)\{OC(Me)N^tBu\}]^+$.[7] In 1997 Erker *et al.* showed that reaction of $[Cp_2ZrMe(THF)]^+$ (**1.17**) with an amino acid derived isocyanate ($MeO(O)CCH(^iPr)NCO$) produced the analogous acetamido insertion product.[8]

Neutral zirconocene complexes have also been shown to react with both isocyanates and carbodiimides to yield the corresponding acetamido and amidinate complexes owing to the large ionic radius of the zirconium centre.[9]

Reaction of [Cp*Ti{NC(N^{i}Pr$_2$)Ph}Me][BF$_{20}$] (**10-[BF$_{20}$]**) with di*iso*propylcarbodiimide or *tert*-butyl*iso*cyanate gave the migratory insertion products in each case, namely [Cp*Ti{NC(N^{i}Pr$_2$)Ph}{MeC(N^{i}Pr)$_2$}][BF$_{20}$] (**35-[BF$_{20}$]**) and [Cp*Ti{NC(N^{i}Pr$_2$)Ph}{OC(Me)N^{t}Bu}][BF$_{20}$] (**36-[BF$_{20}$]**) (Scheme 4.1). **35**$^+$ is related to compound **1.31** reported previously by Stephan *et al.*[1]

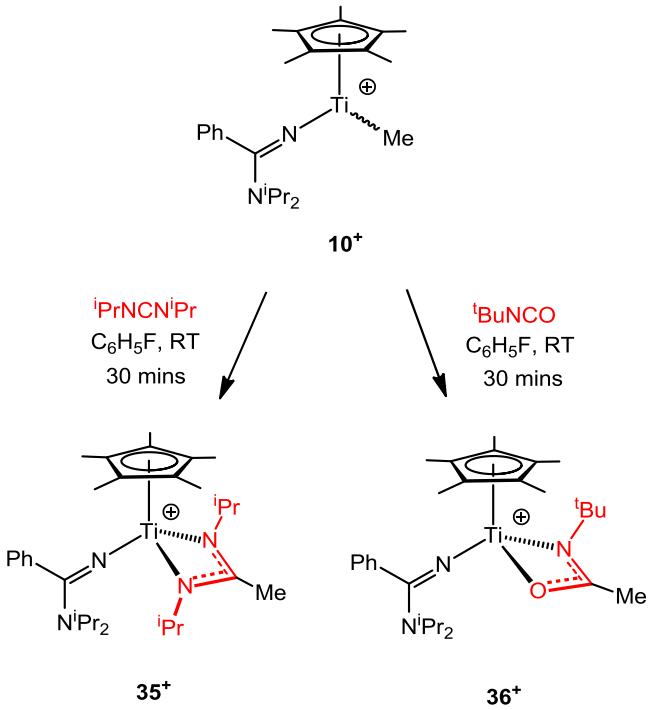

Scheme 4.1 Reaction of cation [Cp*Ti{NC(N^{i}Pr$_2$)Ph}Me]$^+$ (**10**$^+$) with di*iso*propylcarbodiimide and *tert*-butyl*iso*cyanate.

These reactions were carried out by mixing Cp*Ti{NC(N^{i}Pr$_2$)Ph}Me$_2$ (**2.4**) with either of the heterocumulenes followed by the addition of TBF$_{20}$ and both reactions are quantitative by ^{1}H NMR spectroscopy. Complex **35-[BF$_{20}$]** was isolated as a brown powder in 77% yield and **36-[BF$_{20}$]** as a red powder in 66% yield. Both **35-[BF$_{20}$]** and **36-[BF$_{20}$]** were characterised by NMR spectroscopy, IR spectroscopy and elemental analysis. The ^{1}H NMR spectrum of **35**$^+$ is shown in Figure 4.1. The features of this spectrum are the Cp* signal at 2.08 ppm, MeC(N^{i}Pr)$_2$ signal at 2.28 ppm, the κ^2-NCHMe$_2$ signal at 3.67 ppm and the κ^2-NCHMe$_2$ resonances at 1.12 and 0.74 ppm. The two κ^2-NCHMe$_2$ resonances are due to the presence of diastereotopic methyl

groups. The resonances for NC(N^{i}Pr$_2$)Ph are found at 4.21 (br, C<u>H</u>Me$_2$), 3.67 (C<u>H</u>Me$_2$), 1.40 (CH<u>Me</u>$_2$) and 1.09 ppm (CH<u>Me</u>$_2$) alongside the aromatic environments (7.50-7.20 ppm). Overall **35**$^+$ has effective C_s symmetry on the NMR timescale which is indicative of fast rotation about the Ti-N bond. The ^{13}C-{^{1}H} NMR spectrum of **35**$^+$ alongside a ^{1}H-^{13}C HMBC experiment is consistent with the insertion of the carbodiimide into the Ti-Me bond. The ^{13}C NMR chemical shift of the methyl group (13.9 ppm) is significantly downfield when compared to a Ti-<u>Me</u> in an alkyl cation (*ca.* 50-70 ppm see Chapter 3) indicating insertion of the carbodiimide into the Ti-Me bond; the HMBC spectrum shows a correlation between <u>Me</u>C(N^{i}Pr)$_2$ and Me<u>C</u>(N^{i}Pr)$_2$.

Since the vacant coordination site of the titanium has been taken up by the κ^2-amidinate DOSY NMR experiments were carried out to see if it affected the association of the cation with the anion (see Section 3.2.3). In this case the average diffusion constant for the cation by ^{1}H DOSY NMR spectroscopy was 2.78(4) x 10^{-10} m^2 s^{-1} whereas that for the anion by ^{19}F DOSY NMR spectroscopy was 2.80(6) x 10^{-10} m^2 s^{-1}. This shows that they remain associated in C_6D_5Br even after blocking the potential binding site.

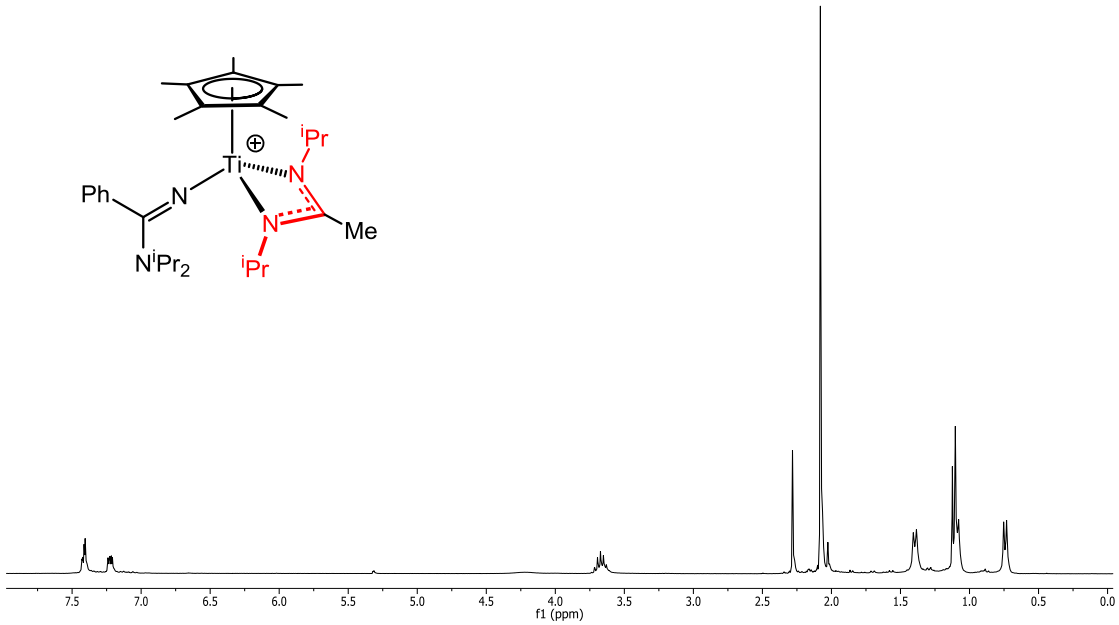

Figure 4.1 ^{1}H NMR spectrum (299.9 MHz, 293 K, CD_2Cl_2) of [Cp*Ti{NC(N^{i}Pr$_2$)Ph}{MeC(N^{i}Pr)$_2$}][BF$_{20}$] (**35-[BF$_{20}$]**).

The ^{1}H NMR spectrum of **36**$^{+}$ is consistent with C_1 symmetry in solution and contains singlet Cp* and ^{t}Bu resonances at 1.61 and 0.79 ppm, respectively. The OC(Me)N^{t}Bu signal is found at 1.99 ppm in the ^{1}H NMR spectrum and 20.7 ppm in the ^{13}C NMR spectrum which is diagnostic of insertion of the heterocumulene into the Ti-Me bond. The resonances for NC(N^{i}Pr$_2$)Ph are found at 3.41 (CHMe$_2$), 3.14 (CHMe$_2$), 1.05 (CHMe$_2$), 1.01 (CHMe$_2$), 0.70 (CHMe$_2$) and 0.64 ppm (CHMe$_2$) alongside the aromatic environments (7.20-6.70 ppm). Analogous to **35**$^{+}$ the ^{1}H-^{13}C HMBC spectrum shows a correlation between OC(Me)N^{t}Bu and OC(Me)N^{t}Bu. **35**$^{+}$ and **36**$^{+}$ are both stable for long periods of time in solution and so these small unsaturated heterocumulenes can be used as efficient traps to form stable isolable derivatives when investigating more unstable species such as the methyl cations discussed in Chapter 2. For example, treatment of the mixture of cationic species on activation of **2.4** (discussed in Section 3.2.5) with di*iso*propylcarbodiimide gives the quantitative formation of **35-[BF$_{20}$]** by ^{1}H NMR spectroscopy which can then be isolated.

Related complex Cp*Ti{NC(N^{i}Pr$_2$)Ar^{F_2}}Me$_2$ (**1.49**), in which the *ortho*-hydrogens on the phenyl group have been replaced by fluorine atoms, following activation with TBF$_{20}$ was reacted with both di*iso*propylcarbodiimide and *tert*-butyl*iso*cyanate. The result of these reactions was the same as the non-fluorinated analogue and followed a migratory insertion reaction pathway to produce [Cp*Ti{NC(N^{i}Pr$_2$)Ar^{F_2}}-{MeC(N^{i}Pr)$_2$}][BF$_{20}$] (**37-[BF$_{20}$]**) and [Cp*Ti{NC(N^{i}Pr$_2$)Ar^{F_2}}{OC(Me)N^{t}Bu}][BF$_{20}$] (**38-[BF$_{20}$]**). Compounds **37-[BF$_{20}$]** and **38-[BF$_{20}$]** were isolated in yields of 61% and 76%, respectively and characterised by NMR spectroscopy, IR spectroscopy and elemental analysis. The NMR data for **37**$^{+}$ and **38**$^{+}$ were analogous to those for **35**$^{+}$ and **36**$^{+}$ and will not be discussed.

In order to try to obtain an X-ray structure of one of these cations the Lewis acid BF$_{15}$ (discussed in Chapter 1) was used to activate **1.49** in presence of di*iso*propylcarbodiimide. Using BF$_{15}$ as a methyl abstraction agent yields the anion [MeBF$_{15}$]$^{-}$ which is more polar than [BF$_{20}$]$^{-}$ and helps confer crystallinity. In this case this allowed the crystallisation of the carbodiimide-trapped cation (**37-[MeBF$_{15}$]**) from CH$_2$Cl$_2$ at room temperature and thus characterisation by single crystal diffraction. The molecular structure of **37**$^{+}$ is displayed in Figure 4.2 and selected distances and angles are listed in Table 4.1. Compound **37-[MeBF$_{15}$]** was also characterised by NMR spectroscopy, IR spectroscopy and elemental analysis. The NMR data are again

analogous to those for **35**$^+$ and **37**$^+$ and so will not be discussed in any detail, the only difference between the ^{1}H NMR spectrum of **37-[BF$_{20}$]** and **37-[MeBF$_{15}$]** being a broad MeBF$_{15}$ signal at 0.93 ppm.

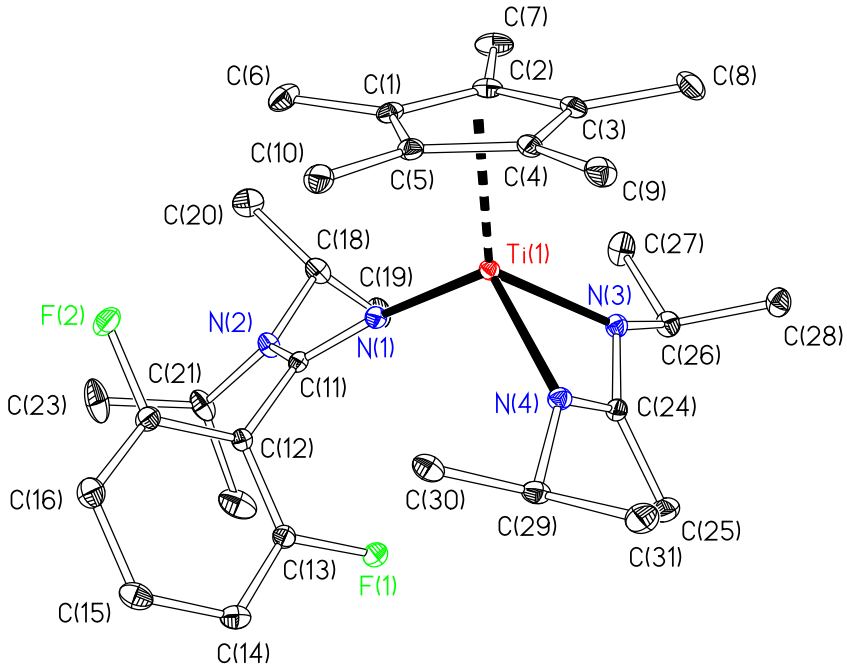

Figure 4.2 Displacement ellipsoid plot (20% probability) of cation [Cp*Ti{NC(N^{i}Pr$_2$)Ar^{F_2}}{MeC(N^{i}Pr)$_2$}]$^+$ (**37**$^+$). H atoms omitted for clarity.

Table 4.1 Selected bond lengths (Å) and angles (°) for [Cp*Ti{NC(N^{i}Pr$_2$)Ar^{F_2}}-{MeC(N^{i}Pr)$_2$}]$^+$ (**37**$^+$). Cp$_{cent}$ is the computed ring centroid.

Ti(1)-Cp$_{cent}$	2.04	Cp$_{cent}$-Ti(1)-N(1)	116.3
Ti(1)-N(1)	1.807(2)	Cp$_{cent}$-Ti(1)-N(3)	124.7
Ti(1)-N(3)	2.039(2)	Cp$_{cent}$-Ti(1)-N(4)	123.3
Ti(1)-N(4)	2.050(2)	Ti(1)-N(1)-C(11)	171.1(2)
N(1)-C(11)	1.301(3)	N(1)-Ti(1)-N(3)	109.30(9)
N(2)-C(11)	1.343(3)	N(1)-Ti(1)-N(4)	106.82(9)
N(3)-C(24)	1.332(3)	N(3)-Ti(1)-N(4)	66.08(9)
N(4)-C(24)	1.343(3)	N(3)-C(24)-N(4)	112.9(2)

The molecular structure of **37**$^+$ contains a *pseudo*-tetrahedral titanium centre with κ^1-amidinate, κ^2-amidinate and Cp* coordinated ligands and shows C_1 symmetry in the solid state. The Ti(1)-N(1) bond length (1.807(2) Å) is longer than in the dimethyl bridged dication **1.26$_{dim}$**$^{2+}$ (1.7913(13) Å).[10] This is as a result of the κ^2-amidinate

ligand which acts as a much better donor than the 3c-2e bridging methyl groups present in $\mathbf{1.26_{dim}}^{2+}$. The Ti(1)-N(3) and Ti(1)-N(4) are only slightly different (2.039(2)Å and 2.050(2) Å) consistent with a symmetrical κ^2-amidinate binding to the metal centre. The Ti(1)-N(2) and Ti(1)-N(3) distances are slightly shorter than those found in isolobal cationic complex $[Ti(N^tBu)(Me_3[9]aneN_3)\{MeC(N^iPr)_2\}]^+$ (**4.1**) (Ti(1)-N(2), 2.102(3) Å and Ti(1)-N(3), 2.120(2) Å)[11] presumably because of the increased electron donation to the titanium centre from ^{t}BuN and $Me_3[9]aneN_3$ compared to Cp* and $NC(N^iPr_2)Ar^{F_2}$ and a reduction of steric bulk around the metal centre going from an octahedral to tetrahedral complex. Also in complex **4.1** there are nitrogen atoms trans to the amidinate which can cause a lengthening of the Ti-N(amidinate) bonds.[12]

4.2.2 Reaction of amidinate-supported cations with nitriles

Several cationic species of the type $[(L)_2Ti\{NC(R)Me\}(NCR)]^+$ (L = Cp, Ind, Cp*; R = Me, Ph, ^{t}Bu, ^{n}Pr) have been reported by Bochmann *et al*. as discussed previously.[13] The insertion of the nitrile into the Ti-Me bond takes *ca.* 1 h for L = Ind but for the Cp analogue it can take 24 h or even 2 weeks in the case of acetonitrile.

The reactions of $\mathbf{10}^+$ and $\mathbf{1.26}^+$ with nitriles were anticipated to form the Lewis base adducts $[Cp^*Ti\{NC(N^iPr_2)Ph\}Me(NCR)]^+$ and $[Cp^*Ti\{NC(N^iPr_2)Ar^{F_2}\}Me(NCR)]^+$ (R = alkyl, aryl) followed by migratory insertion as seen previously for metallocenium systems.[13, 14] When **10-[BF$_{20}$]** and **1.26-[BF$_{20}$]** were generated *in situ* in the presence of two equivalents of MeCN this resulted in immediate and quantitative conversion to $[Cp^*Ti\{NC(N^iPr_2)Ph\}(NCMe_2)(NCMe)][BF_{20}]$ (**39-[BF$_{20}$]**) and $[Cp^*Ti\{NC(N^iPr_2)\text{-}Ar^{F_2}\}(NCMe_2)(NCMe)][BF_{20}]$ (**40-[BF$_{20}$]**) by ^{1}H NMR spectroscopy (Equation 4.1).

Compounds **39-[BF$_{20}$]** and **40-[BF$_{20}$]** were isolated in yields of 81% and 75%, respectively and were fully characterised by NMR spectroscopy, IR spectroscopy and elemental analysis. The rapid insertion of MeCN into the Ti-Me bond of $\mathbf{10}^+$ and $\mathbf{1.26}^+$ is unlike $[Cp_2TiMe][BPh_4]$ which takes 2 weeks to react with this substrate.[13, 15, 16] The ^{1}H NMR spectrum of $\mathbf{39}^+$ contains singlet resonances for Cp*, MeCN and $NC\underline{Me}_2$ at 1.55, 1.60 and 1.65 ppm, respectively. The amidinate ligand's aromatic (7.13-6.87 ppm), $C\underline{H}Me_2$ (3.38, 3.24 ppm) and $CH\underline{Me}_2$ (1.29, 1.23, 0.74 and 0.65 ppm) are also present in the ^{1}H NMR spectrum. $\mathbf{40}^+$ contains analogous resonances to $\mathbf{39}^+$ and so will not be discussed.

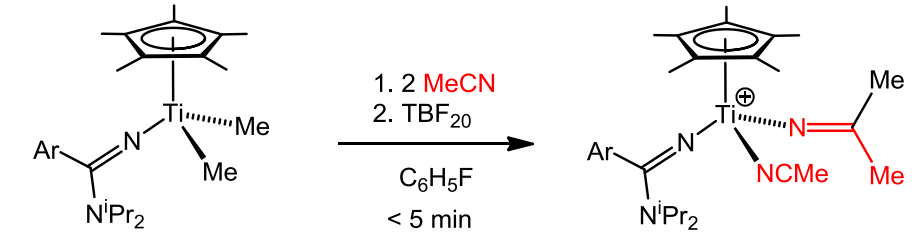

Equation 4.1

Activation of **2.4** and **1.49** in the presence of 2 equivs of benzonitrile also gave rise to the corresponding insertion products [Cp*Ti{NC(N^{i}Pr$_2$)Ph}(NCMePh)(NCPh)][BF$_{20}$] (**41-[BF$_{20}$]**) and [Cp*Ti{NC(N^{i}Pr$_2$)Ar^{F_2}}(NCMePh)(NCPh)][BF$_{20}$] (**42-[BF$_{20}$]**) quantitatively by ^{1}H NMR spectroscopy which could then be isolated in 73% and 80% yields, respectively. Both **41-[BF$_{20}$]** and **42-[BF$_{20}$]** were characterised by NMR spectroscopy, IR spectroscopy and elemental analysis. The ^{1}H NMR spectrum of **41**$^+$ contains resonances corresponding to Cp* (1.63 ppm), NC<u>Me</u>Ph (2.16 ppm), C<u>H</u>Me$_2$ (3.40, 3.22 ppm), CH<u>Me</u>$_2$ (1.30, 0.68 ppm) as well as appropriate signals spanning the aromatic region (7.50-6.90 ppm). **42** contains analogous resonances to **41** and so will not be discussed.

4.2.3 Reaction of guanidinate-supported cations with heterocumulenes

4.2.3.1 Reaction of guanidinate-supported cations with di*iso*propylcarbodiimide

As expected, activation of guanidinate dimethyl complexes **4**, **6** and **7** by TBF$_{20}$ in C$_6$D$_5$Br the presence of di*iso*propylcarbodiimide led to the quantitative production of κ^2-amidinate supported products [Cp*Ti{NC(NMe$_2$)$_2$}{MeC(N^{i}Pr)$_2$}][BF$_{20}$] (**43-[BF$_{20}$]**), [Cp*Ti{NC(NMe^{i}Bu)$_2$}{MeC(N^{i}Pr)$_2$}][BF$_{20}$] (**44-[BF$_{20}$]**) and [Cp*Ti{NC(N(Xyl)CH$_2$)$_2$}{MeC(N^{i}Pr)$_2$}][BF$_{20}$] (**45-[BF$_{20}$]**) by ^{1}H NMR spectroscopy; these complexes were isolated on a preparative scale in 82%, 80% and 72% yield, respectively.

The ^{1}H NMR spectrum of **43**$^+$ is consistent with C_s symmetry in solution and contains singlet resonances at 2.31, 1.75 and 1.73 ppm which can be assigned to NMe$_2$, Me<u>C</u>(N^{i}Pr)$_2$ and Cp*, respectively. The signals for the *iso*propyl C<u>H</u>Me$_2$ and CH<u>Me</u>$_2$ are found at 3.31, 0.79, and 0.70 ppm. The ^{1}H-^{13}C HMBC experiment and ^{13}C-{^{1}H} NMR spectrum again confirms formation of the Ti-Me insertion product (<u>Me</u>C(N^{i}Pr)$_2$, 13.6 ppm). Cation **44**$^+$ contains similar spectral features to **43**$^+$ for the κ^2-amidinate

ligand with resonances in the ^{1}H NMR spectrum at 3.35 ppm (C<u>H</u>Me$_2$), 1.77 (<u>Me</u>C(N^{i}Pr)$_2$) ppm, 0.81 ppm (CH<u>Me$_2$</u>) and 0.72 ppm (CH<u>Me$_2$</u>). The signals for the ligand NC(N^{i}BuMe)$_2$ are straightforward and found at 2.56 ppm (NC<u>H$_2$</u>), 2.38 ppm (N<u>Me</u>), 1.54 ppm (C<u>H</u>Me$_2$) and 0.58 ppm (CH<u>Me$_2$</u>). These resonances alongside that of Cp* (1.76 ppm) are consistent with C_s symmetry in solution. The ^{1}H NMR spectrum of **45**$^+$ is also consistent with C_s symmetry and contains κ^2-amidinate signals at 3.31 (C<u>H</u>Me$_2$), 2.18 (<u>Me</u>C(N^{i}Pr)$_2$), 0.97 (CH<u>Me$_2$</u>) and 0.25 (CH<u>Me$_2$</u>) ppm. The remaining resonances in the spectrum are for C$_6$<u>H$_3$</u>Me$_2$, NC<u>H$_2$</u>, C$_6$H$_3$<u>Me$_2$</u> and Cp* environments found at 7.15, 3.82, 2.41 and 1.92 ppm, respectively.

4.2.3.2 Crystal structure of [Cp*TiNC(N(Xyl)CH$_2$)$_2$}{MeC(N^{i}Pr)$_2$}][BF$_{20}$] (45-[BF$_{20}$])

Diffraction-quality crystals of **45-[BF$_{20}$]** were grown from a solution of CH_2Cl_2 at room temperature. The molecular structure of **45**$^+$ is displayed in Figure 4.3 and selected distances and angles are listed in Table 4.2. The molecular structure of **45**$^+$ contains a *pseudo*-tetrahedral titanium centre with κ^1-iminoimidazolidide, κ^2-amidinate ligand and Cp* ligands coordinated and has approximate C_s symmetry in the solid state. The Ti(1)-N(1) bond length is identical within error to the corresponding distance in **37**$^+$ (1.807(2) Å vs. 1.8012(12) Å) and is, as expected, significantly shorter than in the corresponding neutral complex **7** (1.8335(8) Å). The Ti(1)-N(4) and Ti(1)-N(5) bond distances are identical within error consistent with symmetrical bonding of the κ^2-amidinate to the titanium centre (2.0552(13) and 2.0590(13) Å).

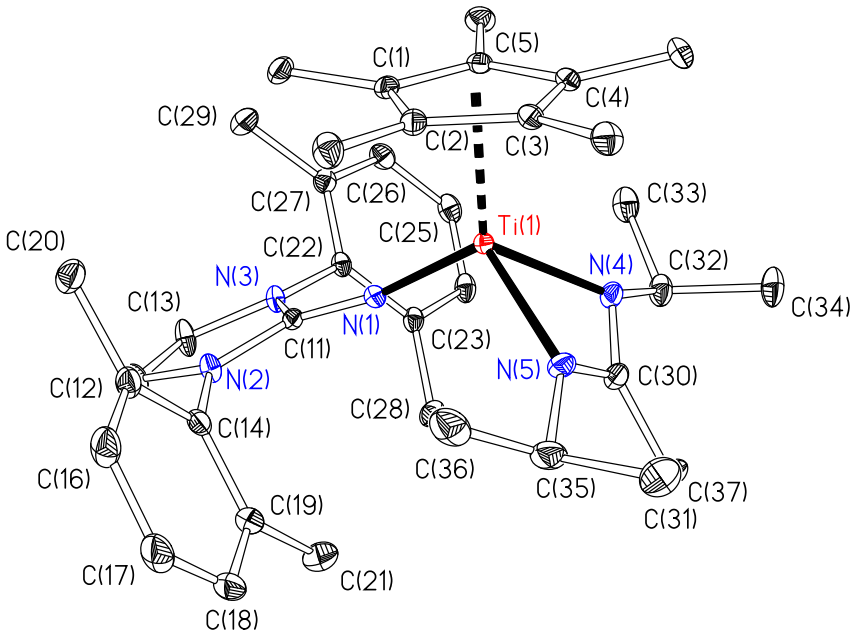

Figure 4.3 Displacement ellipsoid plot (20% probability) of cation $[Cp^*Ti\{NC(N(Xyl)CH_2)_2\}\{MeC(N^iPr)_2\}]^+$ (**45**$^+$). H atoms omitted for clarity.

Table 4.2 Selected bond lengths (Å) and angles (°) for $[Cp^*Ti\{NC(N(Xyl)CH_2)_2\}\{MeC(N^iPr)_2\}]^+$ (**45**$^+$). Cp_{cent} is the computed ring centroid.

Ti(1)-Cp_{cent}	2.04	Cp_{cent}-Ti(1)-N(1)	119.7
Ti(1)-N(1)	1.8012(12)	Cp_{cent}-Ti(1)-N(4)	121.6
Ti(1)-N(4)	2.0552(13)	Cp_{cent}-Ti(1)-N(5)	121.2
Ti(1)-N(5)	2.0590(13)	Ti(1)-N(1)-C(11)	170.41(11)
N(1)-C(11)	1.3064(19)	N(1)-Ti(1)-N(4)	109.01(6)
N(2)-C(11)	1.364(2)	N(1)-Ti(1)-N(5)	107.83(6)
N(3)-C(11)	1.358(2)	N(4)-Ti(1)-N(5)	65.40(6)
N(4)-C(30)	1.332(2)	N(4)-C(24)-N(5)	113.22(14)
N(5)-C(30)	1.329(3)		

4.2.3.3 Reaction of guanidinate-supported cations with *tert*-butyl*iso*cyanate

The activation of the precatalysts **4** and **6** with TBF_{20} in the presence of *tert*-butyl*iso*cyanate produced acetamido complexes $[Cp^*Ti\{NC(NMe_2)_2\}\{OC(Me)N^tBu\}][BF_{20}]$ (**46-[BF$_{20}$]**) and $[Cp^*Ti\{NC(NMe^iBu)_2\}\{OC(Me)N^tBu\}][BF_{20}]$ (**47-[BF$_{20}$]**) in quantitative yield by ^{1}H NMR spectroscopy. Under the same conditions **7** gave a mixture of unidentified products by ^{1}H NMR spectroscopy. Complexes **46-[BF$_{20}$]** and **47-[BF$_{20}$]** could be isolated on a preparative scale in 76%

and 62% yield, respectively, and were subsequently characterised by NMR spectroscopy, IR spectroscopy and elemental analysis.

The ^{1}H NMR spectra of **46**$^{+}$ and **47**$^{+}$ both contained singlet Cp* (2.14 and 2.03 ppm, respectively), OC(Me)N^{t}Bu (2.37 and 2.17 ppm, respectively) and ^{t}Bu (1.24 and 1.12 ppm, respectively) resonances which are consistent with C_1 symmetry in solution. As seen in cationic complexes derived from **4** previously the ligand based NMe_2 signal (2.79 ppm) for **46**$^{+}$ exists as a singlet which is consistent with fast rotation about the Ti-N and C(sp^2)-N bonds. The signals for NC(N^{i}BuMe)$_2$ in **47**$^{+}$ consist of a singlet at 2.64 ppm (NMe), two doublet of doublets at 2.87 and 2.61 ppm (CH_2), a multiplet at 1.72 ppm ($CHMe_2$) and two doublets at 0.83 and 0.79 ppm ($CHMe_2$). The singlet NMe resonance is indicative of fast rotation about the Ti-N bond. The two signals for the CH_2 environments arise because of the diastereotopic methylene groups and the two doublets for the $CHMe_2$ environment because of the diastereotopic methines.

The insertion reactions of di*iso*propylcarbodiimide and *tert*-butyl*iso*cyanate with the previously discussed benzyl equivalent of **4**, Cp*Ti{NC(NMe$_2$)$_2$}Bn$_2$ (**5**), were also carried out. Activation of **5** with TBF_{20} in the presence of di*iso*propylcarbodiimide and *tert*-butyl*iso*cyanate produced [Cp*Ti{NC(NMe$_2$)$_2$}{BnC(N^{i}Pr)$_2$}][BF_{20}] (**48-[BF$_{20}$]**) and [Cp*Ti{NC(NMe$_2$)$_2$}{OC(Bn)N^{t}Bu}][BF_{20}] (**49-[BF$_{20}$]**) quantitatively by ^{1}H NMR spectroscopy. Unlike the $OPPh_3$ adduct **20-[BF$_{20}$]**, **48-[BF$_{20}$]** could be isolated on a preparative scale in 70% yield and was subsequently characterised by NMR spectroscopy, IR spectroscopy and elemental analysis. The ^{1}H NMR spectrum of **48**$^{+}$ is consistent with C_s symmetry and contains the expected singlet Cp* and NMe_2 resonances at 2.36 and 1.77 ppm, respectively. The spectrum also contains signals for $CHMe_2$ (3.40), $CHMe_2$ (0.73 and 0.64) and CH_2Ph (3.65 ppm) alongside the aromatic signals between 7.20-6.70 ppm. The ^{1}H NMR spectrum for the acetamido complex **49**$^{+}$ is consistent with C_1 symmetry in solution and contains singlets for Cp* (1.67 ppm), NMe_2 (2.27 ppm), and ^{t}Bu (0.99 ppm) alongside the aromatic protons CH_2Ph (7.16-6.40 ppm). The CH_2Ph environment is diastereotopic in this complex and so is observed as two doublets (3.65 and 3.54 ppm, ^{2}J = 14.5). Complex **49**$^{+}$ is, however, unstable in solution and could not be isolated. This prevented obtaining ^{13}C-{^{1}H} NMR or elemental analysis data.

4.2.4 Reaction of guanidinate-supported cations with nitriles

To check that they behaved the same as the amidinate complexes the activation of guanidinate complexes **4** and **7** in the presence of 2 equivs of acetonitrile gave the immediate and quantitative formation of the ketimide complexes [Cp*Ti{NC(NMe$_2$)$_2$}(NCMe$_2$)(NCMe)][BF$_{20}$] (**50-[BF$_{20}$]**) and [Cp*Ti{NC(N(Xyl)-CH$_2$)$_2$}(NCMe$_2$)(NCMe)][BF$_{20}$] (**51-[BF$_{20}$]**) by ^{1}H NMR spectroscopy. Complexes **50-[BF$_{20}$]** and **51-[BF$_{20}$]** were isolated in yields of 86% and 58%, respectively and characterised by NMR spectroscopy, IR spectroscopy and elemental analysis. The ^{1}H NMR spectrum of **50**$^+$ and **51**$^+$ contained singlet signals for Cp* (1.99 and 1.37 ppm), NCMe$_2$ (1.95 and 1.57 ppm) and MeCN (2.41 and 1.55 ppm). In **50**$^+$ the guanidinate NMe$_2$ resonance is observed as a singlet as before (2.80 ppm). The iminoimidazolidide signals in **51-[BF$_{20}$]** consist of a singlet at 3.29 ppm (C$\underline{H}_2$) alongside two singlets (2.10 and 2.07 ppm) for the C$_6$H$_3\underline{Me}_2$ environments.

4.2.5 Reaction of Lewis base adducts with d*iso*propylcarbodiimide

In order to ascertain the extent of reactivity of the various Lewis base-stabilised cations discussed previously, di*iso*propylcarbodiimide was utilised since it is known to be highly reactive and produces stable products. Initially the isolated OPPh$_3$ adducts **11**$^+$, **16**$^+$, **22**$^+$ and **26**$^+$ were each dissolved in C$_6$D$_5$Br and di*iso*propylcarbodiimide (1 equiv) was added. In all cases no reactivity was observed even over the period of 2 weeks. This observation is consistent with the high basicity of OPPh$_3$ which cannot be displaced by the less basic carbodiimide before insertion then occurs. Subsequently di*iso*propylcarbodiimide was added to the pyridine adducts **8**$^+$, **12**$^+$, **17**$^+$, **23**$^+$ and **27**$^+$, since pyridine is less basic, and over the period of *ca.* 2 h the insertion reaction went to completion resulting in the formation of complexes **35**$^+$, **37**$^+$, **43**$^+$, **44**$^+$ and **45**$^+$ alongside free pyridine. Accordingly reaction of the THF stabilised cations **9**$^+$, **13**$^+$, **18**$^+$, **24**$^+$ and **28**$^+$ with di*iso*propylcarbodiimide were even more facile than the pyridine adducts occurring immediately and quantitatively by ^{1}H NMR spectroscopy to yield complexes **35**$^+$, **37**$^+$, **43**$^+$, **44**$^+$ and **45**$^+$. The reaction of **18**$^+$ with di*iso*propylcarbodiimide is shown by way of example in Equation 4.2.

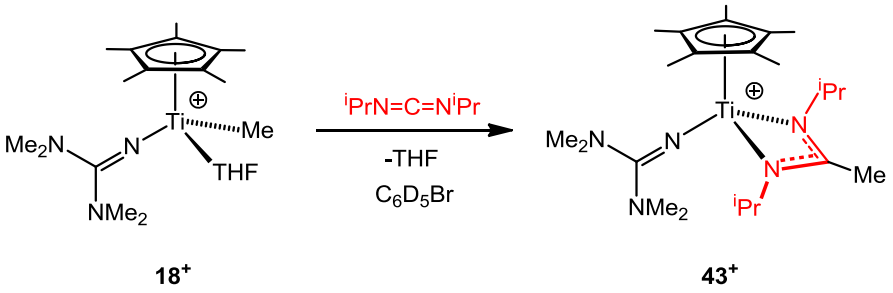

18$^+$ **43**$^+$

Equation 4.2

4.3 Reaction of amidinate-supported cations with alkynes

Following the type of reactivity first carried out by Eisch in 1985 in which the internal alkyne PhCCSiMe$_3$ was inserted into the Ti-Me bond of [Cp$_2$TiMe]$^+$ the cations **10**$^+$ and **1.26**$^+$ were reacted with alkyne substrates.[17] The substrate PhCCSiMe$_3$ was used initially as a direct comparison to the original reaction with the metallocenium cation. Following addition of PhCCSiMe$_3$ to cations **10**$^+$ and **1.26**$^+$ in C$_6$D$_5$Br the formation of two products was observed on the NMR tube scale in each case after 10 mins. This can be clearly observed in the ^{1}H NMR spectra (Figure 4.4) for the reaction products of both **10**$^+$ (forming **52**$^+$) and **1.26**$^+$ (forming **53**$^+$) which each contain two distinct Si<u>Me</u>$_3$ resonances (**52**$^+$, -0.15, -0.52 ppm and **53**$^+$, -0.22, -0.46 ppm). Discussion will initially concentrate on the insertion products (**52**$^+$) obtained from cation **10**$^+$**.**

The ^{1}H NMR spectrum observed after 10 min for **52**$^+$ shows two distinct set of signals for each chemical environment. This is a result of two isomers (**52a**$^+$ and **52b**$^+$) present in solution in a ratio of 3:2 (Figures 4.4 and 4.5). There are two Cp* resonances at 1.65 ppm (**52b**$^+$) and 1.43 ppm (**52a**$^+$), two Me$_3$SiCC(Ph)<u>Me</u> signals at 1.92 (**52a**$^+$) and 1.68 ppm (**52b**$^+$) and two SiMe$_3$ resonances at -0.15 ppm (**52a**$^+$) and -0.52 ppm (**52b**$^+$). The ^{1}H NMR spectrum is consistent with C_1 symmetry for each isomer. The ^{29}Si NMR shifts of the products are -43.2 ppm (**52b**$^+$) and -16.0 ppm (**52a**$^+$). An upfield shift of -43.2 ppm is indicative of the presence of a β-Si-C agostic interaction (*cf.* **1.16**$^+$, -54.9 ppm) whereas -16.0 ppm is typical of a non-bound SiMe$_3$ group. The products of this reaction are in fact γ-C-H (**52a**$^+$) and β-Si-C (**52b**$^+$) agostic isomers of [Cp*Ti{NC(N^{i}Pr$_2$)Ph}{Me$_3$SiCC(Ph)Me}][BF$_{20}$] (Figure 4.5).

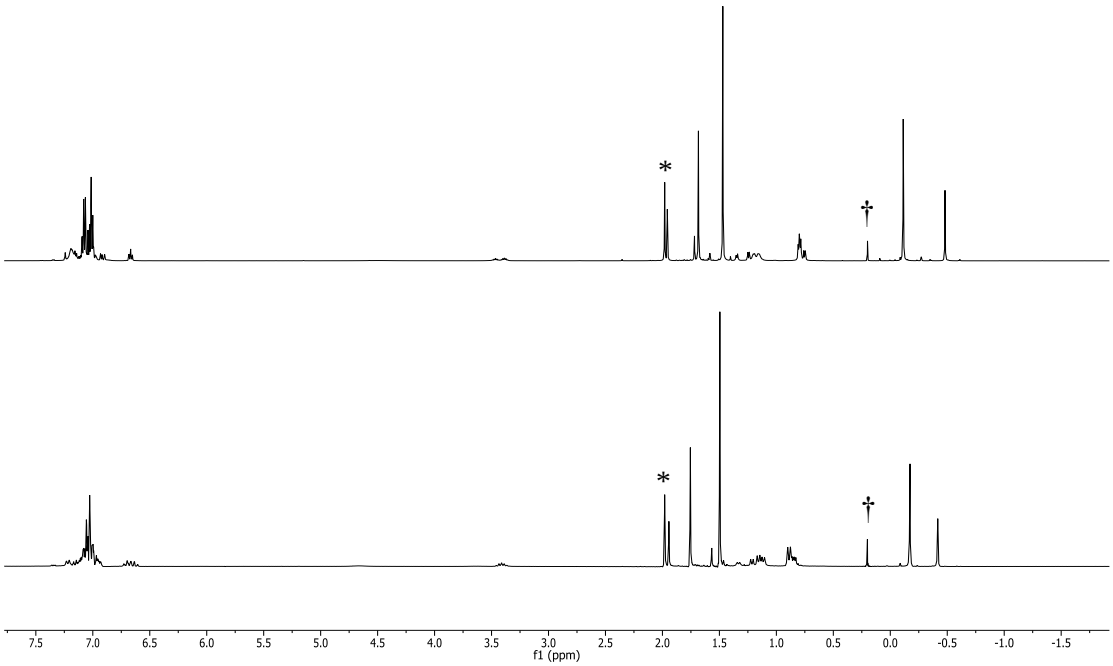

Figure 4.4 ^{1}H NMR spectrum (299.9 MHz, 293K, C_6D_5Br) of [Cp*Ti{NC(N^{i}Pr$_2$)Ph}{Me$_3$SiCC(Ph)Me}][BF$_{20}$] (**52-[BF$_{20}$]**, top) and [Cp*Ti-{NC(N^{i}Pr$_2$)Ar^{F_2}}{Me$_3$SiCC(Ph)Me}][BF$_{20}$] (**53-[BF$_{20}$]**, bottom). Ph$_3$CMe is labelled '*' and free excess Me$_3$SiCCPh is labelled '†'.

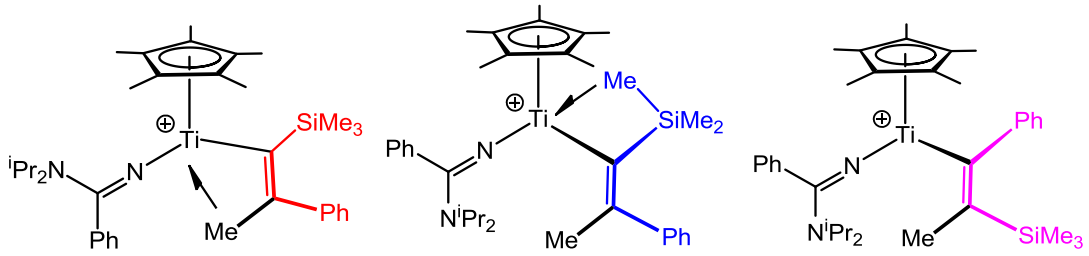

Figure 4.5 Structures of γ-C-H (**52a**$^{+}$, left) and β-Si-C (**52b**$^{+}$, centre) agostic isomers of [Cp*Ti{NC(N^{i}Pr$_2$)Ph}{Me$_3$SiCC(Ph)Me}]$^{+}$ (**52**$^{+}$) resulting from 1,2-insertion and the unobserved 2,1-insertion product [Cp*Ti{NC(N^{i}Pr$_2$)Ph}{PhCC(SiMe$_3$)Me}][BF$_{20}$] (**52c**$^{+}$).

The presence of these two isomers could have been due to the formation of both 1,2- and 2,1-insertion products (e.g. **52b**$^{+}$ and **52c**$^{+}$, Figure 4.5) but as shown in Section 4.3.1 derivatising the mixture leads to a single product and not to two regioisomers.

Another possibility is the formation of monomer-dimer equilibrium in which the dimerisation process broke the β-Si-C agostic interaction. The DOSY ^{1}H NMR spectrum of these two isomers in C_6D_5Br yields diffusion constant values of 2.35(4) x 10^{-10} m^2 s^{-1} and 2.32(4) x 10^{-10} m^2 s^{-1} consistent with two species of the same size in solution. Accordingly a mixture of [Cp*Ti{NC(N^{i}Pr$_2$)Ph}{Me$_3$SiCC(Ph)Me}]$^+$ (**52**$^+$) and [Cp*Ti{NC(N^{i}Pr$_2$)Ar^{F_2}}{Me$_3$SiCC(Ph)Me}]$^+$ (**53**$^+$) (discussed *vide infra*) in solution also shows no formation of dimers [**52-53**]$^{2+}$ which might have been expected to form alongside any dimers [**52-52**]$^{2+}$ or [**53-53**]$^{2+}$. Although these compounds have been fully characterised by NMR spectroscopy they could not be isolated on scale-up. In solution these isomers also decompose over the period of *ca.* 2 hours making extended NMR studies difficult. Interestingly at equilibrium the ratio of 3:2 is in favour of the γ-C-H agostic isomer (discussed further in Section 4.3.2).

The product of the reaction between PhCCSiMe$_3$ and [Cp*Ti{NC(N^{i}Pr$_2$)Ar^{F_2}}-{Me$_3$SiCC(Ph)Me}]$^+$, as seen in the ^{1}H NMR spectrum in Figure 4.4, also results in the formation of two isomers. The ^{29}Si NMR shifts of the products are -42.0 ppm (**53b**$^+$) and -15.8 ppm (**53a**$^+$). These species are again unstable in solution; leaving the reaction mixture in this case for several hours results in the production of a crystalline solid, namely [Cp*$_2$Ti$_2${NC(N^{i}Pr$_2$)Ar^{F_2}}$_2$(μ-Br)$_2$][BF$_{20}$]$_2$ (**54-[BF$_{20}$]$_2$**). This product is formed as a result of solvent activation and may explain the decomposition of both **52**$^+$ and **53**$^+$ in solution over time. The bromo-bridged dimer (**54**$^{2+}$) is insoluble in CH_2Cl_2 and halobenzene solvents and so could not be characterised by NMR spectroscopy. However, it has been characterised by X-ray crystallography (Figure 4.6), elemental analysis and IR spectroscopy.

The molecular structure of **54**$^{2+}$ is displayed in Figure 4.6 and selected distances and angles are listed in Table 4.3. **54**$^{2+}$ contains two titanium atoms which each have a *pseudo* tetrahedral arrangement of ligands and the overall structure has crystallographic C_i symmetry. The Ti(1)-N(1) (1.783(3) Å) and N(2)-C(11) (1.340(5) Å) bond lengths are identical within error to that observed in the previously reported methyl bridged dimer **1.26$_{dim}$**$^{2+}$ (1.7913(13) and 1.340 (2) Å, respectively). The Ti(1)-N(1)-C(11) bond angle is approximately linear (167.4(3)°) again consistent with pπ-dπ Ti-N bonding.

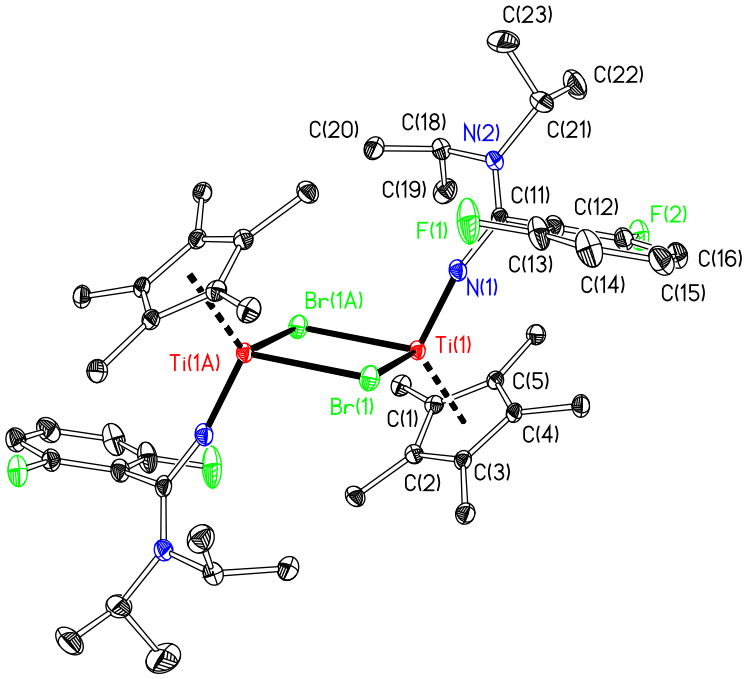

Figure 4.6 Displacement ellipsoid plot (20% probability) of dication $[(Cp^*)_2Ti_2\{NC(Ar^{F_2})N^iPr_2\}_2(\mu\text{-}Br)_2]^{2+}$ (**54**$^{2+}$). H atoms omitted for clarity. Atoms carrying the suffix 'A' are related to their counterparts by the symmetry operator [1-*x*, 1-*y*, 1-*z*].

Table 4.3 Selected bond lengths (Å) and angles (°) for $[Cp^*_2Ti_2\{NC(Ar^{F_2})N^iPr_2\}_2\text{-}(\mu\text{–}Br)_2]^{2+}$ (**54**$^{2+}$). Cp_{cent} is the computed ring centroid.

Ti(1)-Cp_{cent}	2.01	Cp_{cent}-Ti(1)-N(1)	119.1
Ti(1)-N(1)	1.783(3)	Cp_{cent}-Ti(1)-Br(1)	115.6
N(1)-C(11)	1.328(4)	Cp_{cent}-Ti(1)-Br(1A)	118.2
N(2)-C(11)	1.340(5)	Ti(1)-N(1)-C(11)	167.4(3)
Ti(1)-Br(1)	2.5438(7)	N(1)-Ti(1)-Br(1)	104.11(10)
Ti(1)-Br(1A)	2.5770(7)	N(1)-Ti(1)-Br(1A)	106.89(10)
		Br(1)-Ti(1)-Br(1A)	88.19(2)
		Ti(1)-Br(1)-Ti(1A)	91.81(2)

4.3.1 Reaction of agostic isomers 52^+ and 53^+ with di*iso*propylcarbodiimide

It has already been demonstrated that the reaction of monomethyl cations with di*iso*propylcarbodiimide produces κ^2-amidinate supported complexes (Sections 4.2.1 and 4.2.3.1). Reaction of both isomers of **53**$^+$ with di*iso*propylcarbodiimide in C_6D_5Br

gave the immediate formation of a κ^2-amidinate species, [Cp*Ti{NC(N^{i}Pr$_2$)Ar^{F_2}}-{(Me$_3$SiCC(Ph)Me)C(N^{i}Pr)$_2$}][BF$_{20}$] (**55-[BF$_{20}$]**, Equation 4.3). Since the SiMe$_3$ group has now been removed spatially from the titanium centre, preventing agostic interaction, there is now only a single species present in the ^{1}H NMR spectrum. Since the Ti-C(alkenyl) bond has been replaced by more stable Ti-N(κ^2-amidinate) bonds **55-[BF$_{20}$]** is now isolable, unlike **53-[BF$_{20}$]**. Compound **55-[BF$_{20}$]** was isolated in a 77% yield and was characterised by NMR spectroscopy, IR spectroscopy and elemental analysis.

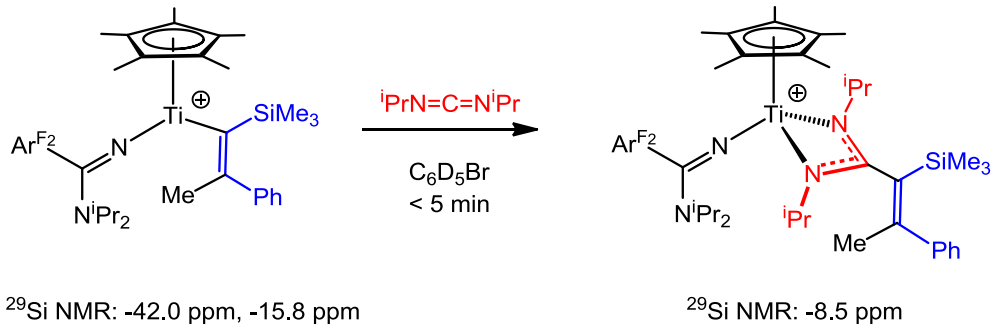

Equation 4.3

NOE experiments indicate that the CC<u>Me</u> group and *ortho*-Ph protons are in close proximity consistent with the proposed structure. The ^{29}Si NMR signal (-8.5 ppm) is also consistent with a non-agostically stabilised species. The ^{1}H NMR spectrum contains singlet resonances for Cp* (2.08 ppm), (Me$_3$SiCC(Ph)<u>Me</u>)C(N^{i}Pr)$_2$ (2.00 ppm) and SiMe$_3$ (0.00 ppm). The κ^2-amidinate ligand has two signals for CH<u>Me</u>$_2$ (1.06 and 0.45 ppm) and a single septet for C<u>H</u>Me$_2$ (3.79 ppm) consistent with previously discussed di*iso*propylcarbodiimide insertion products **35**$^+$, **37**$^+$, **43**$^+$, **44**$^+$, **45**$^+$ and **48**$^+$. The κ^1-amidinate has C<u>H</u>Me$_2$ resonances at 4.68 and 3.47 ppm and CH<u>Me$_2$</u> resonances at 1.12 and 0.95 ppm alongside aromatic resonances in the region of 7.20-6.83 ppm. This reaction provides evidence to further support the presence of two agostic isomers of **53**$^+$. If it were 1,2 *vs.* 2,1 insertion one would expect to see two very different products after treatment with di*iso*propylcarbodiimide.

Reaction of **52**$^+$ with di*iso*propylcarbodiimide gives a similar result to that discussed above and producing [Cp*Ti{NC(N^{i}Pr$_2$)Ph}{(Me$_3$SiCC(Ph)Me)C(N^{i}Pr)$_2$}][BF$_{20}$] (**56-[BF$_{20}$]**) which was subsequently isolated also in a 77% yield. Compound **56-[BF$_{20}$]** was characterised by NMR spectroscopy, IR spectroscopy and elemental analysis. The NMR spectra of **56**$^+$ contains two signals for each environment. For example the ^{29}Si

NMR spectrum contains resonances at -7.7 and -8.1 ppm. The presence of two similar resonances for each environment is likely due some to restricted rotation about the N_2C-$C(SiMe_3)$ bond in **56**$^+$ yielding two isomers. Unfortunately heating this sample in an attempt to coalesce the signals led to immediate decomposition.

4.3.2 DFT calculations on $PhCCSiMe_3$ insertion products

Density Functional Theory calculations at the B3PW91 level were carried out by Dr Betty Coussens to shed light on the relative thermodynamic stabilities of alkyne insertion products **52a**$^+$ and **52b+** as well as transition states involved in their formation. The compound synthesised and characterised by Eisch (**1.16**$^+$) was shown to have a β-Si-C interaction in the X-ray structure; this interaction resulted in a high-field ^{29}Si shift of -54.9 ppm.[18] DFT (B3PW91) calculations on **1.16Q**$^+$ have been carried out previously by Mountford, Clot *et al.* and showed that β-Si-C agostic isomer is more stable than the corresponding γ-C-H isomer by 38.4 kJ mol^{-1}. This study also showed that the ^{29}Si NMR shift can be calculated accurately for the β-Si-C isomer (-51.1 ppm) and showed that the γ-C-H isomer would have a significantly more downfield ^{29}Si NMR chemical shift (+3.4 ppm) comparable to organic vinyl-subsituted trimethyl silanes (-4.3 to -11.5 ppm).[18-20]

The structure of **1.16Q**$^+$ was initially recalculated by DFT with a β-Si-C agostic interaction (**1.16Qa**$^+$) in this study to see how well the method describes the experimentally determined system **1.16**$^+$ (Figure 4.7). The Ti-Cp_{cent} distances in the calculated structure (2.034 Å and 2.045 Å) are only slightly longer than in the isolated complex **1.16**$^+$ (2.008 Å and 2.020 Å). The Cp-Ti-Cp angle in the calculated structure is 133.9° which is in good agreement with **1.16**$^+$ (133.2°). The method also describes the β-Si-C agostic interaction well; the calculated Ti···CSi length is 2.528 Å compared to 2.522 Å in the X-ray structure. The Ti-C-Si angle is 90.0° in **1.16Qa**$^+$ (*cf.* 89.0° in **1.16**$^+$). NMR methods were also used to calculate the ^{29}Si NMR shift of -54.5 ppm which was in good agreement with the experimentally determined value (-54.9 ppm).

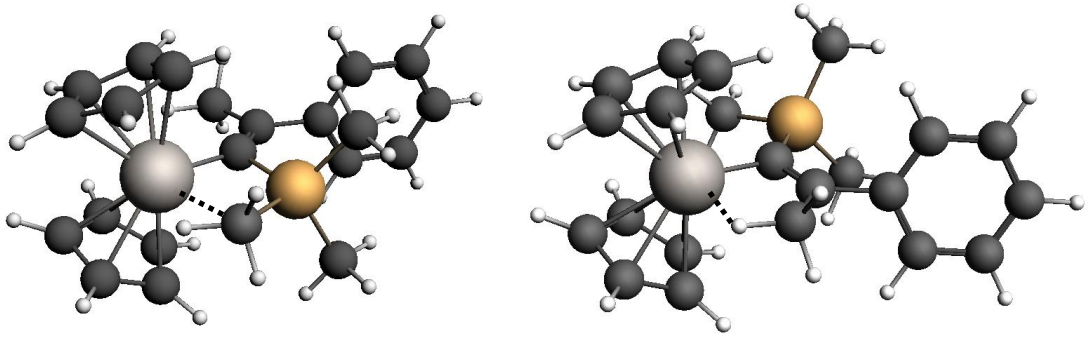

E_{rel} = 0 kJ mol^{-1} E_{rel} = +38.4 kJ mol^{-1}

Figure 4.7 DFT (B3PW91) optimised structures of $[Cp_2Ti(Me_3SiCC(Ph)Me)]^+$ showing a β-Si-C agostic interaction (**1.16Qa**$^+$, left) and a γ-C-H interaction (**1.16Qb**$^+$, left).

The alternative γ-C-H agostic stabilised structure (**1.16Qb**$^+$), which is not observed experimentally in the case of **1.16**, was also optimised (Figure 4.7). In this case the γ-C-H stabilised structure **1.16Qa**$^+$ is 38.4 kJ mol^{-1} less stable than the β-Si-C stabilised structure **1.16Qb**$^+$ consistent with experimental observations. In **1.16Qb**$^+$ the closest Ti···C-Si interaction is now 4.018 Å whereas the closest Ti···H-C interaction is 2.084 Å. The Ti-C-Si angle is now obtuse (134.4°) which is larger than the standard carbon sp^2 angle. The associated C_γ-H bond length is lengthened compared to the other two (1.121 Å *vs.* 1.095, 1.093 Å) as expected from such an agostic interaction. The Cp_2Ti unit is almost identical in this structure (Ti-Cp_{cent} = 2.076, 2.071 Å; Cp_{cent}-Ti-Cp_{cent} = 134.8°) compared to **1.16Qa**$^+$. The ^{29}Si NMR shift for **1.16Qb**$^+$ was calculated to be 1.7 ppm demonstrating the marked difference in ^{29}Si NMR shift between the two types of agostic isomer.

Previous studies by Mountford, Clot *et al.* have shown that $[Ti(N^tBu)(Me_3[9]aneN_3)$-$(Me_3SiCC(Ph)Me)]^+$ forms the γ-C-H isomer exclusively. The ^{29}Si NMR shift was experimentally determined to be -16.8 ppm and calculated by DFT methods (B3PW91) to be -16.1 ppm. The preference of this isomer was found by DFT calculations to be a consequence of steric constraints. This acts as a good example of the delicate balance between the electronics and sterics which ultimately dictate which isomer is observed experimentally.

Table 4.4 Summary of computational results for the compounds $[Cp^*Ti\{NC(N^iPr_2)Ph\}\{Me_3SiCC(Ph)Me\}]^+$ (**52Q**$^+$) and $[Cp_2Ti\{Me_3SiCC(Ph)Me\}]^+$ (**1.16Q**$^+$).

Cation	Isomer	Calculated ^{29}Si /ppm	Experimental ^{29}Si /ppm	Relative electronic energy kJ mol^{-1}
1.16Q$^+$	β-Si-C (**a**)	-54.5	-54.9	0
	γ–C-H (**b**)	1.7		+38.4
52Q$^+$	β-Si-C (**b**)	-50.2	-42.0	0
	γ-C-H (**a**)	-7.3	-15.8	+13.2

The two different agostic structures of $[Cp^*Ti\{NC(N^iPr_2)Ph\}\{Me_3SiCC(Ph)Me\}]^+$ (**52a**$^+$ and **52b**$^+$) were optimised using DFT (B3PW91) and the two resulting structures **52Qa**$^+$ and **52Qb**$^+$ are shown in Figure 4.8. The thermodynamic parameters of the insertion of the alkyne into the Ti-Me bond was calculated and in both cases was determined to be thermodynamically favourable with ΔG (298 K) values of -45.4 and -32.1 kJmol^{-1} for the β-Si-C (**52Qb**$^+$) and γ-C-H (**52Qa**$^+$) stabilised structures, respectively. Structure **52Qb**$^+$ contains a β-Si-C agostic interaction; the distance between Si-C and Ti is 2.449 Å and the Ti-C-Si angle is 91.7° which are similar to the values obtained for **1.16Qa**$^+$. Structure **52Qa**$^+$ has a larger Ti···C-Si distance of 4.405 Å and a more obtuse Ti-C-Si angle of 140.7°. The Ti···H-C distance is 2.009 Å and the associated C_γ-H bond length is longer than the other two (1.118 Å *vs.* 1.093, 1.093 Å). In this situation the electronic energy difference between the isomers is 13.2 kJ mol^{-1} compared to 38.5 kJ mol^{-1} between **1.16Qa**$^+$ **and 1.16Qb**$^+$ (ΔG(298K) = 13.3 kJ mol^{-1}). This reduced difference in energy helps explain why it is possible for both isomers to be observed by ^{1}H NMR spectroscopy in **52**$^+$ but not in **1.16**$^+$. Although there is still a reasonable energy difference between the two isomers this could be due to the calculations being carried out in the gas phase as well as the omission of the anion.

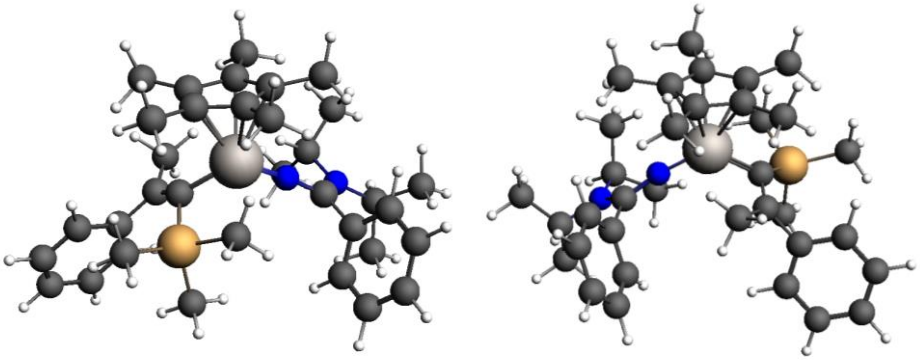

E_{rel} = 0 kJ mol^{-1} E_{rel} = +13.2 kJ mol^{-1}

Figure 4.8 DFT (B3PW91) optimised structures of [Cp*Ti{NC(N^{i}Pr$_2$)Ph}-{Me$_3$SiCC(Ph)Me}]$^+$ with β-Si-C (left, **52Qb**$^+$) and γ-C-H (right, **52Qa**$^+$) agostic interactions.

The calculated 2,1- insertion product (**52Qc**$^+$), which is not observed experimentally, is in fact the lowest in energy (Electronic energy 0.51 kJmol^{-1} lower than **52Qb**$^+$ and Gibb's free energy 2.8 kJ mol^{-1} lower). In an attempt to understand why, the transition states for the 1,2- and 2,1- insertion were calculated using DFT (B3PW91). Each of the optimised transition states had a single imaginary frequency which showed the process of the alkyne insertion into the Ti-Me bond. The $\Delta G^{\ddagger}$ (298 K) for the 1,2-insertion process is 13.0 kJ mol^{-1} more favourable than for the 2,1- insertion process, consistent with the formation of the experimentally observed 1,2-insertion product. The reason the transition state is lower going to the 1,2-insertion product (**52a**$^+$ or **52b**$^+$) is primarily enthalpic ($\Delta H^{\ddagger}$, -8.7 *vs.* -22.4 kJ mol^{-1}). As expected the $\Delta S^{\ddagger}$ of the two processes are similar and negative (1,2- = -247 and 2,1- = -263 J mol^{-1} K^{-1}). The transition state for the 1,2-insertion product has shorter Ti-C(sp^2) (2.17 Å) and Me-C(sp^2) (2.34 Å) distances than the transition state for the 2,1-insertion product (2.26 and 2.41 Å, respectively), which is indicative of stronger and more stable bonding in the former.

4.3.3 Synthesis of [Cp*Ti{NC(N^{i}Pr$_2$)Ph}{Ph$_2$PCC(Tol)Me}][BF$_{20}$] (57-[BF$_{20}$])

Recently Erker *et al.* showed that the reaction of [Cp*$_2$ZrMe][BF$_{20}$] with phosphaalkyne Ph$_2$PCCPh resulted in the formation of a cationic alkenyl product [Cp*$_2$Zr{Ph$_2$PCC(Ph)Me}]$^+$ (**4.2**$^+$, Figure 4.9) with a coordinating phosphine.[21, 22] This is in contrast to the less crowded [Cp$_2$ZrMe][BF$_{20}$] analogue which undergoes an

methyl group migration to phosphorus to produce a system stabilised by an η^2-alkyne interaction, $[Cp_2Zr\{PhCC(PPh_2Me)\}]^+$ (**4.3**$^+$, Figure 4.9).[21]

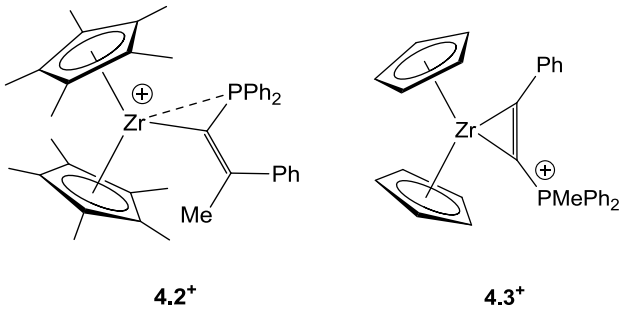

4.2$^+$ **4.3**$^+$

Figure 4.9 Molecular structure of $[Cp^*_2Zr(Ph_2PCC(Ph)Me)][BF_{20}]$ (**4.2**$^+$) and $[Cp_2Zr\{PhCC(PPh_2Me)\}]^+$ (**4.3**$^+$)

As well as **4.2**$^+$ being a stable isolable alkyne insertion product it has also been utilised as a transition metal-based frustrated Lewis pair (FLP).[22] Although non-transition metal FLPs have been widely explored by stoichiometric reactivity with small molecules,[23, 24] the introduction of a transition metal allows catalytic reactivity to take place including the dehydrogenation of amino-boranes and the hydrogenation of alkenes.[22, 25, 26] Wass *et al.* have reported titanocene and zirconocene systems with an additional phospha-alkoxy ligand such as $[Cp_2ZrOC_6H_4P^tBu_2][BF_{20}]$ which are shown to undergo reactivity with small molecules.[25-27]

This Section will describe the reaction of post-metallocene cation **10**$^+$ with the related alkyne $Ph_2PCCTol$. Cation **10**$^+$ was selected as a representative complex for those discussed in this Thesis and the tolyl variant of the alkyne was used since the *para*-methyl substituent acts as a good NMR "handle". The activation of **2.4** in the presence of 1 equiv alkyne $Ph_2PCCTol$ produced alkenyl complex $[Cp^*Ti\{NC(N^iPr_2)Ph\}\{Ph_2PCC(Tol)Me\}][BF_{20}]$ (**57-[BF$_{20}$]**) over a period of 2 h (Equation 4.4). Compound **57-[BF$_{20}$]** was isolated in 66% yield and characterised by NMR spectroscopy, IR spectroscopy and elemental analysis. ROESY NMR spectroscopy showed a through space interaction between $Ph_2PCC(Tol)\underline{Me}$ and (*o*-<u>Tol</u>) which is consistent with the formation of the 1,2-insertion product.

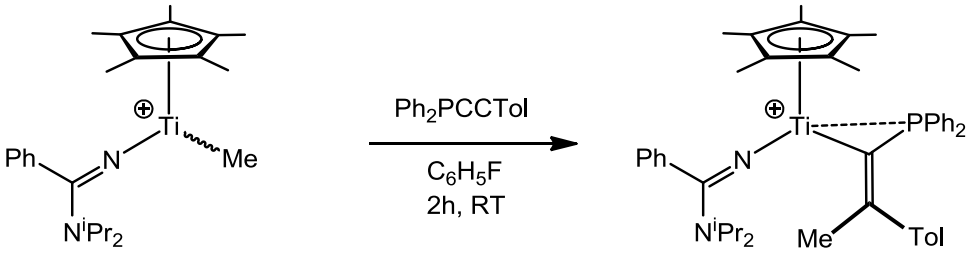

10^{+} **57**$^{+}$

Equation 4.4

The ^{31}P-{^{1}H} NMR spectrum contains a single resonance at 28.0 ppm ($\underline{P}Ph_2$) consistent with a metal bound phosphorus. The ^{1}H NMR spectrum (Figure 4.10) is consistent with C_1 symmetry in solution and the alkenyl methyl group is located at 1.89 ppm as a doublet due to $^{4}J_{PH}$ coupling (1.8 Hz).

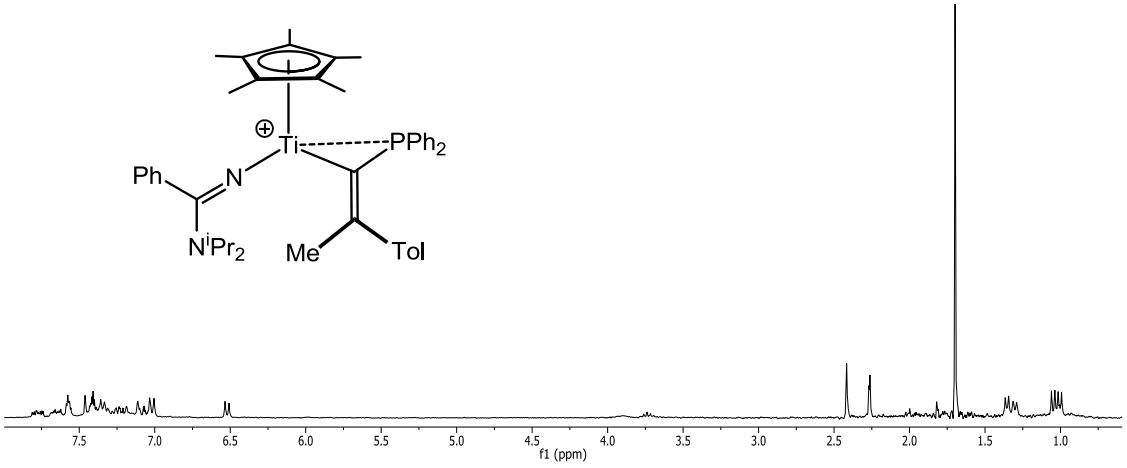

Figure 4.10 ^{1}H NMR spectrum (299.9 MHz, 293 K, C_6D_5Br) of [Cp*Ti{NC(N^{i}Pr$_2$)Ph}{Ph$_2$PCC(Tol)Me}][BF$_{20}$] (**57-[BF$_{20}$]**).

For complex **57**$^{+}$ the signals in the ^{13}C-{^{1}H} NMR spectrum are particularly useful for characterisation because of the diagnostic chemical shifts and distinctive coupling to ^{31}P. The two alkenyl carbons are located at 198.1 (Ti$\underline{C}$CMe) and 165.2 (TiC$\underline{C}$Me) ppm with coupling constants of 101.5 ($^{1}J_{PC}$) and 12.8 Hz ($^{2}J_{PC}$), respectively. The Ph$_2$PCC(Tol)$\underline{Me}$ is located at 26.8 ppm with a coupling constant of 9.6 Hz ($^{3}J_{PC}$). These ^{13}C NMR resonances are consistent with those reported by Erker *et al.* for the equivalent zirconocene derivative **4.2**$^{+}$.[22] The important ^{13}C NMR resonances for **4.2**$^{+}$ are located at 186.2 (Zr$\underline{C}$CMe), 170.6 (ZrC$\underline{C}$Me) and 30.4 ppm (Ph$_2$PCC(Ph)$\underline{Me}$) with coupling constants of 103.7 ($^{1}J_{PC}$), 17.3 ($^{2}J_{PC}$) and 21.6 Hz ($^{3}J_{PC}$), respectively.[21]

Unlike with **52**$^+$ there is only one isomer observed in the ^{1}H NMR spectrum which is not unexpected due to the much greater ability of the phosphine to act as a base compared to $SiMe_3$, discussed further below. Whilst the insertion of $Ph_2PCCTol$ into the Ti-Me bond of **10**$^+$ is taking place a new set of resonances appear in the NMR spectra. Although in the ^{1}H NMR spectrum this is not easily identified due to the presence of multiple overlapping and broad signals, in the ^{31}P-{^{1}H} NMR spectrum there is, alongside the product, an additional resonance at -8.1 ppm which does not correspond to the starting alkyne. It is possible that this intermediate corresponds to the complex $Cp^*Ti\{NC(N^iPr_2)Ph\}(Ph_2PCCTol)Me]^+$ which would be expected contain a σ-bond from the phosphorus to titanium. Over the 2 h reaction time this intermediate converts to the final product **57**$^+$.

4.3.4 DFT calculations on $[Cp^*Ti\{NC(N^iPr_2)Ph\}\{Ph_2PCC(Tol)Me\}]^+$

DFT calculations (B3PW91) were carried out by Dr Betty Coussens in order to investigate the thermodynamic stability and NMR spectra of **57**$^+$. Initial optimisation of the experimentally observed 1,2- insertion product led to the formation of a phosphine stabilised species **57Qa**$^+$ as expected based on experimental data (Figure 4.11). As with **52**$^+$ this insertion of the alkyne into the Ti-C bond was found to be overall thermodynamically favoured ($\Delta G(298\ K) = -115.0$ kJ mol^{-1}). This is even more favourable than the formation of **52Qb**$^+$ ($\Delta G(298\ K) = -45.4$ kJ mol^{-1}) likely because of the formation of strong Ti-P interaction in this case. The ^{31}P NMR shift of this species was calculated, using the free alkyne as a reference, to be 25.3 ppm which is consistent with the experimentally observed value (28.0 ppm). The Ti-P and γ-C-H···Ti distances are 2.49 and 3.26 Å, respectively. Attempts to try and optimise the structure to a local minimum which contained a γ-C-H agostic interaction were unsuccessful and led to the formation of the phosphine stabilised isomer **52Qa**$^+$. In order to calculate the energy of a hypothetical γ-C-H isomer the γ-C-H···Ti distance was constrained to 2.0 Å (the same Ti···H as in **52Qa**$^+$) and the rest of the molecule geometry optimised (Figure 4.11). The resultant structure (**57Qb**$^+$) had an energy 44.5 kJmol^{-1} higher than the phosphine stabilised structure and a larger Ti-P distance of 2.60 Å. Clearly the forced γ-C-H···Ti interaction occurs at the expense of the more stable Ti-P interaction which causes a significant destabilisation overall.

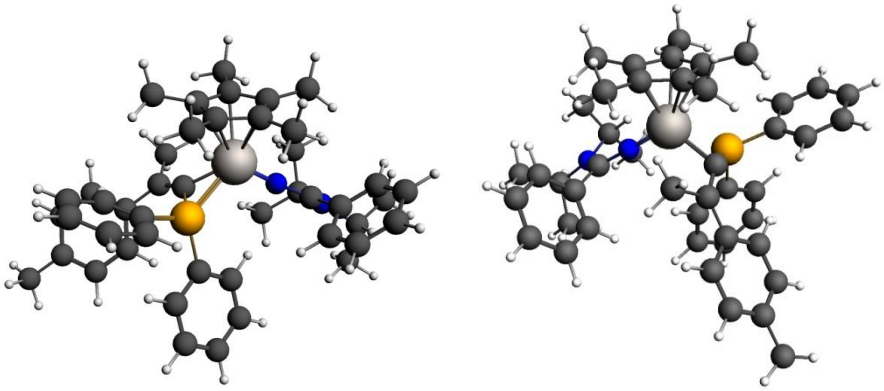

0 kJ mol^{-1} **44.5 kJ mol^{-1}**

Figure 4.11 DFT calculated structures of Cp*Ti{NC(N^{i}Pr$_2$)Ph}{Ph$_2$PCC(Tol)Me}]$^+$ with a Ti-P (**57Qa**$^+$, left) or γ-C-H···Ti (**57Qb**$^+$, right) agostic interaction.

In order to check that the potential energy surface constantly decreased as the γ-C-H···Ti distance increases (and hence enabling a shorter Ti-P distance) geometry optimisations were carried out at various fixed γ-C-H···Ti distances from 1.9-3.1 Å (Figure 4.12). The results were consistent with expectations and showed that the stronger Ti-P interaction is the most significant factor in determining the energy over the entire reaction coordinate.

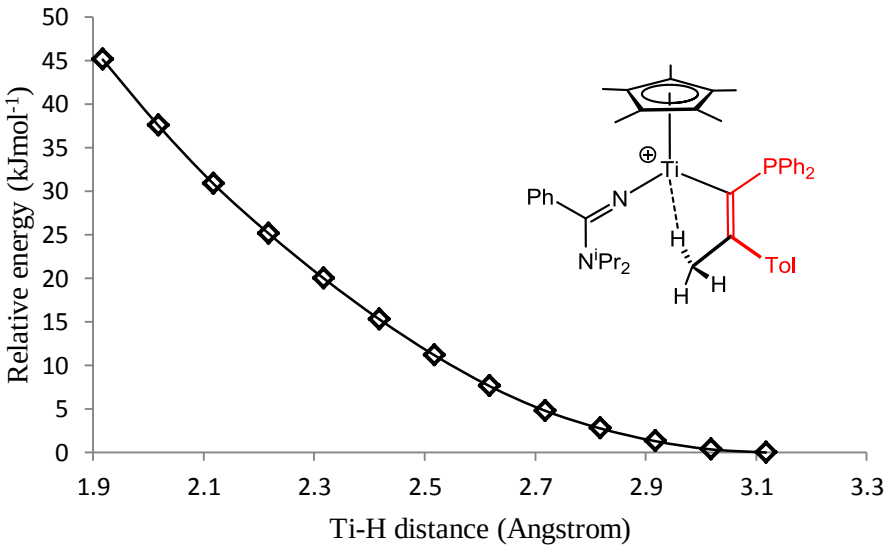

Figure 4.12 Relative energy of **57Q**$^+$ (kJ mol^{-1}) with changing γ-C-H···Ti distance.

The unobserved 2,1- insertion product Cp*Ti{NC(N^{i}Pr$_2$)Ph}{TolCCPPh$_2$Me}]$^+$ (**57Qc**$^+$) was also optimised to give a structure with an electronic energy 37.8 kJ mol^{-1} higher than the lowest energy 1,2-insertion product **57Qa**$^+$. The calculated ^{31}P NMR

shift for this **57Qc**$^+$ is also calculated to be 18.9 ppm, which is in less good agreement with the experimentally observed value (28.0 ppm).

4.3.5 Reaction of [Cp*Ti{NC(N^{i}Pr$_2$)Ph}{Ph$_2$PCC(Tol)Me}]$^+$ (57$^+$) with CO_2 and di*iso*propylcarbodiimide

Although an intensive investigation of the FLP type reactivity of post-metallocene complexes is beyond the scope of this Thesis the reaction of **57**$^+$ with CO_2 was carried out to test the viability of **57**$^+$ as a transition metal based FLP. The reaction of Erker's zirconocene system with CO_2 proceeded readily at room temperature to produce an FLP adduct of CO_2 ([Cp*$_2$Zr(CO_2){Ph$_2$PCC(Ph)Me}]$^+$, **4.4**$^+$) which was subsequently characterised by X-ray crystallography.[22]

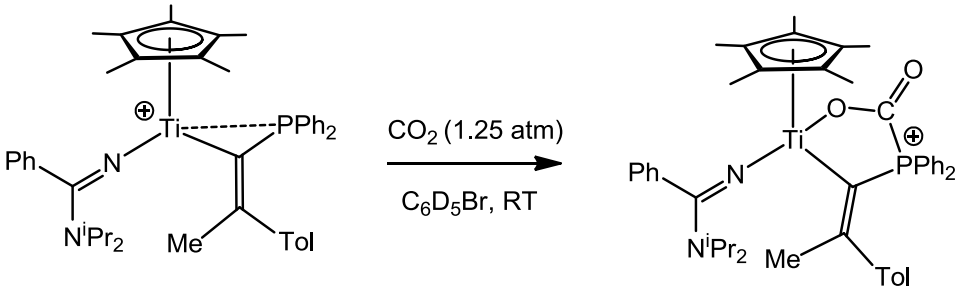

57$^+$ **58**$^+$

Equation 4.5

The reaction of **57**$^+$ with CO_2 was carried out at room temperature by back-filling an NMR tube of **57**$^+$ with CO_2 at 1.25 atm. This proceeded to yield [Cp*Ti{NC(N^{i}Pr$_2$)Ph}(CO_2){Ph$_2$PCC(Tol)Me}]$^+$ (**58**$^+$) over a period of 10 min in quantitative yield by ^{1}H NMR spectroscopy (Equation 4.5). Compound **58-[BF$_{20}$]** was subsequently characterised by ^{1}H, ^{13}C, ^{19}F, ^{11}B and ^{31}P NMR spectroscopy. Unfortunately attempted isolation of this product on scale-up led to significant decomposition.

The ^{1}H NMR spectrum of **58**$^+$ shows resonances for the ancillary supporting ligands for Cp* (1.50 ppm), C<u>H</u>Me$_2$ (3.53 and 3.30 ppm) and CH<u>Me</u>$_2$ (0.96 and 0.70 ppm) alongside the amidinate aromatic signals (7.85-6.83 ppm). The phosphaalkenyl moiety has resonances at 7.85-6.83 (P<u>Ph</u>$_2$), 6.61 (C$_6$<u>H</u>$_4$Me), 6.28 (*m*-C$_6$<u>H</u>$_4$Me), 2.06 (*o*-C$_6$H$_4$<u>Me</u>), 1.76 (Ph$_2$PCC(Tol)<u>Me</u>) ppm. The alkenyl methyl signal is coupled to <u>P</u>Ph$_2$, similar to **58**$^+$, yielding a doublet with a coupling constant of 2.9 Hz ($^4J_{PH}$). The ^{13}C-{^{1}H} NMR spectrum of **58**$^+$ is diagnostic of the CO_2 adduct and contains a

resonance at 166.0 ppm (OCO) which is split into a doublet with a large coupling constant of 123.3 Hz ($^1J_{PC}$). The equivalent resonance in the analogous zirconocene compound **4.4**$^+$ is found at 165.5 ppm and has a coupling constant of 125.1 Hz ($^1J_{PC}$). The alkenyl carbon atoms are now found at 174.9 (TiCCMe) and 155.1 (TiCCMe) ppm with coupling constants of 6.1 ($^2J_{PC}$) and 24.3 Hz ($^1J_{PC}$), respectively. The equivalent carbon environments in **4.4**$^+$ are located at 175.8 (ZrCCMe) and 155.7ppm (ZrCCMe) with coupling constants of 7.2 ($^2J_{PC}$) and 27.0 Hz ($^1J_{PC}$).

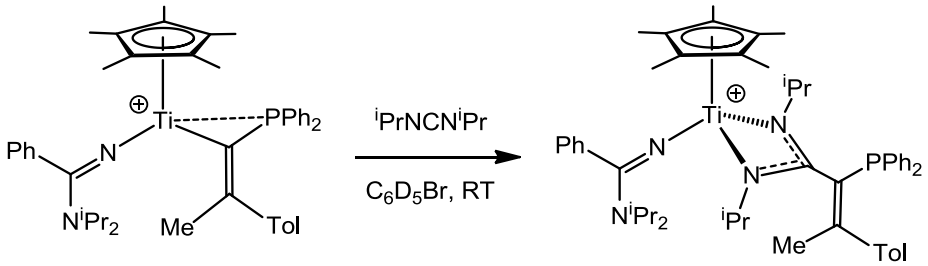

57$^+$ **59**$^+$

Equation 4.6

As an unsaturated substrate that is isoelectronic with CO_2, di*iso*propylcarbodiimide was also reacted with **57**$^+$. The analogous reaction with alkenyl complex **52**$^+$ has already been discussed *vide supra* and the product (**56**$^+$) was identified as a κ^2-amidinate complex resulting from insertion of the heterocumulene into the Ti-C bond. Addition of 1 equiv di*iso*propylcarbodiimide to **57**$^+$ in C_6D_5Br gave the immediate and quantitative formation of κ^2-amidinate product Cp*Ti{NC(N^{i}Pr$_2$)Ph}-{(Ph$_2$PCC(Tol)Me)C(N^{i}Pr)$_2$}][BF$_{20}$] (**59**$^+$) by ^{1}H NMR spectroscopy (Equation 4.6). Compound **59-[BF$_{20}$]** was isolated in a 64% yield and characterised by NMR spectroscopy, IR spectroscopy and elemental analysis.

The ^{1}H NMR spectrum of **59**$^+$ is consistent with the formation of a Ti-C insertion product rather than the FLP type reactivity seen for CO_2. The resonances of the κ^2-amidinate *iso*propyl groups (CHMe$_2$, 3.79 ppm; CHMe$_2$, 0.71 and -0.05 ppm) are consistent with C_s symmetry in solution and not the C_1 symmetry that would be expected if FLP reactivity had taken place to give [Cp*Ti{NC(N^{i}Pr$_2$)Ph}(^{i}PrNCN^{i}Pr){Ph$_2$PCC(Tol)Me}]$^+$. The Ph$_2$PCC(Tol)Me resonance is a doublet found at 1.86 ppm ($^4J_{PH}$ = 1.11 Hz) and the C$_6$H$_4$Me is a singlet at 2.15 ppm. The κ^1-amidinate has the expected signals for CHMe$_2$ and CHMe$_2$, and the phenyl signals are amongst the aromatic region of the spectrum (7.45-6.67 ppm);

the Cp* resonance is found at 1.77 ppm. The ^{13}C-{^{1}H} NMR spectrum of **59**$^{+}$, as for **57**$^{+}$ and **58**$^{+}$, is diagnostic of the environment surrounding $\underline{P}Ph_2$. The coupling between what was the quaternary carbon of the carbodiimide and the phosphorous atom is 33.5 Hz (at 170.8 ppm) which is more consistent with $^{2}J_{PC}$ coupling rather than $^{1}J_{PC}$ expected for the product of FLP reactivity (e.g. **58**$^{+}$, $^{1}J_{PC}$ = 123.3 Hz, *vide supra*). The C$\underline{C}$Me and $\underline{C}$CMe resonances are now found at 139.2 and 129.0 ppm, respectively. This reaction shows that changing the unsaturated substrate can significantly alter the type of reactivity that is observed in these compounds. Overall this Section has shown that these post-metallocene complexes can, much like the metallocene counterparts, act as transition metal FLPs and would likely provide a fruitful avenue for future investigations.

4.4 Polymerisation experiments

EP (ethylene, propylene) polymerisation experiments of dimethyl guanidinate precatalysts Cp*Ti{NC(NMe$_2$)$_2$}Me$_2$ (**4**), Cp*Ti{NC(NMe$_2$)$_2$}Bn$_2$ (**5**), Cp*Ti{NC(N^{i}Bu)$_2$}Me$_2$ (**6**) and Cp*Ti{NC(N(Xyl)CH$_2$)$_2$}Me$_2$ (**7**) as well as preformed cationic compound [Cp*Ti{NC(NMe$_2$)$_2$}(THF)Me][BF$_{20}$] (**18-[BF$_{20}$]**) were carried out in a small-scale batch reactor under industrially relevant conditions by Lanxess Elastomers, the Netherlands at 90 °C. Activation of the dimethyl precatalysts was performed by the addition of 1, 2, 5 or 10 equivs of TBF$_{20}$ or BF$_{15}$ (Table 4.5, [B]:[Ti]). Preactivated cationic catalyst system (**18-[BF$_{20}$]**) which was used as a catalyst was considered as being activated by 1 equiv and if higher equivs of TBF$_{20}$ were used this was accounted for. (Pre)catalysts were assessed using low catalyst loadings (0.05 – 0.50 μmol) to maintain isothermal conditions (exotherms < 3 °C) and reduced the possibility of mass transport limitations. The propylene/ethylene feed was kept at a constant ratio of 80:40 and BHT (4-methyl-2,6-di-*tert*-butylphenol) was used in ratio of 2.22:1 (BHT/Al) as an alkyl aluminium scavenger alongside TiBA (tri*iso*butylaluminum). In the single case when *iso*butylaluminoxane (IBAO-65) was used as a scavenger BHT was not used. The composition of the resultant polymers was analysed using FT-IR and the molecular weight and PDI were obtained from GPC data. The results of these experiments are summarised in Table 4.5.

Table 4.5 EP polymerisation results[a] for Cp*Ti{NC(NMe$_2$)$_2$}Me$_2$ (**4**), [Cp*Ti{NC(NMe$_2$)$_2$}(THF)Me][BF$_{20}$] (**18-[BF$_{20}$]**), [Cp*Ti{NC-(NMe$_2$)$_2$}Me][MeBF$_{15}$] (**14-[MeBF$_{15}$]**) Cp*Ti{NC(NMe$_2$)$_2$}Bn$_2$ (**5**), Cp*Ti{NC(N^{i}Bu)$_2$}Me$_2$ (**6**) and Cp*Ti{NC(N(Xyl)CH$_2$)$_2$}Me$_2$ (**7**).

(Pre)catalyst	Cocatalyst	Cat dosing[b] /μmol	[B]:[Ti][c]	Yield/ g	Productivity/ kg mol^{-1} h^{-1} bar^{-1}	Polymer Analysis			
						C_2/wt.%	C_3/wt.%	M_n/ kg mol^{-1}	M_w/M_n
4	TBF_{20}	0.50	1	6.5	11,000	52	48	590 (1260[e])	2.1
	TBF_{20}	0.50	2	8.5	15,000	47	53	60/1260[f]	-
	TBF_{20}	0.20	5	5.9	25,000	40	60	60/1260[f]	-
	TBF_{20}	0.14	10	11.0	67,000	41	59	60/1260[f]	-
18-[BF$_{20}$]	TBF_{20}	0.28	0	2.47	7,600	51	49	550	2.1
	TBF_{20}	0.28	1	1.80	5,500	51	49	650	2.1
	TBF_{20}	0.28	4	1.68	5,100	51	49	330	3.5
4[d]	BF_{15}	0.50	1	3.68	6,300	47	53	340	2.1
	BF_{15}	0.50	2	4.51	7,700	51	49	-	-
	BF_{15}	0.50	10	4.70	8,100	49	51	340	2.1
5	TBF_{20}	0.14	1	5.8	36,000	48	52	730	2.2
	TBF_{20}	0.07	2	2.6	32,000	52	48	830	2.1
	TBF_{20}	0.07	5	2.9	36,000	49	51	770	2.1
6	TBF_{20}	0.14	1	1.0	6,000	50	50	490	1.9
	TBF_{20}	0.14	2	1.8	11,000	54	46	570	1.9
	TBF_{20}	0.14	5	4.7	29,000	52	48	460	2.2
7	TBF_{20}	0.05	1	12.1	207,000	57	43	240	2.2
	TBF_{20}	0.05	2	11.8	202,000	57	43	-	-
	TBF_{20}	0.05	5	10.3	177,000	56	43	250	2.3

[a]Conditions: T = 90 °C, Pressure: 7 bar, Scavenger: TiBA ([Al] = 0.45 mM), 10 min run time. Solvent pentamethylheptane (1 L) C_3/C_2 = 80/40. Cat. Loading adjusted to limit exotherm < 3 °C. [c]Cocatalyst: $[Ph_3C][BF_{20}]$ or BF_{15} used in ratio [B]:[Ti]. [d]Scavenger: IBAO-65. [e]M_p from GPC trace. [f]M_p of high and low molecular weight peaks for bimodal distribution.

The catalytic performance of **4** with 1 equiv of TBF_{20} is very high (11,000 kg mol^{-1} h^{-1} bar^{-1}) and has a C_2:C_3 ratio of 52:48. GPC analysis reveals that the resultant polymer has a narrow PDI (2.1) and also has a high molecular weight (M_n = 590 kg mol^{-1}). The GPC trace is shown in Figure 4.13. As the number of equivalents of TBF_{20} is increased to 2 the productivity of the catalyst increases (15,000 kg mol^{-1} h^{-1} bar^{-1}). Increasing the amount of TBF_{20} further to 5 and 10 equivs also results in an increase in activity to 25,000 and 67,000 kg mol^{-1} h^{-1} bar^{-1}, respectively.

If the GPC trace of these polymers is analysed there is an introduction of a second lower molecular weight fraction (M_p = 60 kg mol^{-1}) which increases in intensity with increasing TBF_{20} (Figure 4.13) to overall yield a bimodal distribution. The overall C_2:C_3 composition over the entire molecular weight range is 41:59 for 10 equiv TBF_{20} (*cf.* 1 equiv, 52:48). This means the polymer which corresponds to the lower molecular weight fraction has high propylene content, assuming the higher molecular weight fraction has the same composition as seen in the experiment with 1 equiv. The increase in activity seen with increasing equivalents of TBF_{20} has previously been ascribed to a more efficient activation due to a higher concentration of cocatalyst or to the so called "trityl effect".[28] An increase in Ph_3C^+ concentration could potentially cause the formation of aggregates of the form $[L_nTiMe][A^-\cdots Ph_3C^+\cdots A^-]$ which could react faster than mononuclear ion pairs.

Since the isolated dimeric dication **1.26$_{dim}$-[BF_{20}]$_2$** has previously been shown to act as a catalyst,[10] isolated **14-[BF_{20}]** was tested to see if it would also show activity. Unfortunately no activity was seen in this case due to insolubility.

In order to see if this effect was universal for these types of system the related precatalyst Cp*Ti{NC(N^iBuMe)$_2$}Me_2 (**6**) was tested under the same conditions. The activity of **6** with 1 equiv TBF_{20} also gave a high activity, although slightly smaller than **4** (6,000 kg mol^{-1} h^{-1} bar^{-1})[29]; the PDI (1.9), M_n (490) and C_2:C_3 (50:50) data were comparable to **4**. Increasing the activator to 2 equivs increases the productivity to 11,000 kg mol^{-1} h^{-1} bar^{-1} as with **4** but the PDI (1.9), M_n (570 kg mol^{-1}) and C_2:C_3 (54:46) do not change in the same way i.e. there is no introduction of a second lower molecular weight fraction. Increasing further to 5 equivs again led to an increase in productivity (29,000 kg mol^{-1} h^{-1} bar^{-1}) but a similar PDI (2.2), M_n (460 kg mol^{-1}) and C_2:C_3 (52:48) was observed. The increase in activity with increasing TBF_{20} equivalents in this case, similar to with **4**, could be due to more efficient activation or

due to the "trityl effect".[28] When attempting to use the isolated dimethyl-bridged dication **21$_{dim}$-[BF$_{20}$]$_2$** (Section 3.2.12) as a catalyst no activity was observed, again due to insolubility of the dimeric complex.

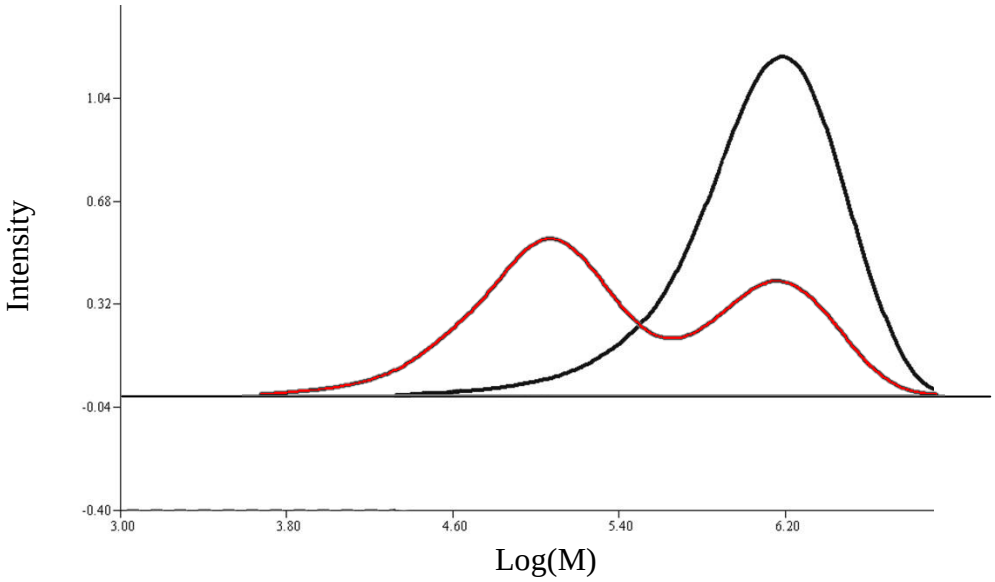

Figure 4.13 Molecular weight distribution obtained by GPC analysis for **4** activated with 1 (black) and 5 (red) equivs of TBF_{20}.

The previously described THF adduct **18-[BF$_{20}$]** has already been shown to be highly active towards the insertion of di*iso*propylcarbodiimide (Section 4.2.5) and thus its activity towards olefin polymerisation was also tested. Using **18-[BF$_{20}$]** with no additional co-catalyst (equal to 1 equiv TBF_{20}) gave a slightly lower activity (7,600 kg mol^{-1} h^{-1} bar^{-1}) but similar M_n (550 kg mol^{-1}) and C_2:C_3 (51:49) to **4** with 1 equiv TBF_{20}. This might be expected since the active polymerisation species should be the same in both cases but in the case of **18-[BF$_{20}$]** THF might also be expected to exhibit an inhibitory effect on the activity by competeting for the active site. During testing **18-[BF$_{20}$]** also did not easily slurry in the solvent which might explain some of the difference in activity compared to **4**. Increasing the amount of TBF_{20} by 1 and 4 equivs did not lead to an increase in activity (5,500 and 5,100 kg mol^{-1} h^{-1} bar^{-1}, respectively) because it was already preactivated, but interestingly the polymer composition did not change either.

The catalytic performance of **4** when activated with BF_{15}, forming **14-[MeBF$_{15}$]**, was also tested. With 1 equiv BF_{15} the activity of the catalyst was determined to be 6,300 kg mol^{-1} h^{-1} bar^{-1} which is lower than when 1 equiv TBF_{20} is used. This is expected as $[MeBF_{15}]^-$ is generally well known to bind to the active site of Group 4 cations as

discussed previously and in this work (Section 3.2.8) has been specifically shown to bind to $\mathbf{14}^{+}$. Although the PDI (2.2) and C_2:C_3 (47:53) is similar to **4** with 1 equiv TBF_{20} the presence of $[MeBF_{15}]^-$ seems to cause a significant reduction in M_n (340 kg mol^{-1}). As opposed to TBF_{20} Increasing the equivalents of BF_{15} seems to make no significant difference to the PDI, C_2:C_3 or activity of the catalyst (Table 4.5). There is a small increase in activity on increasing the equivs of BF_{15} from 1 to 2 which is likely due to more efficient activation of the precatalyst. Increasing from 2 equivs to 10 equivs of the cocatalyst, however, leads to no significant increase in the productivity.

As another data point the polymerisation performance of the related dibenzyl precatalyst **5** was tested. With 1 equiv TBF_{20} **5** produced a higher polymerisation activity (36,000 kg mol^{-1} h^{-1} bar^{-1}) and higher molecular weight polymer (730 kg mol^{-1}) than the dimethyl analogue **4**. The former might be attributed to a more complete activation process or to the reduced tendency of the corresponding benzyl cation to dimerise before the first insertion can take place. The PDI (2.2) and C_2:C_3 ratio (48:52) is comparable to **4** which is expected since the active species will effectively be the same during propagation. Using 2 equivs of activator in this case made little difference to the productivity (32,000 kg mol^{-1} h^{-1} bar^{-1}), M_n (830 kg mol^{-1}), PDI (2.1) or C_2:C_3 ratio (52:48). Further increasing to 5 equivalents of activator again did not significantly effect productivity (36,000 kg mol^{-1} h^{-1} bar^{-1}), M_n (770 kg mol^{-1}), PDI (2.1) or C_2:C_3 ratio (49:51).

To compare these guanidinate systems with an established iminoimidazolidide system, **7** was tested under the same conditions. The productivity of **7** with 1 equiv TBF_{20} was very high (207,000 kg mol^{-1} h^{-1} bar^{-1})[29] and indeed much higher than that seen with **4**, **5**, **6** and **18-[BF_{20}].** This is consistent with the larger steric cone of the ligand in **7** which is known to increase activity in these types of systems.[30] The C_2:C_3 ratio was 57:43 showing that this catalyst have a poorer propylene incorporation. The PDI (2.2) is comparable but the M_n is lower than (240 kg mol^{-1}) the previously discussed catalysts presumably due to an increased rate of β-hydrogen transfer. An increase in the equivs of TBF_{20} in this system did not lead to any change in the productivity or the polymer properties.

The productivity and polymer properties of the amidinate precatalyst **2.4** has already been tested under the same conditions to the κ^1-guanidinate supported systems except the scavenger system used was IBAO (*iso*butylaluminiumoxide) rather than TiBA

(tri*iso*butylaluminium).[31] The productivity of **2.4** is superior to **4**, **5**, **6** and **18-[BF_{20}]** (62,000 kg mol^{-1} h^{-1} bar^{-1}) whilst the PDI is similar (2.3) and the M_n lower (207 kg mol^{-1}). The higher C_2:C_3 ratio (56:44) also shows a lower incorporation of propylene compared to the κ^1-guanidinate supported systems. The productivity change can be ascribed to the larger steric cone of the amidinate ligand. Polymerisation experiments have also been published on **1.49**, although at a higher pressure (8 bar) with the TiBA scavenger and 1 equiv TBF_{20}.[10] The productivity (40,125 kg mol^{-1} h^{-1} bar^{-1}) is very high and comparable to **2.4**; the PDI (2.0) and M_n (210 kg mol^{-1}) are also comparable but the C_2:C_3 (48:52) is quite different. With both of these systems the addition of excess TBF_{20} does not lead to the introduction of a second lower molecular weight polymer.

Overall the appearance of a lower molecular weight fraction to give a bimodal distribution is very specific to precatalyst Cp*Ti{$NC(NMe_2)_2$}Me_2 (**4**) when activated by TBF_{20}. Modifying either the alkyl group or ligand, or indeed using the preactivated THF adduct (**18-[BF20]**), or activating **4** with BF_{15} removes this effect. The lower molecular weight fraction is due to a second unidentified active species in solution which only forms in the case of **4**. Complex **4** has been shown to be different to the other studied amidinate and guanidinate supported-catalysts in that it is capable of forming nitrogen-bridged dimers when activated (Section 3.2.7 and 3.2.19). It could be that the presence of a dimeric nitrogen-bridged active polymerisation species is what differentiates **4** from the others and could be responsible for the lower molecular weight fraction. This is not unprecedented since previous reports by Bochmann *et al.* and Mountford *et al.* have shown that imido-bridged binuclear titanium complexes can act as ethylene polymerisation catalysts, the latter featuring well-defined bimodal molecular weight distributions.[32, 33]

Although there is an established trend that an increase in the steric bulk of the ligand increases the activity of the catalyst, any correlation between the C_2:C_3 incorporation and steric or electronic effect of the ligand is still unclear. DFT calculations coupled with X-ray crystallography have helped in this Thesis to give a better picture of the variation in bonding between the different amidinate and guanidinate catalysts but there is no clear correlation between the Ti-N bonding and the C_2:C_3 incorporation. For example the bonding in **4** and **2.4** has been shown to be very similar but the C_2:C_3 (with 1 equiv TBF_{20}) for the catalysts are 52:48 and 56:44, respectively. Work by

Lanxess Elastomers over multiple catalysts has also shown that the calculated steric factor of the amidinate or guanidinate ligands seems to show no correlation to the C_2:C_3 ratio either. The M_n of the polymers produced also has no clear link to the electronic properties of the ligand for example the electronically similar **4** and **2.4** produce polymers with M_n of 590 kg mol^{-1} and 207 kg mol^{-1}, respectively. There is also again no relation of M_n to the steric factor of the amidinate or guanidinate ligand. The investigation into these effects is still ongoing.

4.5 Summary

This Chapter has described the synthesis and characterisation of products resulting from the insertion of unsaturated species into the Ti-C bond of cationic alkyl species. In all cases insertion of di*iso*propylcarbodiimide gave rise to stable and isolable κ^2-amidinate supported species of the type [$L_nTi(RC(N^iPr)_2)$] (L = ligand(s), R = alkyl). Insertion of *tert*-butyl*iso*cyanate into the Ti-C bond yielded acetamido complexes **36**, **38**, **49** and **50** which could be also be isolated with the exception of **52** which could only be characterised by ^{1}H NMR spectroscopy. Reaction of *tert*-butyl*iso*cyanate with **25**$^+$ gave a mixture of products. Nitriles (MeCN and PhCN) were also shown to undergo rapid insertion into the Ti-C bond to yield ketimide supported complexes (**39**, **40**, **41**, **42**, **53** and **54**). The reaction of κ^1-amidinate supported cations with alkyne $Me_3SiCCPh$ was shown to give 1,2-insertion products which exist as a mixture of agostic isomers in solution. This was further investigated by DFT which showed that the two isomers are reasonably close in energy and also that the transition state for the 1,2-insertion is lower in energy than for the 2,1-insertion. Accordingly addition of di*iso*propylcarbodiimide to this mixture yielded single κ^2-amidinate supported products (**58-[BF$_{20}$]** and **59-[BF$_{20}$]**) which could be isolated and characterised. Reaction of κ^1-amidinate supported cation **10**$^+$ with $Ph_2PCCTol$ resulted in the formation of an alkenyl complex (**57**$^+$) which was isolated and characterised as **57-[BF$_{20}$]**. **57**$^+$ was also shown to react with CO_2 as an FLP to form **58**$^+$ whereas di*iso*propylcarbodiimide undergoes insertion into the Ti-C bond forming **59**$^+$. DFT investigations on **57Q**$^+$ were also detailed and explained why in this case only one isomer was formed. Finally the polymerisation capabilities of the guanidinate and amidinate complexes were described and all were shown to give high activities as well as good PDIs and M_n. In the case of **4** excess equivs of TBF_{20} gave

rise to a bimodal distribution which was not seen with any other system and is possibly due to the formation of homobimetallic dimers.

4.6 References

1. L. Cabrera, E. Hollink, J. C. Stewart, P. Wei and D. W. Stephan, *Organometallics*, 2005, **24**, 1091-1098.
2. P. Mountford, *Chem. Commun.*, 1997, 2127-2134.
3. N. Hazari and P. Mountford, *Acc. Chem. Res.*, 2005, **38**, 839-849.
4. A. P. Duncan and R. G. Bergman, *Chem. Rec.*, 2002, **2**, 431-445.
5. L. H. Gade and P. Mountford, *Coord. Chem. Rev.*, 2001, **216–217**, 65-97.
6. T. K. Panda, A. G. Trambitas, T. Bannenberg, C. G. Hrib, S. Randoll, P. G. Jones and M. Tamm, *Inorg. Chem.*, 2009, **48**, 5462-5472.
7. M. Feliz, P. D. Bolton, P. Mountford and E. Clot, *Organometallics*, 2008, **27**, 6111-6122.
8. M. Oberhoff, G. Erker and R. Fröhlich, *Chem. Eur. J.*, 1997, **3**, 1521-1525.
9. S. Gambarotta, S. Strologo, C. Floriani, A. Chiesi-Villa and C. Guastini, *Inorg. Chem.*, 1985, **24**, 654-660.
10. E. G. Ijpeij, B. Coussens, M. A. Zuideveld, G. H. J. van Doremaele, P. Mountford, M. Lutz and A. L. Spek, *Chem. Commun.*, 2010, **46**, 3339-3341.
11. P. Bolton, *DPhil Thesis, University of Oxford*, 2006.
12. N. Kaltsoyannis and P. Mountford, *J. Chem. Soc., Dalton Trans.*, 1999, 781-790.
13. M. Bochmann, L. M. Wilson, M. B. Hursthouse and M. Motevalli, *Organometallics*, 1988, **7**, 1148-1154.
14. Y. W. Alelyunas, R. F. Jordan, S. F. Echols, S. L. Borkowsky and P. K. Bradley, *Organometallics*, 1991, **10**, 1406-1416.
15. M. Bochmann and L. M. Wilson, *J. Chem. Soc., Chem. Commun.*, 1986, 1610-1611.
16. M. Bochmann, L. M. Wilson, M. B. Hursthouse and R. L. Short, *Organometallics*, 1987, **6**, 2556-2563.
17. J. J. Eisch, A. M. Piotrowski, S. K. Brownstein, E. J. Gabe and F. L. Lee, *J. Am. Chem. Soc.*, 1985, **107**, 7219-7221.
18. P. D. Bolton, M. Feliz, A. R. Cowley, E. Clot and P. Mountford, *Organometallics*, 2008, **27**, 6096-6110.

19. E. Liepiņš, Y. Goldberg, I. Iovel and E. Lukevics, *J. Organomet. Chem.*, 1987, **335**, 301-311.
20. M. Grignon-Dubois and M. Laguerre, *Organometallics*, 1988, **7**, 1443-1446.
21. X. Xu, R. Frohlich, C. G. Daniliuc, G. Kehr and G. Erker, *Chem. Commun.*, 2012, **48**, 6109-6111.
22. X. Xu, G. Kehr, C. G. Daniliuc and G. Erker, *J. Am. Chem. Soc.*, 2013, **135**, 6465-6476.
23. D. W. Stephan and G. Erker, *Angew. Chem. Int. Ed.*, 2010, **49**, 46-76.
24. G. Ménard and D. W. Stephan, *J. Am. Chem. Soc.*, 2010, **132**, 1796-1797.
25. A. M. Chapman, M. F. Haddow and D. F. Wass, *J. Am. Chem. Soc.*, 2011, **133**, 8826-8829.
26. A. M. Chapman, M. F. Haddow and D. F. Wass, *J. Am. Chem. Soc.*, 2011, **133**, 18463-18478.
27. A. M. Chapman, M. F. Haddow and D. F. Wass, *Eur. J. Inorg. Chem.*, 2012, **2012**, 1546-1554.
28. F. Song, R. D. Cannon, S. Lancaster and M. Bochmann, *J. Mol. Catal.*, 2004, **218**, 21-28.
29. G. J. P. Britovsek, V. C. Gibson and D. F. Wass, *Angew. Chem. Int. Ed.*, 1999, **38**, 428-447.
30. M. Tamm, S. Randoll, E. Herdtweck, N. Kleigrewe, G. Kehr, G. Erker and B. Rieger, *Dalton Trans.*, 2006, 459-467.
31. R. Scott, *DPhil Thesis, University of Oxford*, 2013.
32. M. Said, D. L. Hughes and M. Bochmann, *Dalton Trans.*, 2004, 359-360.
33. D. A. Pennington, P. N. Horton, M. B. Hursthouse, M. Bochmann and S. J. Lancaster, *Polyhedron*, 2005, **24**, 151-156.

Chapter 5

Experimental details and characterising data

5.1 General methods and instrumentation.

All manipulations were carried out using standard Schlenk line or dry-box techniques under an atmospfhere of argon or dinitrogen. Solvents were either degassed by sparging with dinitrogen and dried by passing through a column of the appropriate drying agent[1] or refluxed over sodium (toluene), potassium (THF) or Na/K alloy (Et_2O) and distilled. Deuterated solvents were dried over sodium (C_6D_6), P_2O_5 (CD_2Cl_2) or CaH_2 (C_6D_5Br, $CDCl_3$) distilled under reduced pressure and stored under argon in Teflon valve ampoules. NMR samples were prepared under dinitrogen in 5 mm Wilmad 507-PP tubes fitted with J. Young Teflon valves. ^{1}H, ^{13}C, ^{13}C-{^{1}H}, ^{29}Si, ^{31}P-{^{1}H}, ^{11}B and ^{19}F NMR spectra were recorded on Varian Mercury-VX 300, Bruker Ascend 400, Varian Unity Plus 500, Bruker Avance III 500 spectrometers or on a Bruker AVC 500 spectrometer fitted with a ^{13}C cryoprobe. ^{1}H, ^{13}C, ^{29}Si and ^{13}C-{^{1}H} NMR spectra were referenced internally to residual protio-solvent (^{1}H) or solvent (^{13}C) resonances, and are reported relative to tetramethylsilane (δ = 0 ppm). ^{19}F, ^{31}P-{^{1}H}, and ^{11}B were referenced to $CFCl_3$, H_3PO_4 or $Et_2O{\cdot}BF_3$, respectively. Assignments were confirmed as necessary with the use of two dimensional ^{1}H-^{1}H, ^{13}C-^{1}H and ^{29}Si-^{1}H NMR spectra. IR spectra were recorded on a Nicolet Magna 560 E.S.P. FTIR or a Thermo Scientific Nicolet iS5 FTIR spectrometer and samples prepared in a dry-box using NaCl plates as a Nujol mull. CW-EPR spectra were collected in the Centre for Advanced Electron Spin Resonance (CAESR) in the Inorganic Chemistry Laboratory at the University of Oxford. X-band measurements performed with a Bruker-Biospin EMXmicro spectrometer equipped with a PremiumX microwave bridge, a cylindrical TE011-mode resonator (SHQE-W), an ESR-900 liquid helium cryostat, and an ITC-503s temperature controller. Mass spectra were recorded by the mass spectrometry service of Oxford University's Department of Chemistry. Elemental analyses were carried out by Elemental Analysis Service at the London Metropolitan University.

5.2 Literature preparation and starting materials

$HNC(N^iPr_2)Ph$ (**2.1**),[2] $Ph_2PCCTol$,[3] $Cp^*Ti\{NC(N^iPr_2)Ph\}Cl_2$ (**2.3**),[2] $Cp^*Ti\{NC(N^iPr_2)Ph\}Me_2$ (**2.4**),[2] $[Cp^*Ti\{NC(N^iPr_2)Ar^{F_2}\}Me][BF_{20}]$ (**1.26-[BF$_{20}$]**),[4] $[Cp^*_2Ti_2\{NC(N^iPr_2)Ar^{F_2}\}_2Me_2(\mu\text{-}Me)][BF_{20}]$ (**1.50-[BF$_{20}$]**) and $[Cp^*Ti\{NC(N^iPr_2)\text{-}Ar^{F_2}\}(OPPh_3)Me][BF_{20}]$ (**1.51-[BF$_{20}$]**)[4] were prepared according to literature methods.

All other reagents were purchased from Alfa Aesar or Sigma-Aldrich or donated by Lanxess Elastomers and used directly or degassed as appropriate before use.

5.3 Computational details

DFT calculations carried out by the author (Section 2.5) were carried out using the Amsterdam Density Functional program suite ADF 2013.01.[5-7] The generalized gradient approximation was employed, using the local density approximation of Vosko, Wilk, and Nusair[8] together with nonlocal exchange corrections by Becke[9, 10] and non-local correlation corrections by Perdew.[11] TZ2P basis sets were used with triple-ζ accuracy sets of Slater-type orbitals and a polarization function added to the main-group atoms. The default SCF convergence criteria were used, together with a "good" Becke integration grid. Full optimization of geometry was performed without any symmetry constraint, followed by analytical computation of the Hessian matrix to identify the nature of the located extrema as minima or transition states. Fragment analyses use the MOs of the chosen fragments as the basis set for the molecular calculation. AIM analysis[12, 13] of **15Q**$^{+}$ was carried out in ADF 2013.01.[5-7]

DFT calculations carried out by Dr Betty Coussens were carried out in the Gaussian 09 package (Sections 3.2.18, 3.2.19, 3.4.3)[14] or in the Turbomole package (Section 3.2.17).[15-17] In Section 3.2.17 the Turbomole B3LYP functional[18-20] was used and in Sections 3.2.18, 3.2.19 and 3.4.3 the M06 level of theory was used.[21] Sections 3.2.17, 3.2.18 and 3.2.19 used the SV(P) basis set[22] and Section 3.4.3 used the LANL2DZ[23-26] basis set for Ti and SVP[22, 27] for all other atoms. DFT calculations carried out by Dr Betty Coussens in Sections 4.3.2 and 4.3.4 at the B3PW91 level as executed previously by Dr Eric Clot.[20, 28, 29] In this Section the Ti atom was represented by the relativistic effective core potential (RECP) from the Stuttgart group and the SDD basis set, augmented with an f polarisation function (α = 1.506).[30, 31] Si and P atoms were represented by RECP with a MWB10 basis set and were augmented by a d polarisation function (α = 0.284 and 0.387, respectively).[32, 33] The remaining atoms (C, H, N) were represented by a 6-31G(d,p) basis set.[34] NMR parameters were determined using all-electron calculations where for Ti Ahlrich's TZV basis set was used[27] and for all other atoms the IGLOO-II basis set was used.[35] As in Section 2.5 analytical computation of the Hessian matrix was performed to confirm the nature of the located extrema as minima or transition states on the potential energy surface. EPR calculations on **15Q**$^{+}$ were carried out in Gaussian 09 using the B3LYP functional.[18-20] Ti was represented

by the aug-cc-pVTZ-J basis set[36-39], nitrogen was represented by the EPR III basis sets[40] and the remaining atoms by the SV(P) basis set.[22]

5.4 Experimental details for Chapter 2

$Cp^*Ti\{NC(NMe_2)_2\}Cl_2$ (1)

This compound was prepared by adaptation of a patented procedure.[41] To a stirring toluene (20 ml) solution of 1,1,3,3-tetramethylguanidinate (1.99 g, 2.2 ml, 17.3 mmol) at 0 °C was added dropwise ^{n}BuLi (10.8 ml, 1.6 M in hexane, 17.3 mmol). This solution was allowed to warm to room temperature and was stirred for a further 10 min. This solution was then added to Cp^*TiCl_3 (5.0 g, 17.3 mmol) in toluene at -78 °C. This solution was then allowed to warm to room temperature and stirred for a further 16 h. Following removal of the solvent under reduced pressure the orange residue was extracted into CH_2Cl_2 and filtered. After concentration of the solution *in vacuo* to 10 ml and subsequent cooling of the solution to -80 °C an orange solid crystallised which was isolated by filtration, washed with pentane (3 x 10 ml) and dried *in vacuo*. Yield: 5.32 g (84%). ^{1}H NMR (C_6D_6, 299.9 MHz, 293 K) 2.34 (12H, s, NC($N\underline{Me}_2$)$_2$) , 2.09 (15H, s, $C_5\underline{Me}_5$) ppm. ^{13}C-{^{1}H} NMR (C_6D_6, 75.4 MHz, 293 K) 159.6 ($N\underline{C}(NMe_2)_2$), 125.7 ($\underline{C}_5Me_5$), 40.0 (NC($N\underline{Me}_2$)$_2$), 13.1 ($C_5\underline{Me}_5$) ppm. EI-MS *m/z* 367 (5%, $[M]^+$), 253 (90%, $[M\text{-}(NC(NMe_2)_2)]^+$, 135 (100%, $[C_5Me_5]^+$), 114 (70%, $[N\underline{C}(NMe_2)_2]^+$). IR (NaCl plates, Nujol mull, cm^{-1}) 1582 (m), 1512(m), 1502 (m), 1453 (s), 1421 (m), 1412 (m), 1405 (m), 1260 (w), 1145 (w), 1098 (w), 1054 (w), 1023 (w), 858 (w), 800 (w). Anal. Found (calcd. for $C_{15}H_{27}Cl_2N_3Ti$): C, 48.80 (48.93); H, 7.54 (7.39); N, 11.28 (11.41). Single crystals suitable for X-ray diffraction were grown from a saturated benzene solution at room temperature.

$Cp^*Ti\{NC(N^iBuMe)_2\}Cl_2$ (2)

This compound was prepared by adaptation of a patented procedure.[41] To a stirring THF (20 ml) solution of N,N'-diisobutyl-N,N'-dimethylguanidine (0.51 g, 2.5 mmol) at 0 °C was added dropwise ^{n}BuLi (1.6 ml, 1.6 M in hexane, 2.5 mmol). This solution was allowed to warm to room temperature and was stirred for a further 4 h. This solution was then added to a solution of Cp^*TiCl_3 (0.72 g, 2.5 mmol) in THF (10 ml) at -78 °C. This was allowed to warm to room temperature and stirred for a further 16 h. Following removal of the solvent under reduced pressure the orange residue was extracted into hot toluene and filtered. After removal of the volatiles *in vacuo* the

product was washed with pentane (3 x 10 ml) and dried *in vacuo* to yield an orange powder. Yield: 0.92 g (82%). ^{1}H NMR (C_6D_6, 299.9 MHz, 293 K) 2.95 (4H, d, ^{3}J = 7.6 Hz, NC$\underline{H}_2$CHMe$_2$), 2.42 (6H, s, N$\underline{Me}$), 2.10 (15H, s, $C_5\underline{Me}_5$), 1.65 (2H, m, NCH$_2$C$\underline{H}$Me$_2$), 0.81 (12H, d, ^{3}J = 6.6 Hz, NCH$_2$CH$\underline{Me}_2$) ppm. ^{13}C-{^{1}H} NMR (C_6D_6, 75.4 MHz, 293 K) 160.2 (N$\underline{C}$(N^{i}BuMe)$_2$), 126.0 ($\underline{C}_5$Me$_5$), 60.0 (N$\underline{C}$H$_2$CHMe$_2$), 38.9 (NC(N^{i}Bu$\underline{Me}$)$_2$), 27.2 (NCH$_2\underline{C}$HMe$_2$), 20.3 (NCH$_2$CH$\underline{Me}_2$), 13.5 ($C_5\underline{Me}_5$) ppm. EI-MS *m/z* 451 (3%, [M]$^{+}$), 198 (80%, [N$\underline{C}$(N^{i}BuMe)$_2$]$^{+}$), 135 (100%, [C_5Me$_5$]$^{+}$). IR (NaCl plates, Nujol mull, cm^{-1}) 1496 (s), 1413 (s), 1366 (m), 1338 (m), 1267 (w), 1155 (w), 1085 (w), 1022 (w), 965 (w), 857 (m), 803 (w), 722 (w). Anal. Found (calcd. for $C_{21}H_{39}Cl_2N_3Ti$): C, 55.46 (54.76); H, 8.66 (8.69); N, 9.43 (9.29). Single crystals suitable for X-ray diffraction were grown from a saturated benzene solution at 4 °C.

Cp*Ti{NC(N(Xyl)CH$_2$)$_2$}Cl$_2$ (3)

This compound was prepared by the adaption of a patented procedure.[42] To a stirring THF (30 ml) solution of 1,3-(2,6-Me$_2$C$_6$H$_3$)$_2$C$_2$H$_4$N$_2$CNH (3.0 g, 10.2 mmol) at 0 °C was added dropwise ^{n}BuLi (6.4 ml, 1.6 M in hexane, 10.2 mmol). This solution was allowed to warm to room temperature and stirred for a further 10 min. This solution was then added to a solution of Cp*TiCl$_3$ (2.96 g, 10.2 mmol) in THF (10 ml) at -78 °C. This was allowed to warm to room temperature and stirred for a further 16 h. Following removal of the solvent under reduced pressure the orange residue was extracted into hot toluene and filtered. After removal of the volatiles *in vacuo* the product was washed with pentane (3 x 10 ml) and dried *in vacuo* to yield an orange powder. Yield: 4.30 g (77%). ^{1}H NMR (C_6D_6, 399.9 MHz, 293 K) 7.06 (6H, s, C$_6\underline{H}_3$Me$_2$), 3.09 (4H, s, C$\underline{H}_2$C$\underline{H}_2$), 2.44 (12H, s, C$_6$H$_3\underline{Me}_2$), 1.85 (15H, s, $C_5\underline{Me}_5$) ppm. ^{13}C-{^{1}H} NMR (C_6D_6, 100.6 MHz, 293 K) 149.8 (N$\underline{C}$(N(Xyl)CH$_2$)$_2$), 138.0 (*i*-$\underline{C}_6$H$_3$Me$_2$), 136.0 (*o*-$\underline{C}_6$H$_3$Me$_2$), 129.0 (*m*-$\underline{C}_6$H$_3$Me$_2$), 128.5 (*p*-$\underline{C}_6$H$_3$Me$_2$), 126.5 ($\underline{C}_5$Me$_5$), 45.7 ($\underline{C}$H$_2\underline{C}$H$_2$), 18.8 (C$_6$H$_3\underline{Me}_2$), 12.8 ($C_5\underline{Me}_5$) ppm. EI-MS *m/z* 410 (1%, [M-Cp*]$^{+}$), 292 (98%, [NC(N(Xyl)CH$_2$)$_2$]$^{+}$), 277 (100%, [{NC(N(Xyl)CH$_2$)$_2$}-Me]$^{+}$), 135 (10%, [Cp*]$^{+}$), 105 (15%, [Xyl]$^{+}$). IR (NaCl plates, Nujol mull, cm^{-1}) 1597 (m), 1538 (s), 1486 (s), 1300 (w), 1284 (m), 1257 (w), 1196 (w), 1164 (w), 1107 (w), 1026 (w), 1016 (w), 977 (w), 872 (m), 800 (w), 779 (w), 771 (w), 721 (w), 711 (w). Anal. Found (calcd. for $C_{29}H_{37}Cl_2N_3Ti$): C, 63.70 (63.75); H, 6.64 (6.83); N, 7.56 (7.69). Single crystals suitable for X-ray diffraction were grown from a saturated CH_2Cl_2 solution at room temperature.

Cp*Ti{NC(NMe$_2$)$_2$}Me$_2$ (4)

This compound was prepared by adaptation of a patented procedure.[41] MeLi (10.2 ml, 1.6M in Et_2O, 16.30 mmol) was added to a stirring solution of Cp*Ti{NC(NMe$_2$)$_2$}Cl$_2$ (3.0 g, 8.15 mmol) in toluene (30 ml) at 0 °C. The mixture was allowed to warm to room temperature and left to stir for 16 h. The toluene was removed *in vacuo* and the product extracted into pentane (3 x 30 ml). The volume of pentane was reduced *in vacuo* to 20 ml and cooled to -30 °C to produce yellow crystals of the product. Yield: 2.11 g (79%). ^{1}H NMR (C_6D_6, 299.9 MHz, 293 K) 2.47 (12H, s, NC(N$\underline{Me}_2$)$_2$), 1.98 (15H, s, C$_5\underline{Me}_5$), 0.52 (6H, s, Ti-$\underline{Me}$) ppm. ^{13}C-{^{1}H} NMR (C_6D_6, 75.4 MHz, 293 K) 157.4 (N$\underline{C}$(NMe$_2$)$_2$), 119.5 ($\underline{C}_5$Me$_5$), 45.0 (Ti-$\underline{Me}$), 40.3 (NC(N$\underline{Me}_2$)$_2$), 12.6 (C$_5\underline{Me}_5$) ppm. EI-MS *m/z* 213 (60%, [Cp*Ti-$\underline{Me}_2$]$^+$), 177 (20% ,[TiNC(NMe$_2$)$_2$Me]$^+$) 135 (3%, [C$_5$Me$_5$]$^+$), 71.07 (5%, [(NC(NMe$_2$)$_2$)-NMe$_2$]). IR (NaCl plates, Nujol mull, cm^{-1}) 1616 (w), 1573 (s), 1539 (w), 1521 (w), 1506(w), 1496 (w), 1419 (m), 1405 (w), 1395 (w), 1260 (w), 1126 (w), 1094 (w), 1034 (w), 849 (w), 800 (w). Anal. Found (calcd. for $C_{17}H_{33}N_3Ti$): C, 62.52 (62.38); H, 10.15 (10.16), 12.72 (12.84).

Cp*Ti{NC(NMe$_2$)$_2$}Bn$_2$ (5)

This compound was prepared by adaptation of a patented procedure.[41] BnMgCl (5.4 ml, 1.0M in Et_2O, 5.44 mmol) was added to a stirring solution of Cp*Ti{NC(NMe$_2$)$_2$}Cl$_2$ (1.0 g, 2.72 mmol) in toluene (10 ml) at 0 °C. The mixture was allowed to warm to room temperature and left to stir for 16 h. The toluene was removed *in vacuo* and the product extracted into pentane (3 x 30 ml). The volume of pentane was reduced *in vacuo* to 10 ml and cooled to -30 °C to produce orange crystals of the product. Yield: 0.52 g (40%). ^{1}H NMR (C_6D_6, 299.9 MHz, 293 K) 7.19 (4H, m, *m*-C$_6\underline{H}_5$), 7.08 (4H, m, *o*-C$_6\underline{H}_5$), 6.89 (2H, m, *p*-C$_6\underline{H}_5$), 2.38 (2H, d, ^2J = 10.2 Hz, C$\underline{H}_2$), 2.21 (12H, s, NC(N$\underline{Me}_2$)$_2$), 1.99 (2H, d, ^2J = 10.2 Hz, C$\underline{H}_2$), 1.87 (15H, s, C$_5\underline{Me}_5$) ppm. ^{13}C-{^{1}H} NMR (C_6D_6, 75.4 MHz, 293 K) 158.1 (N$\underline{C}$(NMe$_2$)$_2$), 154.8 (*i*-$\underline{C}_6$H$_5$), 128.8 (*o*-$\underline{C}_6$H$_5$), 127.8 (*m*-$\underline{C}_6$H$_5$), 121.4 (*p*-$\underline{C}_6$H$_5$), 120.3 ($\underline{C}_5$Me$_5$), 75.7 ($\underline{C}$H$_2$), 40.3 (NC(N$\underline{Me}_2$)$_2$), 12.9 (C$_5\underline{Me}_5$) ppm. EI-MS *m/z* 388 (20%, [M-Bn]$^+$), 297 (20%, [M-2Bn]$^+$), 135 (5%, [C$_5$Me$_5$]$^+$), 91 (20%, [Bn]$^+$). IR (NaCl plates, Nujol mull, cm^{-1}) 1593 (w), 1528 (m), 1395 (m), 1260 (s), 1093 (s), 1019 (s), 853 (w), 799 (s), 743 (w), 693 (m). Anal. Found (calcd. for $C_{29}H_{41}N_3Ti$): C, 72.83 (72.64); H, 8.75 (8.62); N, 8.91 (8.76). Single crystals suitable for X-ray analysis were grown from a saturated pentane solution at 0 °C.

Cp*Ti{NC(N^{i}BuMe)$_2$}Me$_2$ (6)

This compound was prepared by adaptation of a patented procedure.[41] MeLi (1.38 ml, 1.6M in Et_2O, 2.22 mmol) was added to a stirring solution of Cp*Ti{NC(N^{i}BuMe)$_2$}Cl$_2$ (500 mg, 1.11 mmol) in toluene (30 ml) at 0 °C. The mixture was allowed to warm to room temperature and left to stir for 16 h. The toluene was removed *in vacuo* and the product extracted into pentane (3 x 30 ml). After removal of the pentane *in vacuo* the product was left as yellow solid. Yield: 346 mg (76%). ^{1}H NMR (C_6D_6, 299.9 MHz, 293 K) 2.95 (4H, d, ^3J = 7.6 Hz, NC$\underline{H_2}$CHMe$_2$), 2.54 (6H, s, N$\underline{Me}$), 2.00 (15H, s, C$_5\underline{Me_5}$), 1.73 (2H, m, NCH$_2$C$\underline{H}$Me$_2$), 0.85 (12H, d, ^3J = 6.6 Hz, NCH$_2$CH$\underline{Me_2}$), 0.45 (6H, s, Ti-$\underline{Me}$) ppm. ^{13}C-{^{1}H} NMR (C_6D_6, 75.4 MHz, 293 K) 157.2 (N$\underline{C}$(N^{i}BuMe)$_2$), 119.1 ($\underline{C}_5$Me$_5$), 59.6 (N$\underline{C}$H$_2$CHMe$_2$), 44.9 (Ti-$\underline{Me}$) 38.3 (NC(N^{i}Bu$\underline{Me}$)$_2$), 27.0 (NCH$_2\underline{C}$HMe$_2$), 20.4 (NCH$_2$CH$\underline{Me_2}$), 12.3 (C$_5\underline{Me_5}$) ppm. EI-MS *m/z* 198 (80%, [N$\underline{C}$(N^{i}BuMe)$_2$]$^+$), 135 (40%, [C$_5$Me$_5$]$^+$). IR (NaCl plates, Nujol mull, cm^{-1}) 1557 (s), 1411 (m), 1335 (m), 1299 (w), 1261 (m), 1138 (m), 1104 (w), 1083 (m), 1043 (w), 967 (w), 846 (w), 813 (w), 658 (w). Anal. Found (calcd. for $C_{23}H_{45}N_3Ti$): C, 67.25 (67.13); H, 11.13 (11.02); N, 10.33 (10.21).

Cp*Ti{NC(N(Xyl)CH$_2$)$_2$}Me$_2$ (7)

This compound was prepared by adaptation of a patented procedure.[41] MeLi (4.6 ml, 1.6M in Et_2O, 7.32 mmol) was added to a stirring solution of Cp*Ti{NC(N^{i}BuMe)$_2$}Cl$_2$ (2.0 g, 3.66 mmol) in toluene (30 ml) at 0 °C. The mixture was allowed to warm to room temperature and left to stir for 16 h. The toluene was removed *in vacuo* and the product extracted into pentane (3 x 30 ml). After removal of the pentane *in vacuo* the product was left as yellow solid. Yield: 1.18 g (64%). ^{1}H NMR (C_6D_6, 399.9 MHz, 293 K) 6.98 (6H, s, C$_6\underline{H_3}$Me$_2$), 3.26 (4H, s, C$\underline{H_2}$C$\underline{H_2}$), 2.47 (12H, s, C$_6$H$_3\underline{Me_2}$), 1.74 (15H, s, C$_5\underline{Me_5}$), 0.00 (6H, s, Ti-$\underline{Me}$) ppm. ^{13}C-{^{1}H} NMR (C_6D_6, 100.6 MHz, 293 K) 145.3 (N$\underline{C}$(N(Xyl)CH$_2$)$_2$), 138.2 (*i*-$\underline{C}_6$H$_3$Me$_2$), 138.1 (*o*-$\underline{C}_6$H$_3$Me$_2$), 128.8 (*m*-$\underline{C}_6$H$_3$Me$_2$), 128.0 (*p*-$\underline{C}_6$H$_3$Me$_2$), 119.2 ($\underline{C}_5$Me$_5$), 46.2 (Ti-$\underline{Me}$), 45.1 ($\underline{C}$H$_2\underline{C}$H$_2$), 18.6 (C$_5$H$_3\underline{Me_2}$), 11.8 (C$_5\underline{Me_5}$) ppm. EI-MS *m/z* 475 (1%, [M-2Me]$^+$), 292 (98%, [NC(N(Xyl)CH$_2$)$_2$]$^+$), 277 (100%, [NC(N(Xyl)CH$_2$)$_2$-Me]$^+$), 132 (80%, [Cp*-3H]$^+$), 105 (10%, [Xyl]$^+$). IR (NaCl plates, Nujol mull, cm^{-1}) 1608 (s), 1572 (s), 1403 (m), 1306 (w), 1280 (m), 1260 (m), 1248 (m), 1167 (w), 1108 (m), 1097 (m), 1022 (m), 862 (w), 799 (w), 774 (w), 722 (w), 713 (w). Anal. Found (calcd. for

$C_{31}H_{43}N_3Ti$): C, 73.43 (73.65); H, 8.66 (8.57); N, 8.21 (8.31). Single crystals suitable for X-ray analysis were grown from a saturated pentane solution at -30 °C.

5.5 Experimental details for Chapter 3

[Cp*Ti{NC(N^{i}Pr$_2$)Ar^{F2}}(py)Me][BF$_{20}$] (8-[BF$_{20}$])

Cp*Ti{NC(N^{i}Pr$_2$)Ar^{F2}}Me$_2$ (100 mg, 0.22 mmol) and pyridine (18 mg, 18 μL, 0.22 mmol) were mixed together in fluorobenzene (5 mL), To this a solution of TBF$_{20}$ (204 mg, 0.22 mmol) in fluorobenzene (5 mL) was added dropwise. After 30 min pentane (20 mL) was added resulting in the formation of an orange oil. The pentane/fluorobenzene was decanted and the oil washed with pentane (10 ml). The remaining solvent was removed *in vacuo* to yield the product as a yellow solid. Yield: 203 mg (77%). ^{1}H NMR (C_6D_5Br, 299.9 MHz, 293 K) 7.35 (*m*-py), 7.20-6.50 (6H, m, Ar), 3.79 (1H, br, NC<u>H</u>Me$_2$), 3.36 (1H, sept, ^3J = 6.9 Hz, NC<u>H</u>Me$_2$), 1.50 (C_5<u>Me$_5$</u>), 1.14 (3H, d, ^3J = 6.9 Hz, NCH<u>Me$_2$</u>), 1.10 (3H, d, ^3J = 6.9 Hz, NCH<u>Me$_2$</u>), 1.06 (3H, d, ^3J = 6.9 Hz, NCH<u>Me$_2$</u>), 0.79 (3H, d, ^3J = 6.9 Hz, NCH<u>Me$_2$</u>), 0.78 (Ti-<u>Me</u>) ppm. ^{13}C-{^{1}H} NMR (C_6D_5Br, 75.4 MHz, 293 K) 157.9 (dd, $^1J_{CF}$ = 252 Hz, $^3J_{CF}$ = 6.7 Hz, *o*-<u>C</u>$_6H_3F_2$), 154.3 (N<u>C</u>(N^{i}Pr$_2$)Ar^{F2}), 148.9 (br d, $^1J_{CF}$ = 244.4 Hz, *o*-<u>C</u>$_6F_5$), 138.6 (br d, $^1J_{CF}$ = 247.8 Hz , *p*-<u>C</u>$_6F_5$), 136.8 (br d, $^1J_{CF}$ = 249.0 Hz, *m*-<u>C</u>$_6F_5$), 129.0 (<u>C</u>$_5$Me$_5$), 114.7 (t, $^2J_{CF}$ = 22.7 Hz, *i*-<u>C</u>$_6H_3F_2$), 112.0 (d, $^2J_{CF}$ = 22.0 Hz, *m*-<u>C</u>$_6H_3F_2$), 63.9 (Ti-<u>Me</u>), 49.0 (N<u>C</u>HMe$_2$), 20.7 (NCH<u>Me$_2$</u>), 19.8 (NCH<u>Me$_2$</u>), 11.6 (C_5<u>Me$_5$</u>) ppm. ^{19}F NMR (C_6D_5Br, 282.1 MHz, 293 K) -111.2 (br, C_6H_3<u>F$_2$</u>), -131.8 (m, *o*-C_6F_5), -162.3 (m, *p*-C_6F_5), -166.1 (m, *m*-C_6F_5) ppm. ^{11}B NMR (C_6D_5Br, 96.2 MHz, 293 K) -15.9 ppm. IR (NaCl plates, Nujol mull, cm^{-1}) 1645 (m), 1512 (s), 1349 (w), 1154 (w), 1087 (m), 982 (s), 840 (w), 757 (w), 667 (w). Anal. Found (calcd. for $C_{53}H_{40}BF_{22}N_3Ti$): C, 53.33 (53.24); H, 3.48 (3.37); N, 3.48 (3.51).

[Cp*Ti{NC(N^{i}Pr$_2$)Ar^{F2}}(THF)Me][BF$_{20}$] (9-[BF$_{20}$])

Cp*Ti{NC(N^{i}Pr$_2$)Ar^{F2}}Me$_2$ (100 mg, 0.22 mmol) and THF (16 mg, 18 μL, 0.22 mmol) were mixed together in fluorobenzene (5 mL), To this a solution of TBF$_{20}$ (204 mg, 0.22 mmol) in fluorobenzene (5 mL) was added dropwise. After 30 min pentane (20 mL) was added resulting in the formation of an orange oil. The pentane/fluorobenzene was decanted and the oil washed with pentane (10 ml). The remaining solvent was removed *in vacuo* to yield the product as a yellow solid. Yield: 223 mg (85%).^{1}H NMR (C_6D_5Br, 299.9 MHz, 293 K) 7.03-6.56 (3H, m, C_6<u>H</u>$_3F_2$), 3.85 (1H, br,

NC<u>H</u>Me$_2$), 3.40 (2H, m, OC<u>H</u>$_2$), 3.33 (1H, sept, ^3J = 6.9 Hz, NC<u>H</u>Me$_2$), 3.26 (2H, m, OC<u>H</u>$_2$), 1.58 (15H, s, C$_5$<u>Me</u>$_5$), 1.43 (4H, m, OCH$_2$C<u>H</u>$_2$), 1.18 (3H, br d, NCH<u>Me</u>$_2$), 1.06 (3H, d, ^3J = 6.9 Hz, NCH<u>Me</u>$_2$), 0.80 (3H, d, ^3J = 6.9 Hz, NCH<u>Me</u>$_2$), 0.79 (3H, d, ^3J = 6.9 Hz, NCH<u>Me</u>$_2$), 0.52 (Ti-<u>Me</u>) ppm. ^{13}C-{^{1}H} NMR (C$_6$D$_5$Br, 75.4 MHz, 293 K) 154.5 (N<u>C</u>(N^{i}Pr$_2$)Ar^{F2}), 148.9 (br d, $^1J_{CF}$ = 244.4 Hz, *o*-<u>C</u>$_6$F$_5$), 138.6 (br d, $^1J_{CF}$ = 247.8 Hz, *p*-<u>C</u>$_6$F$_5$), 136.8 (br d, $^1J_{CF}$ = 249.0 Hz, *m*-<u>C</u>$_6$F$_5$), 126.6 (<u>C</u>$_5$Me$_5$), 115.1 (t, $^2J_{CF}$ = 21.5 Hz, *i*-<u>C</u>$_6$H$_3$F$_2$), 112.2 (d, $^2J_{CF}$ = 22.1 Hz, *m*-<u>C</u>$_6$H$_3$F$_2$), 75.3 (O<u>C</u>H$_2$), 63.6 (Ti-<u>Me</u>), 49.0 (N<u>C</u>HMe$_2$), 25.2 (OCH$_2$C<u>H</u>$_2$), 21.0 (NCH<u>Me</u>$_2$), 20.2 (NCH<u>Me</u>$_2$), 19.7 (NCH<u>Me</u>$_2$), 11.6 (C$_5$<u>Me</u>$_5$) ppm. ^{19}F NMR (C$_6$D$_5$Br, 282.1 MHz, 293 K) -110.6 (br, C$_6$H$_3$<u>F</u>$_2$), -131.8 (m, *o*-C$_6$F$_5$), -162.3 (m, *p*-C$_6$F$_5$), -166.1 (m, *m*-C$_6$F$_5$) ppm. ^{11}B NMR (C$_6$D$_5$Br, 96.2 MHz, 293 K) -16.1 ppm. IR (NaCl plates, Nujol mull, cm^{-1}) 1644 (w), 1598 (w), 1533 (m), 1455 (s), 1419 (m), 1262 (w), 1085 (m), 1021 (m), 980 (m), 757 (w), 728 (w), 681 (w). Anal. Found (calcd. for C$_{52}$H$_{43}$BF$_{22}$N$_2$OTi): C, 52.37 (52.55); H, 3.55 (3.65); N, 2.46 (2.36).

NMR tube scale synthesis of [Cp*Ti{NC(N^{i}Pr$_2$)Ph}Me][BF$_{20}$] (10-[BF$_{20}$])

To a solution of Cp*Ti{NC(N^{i}Pr$_2$)Ph}Me$_2$ (20 mg, 0.05 mmol) in C$_6$D$_5$Br (0.5 ml) was added TBF$_{20}$ (44 mg, 0.05 mmol) resulting in the formation of a red solution. The red solution was transferred to an NMR tube and the ^{1}H NMR spectrum recorded after 5 min. There are three isomers of the product **10a**$^+$, **10b**$^+$ and **10c**$^+$ in a ratio of 2:1:1 by Cp* integration or 4:2:1 if product **10b**$^+$ is considered a dimer. Major isomer **10a**$^+$: ^{1}H NMR (C$_6$D$_5$Br, 299.9 MHz, 293 K) 7.30-6.80 (5H, m, C$_6$<u>H</u>$_5$), 3.49 (1H, br, NC<u>H</u>Me$_2$), 3.45 (1H, sept, ^3J = 6.7 Hz, NC<u>H</u>Me$_2$), 1.49 (15H, s, C$_5$<u>Me</u>$_5$), 1.19 (3H, d, ^3J = 6.7 Hz, NCH<u>Me</u>$_2$), 0.74 (3H, s, Ti-<u>Me</u>), 0.73 (3H, d, ^3J = 6.7 Hz, NCH<u>Me</u>$_2$) ppm. **10b**$^+$**:** 1.55 (30H, s, C$_5$<u>Me</u>$_5$) ppm **10c**$^+$**:** 1.73 (15H, s, C$_5$<u>Me</u>$_5$) ppm. The remaining resonances could not be assigned unambiguously to either **10b**$^+$ or **10c**$^+$ due to the overlapping and broad nature of the peaks, although the type of chemical environment could be assigned by their chemical shift: 4.36 (sept, ^3J = 6.7 Hz, NC<u>H</u>Me$_2$), 4.29 (sept, ^3J = 6.7 Hz, NC<u>H</u>Me$_2$), 3.76 (sept, ^3J = 6.7 Hz, NC<u>H</u>Me$_2$), 1.26 (br d) , 0.91 (d, ^3J = 6.5 Hz, NCH<u>Me</u>$_2$), 0.82 (br d, NCH<u>Me</u>$_2$), 0.36 (s, Ti-Me), 0.04 (s, Ti-Me), -0.35 (s, Ti-Me), -0.43 (s, Ti-Me), -0.59 (s, Ti-Me), -0.85 (s, Ti-Me), -0.95 (s, Ti-Me) ppm.

NMR tube scale reaction of [Cp*Ti{NC(N^{i}Pr$_2$)Ph}Me][BF$_{20}$] with OPPh$_3$

[Cp*Ti{NC(N^{i}Pr$_2$)Ph}Me][BF$_{20}$] was generated from Cp*Ti{NC(N^{i}Pr$_2$)Ph}Me$_2$ (20 mg, 0.05 mmol) and TBF$_{20}$ (44 mg, 0.05 mmol) in C_6D_5Br (0.5 ml). After 2 min OPPh$_3$ (13.4 mg, 0.05 mmol) was added resulting in a colour change from red to yellow. The yellow solution was transferred to an NMR tube and the ^{1}H NMR spectrum recorded after 5 min revealing quantitative conversion of the mixture of cations to **11-[BF$_{20}$]**.

[Cp*Ti{NC(N^{i}Pr$_2$)Ph}(OPPh$_3$)Me][BF$_{20}$] (11-[BF$_{20}$])

Cp*Ti{NC(N^{i}Pr$_2$)Ph}Me$_2$ (100 mg, 0.24 mmol) and OPPh$_3$ (67 mg, 0.24 mmol) were mixed together in fluorobenzene (10 ml). To this a solution of TBF$_{20}$ (221 mg, 0.24 mmol) in fluorobenzene (5 ml) was added. After 30 min pentane (30 ml) was added resulting in the formation of a yellow solid. The pentane/fluorobenzene was decanted and the solid washed further with pentane (10 ml). The yellow solid was dried *in vacuo* yielding the product. Yield: 172 mg (53%). ^{1}H NMR (C_6D_5Br, 299.9 MHz, 293 K) 7.55-6.80 (20H, OP<u>Ph</u>$_3$ and NC(N^{i}Pr$_2$)<u>Ph</u>) 3.62 (1H, br, NC<u>H</u>Me$_2$), 3.50 (1H, sept, ^3J = 6.7 Hz, NC<u>H</u>Me$_2$), 1.60 (15H, C$_5$<u>Me</u>$_5$), 1.49 (3H, d, ^3J = 6.7 Hz, NCH<u>Me</u>$_2$), 1.29 (3H, d, ^3J = 6.7 Hz, NCH<u>Me</u>$_2$), 0.88 (3H, d, ^3J = 6.7 Hz, NCH<u>Me</u>$_2$), 0.83 (3H, d, ^3J = 6.7 Hz, NCH<u>Me</u>$_2$), 0.50 (3H, s, Ti-<u>Me</u>) ppm. ^{13}C-{^{1}H} NMR (C_6D_5Br, 75.4 MHz, 293 K) 165.8 (N<u>C</u>(N^{i}Pr$_2$)Ph), 148.9 (br d, $^1J_{CF}$ = 244.4 Hz, *o*-<u>C</u>$_6$F$_5$), 139.3 (*i*-NC(N^{i}Pr$_2$)<u>Ph</u>), 138.6 (br d, $^1J_{CF}$ = 247.8 Hz , *p*-<u>C</u>$_6$F$_5$), 136.8 (br d, $^1J_{CF}$ = 249.0 Hz, *m*-<u>C</u>$_6$F$_5$), 134.9 (*p*-OP<u>Ph</u>$_3$), 132.4 (d, $^2J_{CP}$ = 11.4 Hz, *o*-OP<u>Ph</u>$_3$), 129.6 (*o*-NC(N^{i}Pr$_2$)<u>Ph</u>), 128.9 (*m*-NC(N^{i}Pr$_2$)<u>Ph</u>), 125.8 (*p*-NC(N^{i}Pr$_2$)<u>Ph</u>), 123.6 (<u>C</u>$_5$Me$_5$), 52.3 (N<u>C</u>HMe$_2$), 49.3 (Ti-<u>Me</u>), 47.8 (N<u>C</u>HMe$_2$), 21.1 (NCH<u>Me</u>$_2$), 20.8 (NCH<u>Me</u>$_2$), 20.4 (NCH<u>Me</u>$_2$), 20.3 (NCH<u>Me</u>$_2$), 11.8 (C$_5$<u>Me</u>$_5$). ^{31}P-{^{1}H} NMR (C_6D_5Br, 121.4 MHz, 293 K) 49.6 ppm, ^{19}F NMR (C_6D_5Br, 282.1 MHz, 293 K) -131.8 (m, *o*-C_6F_5), -162.2 (m, *p*-C_6F_5), -166.0 (m, *m*-C_6F_5) ppm. ^{11}B NMR (C_6D_5Br, 96.2 MHz, 293 K) -15.9 ppm. IR (NaCl plates, Nujol mull, cm^{-1}) 1643 (m), 1593 (w), 1527 (s), 1514 (s), 1340 (m), 1275 (m), 1217 (w), 1155 (w), 1125 (s), 1083 (s), 1026 (m), 980 (s), 891 (w), 785 (w), 756 (w), 728 (w), 684 (w), 668 (m), 660 (w). Anal. Found (calcd. for $C_{66}H_{52}BF_{20}N_2OPTi$) C, 58.20 (58.34); H, 3.74 (3.86); N, 2.16 (2.06).

[Cp*Ti{NC(N^{i}Pr$_2$)Ph}(py)Me][BF$_{20}$] (12-[BF$_{20}$])

Cp*Ti{NC(N^{i}Pr$_2$)Ph}Me$_2$ (20 mg, 0.05 mmol) and pyridine (4 mg, 4 μL, 0.05 mmol) were mixed together in fluorobenzene (5 mL), To this a solution of TBF$_{20}$ (44 mg, 0.05 mmol) in fluorobenzene (5 mL) was added dropwise. After 30 min pentane (20 mL) was added resulting in the formation of an orange oil. The pentane/fluorobenzene was decanted and the oil washed with pentane (10 ml). The remaining solvent was removed *in vacuo* to yield the product as a yellow solid. Yield: 34 mg (77%). ^{1}H NMR (C$_6$D$_5$Br, 299.9 MHz, 293 K) 7.30-6.75 (10H, m, py and C$_6$H$_5$), 3.65 (1H, br, NCHMe$_2$), 3.33 (1H, sept, ^3J = 6.8 Hz, NCHMe$_2$), 1.43 (15H, s, C$_5$Me$_5$), 1.18 (3H, br d, NCHMe$_2$), 1.05 (3H, br d, NCHMe$_2$), 0.68 (6H, d, ^3J = 6.8 Hz, NCHMe$_2$), 0.67 (3H, s, Ti-Me) ppm. ^{13}C-{^{1}H} NMR (C$_6$D$_5$Br, 75.4 MHz, 293 K) 167.3 (NC(N^{i}Pr$_2$)Ph), 137.7 (*i*-C$_6$H$_5$), 126.1 (C$_5$Me$_5$), 125.6 (*m*-py), 61.5 (Ti-Me), 51.9 (NCHMe$_2$), 48.7 (NCHMe$_2$), 21.2 (NCHMe$_2$), 20.6 (NCHMe$_2$), 19.9 (NCHMe$_2$), 12.0 (C$_5$Me$_5$) ppm. ^{19}F NMR (C$_6$D$_5$Br, 282.1 MHz, 293 K) -131.8 (m, *o*-C$_6$F$_5$), -162.2 (m, *p*-C$_6$F$_5$), -166.0 (m, *m*-C$_6$F$_5$) ppm. ^{11}B NMR (C$_6$D$_5$Br, 96.2 MHz, 293 K) -16.0 ppm. IR (NaCl plates, Nujol mull, cm^{-1}) 1643 (m), 1608 (w), 1514 (s), 1345(m), 1274 (m), 1217 (w), 1153 (w), 1137 (w), 1024 (w), 1086 (s), 1023 (w), 979 (s), 798 (w), 756 (w), 701(w), 684 (w), 668 (w). Anal. Found (calcd. for C$_{53}$H$_{42}$BF$_{20}$N$_3$Ti) C, 55.06 (54.90); H, 3.52 (3.65); N, 3.76 (3.62).

[Cp*Ti{NC(N^{i}Pr$_2$)Ph}(THF)Me][BF$_{20}$] (13-[BF$_{20}$])

Cp*Ti{NC(N^{i}Pr$_2$)Ph}Me$_2$ (100 mg, 0.24 mmol) and THF (17 mg, 19 μL, 0.24 mmol) were mixed together in fluorobenzene (10 ml). To this a solution of TBF$_{20}$ (221 mg, 0.24 mmol) in fluorobenzene (5 ml) was added. After 30 min pentane (20 ml) was added resulting in the formation of an orange oil. The pentane/fluorobenzene was decanted and the oil washed further with pentane (10 ml). The remaining solvent was removed *in vacuo* yielding the product as a yellow solid. Yield: 193 mg (70%) ^{1}H NMR (C$_6$D$_5$Br, 299.9 MHz, 293 K) 7.20-6.70 (5H, m, C$_6$H$_5$), 3.47 (1H, br, NCHMe$_2$), 3.39 (1H, sept, ^3J = 6.8 Hz, NCHMe$_2$), 3.29 (2H, m, OCH$_2$), 3.18 (2H, m, OCH$_2$), 1.54 (15H, s, C$_5$Me$_5$), 1.41 (4H, m, OCH$_2$CH$_2$), 1.23 (1H, d, ^3J = 6.8 Hz, NCHMe$_2$), 1.10 (1H, d, ^3J = 6.8 Hz, NCHMe$_2$), 0.73 (2H, d, ^3J = 6.6 Hz, NCHMe$_2$), 0.51 (3H, s, Ti-Me) ppm. ^{13}C-{^{1}H} NMR (C$_6$D$_5$Br, 75.4 MHz, 293 K) 167.6 (NC(N^{i}Pr$_2$)Ph), 148.9 (br d, $^1J_{CF}$ = 244.4 Hz, *o*-C$_6$F$_5$), 138.6 (br d, $^1J_{CF}$ = 247.8 Hz , *p*-C$_6$F$_5$), 137.7 (*i*-C$_6$H$_5$), 136.8 (br d, $^1J_{CF}$ = 249.0 Hz, *m*-C$_6$F$_5$), 129.5 (*o*-C$_6$H$_5$), 128.9 (*m*-C$_6$H$_5$), 125.6 (C$_5$Me$_5$),

75.1 (O<u>C</u>H$_2$CH$_2$), 58.8 (Ti-<u>Me</u>), 52.3 (NC<u>H</u>Me$_2$), 48.5 (NC<u>H</u>Me$_2$), 25.2 (OCH$_2$<u>C</u>H$_2$), 21.5 (NCH<u>Me</u>$_2$), 21.0 (NCH<u>Me</u>$_2$), 20.5 (NCH<u>Me</u>$_2$), 19.8 (NCH<u>Me</u>$_2$), 11.7 (C$_5$<u>Me</u>$_5$) ppm. ^{19}F NMR (C$_6$D$_5$Br, 282.1 MHz, 293 K) -131.5 (m, *o*-C$_6$F$_5$), -161.9 (m, *p*-C$_6$F$_5$), -165.8 (m, *m*-C$_6$F$_5$) ppm. ^{11}B NMR (C$_6$D$_5$Br, 96.2 MHz, 293 K) -15.9 ppm. IR (NaCl plates, Nujol mull, cm^{-1}) 1643 (m), 1595 (w), 1514 (s), 1345 (w), 1261 (w), 1153 (w), 1086 (m), 1023 (w), 980 (s), 891 (w), 844 (w), 789 (w), 775 (w), 756 (w), 668 (w). Anal. Found (calcd. for C$_{52}$H$_{45}$B F$_{20}$N$_2$OTi) C, 53.98 (54.19); H, 3.90 (3.94); N, 2.56 (2.43).

[Cp*$_2$Ti$_2${NC(NMe$_2$)$_2$}$_2$(μ-Me)$_2$][BF$_{20}$]$_2$ (14$_{dim}$-[BF$_{20}$]$_2$)

Cp*Ti{NC(NMe$_2$)$_2$}Me$_2$ (200 mg, 0.61 mmol) and TBF$_{20}$ were mixed together and to this fluorobenzene (10 ml) was added. After 30 min the fluorobenzene was removed by filtration and the resultant red solid washed with pentane (10 ml) to yield the product. Yield: 0.45g (75%). IR (NaCl plates, Nujol mull, cm^{-1}) 1644 (w), 1595 (w), 1548 (m), 1513 (s), 1419 (m), 1286 (m), 1221 (m), 1157 (w), 1085 (s), 978 (s), 806 (w), 774 (w) 756 (w), 750 (w), 683 (w), 661 (w). Anal. Found (calcd. for C$_{40}$H$_{30}$BF$_{20}$N$_3$Ti): C, 48.62 (48.46); H, 2.87 (3.05); N, 4.06 (4.24).

NMR tube scale synthesis of [Cp*Ti{NC(NMe$_2$)$_2$}Me][MeBF$_{15}$] (14-[MeBF$_{15}$])

To a solution of Cp*Ti{NC(NMe$_2$)$_2$}Me$_2$ (20 mg, 0.06 mmol) in C$_6$D$_5$Br (0.5 ml) was added BF$_{15}$ (31 mg, 0.06 mmol) resulting in the formation of a red solution. The red solution was transferred to an NMR tube and the NMR spectra recorded after 5 min. ^{1}H NMR (C$_6$D$_5$Br, 299.9 MHz, 293 K) 2.47 (12H, s, NC(N<u>Me</u>$_2$)$_2$), 1.62 (15H, s, C$_5$<u>Me</u>$_5$), 1.46 (3H, s, Ti-Me) and 0.90 (3H, s, [<u>Me</u>BF$_{15}$]$^-$) ppm. ^{19}F NMR -132.1 (m, *o*-C$_6$F$_5$), -160.0 (m, *p*-C$_6$F$_5$) and -164.4 (m, *m*-C$_6$F$_5$) ppm.

NMR tube scale reaction [Cp*Ti{NC(NMe$_2$)$_2$}Me][MeBF$_{15}$] with ^{i}PrNCN^{i}Pr

To a solution of Cp*Ti{NC(NMe$_2$)$_2$}Me$_2$ (20 mg, 0.06 mmol) in C$_6$D$_5$Br (0.5 ml) was added BF$_{15}$ (31 mg, 0.06 mmol) resulting in the formation of a red solution. After 1 minute ^{i}PrNCN^{i}Pr (10 μl ,8 mg, 0.06 mmol) was added resulting in the formation of a brown solution which was transferred to an NMR tube and the NMR spectra recorded after 5 min. The ^{1}H NMR spectrum showed quantitative conversion to [Cp*Ti{NC(NMe$_2$)$_2$}{MeC(N^{i}Pr)$_2$][MeBF$_{15}$] **(43-[MeBF$_{15}$])**. The ^{1}H NMR spectrum of **43-[MeBF$_{15}$]** is identical to **43-[BF$_{20}$]** with the addition of a resonance at 0.98 (3H,

br, [MeBF$_{15}$]$^-$) ppm. ^{19}F NMR -131.8 (m, *o*-C$_6$F$_5$), -164.0 (m, *p*-C$_6$F$_5$) and -166.5 (m, *m*-C$_6$F$_5$) ppm.

[Cp*$_2$Ti$_2${μ-NC(NMe$_2$)$_2$}$_2$Me$_2$][BF$_{20}$] (15-[BF$_{20}$])

[Cp*$_2$Ti$_2${NC(NMe$_2$)$_2$}$_2$(μ-Me)$_2$][BF$_{20}$]$_2$ (**14$_{dim}$-[BF$_{20}$]$_2$**, 500 mg, 0.25 mmol) was left to stand in C$_6$D$_5$Br for 2 weeks which led to the crystallization of a teal solid as the product. Yield: 85 mg (26%). IR (NaCl plates, Nujol mull, cm^{-1}) 1641 (w), 1530 (w), 1509 (w), 1419 (w), 1413 (w), 1303 (m), 1279 (m), 1264 (w), 1222 (m), 1080 (m), 1058 (m), 1021 (w), 979 (s), 797 (w), 775 (w), 722 (w), 682 (w), 659 (w). Anal. Found (calcd. for C$_{56}$H$_{60}$BF$_{20}$N$_6$Ti$_2$): C, 51.73 (51.59); H, 4.51 (4.64); N, 6.27 (6.45). EPR (298 K) g = 1.98, A(^{47}Ti) = 13.6 MHz, $A_\perp$(^{14}N) = 8.3±0.2 MHz, $A_\parallel$(^{14}N) = 9.5±2 MHz, with a Gaussian line width (f.w.h.h.) of $LW_\perp$ = 7 MHz, $Lw_\parallel$ = 33 MHz. Single crystals suitable for X-ray analysis were grown from a saturated C$_6$D$_5$Br solution.

[Cp*Ti{NC(NMe$_2$)$_2$}(OPPh$_3$)Me][BF$_{20}$] (16-[BF$_{20}$])

Cp*Ti{NC(NMe$_2$)$_2$}Me$_2$ (300 mg, 0.91 mmol) and OPPh$_3$ (255 mg, 0.91 mmol) were mixed together in fluorobenzene (15 ml). To this a solution of TBF$_{20}$ (845 mg, 0.91 mmol) in fluorobenzene (10 ml) was added dropwise. After 30 min pentane (20 ml) was added resulting in the formation of an orange oil. The pentane/fluorobenzene was decanted and the oil washed further with pentane (10 ml). The remaining solvent was removed *in vacuo* to yield a yellow solid as the product. Yield: 838 mg (72%). ^{1}H NMR (C$_6$D$_5$Br, 299.9 MHz, 293 K) 7.40-7.00 (15H, m, OPPh$_3$), 2.28 (12H, s, NC(NMe$_2$)$_2$), 1.65 (15H, s, C$_5$Me$_5$), 0.22 (3H, s, Ti-Me) ppm. ^{13}C-{^{1}H} NMR (C$_6$D$_5$Br, 75.4 MHz, 293 K), 159.8 (NC(NMe$_2$)$_2$), 148.9 (br d, $^1J_{CF}$ = 244.4 Hz, *o*-C$_6$F$_5$), 138.6 (br d, $^1J_{CF}$ = 247.8 Hz , *p*-C$_6$F$_5$), 136.8 (br d, $^1J_{CF}$ = 249.0 Hz, *m*-C$_6$F$_5$), 134.7 (d, $^4J_{CP}$ = 2.8 Hz, *p*-C$_6$H$_5$), 132.5 (d, $^2J_{CP}$ = 11.2 Hz, *o*-C$_6$H$_5$), 122.7 (C$_5$Me$_5$), 48.1 (Ti-Me), 39.7 (NC(NMe$_2$)$_2$), 12.1 (C$_5$Me$_5$) ppm. ^{31}P-{^{1}H} NMR (C$_6$D$_5$Br, 121.4 MHz, 293 K), 49.4 ppm. ^{19}F NMR (C$_6$D$_5$Br, 282.1 MHz, 293 K) -131.5 (m, *o*-C$_6$F$_5$)), -161.9 (m, *p*-C$_6$F$_5$), -165.8 (m, *m*-C$_6$F$_5$) ppm. ^{11}B NMR (C$_6$D$_5$Br, 96.2 MHz, 293 K) -16.1 ppm. IR (NaCl plates, Nujol mull, cm^{-1}) 1642 (m), 1591 (w), 1563 (w), 1529 (s), 1513 (s), 1502 (m), 1453 (s), 1421 (m), 1404 (m), 1261 (m), 1124 (m), 1085 (m), 980 (s), 798 (w), 756 (w), 728 (w). Anal. Found (calcd. for C$_{58}$H$_{45}$BF$_{20}$N$_3$OPTi): C, 54.81 (54.87); H, 3.67 (3.57); N, 3.23 (3.31).

[Cp*Ti{NC(NMe$_2$)$_2$}(py)Me][BF$_{20}$] (17-[BF$_{20}$])

Cp*Ti{NC(NMe$_2$)$_2$}Me$_2$ (300 mg, 0.91 mmol) and pyridine (72 mg, 74μL, 0.91 mmol) were mixed together in fluorobenzene (15 ml). To this a solution of TBF$_{20}$ (845 mg, 0.91 mmol) in fluorobenzene (10 ml) was added dropwise. After 30 min pentane (20 ml) was added resulting in the formation of a red oil. The pentane/fluorobenzene was decanted and the oil washed further with pentane (10 ml). The remaining solvent was removed *in vacuo* to yield a orange solid as the product. Yield: 765 mg (78%). ^{1}H NMR (C_6D_5Br, 299.9 MHz, 293 K) 7.73 (2H, d, ^3J = 5.3, *o*-py), 7.36 (1H, t, ^3J = 7.5 Hz, *p*-py), 7.01 (2H, m, *m*-py), 2.43 (12H, s, NC(N$\underline{Me}_2$)$_2$, 1.55 (15H, s, $C_5\underline{Me}_5$), 0.63 (3H, s, Ti-$\underline{Me}$) ppm. ^{13}C-{^{1}H} NMR (C_6D_5Br, 75.4 MHz, 293 K) 161.2 (N$\underline{C}$(NMe$_2$)$_2$), 148.9 (br d, $^1J_{CF}$ = 244.4 Hz, *o*-$\underline{C}_6F_5$), 147.8 (*o*-py), 141.3 (*p*-py), 138.6 (br d, $^1J_{CF}$ = 247.8 Hz , *p*-$\underline{C}_6F_5$), 136.8 (br d, $^1J_{CF}$ = 249.0 Hz, *m*-$\underline{C}_6F_5$), 125.9 (*m*-py), 124.8 ($\underline{C}_5Me_5$), 58.1 (Ti-$\underline{Me}$), 40.0 (NC(N$\underline{Me}_2$)$_2$), 11.9 ($C_5\underline{Me}_5$) ppm. ^{19}F NMR (C_6D_5Br, 282.1 MHz, 293 K) -131.5 (m, *o*-C_6F_5), -161.8 (m, *p*-C_6F_5), -165.8 (m, *m*-C_6F_5) ppm. ^{11}B NMR (C_6D_5Br, 96.2 MHz, 293 K) -16.0 ppm. IR (NaCl plates, Nujol mull, cm^{-1}) 1642 (w), 1608 (w), 1513 (s), 1503 (m), 1467 (s), 1453 (s), 1420 (w), 1402 (w), 1274 (w), 1217 (w), 1150 (w), 1086 (m), 1017 (w), 979 (m), 858 (w), 800 (w), 756 (w) 774 (w), 684 (w), 661 (w). Anal. Found (calcd. for $C_{45}H_{35}BF_{20}N_4Ti$): C, 50.32 (50.49); H, 3.19 (3.30); N, 5.15 (5.23).

[Cp*Ti{NC(NMe$_2$)$_2$}(THF)Me][BF$_{20}$] (18-[BF$_{20}$])

Cp*Ti{NC(NMe$_2$)$_2$}Me$_2$ (300 mg, 0.91 mmol) and THF (66 mg, 74 μL, 0.91 mmol) were mixed together in fluorobenzene (15 ml).To this a solution of TBF$_{20}$ (845 mg, 0.91 mmol) in fluorobenzene (10 ml) was added dropwise. After 30 min pentane (20 ml) was added resulting in the formation of an orange oil. The pentane/fluorobenzene was decanted and the oil washed further with pentane (10 ml). The remaining solvent was removed *in vacuo* to yield a yellow solid as the product. Yield: 0.78 g (80%). ^{1}H NMR (C_6D_5Br, 299.9 MHz, 293 K) 3.69 (2H, m, OC$\underline{H}_2$) 3.48 (2H, m, OC$\underline{H}_2$), 2.37 (12H, s, NC(N$\underline{Me}_2$)$_2$), 1.60 (15H, s, $C_5\underline{Me}_5$), 1.48 (4H, m, OCH$_2$C$\underline{H}_2$), 0.40 (3H, s, Ti-$\underline{Me}$) ppm. ^{13}C-{^{1}H} NMR (C_6D_5Br, 75.4 MHz, 293 K) 161.0 (N$\underline{C}$(NMe$_2$)$_2$), 148.9 (br d, $^1J_{CF}$ = 244.4 Hz, *o*-$\underline{C}_6F_5$), 138.6 (br d, $^1J_{CF}$ = 247.8 Hz , *p*-$\underline{C}_6F_5$), 136.8 (br d, $^1J_{CF}$ = 249.0 Hz, *m*-$\underline{C}_6F_5$), 124.2 ($\underline{C}_5Me_5$), 77.3 (OC$\underline{H}_2$), 54.5 (Ti-$\underline{Me}$), 39.9 (NC(N$\underline{Me}_2$)$_2$), 25.6 (OCH$_2$C$\underline{H}_2$), 11.9 ($C_5\underline{Me}_5$) ppm. ^{19}F NMR (C_6D_5Br, 282.1 MHz, 293 K) -131.5 (m, *o*-C_6F_5), -161.9 (m, *p*-C_6F_5), -165.8 (m, *m*-C_6F_5) ppm. ^{11}B NMR (C_6D_5Br, 96.2

MHz, 293 K) -16.0 ppm. IR (NaCl plates, Nujol mull, cm^{-1}) 1642 (w), 1595 (w), 1513 (m), 1503 (m), 1453 (s), 1421 (m), 1402 (m), 1261 (w), 1151 (w), 1086 (m), 1021 (m), 979 (m), 858 (w), 801 (w), 756 (w), 724 (w), 683 (w), 661 (w). Anal. Found (calcd. for $C_{44}H_{38}BF_{20}N_3OTi$) C, 49.76 (49.69); H, 3.47 (3.60); N, 3.83 (3.95).

NMR tube scale synthesis of [Cp*Ti{NC(NMe$_2$)$_2$}Bn][BF$_{20}$] (19-[BF$_{20}$])

To a solution of Cp*Ti{NC(NMe$_2$)$_2$}Bn$_2$ (20 mg, 0.04 mmol) in C_6D_5Br (0.5 ml) was added TBF_{20} (38 mg, 0.04 mmol) resulting in the formation of a red solution. The red solution was transferred to an NMR tube and the NMR spectra recorded after 5 min. ^{1}H NMR (C_6D_5Br, 299.9 MHz, 293 K) 7.15-6.48 (5H, m, $CH_2\underline{Ph}$), 2.91 (2H, s, $C\underline{H}_2$), 2.30 (12H, s, $N\underline{Me}_2$), 1.58 (15H, s, $C_5\underline{Me}_5$) ppm. ^{13}C-{^{1}H} NMR (C_6D_5Br, 75.4 MHz, 293 K) 160.5 ($N\underline{C}(NMe_2)_2$), 122.5 ($\underline{C}_5Me_5$), 75.4 ($\underline{C}H_2$), 40.0 ($N\underline{Me}_2$), 12.4 ($C_5\underline{Me}_5$). ^{13}C-NMR (C_6D_5Br, 75.4 MHz, 293 K) 160.5 (s, $N\underline{C}(NMe_2)_2$), 122.5 (s, $\underline{C}_5Me_5$), 75.4 (t, $^1J_{CH}$ = 144.7 Hz, $\underline{C}H_2$), 40.0 (q, $^1J_{CH}$ = 138.0, NMe_2), 12.4 (t, $^1J_{CP}$ = 126.5 Hz, $C_5\underline{Me}_5$) ppm. ^{19}F NMR (C_6D_5Br, 282.1 MHz, 293 K) -131.5 (m, *o*-C_6F_5), -161.9 (m, *p*-C_6F_5), -165.8 (m, *m*-C_6F_5) ppm. ^{11}B NMR (C_6D_5Br, 96.2 MHz, 293 K) -16.0 ppm.

NMR tube scale synthesis of [Cp*Ti{NC(NMe$_2$)$_2$}(OPPh$_3$)Bn][BF$_{20}$] (20-[BF$_{20}$])

Cp*Ti{NC(NMe$_2$)$_2$}Bn$_2$ (30 mg, 0.06 mmol) and $OPPh_3$ (17 mg, 0.06 mmol) were mixed in C_6D_5Br. To this TBF_{20} (58 mg, 0.06 mg) was added resulting in a yellow solution. The yellow solution was transferred to an NMR tube and NMR spectra recorded after 5 min. The product shows significant decomposition to give a green solution and complicated NMR spectra after *ca.* 30 min. ^{1}H NMR (C_6D_5Br, 299.9 MHz, 293 K) 7.45-6.45 (20H, $OP\underline{Ph}_3$ and $TiCH_2\underline{Ph}$), 2.41 (1H, d, ^2J = 10.8 Hz, $TiC\underline{H}HPh$), 2.37 (12H, s, $NC(N\underline{Me}_2)_2$), 1.99 (1H, d, ^2J = 10.8 Hz, $TiCH\underline{H}Ph$), 1.68 (15H, s, $C_5\underline{Me}_5$) ppm. ^{31}P-{^{1}H} NMR (C_6D_5Br, 121.4 MHz, 293 K) 50.8 ppm, ^{19}F NMR (C_6D_5Br, 282.1 MHz, 293 K) -131.7 (m, *o*-C_6F_5), -162.2 (m, *p*-C_6F_5), -166.0 (m, *m*-C_6F_5) ppm. Due to the instability of the product in solution the ^{13}C-{^{1}H} NMR spectrum was not recorded.

NMR tube scale synthesis of [Cp*Ti{NC(N^{i}BuMe)$_2$}Me][BF$_{20}$] (21-[BF$_{20}$])

To a solution of Cp*Ti{NC(N^{i}BuMe)$_2$}Me$_2$ (20 mg, 0.05 mmol) in C_6D_5Br (0.5 ml) was added TBF_{20} (45 mg, 0.05 mmol) resulting in the formation of a red solution. The red solution was transferred to an NMR tube and the ^{1}H NMR spectrum recorded after 5 min. The resultant spectrum contained a mixture of isomers (**21a**$^+$, **21b**$^+$ and **21c**$^+$) in

a ratio of 7:5:1 one of which could be assigned to a major isomer **21a**$^+$. Major isomer **21a**$^+$: ^{1}H NMR (C_6D_5Br, 299.9 MHz, 293 K) 2.71 (4H, d, ^3J = 7.6 Hz, NC$\underline{H_2}$CHMe$_2$), 2.36 (6H, s, N$\underline{Me}$) 1.69 (15H, s, $C_5\underline{Me_5}$), 1.47 (2H, m, NCH$_2$C$\underline{H}$Me$_2$), 0.62 (3H, s, Ti-$\underline{Me}$) 0.56 (12H, d, ^3J = 6.6 Hz, NCH$_2$CH$\underline{Me_2}$) ppm. **21b**$^+$: 1.18 ppm (s, C_5Me_5) **21c**$^+$: (s, C_5Me_5). As with **10-[BF$_{20}$]** the remaining resonances could not be unambiguously assigned to either **21b**$^+$ or **21c**$^+$ due to the overlapping and broad nature of the peaks, although the type of chemical environment could be assigned by their chemical shift: 2.62 (s, N$\underline{Me}$), 2.53 (m, NC$\underline{H_2}$CHMe$_2$), 1.62 (br, NCH$_2$C$\underline{H}$Me$_2$), 0.69 (m, NCH$\underline{Me_2}$), 0.66 (m, NCH$\underline{Me_2}$), 0.20 (s, Ti-Me), 0.17 (s, Ti-Me), 0.05 (s, Ti-Me), -0.29 (s, Ti-Me), -0.45 (s, Ti-Me), -0.49 (s, Ti-Me) ppm. Single crystals of **21$_{dim}$-[BF$_{20}$]** suitable for X-ray analysis were grown from a saturated C_6D_5Br solution at room temperature.

NMR tube scale reaction of [Cp*Ti{NC(N^{i}BuMe)$_2$}Me][BF$_{20}$] with OPPh$_3$

[Cp*Ti{NC(N^{i}BuMe)$_2$}Me][BF$_{20}$] was generated from Cp*Ti{NC(N^{i}BuMe)$_2$}Me$_2$ (20 mg, 0.05 mmol) and TBF$_{20}$ (45 mg, 0.05 mmol) in C_6D_5Br (0.5 ml). After 2 min OPPh$_3$ (14 mg, 0.05 mmol) was added resulting in a colour change from red to yellow. The yellow solution was transferred to an NMR tube and the ^{1}H NMR spectrum recorded after 5 min revealing quantitative conversion of the mixture of cations to **22-[BF$_{20}$]**.

[Cp*Ti{NC(N^{i}BuMe)$_2$}(OPPh$_3$)Me][BF$_{20}$] (22-[BF$_{20}$])

Cp*Ti{NC(N^{i}BuMe)$_2$}Me$_2$ (123 mg, 0.30 mmol) and OPPh$_3$ (83 mg, 0.30 mmol) were mixed together in fluorobenzene (15 ml). To this a solution of TBF$_{20}$ (276 mg, 0.30 mmol) in fluorobenzene (10 ml) was added dropwise. After 30 min pentane (20 ml) was added resulting in the formation of an orange oil. The pentane/fluorobenzene was decanted and the oil washed further with pentane (10 ml). The remaining solvent was removed *in vacuo* to yield a yellow solid as the product. Yield: 260 mg (64%). ^{1}H NMR (C_6D_5Br, 299.9 MHz, 293 K) 2.89 (2H, dd, ^2J = 12.3 Hz, ^3J = 8.2 Hz, NC$\underline{H_2}$CHMe$_2$), 2.40 (6H, s, N$\underline{Me}$), 2.21 (2H, dd, ^2J = 12.3 Hz, ^3J = 6.7 Hz, NC$\underline{H_2}$CHMe$_2$), 1.65 (15H, s, $C_5\underline{Me_5}$), 1.47 (2H, m, NCH$_2$C$\underline{H}$Me$_2$), 0.58 (6H, d, ^3J = 6.4 Hz, NCH$_2$CH$\underline{Me_2}$), 0.54 (6H, d, ^3J = 6.4 Hz, NCH$_2$CH$\underline{Me_2}$), 0.24 (3H, s, Ti-$\underline{Me}$) ppm. ^{13}C-{^{1}H} NMR (C_6D_5Br, 75.4 MHz, 293 K) 160.2 (N$\underline{C}$(N^{i}BuMe)$_2$), 148.9 (br d, $^1J_{CF}$ = 244.4 Hz, *o*-$\underline{C_6}F_5$), 138.6 (br d, $^1J_{CF}$ = 247.8 Hz , *p*-$\underline{C_6}F_5$), 136.8 (br d, $^1J_{CF}$ = 249.0 Hz, *m*-$\underline{C_6}F_5$), 134.3 (*p*-OP$\underline{Ph_3}$), 132.1 (*o*-OP$\underline{Ph_3}$, $^2J_{CP}$ = 11.2 Hz), 129.3 (*m*-

OPPh$_3$) 122.7 (C_5Me_5), 58.9 (NCH_2CHMe_2), 48.8 (Ti-Me), 38.8 ($NC(N^iBuMe)_2$), 26.4 (NCH_2CHMe_2), 20.1 (NCH_2CHMe_2), 19.7 (NCH_2CHMe_2), 12.1 (C_5Me_5) ppm. ^{19}F NMR (C_6D_5Br, 282.1 MHz, 293 K) -131.5 (m, *o*-C_6F_5), -162.1 (m, *p*-C_6F_5), -166.0 (m, *m*-C_6F_5) ppm. ^{11}B NMR (C_6D_5Br, 96.2 MHz, 293 K) -16.1 ppm. IR (NaCl plates, Nujol mull, cm^{-1}) 1642 (m), 1591 (w), 1513 (s), 1417 (m), 1341 (m), 1274 (m), 1124 (m), 1083 (s), 1026 (w), 979 (s), 859 (w), 775 (m), 755 (m), 726 (m), 683 (m), 660 (m). Anal. Found (calcd. for $C_{64}H_{57}BF_{20}N_3OPTi$): C, 56.63 (56.78); H, 4.15 (4.24); N, 3.23 (3.10).

[Cp*Ti{NC(N^{i}BuMe)$_2$}(py)Me][BF$_{20}$] (23-[BF$_{20}$])

Cp*Ti{NC(N^{i}BuMe)$_2$}Me$_2$ (121 mg, 0.29 mmol) and pyridine (24 mg, 24 µl, 0.29 mmol) were mixed together in fluorobenzene (15 ml). To this a solution of TBF_{20} (271 mg, 0.29 mmol) in fluorobenzene (10 ml) was added dropwise. After 30 min pentane (20 ml) was added resulting in the formation of an orange oil. The pentane/fluorobenzene was decanted and the oil washed further with pentane (10 ml). The remaining solvent was removed *in vacuo* to yield a yellow solid as the product. Yield: 224 mg (66%). ^{1}H NMR (C_6D_5Br, 299.9 MHz, 293 K) 7.75 (2H, d, ^3J = 5.3, *o*-py), 7.35 (1H, t, ^3J = 7.5 Hz, *p*-py) 7.00 (2H, m, *m*-py), 3.02 (2H, dd, ^2J =12.3 Hz, ^3J = 9.9 Hz NCH_2CHMe_2), 2.48 (6H, s, NMe), 2.45 (2H, dd, ^2J =12.3 Hz, ^2J = 8.9 Hz, NCH_2CHMe_2), 2.41 (1H, d, ^2J =12.0 Hz, NCH_2CHMe_2), 1.59 (15H, s, C_5Me_5), 0.67 (5H, s, Ti-Me and NCH_2CHMe_2 overlapping), 0.63 (6H, d, ^3J = 6.6 Hz, NCH_2CHMe_2), 0.61 (6H, d, ^3J = 6.6 Hz, NCH_2CHMe_2) ppm. ^{13}C-{^{1}H} NMR (C_6D_5Br, 75.4 MHz, 293 K) 161.6 ($NC(N^iBuMe)_2$), 148.9 (br d, $^1J_{CF}$ = 244.4 Hz, *o*-C_6F_5), 147.7 (*o*-py), 141.3 (*p*-py), 138.6 (br d, $^1J_{CF}$ = 247.8 Hz , *p*-C_6F_5), 136.8 (br d, $^1J_{CF}$ = 249.0 Hz, *m*-C_6F_5), 125.9 (*m*-py), 124.9 (C_5Me_5), 59.5 (NCH_2CHMe_2) , 58.5 (Ti-Me), 38.7 (NMe), 26.6 (NCH_2CHMe_2), 20.2 (NCH_2CHMe_2), 19.5 (NCH_2CHMe_2), 12.0 (C_5Me_5) ppm. ^{19}F NMR (C_6D_5Br, 282.1 MHz, 293 K) -131.5 (m, *o*-C_6F_5), -162.1 (m, *p*-C_6F_5), -166.0 (m, *m*-C_6F_5) ppm. ^{11}B NMR (C_6D_5Br, 96.2 MHz, 293 K) -16.0 ppm. IR (NaCl plates, Nujol mull, cm^{-1}) 1642 (m), 1593 (m), 1556 (w), 1513 (s), 1410 (m), 1341 (m), 1272 (m), 1217 (w), 1150 (w), 1084 (s), 978 (s), 848 (w), 787 (m), 774 (m), 755 (m), 725 (w), 682 (m), 660 (m). Anal. Found (calcd. for $C_{51}H_{47}BF_{20}N_4Ti$): C, 53.15 (53.05); H, 4.27 (4.10); N, 5.03 (4.85).

[Cp*Ti{NC(N^{i}BuMe)$_2$}(THF)Me][BF$_{20}$] (24-[BF$_{20}$])

Cp*Ti{NC(N^{i}BuMe)$_2$}Me$_2$ (104 mg, 0.25 mmol) and THF (18 mg, 21 μl, 0.25 mmol) were mixed together in fluorobenzene (15 ml). To this a solution of TBF$_{20}$ (233 mg, 0.25 mmol) in fluorobenzene (10 ml) was added dropwise. After 30 min pentane (20 ml) was added resulting in the formation of an orange oil. The pentane/fluorobenzene was decanted and the oil washed further with pentane (10 ml). The remaining solvent was removed *in vacuo* to yield a yellow solid as the product. Yield: 218 mg (75%). ^{1}H NMR (C_6D_5Br, 299.9 MHz, 293 K) 3.73 (2H, m, OC$\underline{H}_2$), 3.53 (2H, m, OC$\underline{H}_2$), 2.95 (2H, dd, ^{2}J = 12.5 Hz, ^{3}J = 9.8 Hz, NC$\underline{H}_2$CHMe$_2$), 2.44 (6H, s, N$\underline{Me}$), 2.35 (2H, dd, ^{2}J =12.5 Hz, ^{3}J = 5.3 Hz, NC$\underline{H}_2$CHMe$_2$), 1.64 (15H, s, C$_5\underline{Me}_5$), 1.51 (6H, m, overlapping OCH$_2$C$\underline{H}_2$ and NCH$_2$C$\underline{H}$Me$_2$), 0.64, (6H, d, ^{3}J = 6.8 Hz, NCH$_2$CH$\underline{Me}_2$), 0.61 (6H, d, ^{3}J = 6.8 Hz, NCH$_2$CH$\underline{Me}_2$), 0.43 (3H, s, Ti-$\underline{Me}$) ppm. ^{13}C-{^{1}H} NMR (C_6D_5Br, 75. MHz, 293 K) 161.8 (N$\underline{C}$(N^{i}BuMe)$_2$), 148.9 (br d, $^{1}J_{CF}$ = 244.4 Hz, *o*-$\underline{C}_6F_5$), 138.6 (br d, $^{1}J_{CF}$ = 247.8 Hz , *p*-$\underline{C}_6F_5$), 136.8 (br d, $^{1}J_{CF}$ = 249.0 Hz, *m*-$\underline{C}_6F_5$), 124.4 ($\underline{C}_5Me_5$), 77.4 (O$\underline{C}$H$_2$), 59.3 (N$\underline{C}$H$_2$CHMe$_2$), 55.1 (Ti-$\underline{Me}$), 38.7 (NC(N^{i}Bu$\underline{Me}$)$_2$), 26.6 (NCH$_2\underline{C}$HMe$_2$), 25.5 (OCH$_2\underline{C}$H$_2$), 20.2 (NCH$_2$CH$\underline{Me}_2$), 19.5 (NCH$_2$CH$\underline{Me}_2$), 11.9 (C$_5\underline{Me}_5$) ppm. ^{19}F NMR (C_6D_5Br, 282.1 MHz, 293 K) -131.5 (m, *o*-C_6F_5), -162.1 (m, *p*-C_6F_5), -166.0 (m, *m*-C_6F_5) ppm. ^{11}B NMR (C_6D_5Br, 96.2 MHz, 293 K) -16.0 ppm. IR (NaCl plates, Nujol mull, cm^{-1}) 1643 (m), 1596 (w), 1513 (s), 1377 (s), 1261 (m), 1151 (w), 1085 (s), 1023 (m), 979 (m), 927 (w), 847 (w), 800 (m), 774 (m), 756 (m), 726 (w), 684 (m), 661 (m). Anal. Found (calcd. for $C_{50}H_{50}BF_{20}N_3OTi$): C, 52.03 (52.33); H, 4.19 (4.39); N, 3.80 (3.66).

NMR tube scale synthesis of [Cp*Ti{NC(N(Xyl)CH$_2$)$_2$}Me][BF$_{20}$] (25-[BF$_{20}$])

Cp*Ti{NC(N(Xyl)CH$_2$)$_2$}Me$_2$ (20 mg, 0.04 mmol) and TBF$_{20}$ (36 mg, 0.04mmol) were mixed together in C_6D_5Br (0.5 ml). The red solution was transferred to an NMR tube and the NMR spectra recorded after 5 min. ^{1}H NMR (C_6D_5Br, 299.9 MHz, 293 K) 7.07-6.88 (6H, m, C$_6\underline{H}_3$Me$_2$) 3.42 (4H, s, C$\underline{H}_2$C$\underline{H}_2$), 2.20 (12H, s, C$_6$H$_3\underline{Me}_2$), 1.28 (15H, s, C$_5\underline{Me}_5$), 0.57 (3H, s, Ti-$\underline{Me}$) ppm. ^{13}C-{^{1}H} NMR (C_6D_5Br, 75.4 MHz, 293 K) 153.2 (N$\underline{C}$(N(Xyl)CH$_2$)$_2$), 148.7 (br d, $^{1}J_{CF}$ = 241.7 Hz, *o*-$\underline{C}_6F_5$), 139.0 (br d, $^{1}J_{CF}$ = 245.1 Hz, *p*-$\underline{C}_6F_5$), 137.1 (*i*-$\underline{C}_6H_5Me_2$), 136.9 (br d, $^{1}J_{CF}$ = 244.4 Hz, *m*-$\underline{C}_6F_5$), 135.0 (*o*-$\underline{C}_6H_5Me_2$), 130.0 (*m*-$\underline{C}_6H_5Me_2$), 128.2 ($\underline{C}_5Me_5$), 68.6 (Ti-$\underline{Me}$), 46.3 ($\underline{C}H_2\underline{C}H_2$), 18.1 (C$_6H_5\underline{Me}_2$), 12.0 (C$_5\underline{Me}_5$) ppm. ^{19}F NMR ($C_6D_5Br$, 282.1 MHz, 293 K) -131.5 (m, *o*-

C_6F_5), -162.1 (m, *p*-C_6F_5), -166.0 (m, *m*-C_6F_5) ppm. ^{11}B NMR (C_6D_5Br, 96.2 MHz, 293 K) -16.1 ppm.

[Cp*Ti{NC(N(Xyl)CH_2)$_2$}(OPPh_3)Me][BF_{20}] (26-[BF_{20}])

Cp*Ti{NC(N(Xyl)CH_2)$_2$}Me_2 (80 mg, 0.16 mmol) and OPPh_3 (44 mg, 0.16 mmol) were mixed together in fluorobenzene (15 ml). To this a solution of TBF_{20} (146 mg, 0.16 mmol) in fluorobenzene (10 ml) was added dropwise. After 30 min pentane (20 ml) was added resulting in the formation of an orange oil. The pentane/fluorobenzene was decanted and the oil washed further with pentane (10 ml). The remaining solvent was removed *in vacuo* to yield a yellow solid as the product. Yield: 229 mg (65%). ^{1}H NMR (C_6D_5Br, 299.9 MHz, 293 K) 7.40-6.60 (21H, m, $C_6\underline{H}_3Me_2$ & OP$\underline{Ph}_3$), 3.71 (4H, s, $C\underline{H}_2C\underline{H}_2$), 2.61 (6H, s, $C_6H_3\underline{Me}Me$), 2.24 (6H, s, $C_6H_3Me\underline{Me}$), 1.65 (15H, s, $C_5\underline{Me}_5$), 0.11 (3H, s, Ti-$\underline{Me}$) ppm. ^{13}C-{^{1}H} NMR (C_6D_5Br, 75.4 MHz, 293 K) 149.7 (N$\underline{C}$(N(Xyl)CH_2)$_2$), 148.9 (br d, $^1J_{CF}$ = 244.4 Hz, *o*-$\underline{C}_6F_5$), 138.6 (br d, $^1J_{CF}$ = 247.8 Hz, *p*-$\underline{C}_6F_5$), 137.1 (*i*-$\underline{C}_6H_3Me_2$), 136.8 (br d, $^1J_{CF}$ = 249.0 Hz, *m*-$\underline{C}_6F_5$), 136.7 (*o*-$\underline{C}_6H_3Me_2$), 136.0 (*o*-$\underline{C}_6H_3Me_2$), 134.7 (*p*-OP$\underline{Ph}_3$), 132.7 (d, $^2J_{CP}$ = 11.4 Hz, *o*-OP$\underline{Ph}_3$), 129.6 (*m*-OP$\underline{Ph}_3$), 129.4 (*m*-OP$\underline{Ph}_3$), 129.2 (*m*-$\underline{C}_6H_3Me_2$), 128.8 (*m*-$\underline{C}_6H_3Me_2$), 128.5 (*p*-$\underline{C}_6H_3Me_2$), 122.5 ($\underline{C}_5Me_5$), 49.0 (Ti-$\underline{Me}$), 45.6 ($\underline{C}H_2\underline{C}H_2$),18.7 ($C_6H_3\underline{Me}Me$), 18.4 ($C_6H_3Me\underline{Me}$), 11.8 ($C_5\underline{Me}_5$) ppm. ^{31}P-{^{1}H} NMR (C_6D_5Br, 121.4 MHz, 293 K) 48.0 ppm, ^{19}F NMR (C_6D_5Br, 282.1 MHz, 293 K) -131.5 (m, *o*-C_6F_5), -161.8 (m, *p*-C_6F_5), -165.8 (m, *m*-C_6F_5) ppm. ^{11}B NMR (C_6D_5Br, 96.2 MHz, 293 K) -16.1 ppm. IR (NaCl plates, Nujol mull, cm^{-1}) 1643 (w), 1599 (w), 1545 (m), 1513 (m), 1261 (w), 1124 (m), 1083 (s), 1026 (m), 980 (s), 867 (w), 799 (m), 774 (w), 756 (w), 726 (m), 683 (w), 660 (w). Anal. Found (calcd. for $C_{66}H_{52}BF_{20}N_2OPTi$) C, 59.53 (59.73); H, 3.66 (3.83); N, 2.99 (2.90).

[Cp*Ti{NC(N(Xyl)CH_2)$_2$}(py)Me][BF_{20}] (27-[BF_{20}])

Cp*Ti{NC(N(Xyl)CH_2)$_2$}Me_2 (20 mg, 0.04 mmol) and pyridine (3 mg, 3 µl, 0.04 mmol) were mixed together in fluorobenzene (15 ml). To this a solution of TBF_{20} (36 mg, 0.04 mmol) in fluorobenzene (10 ml) was added dropwise. After 30 min pentane (20 ml) was added resulting in the formation of an orange oil. The pentane/fluorobenzene was decanted and the oil washed further with pentane (10 ml). The remaining solvent was removed *in vacuo* to yield a yellow solid as the product. Yield: 49 mg (60%). ^{1}H NMR (C_6D_5Br, 299.9 MHz, 293 K) 7.30-6.63 (5H, m, py),

3.37 (4H, s, C$\underline{H_2}$C$\underline{H_2}$), 2.21 (6H, s, $C_6H_3\underline{Me}Me$), 1.99 (6H, s, $C_6H_3Me\underline{Me}$), 1.27 (15H, s, $C_5\underline{Me_5}$), 0.40 (3H, s, Ti-$\underline{Me}$) ppm. ^{13}C-{^{1}H} NMR (C_6D_5Br, 75.4 MHz, 293 K) 151.8 (N$\underline{C}$(N(Xyl)CH_2)$_2$), 148.9 (br d, $^1J_{CF}$ = 244.4 Hz, *o*-$\underline{C}_6F_5$), 146.8 (*o*-py), 140.3 (*p*-py), 138.6 (br d, $^1J_{CF}$ = 247.8 Hz, *p*-$\underline{C}_6F_5$), 137.5 (*i*-$\underline{C}_6H_3Me_2$), 137.2 (*o*-$\underline{C}_6H_3Me_2$), 136.8 (br d, $^1J_{CF}$ = 249.0 Hz, *m*-$\underline{C}_6F_5$), 135.7 (*o*-$\underline{C}_6H_3Me_2$), 129.3 (*m*-$\underline{C}_6H_3Me_2$), 129.2 (*p*-$\underline{C}_6H_3Me_2$), 126.0 ($\underline{C}_5Me_5$), 125.7 (*m*-py), 62.4 (Ti-$\underline{Me}$), 45.9 ($\underline{C}H_2\underline{C}H_2$), 18.3 ($C_6H_5\underline{Me}Me$), 18.0 ($C_6H_5Me\underline{Me}$), 11.7 ($C_5\underline{Me_5}$) ppm. ^{19}F NMR ($C_6D_5Br$, 282.1 MHz, 293 K) -131.5 (m, *o*-C_6F_5), -162.1 (m, *p*-C_6F_5), -166.0 (m, *m*-C_6F_5) ppm. ^{11}B NMR (C_6D_5Br, 96.2 MHz, 293 K) -16.0 ppm. IR (NaCl plates, Nujol mull, cm^{-1}) 1644 (m), 1592 (m), 1555 (w), 1512 (s), 1342 (m), 1272 (m), 1149 (w), 1082 (s), 978 (s), 850 (m), 787 (m), 753 (m), 725 (w), 682 (m). Anal. Found (calcd. for $C_{59}H_{45}BF_{20}N_4Ti$): C, 56.85 (56.75); H, 3.50 (3.63); N, 4.35 (4.49).

[Cp*Ti{NC(N(Xyl)CH$_2$)$_2$}(THF)Me][BF$_{20}$] (28-[BF$_{20}$])

Cp*Ti{NC(N(Xyl)CH_2)$_2$}Me_2 (80 mg, 0.16 mmol) and THF (11 mg, 13 µl, 0.16 mmol) were mixed together in fluorobenzene (15 ml). To this a solution of TBF_{20} (146 mg, 0.16 mmol) in fluorobenzene (10 ml) was added dropwise. After 30 min pentane (20 ml) was added resulting in the formation of an orange oil. The pentane/fluorobenzene was decanted and the oil washed further with pentane (10 ml). The remaining solvent was removed *in vacuo* to yield a yellow solid as the product. Yield: 118 mg (60%). ^{1}H NMR (C_6D_5Br, 299.9 MHz, 293 K) 6.82 (6H, s, $C_6\underline{H}_3Me_2$), 3.35 (4H, s, C$\underline{H_2}$C$\underline{H_2}$), 2.75 (2H, m, OC$\underline{H_2}$), 2.53 (2H, m, OC$\underline{H_2}$), 2.18 (6H, s, $C_6H_3\underline{Me}Me$), 2.10 (6H, s, $C_6H_3Me\underline{Me}$), 1.37 (15H, s, $C_5\underline{Me_5}$), 1.30 (2H, m, OCH_2C$\underline{H_2}$), 1.22 (2H, m, OCH_2C$\underline{H_2}$), 0.21 (Ti-$\underline{Me}$) ppm. ^{13}C-{^{1}H} NMR (C_6D_5Br, 75. MHz, 293 K) 152.0 (N$\underline{C}$(N(Xyl)CH_2)$_2$), 148.9 (br d, $^1J_{CF}$ = 244.4 Hz, *o*-$\underline{C}_6F_5$), 138.6 (br d, $^1J_{CF}$ = 247.8 Hz, *p*-$\underline{C}_6F_5$), 137.6 (*i*-$\underline{C}_6H_3Me_2$), 136.8 (br d, $^1J_{CF}$ = 249.0 Hz, *m*-$\underline{C}_6F_5$), 136.7 (*o*-$\underline{C}_6H_3Me_2$), 135.7 (*o*-$\underline{C}_6H_3Me_2$), 129.3 (*m*-$\underline{C}_6H_3Me_2$), 129.1 (*p*-$\underline{C}_6H_3Me_2$), 125.7 ($\underline{C}_5Me_5$), 74.5 (O$\underline{C}H_2$), 61.8 (Ti-$\underline{Me}$), 45.9 ($\underline{C}H_2\underline{C}H_2$), 25.3 (OC$H_2\underline{C}H_2$), 18.3 ($C_6H_5\underline{Me}Me$), 18.1 ($C_6H_5Me\underline{Me}$), 11.7 ($C_5\underline{Me_5}$) ppm. ^{19}F NMR ($C_6D_5Br$, 282.1 MHz, 293 K) -131.5 (m, *o*-C_6F_5), -162.1 (m, *p*-C_6F_5), -166.0 (m, *m*-C_6F_5) ppm. ^{11}B NMR (C_6D_5Br, 96.2 MHz, 293 K) -16.0 ppm. IR (NaCl plates, Nujol mull, cm^{-1}) 1643 (w), 1597 (w), 1532 (s), 1512 (s), 1260 (m), 1084 (s), 1016 (w), 978 (s), 870 (w), 798 (w), 774 (w), 721 (w), 660 (w). Anal. Found (calcd. for $C_{58}H_{48}BF_{20}N_3OTi$): C, 56.41 (56.10); H, 3.82 (3.90); N, 3.35 (3.38).

NMR tube scale synthesis of [Cp*$_2$Ti$_2${NC(N^{i}Pr$_2$)Ph}$_2$(μ-Me)Me$_2$][BF$_{20}$] (29-[BF$_{20}$])

Cp*Ti{NC(N^{i}Pr$_2$)Ph}Me$_2$ (20 mg, 0.05 mmol) and TBF$_{20}$ (22 mg, 0.02 mmol) were mixed together in C_6D_5Br (0.5 ml). The brown/yellow solution was transferred to an NMR tube and the NMR spectra recorded after 5 min. The product exists as a mixture of diastereoisomers (**29a**$^+$ and **29b**$^+$) in a 3:2 ratio. The quoted intensities given are self-consistent within each isomer. ^{1}H NMR (C_6D_5Br, 299.9 MHz, 293 K) 7.20-6.95 (10H, NC(N^{i}Pr$_2$)Ph, **29a**$^+$ and **29b**$^+$), 3.56 (4H, br, NCHMe$_2$, **29a**$^+$ and **29b**$^+$), 1.54 (30H, s, C$_5$Me$_5$, **29a**$^+$ and **29b**$^+$), 1.46 (6H, br, NCHMe$_2$, **29a**$^+$ and **29b**$^+$), 1.25 (6H, br, NCHMe$_2$, **29a**$^+$ and **29b**$^+$), 0.81 (12H, br, NCHMe$_2$, **29a**$^+$ and **29b**$^+$), 0.35 (6H, s, Ti-Me, **29a**$^+$ and **29b**$^+$) -0.84 (3H, s, Ti(μ-Me)Ti, **29b**$^+$), -0.96 (3H, s, Ti(μ-Me)Ti, **29a**$^+$). ^{13}C-{^{1}H} NMR (C_6D_5Br, 75.4 MHz, 293 K) 166.7 (NC(N^{i}Pr$_2$)Ph, **29b**$^+$), 166.3 (NC(N^{i}Pr$_2$)Ph, **29a**$^+$), 148.9 (br d, $^1J_{CF}$ = 244.4 Hz, *o*-C$_6$F$_5$), 138.6 (br d, $^1J_{CF}$ = 247.8 Hz, *p*-C$_6$F$_5$), 136.8 (br d, $^1J_{CF}$ = 249.0 Hz, *m*-C$_6$F$_5$), 123.8 (C$_5$Me$_5$, **29b**$^+$), 123.9 (C$_5$Me$_5$, **29a**$^+$), 139.4 (*i*-C$_6$H$_5$, **29b**$^+$), 139.3 (*i*-C$_6$H$_5$, **29a**$^+$), 129.4 (*m*-C$_6$H$_5$, **29b**$^+$), 129.3 (*m*-C$_6$H$_5$, **29a**$^+$), 126.0 (*p*-C$_6$H$_5$, **29a**$^+$ or **29b**$^+$), 55.2 (Ti-Me, **29b**$^+$), 55.0 (Ti-Me, **29a**$^+$), 48.0 (NCHMe$_2$, **29a**$^+$), 47.6 (NCHMe$_2$, **29b**$^+$), 43.7 (Ti(μ-Me)Ti, **29a**$^+$), 43.3 (Ti(μ-Me)Ti, **29b**$^+$), 20.8 (NCHMe$_2$, **29a**$^+$ or **29b**$^+$), 20.6 (NCHMe$_2$, **29a**$^+$ or **29b**$^+$), 20.4 (NCHMe$_2$, **29a**$^+$ or **29b**$^+$), 20.1 (NCHMe$_2$, **29a**$^+$ or **29b**$^+$), 12.0 (C$_5$Me$_5$, **29b**$^+$), 11.9 (C$_5$Me$_5$, **29a**$^+$) ppm. ^{19}F NMR (C_6D_5Br, 282.1 MHz, 293 K) -131.5 (m, *o*-C$_6$F$_5$), -162.1 (m, *p*-C$_6$F$_5$), -166.0 (m, *m*-C$_6$F$_5$) ppm. ^{11}B NMR (C_6D_5Br, 96.2 MHz, 293 K) -16.0 ppm.

NMR tube scale reaction of [Cp*$_2$Ti$_2${NC(N^{i}Pr$_2$)Ph}$_2$(μ-Me)Me$_2$][BF$_{20}$] with OPPh$_3$

[Cp*$_2$Ti$_2${NC(N^{i}Pr$_2$)Ph}$_2$(μ-Me)Me$_2$][BF$_{20}$] was generated *in situ* from Cp*Ti{NC(N^{i}Pr$_2$)Ph}Me$_2$ (20 mg, 0.05 mmol) and TBF$_{20}$ (22 mg, 0.02 mmol) in C_6D_5Br. After 2 min OPPh$_3$ (7 mg, 0.02 mmol) was added resulting in the quantitative formation of **2.4** and **11-[BF$_{20}$]** by ^{1}H NMR spectroscopy.

NMR tube scale synthesis of [Cp*$_2$Ti$_2${NC(NMe$_2$)$_2$}$_2$(μ-Me)Me$_2$][BF$_{20}$] (30-[BF$_{20}$])

Cp*Ti{NC(NMe$_2$)$_2$}Me$_2$ (30 mg, 0.09 mmol) and TBF$_{20}$ (43 mg, 0.05 mmol) were mixed together in C_6D_5Br The brown/yellow solution was transferred to an NMR tube and the NMR spectra recorded after 5 min. The product exists as a mixture of

diastereoisomers (**30a**$^+$ and **30b**$^+$) in a 3:2 ratio. The quoted intensities given are self-consistent within each isomer. ^{1}H NMR (C_6D_5Br, 299.9 MHz, 293 K) 2.27 (12H, s, NC(N$\underline{Me}_2$)$_2$, **30a**$^+$), 2.24 (12H, s, NC(N$\underline{Me}_2$)$_2$, **30b**$^+$), 1.48 (15H, s, $C_5\underline{Me}_5$, **30b**$^+$), 1.47 (15H, s, $C_5\underline{Me}_5$, **30a**$^+$), 0.03 (6H, s, Ti-$\underline{Me}$, **30b**$^+$), 0.00 (6H, s, Ti-$\underline{Me}$, **30a**$^+$), -0.75 (3H, s, Ti(μ-$\underline{Me}$)Ti, **30b**$^+$) , -0.76 (3H, s, Ti-(μ-$\underline{Me}$-Ti, **30a**$^+$) ppm.^{13}C-{^{1}H} NMR (C_6D_5Br, 75.4 MHz, 293 K) 160.3 (N$\underline{C}$(NMe$_2$)$_2$), 148.9 (br d, $^1J_{CF}$ = 244.4 Hz, *o*-$\underline{C}_6F_5$), 138.6 (br d, $^1J_{CF}$ = 247.8 Hz, *p*-$\underline{C}_6F_5$), 136.8 (br d, $^1J_{CF}$ = 249.0 Hz, *m*-$\underline{C}_6F_5$), 122.9 ($\underline{C}_5Me_5$, **30a**$^+$), 122.8 ($\underline{C}_5Me_5$, **30b**$^+$), 52.2 (Ti-$\underline{Me}$, **30b**$^+$), 51.8 (Ti-$\underline{Me}$, **30a**$^+$), 40.2 (Ti(μ-$\underline{Me}$)Ti, **30b**$^+$), 40.1 (Ti(μ-$\underline{Me}$)Ti, **30a**$^+$), 40.0 (NC(N$\underline{Me}_2$)$_2$, **30b**$^+$), 39.9 (NC(N$\underline{Me}_2$)$_2$, **30a**$^+$), 12.2 ($C_5\underline{Me}_5$, **30a**$^+$ and **30b**$^+$) ppm. ^{19}F NMR (C_6D_5Br, 282.1 MHz, 293 K) -131.4 (m, *o*-C_6F_5), -162.0 (m, *p*-C_6F_5), -165.9 (m, *m*-C_6F_5) ppm. ^{11}B NMR (C_6D_5Br, 96.2 MHz, 293 K) -16.1 ppm.

NMR tube scale reaction of [Cp*$_2$Ti$_2${NC(NMe$_2$)$_2$}$_2$(μ-Me)Me$_2$][BF$_{20}$] with OPPh$_3$

[Cp*$_2$Ti$_2${NC(NMe$_2$)$_2$}$_2$(μ-Me)Me$_2$][BF$_{20}$] was generated *in situ* from Cp*Ti{NC(NMe$_2$)$_2$}Me$_2$ (20 mg, 0.06 mmol) and TBF$_{20}$ (28 mg, 0.03 mmol) in C_6D_5Br. After 2 min OPPh$_3$ (9 mg, 0.02 mmol) was added resulting in the quantitative formation of **4** and **16-[BF$_{20}$]** by ^{1}H NMR spectroscopy.

NMR tube scale synthesis of [Cp*$_2$Ti$_2${NC(N^{i}BuMe)$_2$}$_2$(μ-Me)Me$_2$][BF$_{20}$] (31-[BF$_{20}$])

Cp*Ti{NC(N^{i}BuMe)$_2$}Me$_2$ (30 mg, 0.07 mmol) and TBF$_{20}$ (34 mg, 0.04 mmol) were mixed together in C_6D_5Br The brown/yellow solution was transferred to an NMR tube and the NMR spectra recorded after 5 min. The product exists as a mixture of diastereoisomers (**31a**$^+$ and **31b**$^+$) in a 3:2 ratio. The quoted intensities given are self-consistent within each isomer. ^{1}H NMR (C_6D_5Br, 299.9 MHz, 293 K) 3.11-2.99 (4H, overlapping CH_2 for **31a**$^+$ and **31b**$^+$), 2.53 (3H, s, N$\underline{Me}$, **31b**$^+$), 2.52 (3H, s, N$\underline{Me}$, **31a**$^+$), 2.47-2.40 (4H, overlapping CH_2 for **31a**$^+$ and **31b**$^+$), 1.72 (15H , s, $C_5\underline{Me}_5$, **31a**$^+$), 1.71 (15H, s, $C_5\underline{Me}_5$, **31b**$^+$), 1.64 (4H, overlapping NCH$_2$C$\underline{H}$Me$_2$ sept for **31a**$^+$ and **31b**$^+$), 0.69 (24H, d, ^3J = 6.3 Hz, NCH$_2$CH$\underline{Me}_2$, **31a**$^+$ and **31b**$^+$), 0.20 (6H, s, Ti-$\underline{Me}$, **31a**$^+$), 0.17 (6H, s, Ti-$\underline{Me}$ **31b**$^+$), -0.46 (3H, s, Ti(μ-$\underline{Me}$)Ti, **31b**$^+$), -0.49 (3H, s, Ti(μ-$\underline{Me}$)Ti, **31a**$^+$) ppm. ^{13}C-{^{1}H} NMR (C_6D_5Br, 75.4 MHz, 293 K) 160.7 (N$\underline{C}$(N^{i}BuMe)$_2$), 148.9 (br d, $^1J_{CF}$ = 244.4 Hz, *o*-$\underline{C}_6F_5$), 138.6 (br d, $^1J_{CF}$ = 247.8 Hz , *p*-$\underline{C}_6F_5$), 136.8 (br d, $^1J_{CF}$ = 249.0 Hz, *m*-$\underline{C}_6F_5$), 122.8 ($\underline{C}_5Me_5$, **31b**$^+$), 122.7 ($\underline{C}_5Me_5$,

31a$^+$), 59.4 (N<u>C</u>H$_2$CHMe$_2$, **31a**$^+$), 59.3 (N<u>C</u>H$_2$CHMe$_2$, **31b**$^+$), 52.7 (Ti-<u>Me</u>, **31a**$^+$), 52.6 (Ti-<u>Me</u>, **31b**$^+$), 38.9 (N<u>Me</u>, **31b**$^+$), 38.8 (N<u>Me</u>, **31a**$^+$), 37.4 (Ti(μ-<u>Me</u>)Ti, **31b**$^+$), 36.1 (Ti(μ-<u>Me</u>)Ti, **31a**$^+$), 26.7 (NCH$_2$<u>C</u>HMe$_2$, **31a**$^+$), 26.6 (NCH$_2$<u>C</u>HMe$_2$, **31b**$^+$), 20.4 (NCH$_2$CH<u>Me</u>$_2$, **31a**$^+$), 19.8 (NCH$_2$CH<u>Me</u>$_2$, **31b**$^+$), 12.4 (C$_5$<u>Me</u>$_5$, **31a**$^+$ and **31b**$^+$) ppm. ^{19}F NMR (C$_6$D$_5$Br, 282.1 MHz, 293 K) -131.4 (m, *o*-C$_6$F$_5$), -162.0 (m, *p*-C$_6$F$_5$), -165.9 (m, *m*-C$_6$F$_5$) ppm. ^{11}B NMR (C$_6$D$_5$Br, 96.2 MHz, 293 K) -15.9 ppm.

NMR tube scale reaction of [Cp*$_2$Ti$_2${NC(N^{i}BuMe)$_2$}$_2$(μ-Me)Me$_2$][BF$_{20}$] with OPPh$_3$

[Cp*$_2$Ti$_2${NC(N^{i}BuMe)$_2$}$_2$(μ-Me)Me$_2$][BF$_{20}$] was generated *in situ* from Cp*Ti{NC(N^{i}BuMe)$_2$}Me$_2$ (20 mg, 0.05 mmol) and TBF$_{20}$ (22 mg, 0.02 mmol) in C$_6$D$_5$Br. After 2 min OPPh$_3$ (7 mg, 0.02 mmol) was added resulting in the quantitative formation of **6** and **22-[BF$_{20}$]** by ^{1}H NMR spectroscopy.

NMR tube scale synthesis of [Cp*$_2$Ti$_2${NC(N(Xyl)CH$_2$)$_2$}$_2$(μ-Me)Me$_2$][BF$_{20}$] (32-[BF$_{20}$])

Cp*Ti{NC(N(Xyl)CH$_2$)$_2$}Me$_2$ (30 mg, 0.05 mmol) and TBF$_{20}$ (25 mg, 0.03 mmol) were mixed together in C$_6$D$_5$Br The brown/yellow solution was transferred to an NMR tube and the NMR spectra recorded after 5 min. The product exists as a mixture of diastereoisomers (**32a**$^+$ and **32b**$^+$) in a 3:2 ratio alongside monomeric cation **25**$^+$ and dimethyl precatalyst **7**. Only the resonances for **32**$^+$ will be reported in this Section. The quoted intensities given are self-consistent within each isomer. ^{1}H NMR (C$_6$D$_5$Br, 299.9 MHz, 293 K) 7.11-6.88 (12H, m, C$_6$<u>H</u>$_3$Me$_2$), 3.45-3.34 (8H, m, overlapping peaks from **32a**$^+$ and **32b**$^+$ C<u>H</u>$_2$C<u>H</u>$_2$), 3.30 (6H, s, C$_6$H$_3$<u>Me</u>$_2$ **32a**$^+$), 2.24 (6H, s, C$_6$H$_3$<u>Me</u>$_2$, **32b**$^+$), 2.20 (6H, s, C$_6$H$_3$<u>Me</u>$_2$ **32a**$^+$), 2.07 (6H, s, C$_6$H$_3$<u>Me</u>$_2$, **32b**$^+$), 1.42 (15H, s, C$_5$<u>Me</u>$_5$, **32b**$^+$), 1.33 (15H, s, C$_5$<u>Me</u>$_5$, **32a**$^+$), -0.39 (6H, s, Ti-<u>Me</u>, **32a**$^+$), -0.47 (6H, s, Ti-<u>Me</u>, **32b**$^+$), -1.42 (3H, s, Ti(μ-<u>Me</u>)Ti, **32b**$^+$), -1.55 (3H, s, Ti(μ-<u>Me</u>)Ti, **32a**$^+$) ppm. ^{13}C-{^{1}H} NMR (C$_6$D$_5$Br, 75.4 MHz, 293 K) 151.6 (N<u>C</u>(N(Xyl)CH$_2$)$_2$, **32a**$^+$ and **32b**$^+$), 148.7 (br d, $^1J_{CF}$ = 241.7 Hz, *o*-<u>C</u>$_6$F$_5$), 139.0 (br d, $^1J_{CF}$ = 245.1 Hz, *p*-<u>C</u>$_6$F$_5$), 136.9 (br d, $^1J_{CF}$ = 244.4 Hz, *m*-<u>C</u>$_6$F$_5$), 137.1 (*i*-<u>C</u>$_6$H$_3$Me$_2$, **32a**$^+$ and **32b**$^+$), 135.0 (*o*-<u>C</u>$_6$H$_3$Me$_2$, **32a**$^+$ and **32b**$^+$), 128.4 (*p*-<u>C</u>$_6$H$_3$Me$_2$, **32a**$^+$ and **32b**$^+$), 123.4 (<u>C</u>$_5$Me$_5$, **32a**$^+$), 122.7 (<u>C</u>$_5$Me$_5$, **32b**$^+$), 54.9 (Ti-<u>Me</u>, **32a**$^+$), 53.9 (Ti-<u>Me</u>, **32b**$^+$), 46.3 (<u>C</u>H$_2$<u>C</u>H$_2$, **32a**$^+$), 46.0 (<u>C</u>H$_2$<u>C</u>H$_2$,**32b**$^+$), 45.9 (<u>C</u>H$_2$<u>C</u>H$_2$, **32a**$^+$), 45.2 (<u>C</u>H$_2$<u>C</u>H$_2$, **32b**$^+$) 40.7 (Ti(μ-<u>Me</u>)Ti, **32a**$^+$), 39.4 (Ti(μ-<u>Me</u>)Ti, **32b**$^+$), 12.2 (C$_5$<u>Me</u>$_5$), 12.1 (C$_5$<u>Me</u>$_5$) ppm. ^{19}F NMR (C$_6$D$_5$Br, 282.1

MHz, 293 K) -131.4 (m, *o*-C_6F_5), -162.0 (m, *p*-C_6F_5), -165.9 (m, *m*-C_6F_5) ppm. ^{11}B NMR (C_6D_5Br, 96.2 MHz, 293 K) -16.1 ppm.

NMR tube scale reaction of [Cp*$_2$Ti$_2${NC(N(Xyl)CH$_2$)$_2$}$_2$(μ-Me)Me$_2$][BF$_{20}$] with OPPh$_3$

[Cp*$_2$Ti$_2${NC(N(Xyl)CH$_2$)$_2$}$_2$(μ-Me)Me$_2$][BF$_{20}$] was generated *in situ* from Cp*Ti{NC(N(Xyl)CH$_2$)$_2$}Me$_2$ (30 mg, 0.05 mmol) and TBF$_{20}$ (25 mg, 0.03 mmol) in C_6D_5Br. After 2 min $OPPh_3$ (8 mg, 0.03 mmol) was added resulting in the quantitative formation of **7** and **26-[BF$_{20}$]** by ^{1}H NMR spectroscopy.

NMR tube scale synthesis of [Cp*Ti{NC(NMe$_2$)$_2$}Me(μ-Me)AlMe$_2$][BF$_{20}$] (33-[BF$_{20}$])

Cp*Ti{NC(NMe$_2$)$_2$}Me$_2$ (30 mg, 0.09 mmol) and $AlMe_3$ (6.6 mg, 8.8μL, 0.09 mmol) were mixed together in C_6D_5Br and TBF$_{20}$ (845 mg, 0.09 mmol) added. The red solution was transferred to an NMR tube and all NMR spectra recorded after 5 min. ^{1}H NMR (C_6D_5Br, 299.9 MHz, 298 K) 2.37 (12H, s, NC(N$\underline{Me}_2$)$_2$), 1.59 (15H, s, $C_5\underline{Me}_5$), 0.66 (6H, s, Ti-$\underline{Me}$ and Ti(μ-$\underline{Me}$)Al), -0.70 (6H, s, Al$\underline{Me}_2$) ppm. ^{13}C-{^{1}H} NMR (C_6D_5Br, 75.4 MHz, 298 K) 163.7 (N$\underline{C}$(NMe$_2$)$_2$), 148.9 (br d, $^1J_{CF}$ = 244.4 Hz, *o*-$\underline{C}_6F_5$), 138.6 (br d, $^1J_{CF}$ = 247.8 Hz , *p*-$\underline{C}_6F_5$), 136.8 (br d, $^1J_{CF}$ = 249.0 Hz, *m*-$\underline{C}_6F_5$), 128.1 ($\underline{C}_5Me_5$), 64.7 (Ti(μ-$\underline{Me}$)Al), 41.3 (NC(N$\underline{Me}_2$)$_2$), 12.3 ($C_5\underline{Me}_5$), -8.7 (Al$\underline{Me}_2$) ppm. ^{1}H NMR (CD_2Cl_2, 499.9 MHz, 183 K) 3.11 (3H, br s, N$\underline{Me}$), 2.98 (6H, br s, N$\underline{Me}_2$), 2.80 (3H, br s, N$\underline{Me}$), 1.97 (15H, s, $C_5\underline{Me}_5$), 1.04 (3H, s, Ti-$\underline{Me}$), 0.75 (3H, s, Ti(μ-$\underline{Me}$)Al), -0.43 (3H, s, Al-$\underline{Me}$), -0.65 (3H, s, Al-$\underline{Me}$) ppm. ^{13}C-{^{1}H} NMR (CD_2Cl_2, 125.7 MHz, 183 K) 162.7 (N$\underline{C}$(NMe$_2$)$_2$), 147.1 (br d, $^1J_{CF}$ = 241.7 Hz, *o*-$\underline{C}_6F_5$), 137.6 (br d, $^1J_{CF}$ = 245.1 Hz, *p*-$\underline{C}_6F_5$), 135.7 (br d, $^1J_{CF}$ = 244.4 Hz, *m*-$\underline{C}_6F_5$), 127.7 ($\underline{C}_5Me_5$), 70.6 (Ti-$\underline{Me}$), 57.2 (Ti(μ-$\underline{Me}$)Al), 44.1 (NC(N$\underline{Me}_2$)$_2$), 42.4 (NC(N$\underline{Me}_2$)$_2$), 42.1 (NC(N$\underline{Me}_2$)$_2$) 39.5 (NC(N$\underline{Me}_2$)$_2$), 13.1 ($C_5\underline{Me}_5$), -9.2 (Al-$\underline{Me}$), -9.7 (Al-$\underline{Me}$) ppm. ^{19}F NMR (C_6D_5Br, 282.1 MHz, 298 K) -131.8 (m, *o*-C_6F_5), -162.1 (m, *p*-C_6F_5), -165.9 (m, *m*-C_6F_5) ppm. ^{11}B NMR (C_6D_5Br, 96.2 MHz, 298 K) -16.1 ppm.

NMR tube scale reaction of [Cp*Ti{NC(NMe$_2$)$_2$}(μ-Me)$_2$AlMe$_2$][BF$_{20}$] (33-[BF$_{20}$]) with ^{i}PrNCN^{i}Pr

[Cp*Ti{NC(NMe$_2$)$_2$}(μ-Me)$_2$AlMe$_2$][BF$_{20}$] was generated *in situ* from Cp*Ti{NC(NMe$_2$)$_2$}Me$_2$ (30 mg, 0.09 mmol) and $AlMe_3$ (6.6 mg, 8.8μL, 0.09 mmol) in C_6D_5Br and 2 equivs ^{i}PrNCN^{i}Pr (23.2 mg, 28.8 μl, 0.18 mmol) was added. The

brown solution was transferred to an NMR tube and a ^{1}H NMR spectrum ran after 5 minutes. The reaction proceeded quantitatively such that the ^{1}H NMR spectrum consisted of a mixture of **35-[BF$_{20}$]** and {MeC(N^{i}Pr)$_2$}AlMe$_2$ after 2 h.

[Cp*Ti{NC(NMe$_2$)$_2$}Me(μ-Cl)AlMe$_2$][BF$_{20}$] (34-[BF$_{20}$])

Cp*Ti{NC(NMe$_2$)$_2$}Me$_2$ (100 mg, 0.31 mmol) and Me$_2$AlCl (28 mg , 28 μl, 0.31 mmol) were mixed together in fluorobenzene (5 ml). To this a solution of TBF$_{20}$ (282 mg, 0.31 mmol) in fluorobenzene (2 ml) was added dropwise. After 30 min pentane (20 ml) was added resulting in the formation of a red oil. The pentane/fluorobenzene was decanted and the oil washed further with pentane (10 ml). The remaining solvent was removed *in vacuo* to yield a red solid as the product. Yield: 172 mg (52%). ^{1}H NMR (C$_6$D$_5$Br, 299.9 MHz, 298 K) 3.02 (12H, s, NMe$_2$), 2.19 (15H, s, C$_5$Me$_5$), 1.70 (3H, Ti-Me), -0.40 (Al-Me) ppm. ^{13}C-{^{1}H} NMR (C$_6$D$_5$Br, 75.4 MHz, 298 K) 164.1 (NC(NMe$_2$)$_2$), 148.9 (br d, $^{1}J_{CF}$ = 244.4 Hz, *o*-C$_6$F$_5$), 138.6 (br d, $^{1}J_{CF}$ = 247.8 Hz, *p*-C$_6$F$_5$), 137.1 (*i*-C$_6$H$_3$Me$_2$), 136.8 (br d, $^{1}J_{CF}$ = 249.0 Hz, *m*-C$_6$F$_5$), 126.1 (C$_5$Me$_5$), 80.7 (Ti-Me), 41.5 (NMe$_2$), 13.0 (C$_5$Me$_5$), -8.3 (Al-Me) ppm. ^{1}H NMR (CD$_2$Cl$_2$, 499.99 MHz, 208 K), 3.17 (3H, br s, NMe$_2$), 2.95 (3H, br s, NMe$_2$), 2.87 (3H, br s, NMe$_2$), 2.86 (3H, br s, NMe$_2$) 2.11 (15H, s, C$_5$Me$_5$), 1.59 (3H, s, Ti-Me) , -0.46 (3H, s, Al-Me), -0.54 (3H, s, Al-Me) ppm. ^{13}C-{^{1}H} NMR (CD$_2$Cl$_2$, 125.7 MHz, 208 K) 162.8 (NC(NMe$_2$)$_2$),147.1 (br d, $^{1}J_{CF}$ = 241.7 Hz, *o*-C$_6$F$_5$), 137.6 (br d, $^{1}J_{CF}$ = 245.1 Hz, *p*-C$_6$F$_5$), 135.7 (br d, $^{1}J_{CF}$ = 244.4 Hz, *m*-C$_6$F$_5$), 132.3 (C$_5$Me$_5$), 70.9 (Ti-Me), 44.1 (NC(NMe$_2$)$_2$), 42.1 (NC(NMe$_2$)$_2$), 41.9 (NC(NMe$_2$)$_2$), 38.8 (NC(NMe$_2$)$_2$), 13.1 (C$_5$Me$_5$), -8.6 (Al-Me), -9.4 (Al-Me) ppm. ^{19}F NMR (C$_6$D$_5$Br, 282.1 MHz, 293 K) -131.5 (m, *o*-C$_6$F$_5$), -162.1 (m, *p*-C$_6$F$_5$), -166.0 (m, *m*-C$_6$F$_5$) ppm. ^{11}B NMR (C$_6$D$_5$Br, 96.2 MHz, 298 K) -16.0 ppm. IR (NaCl plates, Nujol mull, cm^{-1}) 1643 (m), 1594 (m), 1556 (w), 1513 (s), 1422 (m), 1401 (m), 1274 (m), 1204 (w), 1086 (m), 978 (s), 805 (w), 775 (m), 756 (m), 684 (w), 661 (w). Anal. Found (calcd. for C$_{42}$H$_{36}$AlBClF$_{20}$N$_3$Ti): C, 46.37 (46.54); H, 3.16 (3.35); N, 3.97 (3.88).

5.6 Experimental details for Chapter 4

[Cp*Ti{NC(N^{i}Pr$_2$)Ph}{MeC(N^{i}Pr)$_2$}][BF$_{20}$] (35-[BF$_{20}$])

Cp*Ti{NC(N^{i}Pr$_2$)Ph}Me$_2$ (100 mg, 0.24 mmol) and ^{i}PrNCN^{i}Pr (30 mg, 37 μL, 0.24 mmol) were mixed together in fluorobenzene (10 ml). To this a solution of TBF$_{20}$ (221 mg, 0.24 mmol) in fluorobenzene (5 ml) was added. After 30 min pentane (20 ml) was

added resulting in the formation of a brown solid. The pentane/fluorobenzene was decanted and the solid washed further with pentane (10 ml). The solid was dried *in vacuo* yielding the product as a brown solid. Yield: 220 mg (77 %). ^{1}H NMR (CD_2Cl_2, 299.9 MHz, 293 K) 7.50-7.20 (5H, m, $C_6\underline{H}_5$), 4.21 (1H, br, κ^1-NC$\underline{H}$Me$_2$), 3.67 (3H, overlapping sept, κ^1 and κ^2-NC$\underline{H}$Me$_2$), 2.28 (1H, s, $\underline{Me}$C(N^{i}Pr)$_2$), 2.08 (15H, s, $C_5\underline{Me}_5$), 1.40 (6H, d, ^3J = 6.9 Hz, κ^1-NCH$\underline{Me}_2$), 1.12 (6H, d, ^3J = 6.4 Hz, κ^2-NCH$\underline{Me}_2$), 1.09 (6H, d, ^3J = 6.9 Hz, κ^1-NCH$\underline{Me}_2$), 0.74 (6H, d, ^3J = 6.4 Hz, κ^2-NCH$\underline{Me}_2$) ppm. ^{13}C-{^{1}H} NMR (CD_2Cl_2, 75.4 MHz, 293K) 170.0 (Me$\underline{C}$(N^{i}Pr)$_2$), 168.5 (N$\underline{C}$(N^{i}Pr$_2$)Ph), 148.7 (br d, $^1J_{CF}$ = 241.7 Hz, *o*-$\underline{C}_6F_5$), 139.0 (br d, $^1J_{CF}$ = 245.1 Hz, *p*-$\underline{C}_6F_5$), 137.4 (*i*-$\underline{C}_6H_5$), 136.9 (br d, $^1J_{CF}$ = 244.4 Hz, *m*-$\underline{C}_6F_5$), 130.4 ($\underline{C}_5Me_5$), 130.1 (*o*-$\underline{C}_6H_5$), 129.4 (*m*-$\underline{C}_6H_5$), 127.1 (*p*-$\underline{C}_6H_5$), 51.5 (κ^2-N$\underline{C}$HMe$_2$), 49.4 (br, κ^1-N$\underline{C}$HMe$_2$), 25.8 (κ^2-NCH$\underline{Me}_2$), 24.9 (κ^2-NCH$\underline{Me}_2$), 22.2 (br, κ^1-NCH$\underline{Me}_2$), 20.7 (κ^1-NCH$\underline{Me}_2$), 13.9 ($\underline{Me}$C(N^{i}Pr)$_2$), 13.5 ($C_5\underline{Me}_5$) ppm. ^{19}F NMR (CD_2Cl_2, 282.1 MHz, 293K) -133.0 (m, *o*-C_6F_5), -163.8 (m, *p*-C_6F_5), -167.6 (m, *m*-C_5F_5) ppm. ^{11}B NMR (CD_2Cl_2, 96.2 MHz, 293K) -16.5 ppm. IR (NaCl plates, Nujol mull, cm^{-1}) 1643 (m), 1596 (w), 1557 (w), 1540 (m), 1514 (s), 1339 (w), 1311 (w), 1210 (w), 1151 (w), 1085 (s), 1023 (m), 980 (s), 803 (m), 775 (w), 756 (w), 683 (w), 668 (w). Anal. found (calcd. for $C_{55}H_{51}BF_{20}N_4Ti$) C, 54.51 (57.74); H, 4.13 (4.26); N, 4.78 (4.64).

[Cp*Ti{NC(N^{i}Pr$_2$)Ph}{OC(Me)N^{t}Bu}][BF$_{20}$] (36-[BF$_{20}$])

Cp*Ti{NC(N^{i}Pr$_2$)Ph}Me$_2$ (100 mg, 0.24 mmol) and ^{t}BuNCO (24 mg, 27 μL, 0.24 mmol) were mixed together in fluorobenzene (10 ml). To this a solution of TBF$_{20}$ (221 mg, 0.24 mmol) in fluorobenzene (5 ml) was added. After 30 min pentane (10 ml) was added to resulting in the formation of a red oil. The pentane/fluorobenzene was decanted and the oil washed further with pentane (10 ml). The remaining solvent was removed *in vacuo* yielding the product as a red solid. Yield: 183 mg (66%). ^{1}H NMR (C_6D_5Br, 299.9 MHz, 293 K) 7.20-6.70 (5H, m, $C_6\underline{H}_5$), 3.41 (1H, sept, ^3J = 6.9 Hz, NC$\underline{H}$Me$_2$), 3.14 (1H, sept, ^3J = 6.9 Hz, NC$\underline{H}$Me$_2$), 1.99 (3H, s, OC($\underline{Me}$)N^{t}Bu), 1.61 (15H, s, $C_5\underline{Me}_5$), 1.05 (3H, d, ^3J = 6.9 Hz, NCH$\underline{Me}_2$), 1.01 (3H, d, ^3J = 6.9 Hz, NCH$\underline{Me}_2$), 0.79 (9H, s, ^{t}Bu), 0.70 (3H, ^3J = 6.9 Hz, NCH$\underline{Me}_2$), 0.64 (3H, d, ^3J = 6.9 Hz, NCH$\underline{Me}_2$) ppm. ^{13}C-{^{1}H} NMR (C_6D_5Br, 75.4 MHz, 293 K) 178.0 (O$\underline{C}$(Me)N^{t}Bu), 168.5 (N$\underline{C}$(N^{i}Pr$_2$)Ph), 148.9 (br d, $^1J_{CF}$ = 244.4 Hz, *o*-$\underline{C}_6F_5$), 138.6 (br d, $^1J_{CF}$ = 247.8 Hz , *p*-$\underline{C}_6F_5$), 136.8 (br d, $^1J_{CF}$ = 249.0 Hz, *m*-$\underline{C}_6F_5$), 136.1 (*i*-$\underline{C}_6H_5$), 131.2 ($\underline{C}_5Me_5$), 130.3 (*o*-$\underline{C}_6H_5$), 129.4 (*m*-$\underline{C}_6H_5$), 125.8 (*p*-$\underline{C}_6H_5$), 55.3 (N$\underline{C}$Me$_3$), 54.0

(N<u>C</u>HMe$_2$), 48.5 (N<u>C</u>HMe$_2$), 30.4 (NC<u>Me</u>$_3$), 20.7 (OC(<u>Me</u>)N^{t}Bu), 20.4 (NCH<u>Me</u>$_2$), 20.1 (NCH<u>Me</u>$_2$), 19.7 (NCH<u>Me</u>$_2$), 19.2 (NCH<u>Me</u>$_2$), 12.0 (C$_5$<u>Me</u>$_5$) ppm. ^{19}F NMR (C$_6$D$_5$Br, 282.1 MHz, 293 K) -131.4 (m, *o*-C$_6$F$_5$), -162.0 (m, *p*-C$_6$F$_5$), -165.8 (m, *m*-C$_6$F$_5$) ppm. ^{11}B NMR (C$_6$D$_5$Br, 96.2 MHz, 293 K) -16.1 ppm. IR (NaCl plates, Nujol mull, cm^{-1}) 1643 (m), 1596 (w), 1583 (w), 1514 (s), 1375 (m), 1350 (m), 1339 (w), 1261 (m), 1151 (w), 1086 (s), 1032 (m), 1023 (m). 980 (s), 894 (w), 836 (w), 789 (m), 775 (w), 756 (w), 964 (w), 668 (m) 661 (w). Anal. found (calcd. for C$_{53}$H$_{46}$BF$_{20}$N$_3$OTi) C, 53.86 (53.96); H, 4.08 (3.93); N, 3.46 (3.56).

[Cp*Ti{NC(N^{i}Pr$_2$)Ar^{F2}}{MeC(N^{i}Pr)$_2$}][BF$_{20}$] (37-[BF$_{20}$])

Cp*Ti{NC(N^{i}Pr$_2$)Ar^{F2}}Me$_2$ (300 mg, 0.66 mmol) and ^{i}PrNCN^{i}Pr (103 µl, 84 mg, 0.66 mmol) were mixed together in fluorobenzene (10 ml). To this a solution of TBF$_{20}$ (612 mg, 0.66 mmol) in fluorobenzene (20 ml) was added. After 30 min pentane (20 mL) was added resulting in the formation of an brown oil. The pentane/fluorobenzene was decanted and the oil washed with pentane (10 ml). The solid was dried *in vacuo* yielding the product as a brown/red solid. Yield: 505 mg (61%). ^{1}H NMR (C$_6$D$_5$Br, 299.9 MHz, 293 K) 6.95-6.54 (3H, m, C$_6$<u>H</u>$_3$F$_2$), 4.11 (1H, br, κ^1-NC<u>H</u>Me$_2$), 3.19 (1H, sept, ^3J = 6.9 Hz, κ^1-NC<u>H</u>Me$_2$), 3.17 (2H, sept, J = 6.3 Hz, κ^2- NC<u>H</u>Me$_2$), 1.78 (3H, s, <u>Me</u>C(N^{i}Pr)$_2$), 1.77 (15H, s, C$_5$<u>Me</u>$_5$), 0.96 (6H, d, ^3J = 6.9 Hz, κ^1-NCH<u>Me</u>$_2$), 0.76 (6H, d, ^3J = 6.3 Hz, κ^2-NCH<u>Me</u>$_2$), 0.72 (6H, d, ^3J = 6.9 Hz, κ^1-NCH<u>Me</u>$_2$), 0.26 (6H, d, ^3J = 6.3 Hz, κ^2-NCH<u>Me</u>$_2$) ppm. ^{13}C-{^{1}H} NMR (C$_6$D$_5$Br, 75.4 MHz, 293 K) 169.7 (Me<u>C</u>(N^{i}Pr)$_2$), 158.1 (dd, $^1J_{CF}$ = 247 Hz, $^3J_{CF}$ = 6.9 Hz *o*-<u>C</u>$_6$H$_3$F$_2$), 154.1 (N<u>C</u>(N^{i}Pr$_2$)Ar^{F2}), 148.9 (br d, $^1J_{CF}$ = 244.4 Hz, *o*-<u>C</u>$_6$F$_5$), 138.6 (br d, $^1J_{CF}$ = 247.8 Hz, *p*-<u>C</u>$_6$F$_5$), 136.8 (br d, $^1J_{CF}$ = 249.0 Hz, *m*-<u>C</u>$_6$F$_5$), 130.7 (<u>C</u>$_5$Me$_5$), 114.8 (t, $^2J_{CF}$ = 19.2 Hz, *i*-<u>C</u>$_6$H$_3$F$_2$), 112.1 (dd, $^2J_{CF}$ = 21.7 Hz, $^4J_{CF}$ = 2.9 Hz, *m*-<u>C</u>$_6$H$_3$F$_2$), 51.1 (κ^2-N<u>C</u>HMe$_2$), 49.1 (κ^1-N<u>C</u>HMe$_2$), 25.4 (κ^2-NCH<u>Me</u>$_2$), 24.2 (κ^2-NCH<u>Me</u>$_2$), 21.4 (κ^1-NCH<u>Me</u>$_2$), 19.9 (κ^1-NCH<u>Me</u>$_2$), 13.1 (C$_5$<u>Me</u>$_5$), 12.6 (<u>Me</u>C(N^{i}Pr)$_2$) ppm. ^{19}F NMR (C$_6$D$_5$Br, 282.1 MHz, 293 K) -111.8 (br, C$_6$H$_3$<u>F</u>$_2$), -131.8 (m, *o*-C$_6$F$_5$), -162.3 (m, *p*-C$_6$F$_5$), -166.1 (m, *m*-C$_6$F$_5$) ppm. ^{11}B NMR (C$_6$D$_5$Br, 96.2 MHz, 293 K) -15.9 ppm. IR (NaCl plates, Nujol mull, cm^{-1}) 1642 (m), 1621(m), 1590 (w), 1548(s), 1513 (s), 1503 (m), 1468 (s), 1451(s), 1329 (m), 1275.4 (w). 1155 (w), 1085 (m), 1003 (w), 979 (m), 767 (w), 755 (w), 684 (w), 660 (w). Anal. Found (calcd. for C$_{55}$H$_{50}$BF$_{22}$N$_4$Ti): C, 53.23 (53.12); H, 3.92 (4.05); N, 4.44 (4.51).

[Cp*Ti{NC(N^{i}Pr$_2$)Ar^{F2}}{MeC(N^{i}Pr)$_2$}][MeBF$_{15}$] (37-[MeBF$_{15}$])

Cp*Ti{NC(N^{i}Pr$_2$)Ar^{F2}}Me$_2$ (200 mg, 0.44 mmol) and ^{i}PrNCN^{i}Pr (68 µl, 56 mg, 0.44 mmol) were mixed together in fluorobenzene (10 ml). To this a solution of BF_{15} (226 mg, 0.44 mmol) in fluorobenzene (20 ml) was added. After 30 min pentane (20 mL) was added resulting in the formation of a brown oil. The pentane/fluorobenzene was decanted and the oil washed with pentane (10 ml). The remaining solvent was removed *in vacuo* yielding the product as a brown solid. Yield: 313 mg (65%). ^{1}H NMR (C_6D_5Br, 299.9 MHz, 293 K) 6.95-6.54 (3H, m, $C_6\underline{H}_3F_2$), 4.12 (1H, br, κ^1-NC$\underline{H}$Me$_2$), 3.19 (1H, sept, ^3J = 6.9 Hz, κ^1-NC$\underline{H}$Me$_2$), 3.18 (2H, sept, J = 6.30 Hz, κ^2- NC$\underline{H}$Me$_2$), 1.78 (3H, s, $\underline{Me}$C(N^{i}Pr)$_2$), 1.77 (15H, s, $C_5\underline{Me}_5$), 0.97 (6H, d, ^3J = 6.9 Hz, κ^1-NCH$\underline{Me}_2$), 0.93 ($\underline{Me}BF_{15}$), 0.76 (6H, d, ^3J = 6.3 Hz, κ^2-NCH$\underline{Me}_2$), 0.72 (6H, d, ^3J = 6.9 Hz, κ^1-NCH$\underline{Me}_2$), 0.26 (6H, d, ^3J = 6.3 Hz, κ^2-NCH$\underline{Me}_2$) ppm. ^{13}C-{^{1}H} NMR (C_6D_5Br, 75.4 MHz, 293 K) 169.7 (Me$\underline{C}$(N^{i}Pr)$_2$), 158.1 (dd, $^1J_{CF}$ = 247 Hz, $^3J_{CF}$ = 6.9 Hz *o*-$\underline{C}_6H_3F_2$), 154.2 (N$\underline{C}$(N^{i}Pr$_2$)Ar^{F2}), 148.7 (br d, $^1J_{CF}$ = 250.1 Hz, *o*-$\underline{C}_6F_5$), 137.3 (br d, $^1J_{CF}$ = 247.8 Hz, *p*-C_6F_5), 136.8 (br d, $^1J_{CF}$ = 249.0 Hz, *m*-C_6F_5), 130.7 ($\underline{C}_5Me_5$), 114.8 (t, $^2J_{CF}$ = 19.2 Hz, *i*-$C_6\underline{H}_3F_2$), 112.1 (dd, $^2J_{CF}$ = 21.7 Hz, $^4J_{CF}$ = 2.9 Hz, *m*-$C_6\underline{H}_3F_2$), 51.2 (κ^2-N$\underline{C}$HMe$_2$), 49.0 (κ^1-N$\underline{C}$HMe$_2$), 25.5 (κ^2-NCH$\underline{Me}_2$), 24.1 (κ^2-NCH$\underline{Me}_2$), 21.4 (κ^1-NCH$\underline{Me}_2$), 20.0 (κ^1-NCH$\underline{Me}_2$), 13.1 ($C_5\underline{Me}_5$), 12.6 ($\underline{Me}$C(N^{i}Pr)$_2$) ppm. ^{19}F NMR (C_6D_5Br, 282.1 MHz, 293 K) -111.8 (br, $C_6H_3\underline{F}_2$), -131.8 (m, *o*-C_6F_5), -164.2 (m, *p*-C_6F_5), -166.7 (m, *m*-C_6F_5) ppm. ^{11}B NMR (C_6D_5Br, 96.2 MHz, 293 K) -14.1 ppm. IR (NaCl plates, Nujol mull, cm^{-1}) 1641 (w), 1622 (w), 1525 (s), 1330 (w), 1331 (w), 1261 (w), 1138 (w), 1086 (s), 1077 (s), 1018 (m), 965 (w), 952 (w), 798 (m), 769 (w), 658 (w). Anal. Found (calcd. for $C_{50}H_{52}BF_{17}N_4Ti$): C, 55.13 (55.06); H, 4.77 (4.81); N, 5.01 (5.14). Single crystals suitable for X-ray analysis were grown from a saturated CH_2Cl_2 solution at room temperature.

[Cp*Ti{NC(N^{i}Pr$_2$)Ar^{F2}}{OC(Me)N^{t}Bu}][BF$_{20}$] (38-[BF$_{20}$])

Cp*Ti{NC(N^{i}Pr$_2$)Ar^{F2}}Me$_2$ (300 mg, 0.66 mmol) and ^{t}BuNCO (76 µl, 66 mg, 0.66 mmol) were mixed together in fluorobenzene (10 ml). To this a solution of TBF_{20} (612 mg, 0.66 mmol) in fluorobenzene (10 ml) was added. After 30 min pentane (20 mL) was added resulting in the formation of a red oil. The pentane/fluorobenzene was decanted and the oil washed with pentane (10 ml). The remaining solvent was removed *in vacuo* yielding the product as a red solid. Yield: 0.50 g (62%). ^{1}H NMR (CD_2Cl_2, 299.9 MHz, 293 K) 7.47 (1H, m, *p*-$C_6\underline{H}_3F_2$), 7.16 (1H, m, *m*-$C_6\underline{H}_3F_2$), 7.03 (1H, m, *m*-

$C_6\underline{H}_3F_2$), 3.71 (2H, sept, two overlapping, NC$\underline{H}$Me$_2$), 2.42 (3H, s, OC($\underline{Me}$)N^{t}Bu), 2.06 (15H, s, $C_5\underline{Me}_5$), 1.36 (3H, d, ^3J = 6.8 Hz, NCH$\underline{Me}_2$), 1.34 (3H, d, ^3J = 6.8 Hz, NCH$\underline{Me}_2$), 1.22 (3H, d, ^3J = 6.8 Hz, NCH$\underline{Me}_2$), 1.15 (9H, s, ^{t}Bu), 1.13 (3H, d, ^3J = 6.8 Hz, NCH$\underline{Me}_2$) ^{13}C-{^{1}H} NMR (CD_2Cl_2, 75.4 MHz, 293 K) 178.3 (O$\underline{C}$(Me)N^{t}Bu), 156.6 (N$\underline{C}$(N^{i}Pr$_2$)Ar^{F2}), 148.7 (br d, $^1J_{CF}$ = 241.7 Hz, *o*-$\underline{C}_6F_5$), 139.0 (br d, $^1J_{CF}$ = 245.1 Hz, *p*-$\underline{C}_6F_5$), 136.9 (br d, $^1J_{CF}$ = 244.4 Hz, *m*-$\underline{C}_6F_5$), 132.8 ($\underline{C}_5Me_5$), 128.8 (t, $^3J_{CF}$ = 7.0 Hz, *p*-$\underline{C}_6H_3F_2$), 114.0 (t, $^2J_{CF}$ = 20.0 Hz, *i*-$\underline{C}_6H_3F_2$), 113.0 (dd, $^2J_{CF}$ = 21.5 Hz, $^4J_{CF}$ = 3.0 Hz, *m*-$\underline{C}_6H_3F_2$), 56.13 (N$\underline{C}$Me$_3$), 49.2 (κ^1-N$\underline{C}$HMe$_2$) 30.8 (NCH$\underline{Me}_2$), 21.4 (NCH$\underline{Me}_2$), 20.8 (OC($\underline{Me}$)N^{t}Bu), 20.4 (NCH$\underline{Me}_2$), 19.3 (NCH$\underline{Me}_2$), 12.5 ($C_5\underline{Me}_5$), ppm. ^{19}F NMR (CD_2Cl_2, 282.1 MHz, 293K) -111.5 ($C_6H_3\underline{F}_2$), -133.0 (m, *o*-C_6F_5), -163.7 (m, *p*-C_6F_5), -167.6 (m, *m*-C_6F_5) ppm. ^{11}B NMR (CD_2Cl_2, 96.2 MHZ, 293K) -16.1 ppm. IR (NaCl plates, Nujol mull, cm^{-1}) 1643 (w), 1622(w), 1591 (w), 1562 (w), 1546 (m), 1503 (w), 1467 (s), 1453 (s), 1306 (w), 1260 (m), 1209 (w), 1087 (s), 1019 (m), 980 (m), 798 (w), 756 (w), 684 (w). Anal. Found (calcd. for $C_{53}H_{45}BF_{22}N_3OTi$): C, 51.60 (52.32); H, 3.69 (3.73); N, 3.02 (3.45).

[Cp*Ti{NC(N^{i}Pr$_2$)Ph}(NCMe$_2$)(NCMe)][BF$_{20}$] (39-[BF$_{20}$])

Cp*Ti{NC(N^{i}Pr$_2$)Ph}Me$_2$ (100 mg, 0.24 mmol) and 2 equivs of MeCN (25 µl, 20 mg, 0.48 mmol) were mixed together in fluorobenzene (10 ml). To this a solution of TBF$_{20}$ (224 mg, 0.24 mmol) in fluorobenzene (20 ml) was added. After 30 min pentane (20 mL) was added resulting in the formation of a red oil. The pentane/fluorobenzene was decanted and the oil washed with pentane (10 ml). The remaining solvent was removed *in vacuo* yielding the product as an orange solid. Yield: 226 mg (81%). ^{1}H NMR (C_6D_5Br, 299.9 MHz, 293 K) 7.13-6.87 (5H, $C_6\underline{H}_5$), 3.38 (1H, br, NC$\underline{H}$Me$_2$), 3.24 (1H, sept, ^3J = 6.7 Hz, NC$\underline{H}$Me$_2$), 1.65 (6H, s, NC$\underline{Me}_2$), 1.60 ($\underline{Me}$CN), 1.55 ($C_5\underline{Me}_5$), 1.29 (6H, d, ^3J = 6.7 Hz, NCH$\underline{Me}_2$), 1.23 (6H, d, ^3J = 6.7 Hz, NCH$\underline{Me}_2$), 0.74 (6H, d, ^3J = 6.7 Hz, NCH$\underline{Me}_2$), 0.65 (6H, d, ^3J = 6.7 Hz, NCH$\underline{Me}_2$) ppm. ^{13}C-{^{1}H} NMR (C_6D_5Br, 75.4 MHz, 293 K) 180.0 (NC$\underline{Me}_2$), 164.1 (N$\underline{C}$(N^{i}Pr$_2$)Ph), 148.9 (br d, $^1J_{CF}$ = 244.4 Hz, *o*-$\underline{C}_6F_5$), 138.6 (br d, $^1J_{CF}$ = 247.8 Hz, *p*-$\underline{C}_6F_5$), 138.7 (*i*-$\underline{C}_6H_5$), 136.8 (br d, $^1J_{CF}$ = 249.0 Hz, *m*-C_6F_5), 129.9 (Me$\underline{C}$N), 126.9 (*m*-$\underline{C}_6H_5$), 126.6 (*p*-$\underline{C}_6H_5$), 122.0 ($\underline{C}_5Me_5$), 53.0 (N$\underline{C}$HMe$_2$), 47.4 (N$\underline{C}$HMe$_2$), 29.1 (NC$\underline{Me}_2$), 20.1 (NCH$\underline{Me}_2$), 20.0 (NCH$\underline{Me}_2$), 19.5 (NCH$\underline{Me}_2$), 19.3 (NCH$\underline{Me}_2$), 11.6 ($C_5\underline{Me}_5$), 1.6 ($\underline{Me}$CN) ppm. ^{19}F NMR (CD_2Cl_2, 282.1 MHz, 293K) -133.0 (m, *o*-C_6F_5), -163.8 (m, *p*-C_6F_5), -167.6 (m, *m*-C_5F_5) ppm. ^{11}B NMR (CD_2Cl_2, 96.2 MHz, 293K) -16.1 ppm. IR (NaCl plates, Nujol mull, cm^{-1})

2316 (w), 2288 (w), 1678 (w), 1642 (m), 1514 (s), 1340 (m), 1273 (w), 1153 (w), 1085 (m), 1034 (w), 979 (m), 784 (w), 774 (w), 668 (w). Anal. Found (calcd. for $C_{52}H_{43}BF_{20}N_4Ti$) C, 53.64 (53.72); H, 3.59 (3.73); N, 4.66 (4.82).

[Cp*Ti{NC(N^{i}Pr$_2$)Ar^{F2}}(NCMe$_2$)(NCMe)][BF$_{20}$] (40-[BF$_{20}$])

Cp*Ti{NC(N^{i}Pr$_2$)Ar^{F2}}Me$_2$ (300 mg, 0.66 mmol) and 2 equivs of MeCN (54 mg, 69 µl, 1.32 mmol) were mixed together in fluorobenzene (10 ml). To this a solution of TBF_{20} (612 mg, 0.66 mmol) in fluorobenzene (10 ml) was added. After 30 min pentane (20 mL) was added resulting in the formation of a red oil. The pentane/fluorobenzene was decanted and the oil washed with pentane (10 ml). The remaining solvent was removed *in vacuo* yielding the product as an orange solid. Yield: 596 mg (75%). ^{1}H NMR (CD_2Cl_2, 299.9 MHz, 293 K) 7.35 (1H, m, *p*-$C_6\underline{H}_3F_2$), 6.98 (2H, m, *m*-$C_6\underline{H}_3F_2$), 3.73 (1H, sept, ^3J = 6.6 Hz, NC$\underline{H}$Me$_2$), 3.62 (1H, sept, ^3J = 6.6 Hz, NC$\underline{H}$Me$_2$), 2.36 (3H, br s, $\underline{Me}$CN), 1.93 (6H, s, NC$\underline{Me}_2$), 1.87 (15H, s, $C_5\underline{Me}_5$), 1.54 (6H, br d, ^3J = 6.6 Hz, NCH$\underline{Me}_2$), 1.15 (6H, d, ^3J = 6.6 Hz, NCH$\underline{Me}_2$) ppm. ^{13}C-{^{1}H} NMR (CD_2Cl_2, 75.4 MHz, 293 K) 180.6 (NC$\underline{Me}_2$), 152.0 (N$\underline{C}$(N^{i}Pr$_2$)Ar^{F2}), 148.7 (br d, $^1J_{CF}$ = 241.7 Hz, *o*-$\underline{C}_6F_5$), 139.0 (br d, $^1J_{CF}$ = 245.1 Hz, *p*-$\underline{C}_6F_5$), 136.9 (br d, $^1J_{CF}$ = 244.4 Hz, *m*-$\underline{C}_6F_5$), 131.0 (t, $^3J_{CF}$ = 8.7 Hz, *p*-$C_6\underline{H}_3F_2$), 128.6 (Me$\underline{C}$N), 123.5 ($\underline{C}_5Me_5$), 116.6 (t, $^2J_{CF}$ = 22.1 Hz, *i*-$\underline{C}_6H_3F_2$), 115.8 (d, $^2J_{CF}$ = 20.5 Hz, *m*-$\underline{C}_6H_3F_2$), 53.9 (N$\underline{C}$HMe$_2$), 48.4 (N$\underline{C}$HMe$_2$), 29.2 (NC$\underline{Me}_2$), 20.8 (NCH$\underline{Me}_2$), 20.0 (NCH$\underline{Me}_2$), 11.9 ($C_5\underline{Me}_5$), 3.2 ($\underline{Me}$CN) ppm. ^{19}F NMR (CD_2Cl_2, 282.1 MHz, 293K) -113.2 ($C_6H_3\underline{F}_2$), -133.1 (m, *o*-C_6F_5), -163.7 (m, *p*-C_6F_5), -167.6 (m, *m*-C_6F_5) ppm. ^{11}B NMR (CD_2Cl_2, 96.2 MHZ, 293K) -16.2 ppm. IR (NaCl plates, Nujol mull, cm^{-1}) 2316 (w), 2287.89 (w), 1678 (w), 1642 (w), 1621 (w), 1587 (w), 1563 (w), 1548 (m), 1536 (m), 1467 (s), 1452 (s), 1338 (m), 1274 (w), 1236 (w), 1155 (w), 1085 (m), 1030 (w), 1002 (w), 980 (m), 893 (w), 795 (w), 757 (w), 684 (w), 661 (w). Anal. Found (calcd. for $C_{52}H_{41}BF_{22}N_4Ti$): C, 52.37 (52.11); H, 3.38 (3.45); N, 4.80 (4.67).

[Cp*Ti{NC(N^{i}Pr$_2$)Ph}(NCMePh)(NCPh)][BF$_{20}$] (41-[BF$_{20}$])

Cp*Ti{NC(N^{i}Pr$_2$)Ph}Me$_2$ (100 mg, 0.24 mmol) and 2 equivs of PhCN (50 mg, 50 µl, 0.48 mmol) were mixed together in fluorobenzene (10 ml). To this a solution of TBF_{20} (221 mg, 0.24 mmol) in fluorobenzene (10 ml) was added. After 30 min pentane (20 mL) was added resulting in the formation of a red oil. The pentane/fluorobenzene was decanted and the oil washed with pentane (10 ml). The remaining solvent was removed

in vacuo yielding the product as an orange solid. Yield: 226 mg (73%). ^{1}H NMR (C_6D_5Br, 299.9 MHz, 293 K) 7.50-6.90 (15H, m, Ar), 3.40 (1H, sept, ^{3}J = 6.7 Hz, NC<u>H</u>Me$_2$), 3.22 (1H, br, NC<u>H</u>Me$_2$), 2.16 (3H, s, NC<u>Me</u>Ph), 1.63 (15H, s, C_5<u>Me$_5$</u>), 1.30 (6H, br d, NCH<u>Me$_2$</u>), 0.68 (6H, br d, NCH<u>Me$_2$</u>) ppm. ^{13}C-{^{1}H} NMR (C_6D_5Br, 75.4 MHz, 293 K) 174.9 (N<u>C</u>MePh), 164.6 (N<u>C</u>(N^{i}Pr$_2$)Ph), 148.9 (br d, $^{1}J_{CF}$ = 244.4 Hz, *o*-<u>C</u>$_6F_5$), 138.7 (*i*-NC(N^{i}Pr$_2$)<u>Ph</u>), 138.6 (br d, $^{1}J_{CF}$ = 247.8 Hz, *p*-C_6F_5), 137.3 (*i*-NCMe<u>Ph</u>), 136.8 (br d, $^{1}J_{CF}$ = 249.0 Hz, *m*-C_6F_5), 132.4 (Ar), 129.0 (*o*-N<u>C</u>(N^{i}Pr$_2$)Ph), 128.8 (Ar), 127.2 (Ar), 122.7 (<u>C</u>$_5$Me$_5$), 110.4 (*i*-<u>Ph</u>CN), 53.0 (NC<u>H</u>Me$_2$), 47.6 (NC<u>H</u>Me$_2$), 26.0 (NC<u>Me</u>Ph), 20.2 (NCH<u>Me$_2$</u>), 19.6 (NCH<u>Me$_2$</u>), 11.8 (C_5<u>Me$_5$</u>) ppm. Resonances labeled Ar could not be unambiguously assigned. ^{19}F NMR (C_6D_5Br, 282.1 MHz, 293 K) -131.5 (m, *o*-C_6F_5), -162.1 (m, *p*-C_6F_5), -166.0 (m, *m*-C_6F_5) ppm. ^{11}B NMR (C_6D_5Br, 96.2 MHz, 293 K) -16.0 ppm. IR (NaCl plates, Nujol mull, cm^{-1}) 2252 (w), 1644 (m), 1578 (w), 1514 (s), 1341 (m), 1274 (w), 1180 (w), 1085 (m), 979(s), 890 (w), 784 (w), 756 (w), 683 (w). Anal. Found (calcd. for $C_{62}H_{47}BF_{20}N_4Ti$): C, 57.68 (57.87); H, 3.64 (3.68); N, 4.39 (4.35).

[Cp*Ti{NC(N^{i}Pr$_2$)Ar^{F2}}(NCMePh)(NCPh)][BF$_{20}$] (42-[BF$_{20}$])

Cp*Ti{NC(N^{i}Pr$_2$)Ar^{F2}}Me$_2$ (100 mg, 0.22 mmol) and 2 equivs of PhCN (46 mg, 46 µl, 0.44 mmol) were mixed together in fluorobenzene (10 ml). To this a solution of TBF_{20} (204 mg, 0.22 mmol) in fluorobenzene (10 ml) was added. After 30 min pentane (20 mL) was added resulting in the formation of a red oil. The pentane/fluorobenzene was decanted and the oil washed with pentane (10 ml). The pentane/fluorobenzene was decanted and the oil washed with pentane (10 ml). The remaining solvent was removed *in vacuo* to yield the product as an orange solid. Yield: 234 mg (80%). ^{1}H NMR (C_6D_5Br, 299.9 MHz, 293 K) 7.38-6.50 (13H, m, Ar), 3.34 (1H, sept, ^{3}J = 6.8 Hz, NC<u>H</u>Me$_2$), 3.30 (1H, br, NC<u>H</u>Me$_2$), 2.12 (3H, s, NC<u>Me</u>Ph), 1.70 (15H, s, C_5Me_5), 1.27 (6H, d, ^{3}J = 6.8 Hz, NCH<u>Me$_2$</u>), 0.75 (6H, d, ^{3}J = 6.8 Hz, NCH<u>Me$_2$</u>) ppm. ^{13}C-{^{1}H} NMR (C_6D_5Br, 75.4 MHz, 293 K) 175.4 (N<u>C</u>MePh), 157.8 (dd, $^{1}J_{CF}$ = 244.8 Hz, $^{3}J_{CF}$ = 6.9 Hz, *o*-<u>C</u>$_6H_3F_2$), 151.8 (N<u>C</u>(N^{i}Pr$_2$)Ar^{F2}), 148.9 (br d, $^{1}J_{CF}$ = 244.4 Hz, *o*-<u>C</u>$_6F_5$), 138.6 (br d, $^{1}J_{CF}$ = 247.8 Hz, *p*-<u>C</u>$_6F_5$), 137.1 (*i*-NCMe<u>Ph</u>), 136.8 (br d, $^{1}J_{CF}$ = 249.0 Hz, *m*-<u>C</u>$_6F_5$), 132.6 (Ar), 128.8 (Ar), 127.2 (Ar), 123.4 (<u>C</u>$_5$Me$_5$), 115.9 (t, $^{2}J_{CF}$ = 23.4 Hz, *i*-<u>C</u>$_6H_3F_2$), 110.3 (*i*-<u>Ph</u>CN), 53.7 (N<u>C</u>HMe$_2$), 48.0 (N<u>C</u>HMe$_2$), 25.8 (NC<u>Me</u>Ph), 20.2 (NC<u>H</u>Me$_2$), 19.5 (NC<u>H</u>Me$_2$), 11.7 (C_5Me_5) ppm. Resonances labeled Ar could not be unambiguously assigned. ^{19}F NMR (C_6D_5Br, 282.1 MHz, 293 K) -112.7 (br, C_6H_3<u>F$_2$</u>),

-131.5 (m, *o*-C_6F_5), -162.1 (m, *p*-C_6F_5), -166.0 (m, *m*-C_6F_5) ppm. ^{11}B NMR (C_6D_5Br, 96.2 MHz, 293 K) -16.1 ppm. IR (NaCl plates, Nujol mull, cm^{-1}) 2250 (w), 1644 (w), 1536 (s), 1511 (m), 1272 (m), 1236 (w), 1083 (m), 1029 (w), 976 (s), 755 (m), 723 (w), 683 (w). Anal. Found (calcd. for $C_{62}H_{45}BF_{22}N_4Ti$): C, 56.22 (56.30); H, 3.59 (3.43); N, 4.36 (4.24).

[Cp*Ti{NC(NMe$_2$)$_2$}{MeC(N^{i}Pr)$_2$}][BF$_{20}$] (43-[BF$_{20}$])

Cp*Ti{NC(NMe$_2$)$_2$}Me$_2$ (500 mg, 1.53 mmol) and ^{i}PrNCN^{i}Pr (0.19 g, 0.24 ml, 1.53 mmol) were mixed together in fluorobenzene (20 ml). To this a solution of TBF_{20} (1.41 g, 1.53 mmol) in fluorobenzene (10 ml) was added dropwise. After 30 min pentane (20 mL) was added resulting in the formation of a brown oil. The pentane/fluorobenzene was decanted and the oil washed with pentane (10 ml). The remaining solvent was removed *in vacuo* to yield the product as a brown solid. Yield: 1.41 g (82%). ^{1}H NMR (C_6D_5Br, 299.9 MHz, 293 K) 3.31 (2H, sept, ^3J = 6.5 Hz, NC<u>H</u>Me$_2$), 2.31 (12H, s, NC(N<u>Me</u>$_2$)$_2$), 1.75 (3H, s, <u>Me</u>C(N^{i}Pr)$_2$), 1.73 (15H, C_5<u>Me</u>$_5$), 0.79 (6H, d, ^3J = 6.5 Hz, NCH<u>Me</u>$_2$), 0.70 (6H, d, ^3J = 6.5 Hz, NCH<u>Me</u>$_2$) ppm. ^{13}C-{^{1}H} NMR (C_6D_5Br, 75.4 MHz, 293 K) 168.4 (Me<u>C</u>(N^{i}Pr)$_2$), 161.1 (N<u>C</u>(NMe$_2$)$_2$), 148.9 (br d, $^1J_{CF}$ = 244.4 Hz, *o*-<u>C</u>$_6F_5$), 138.6 (br d, $^1J_{CF}$ = 247.8 Hz , *p*-C_6F_5), 136.8 (br d, $^1J_{CF}$ = 249.0 Hz, *m*-C_6F_5), 128.2 (<u>C</u>$_5$Me$_5$), 50.5 (N<u>C</u>HMe$_2$), 40.1 (NC(N<u>Me</u>$_2$)$_2$), 25.2 (NCH<u>Me</u>$_2$), 24.4 (NCH<u>Me</u>$_2$), 13.6 (<u>Me</u>C(N^{i}Pr)$_2$), 12.9 (C_5<u>Me</u>$_5$) ppm. ^{19}F NMR (C_6D_5Br, 282.1 MHz, 293 K) -131.4 (m, *o*-C_6F_5), -162.0 (m, *p*-C_6F_5), -165.8 (m, *m*-C_6F_5) ppm. ^{11}B NMR (C_6D_5Br, 96.2 MHz, 293 K) -16.0 ppm. IR (NaCl plates, Nujol mull, cm^{-1}) 1642 (w), 1513 (s), 1419 (m), 1402 (m), 1276 (w), 1211 (w), 1153 (w), 1086 (m), 1020 (w), 979 (s), 859 (w), 775 (w), 769 (w), 756 (w), 684 (w). Anal. found (calcd. for $C_{47}H_{44}BF_{20}N_5Ti$) C, 50.51 (50.47); H, 3.97 (4.06); N, 6.27 (6.26).

[Cp*Ti{NC(N^{i}BuMe)$_2$}{MeC(N^{i}Pr)$_2$}][BF$_{20}$] (44-[BF$_{20}$])

Cp*Ti{NC(N^{i}BuMe)$_2$}Me$_2$ (98 mg, 0.24 mmol) and ^{i}PrNCN^{i}Pr (30 mg, 37 µL, 0.24 mmol) were mixed together in fluorobenzene (10 ml). To this a solution of TBF_{20} (220 mg, 0.24 mmol) in fluorobenzene (5 ml) was added dropwise. After 30 min pentane (20 mL) was added resulting in the formation of a brown oil. The pentane/fluorobenzene was decanted and the oil washed with pentane (10 ml). The remaining solvent was removed *in vacuo* to yield the product as a brown solid. Yield: 172 mg (80%).^{1}H NMR (C_6D_5Br, 299.9 MHz, 293 K) 3.35 (2H, sept, ^3J = 6.5 Hz,

NC<u>H</u>Me$_2$), 2.56 (4H, d, ^3J = 7.6 Hz, NC<u>H$_2$</u>CHMe$_2$), 2.38 (6H, s, N<u>Me</u>), 1.77 (3H, s, <u>Me</u>C(N^{i}Pr)$_2$), 1.76 (15H, s, C$_5$<u>Me$_5$</u>), 1.54 (2H, sept, ^3J = 6.6 Hz NCH$_2$C<u>H</u>Me$_2$), 0.81 (6H, d, ^3J = 6.5 Hz, NCH<u>Me$_2$</u>), 0.72 (6H, d, ^3J = 6.5 Hz, NCH<u>Me$_2$</u>), 0.58 (12H, d, ^3J = 6.6 Hz, NCH$_2$CH<u>Me$_2$</u>) ppm. ^{13}C-{^{1}H} NMR (C$_6$D$_5$Br, 75.4 MHz, 293 K) 168.2 (Me<u>C</u>(N^{i}Pr)$_2$), 162.1 (N<u>C</u>(N^{i}BuMe)$_2$), 148.9 (br d, $^1J_{CF}$ = 244.4 Hz, *o*-<u>C</u>$_6$F$_5$), 138.6 (br d, $^1J_{CF}$ = 247.8 Hz , *p*-<u>C</u>$_6$F$_5$), 136.8 (br d, $^1J_{CF}$ = 249.0 Hz, *m*-<u>C</u>$_6$F$_5$), 128.4 (<u>C</u>$_5$Me$_5$), 59.4 (N<u>C</u>H$_2$CHMe$_2$), 50.5 (N<u>C</u>HMe$_2$), 38.4 (NC(N^{i}Bu<u>Me</u>)$_2$), 26.5 (NCH$_2$<u>C</u>HMe$_2$), 25.3 (NCH<u>Me$_2$</u>), 24.7 (NCH<u>Me$_2$</u>), 19.7 (NCH$_2$CH<u>Me$_2$</u>), 13.4 (<u>Me</u>C(N^{i}Pr)$_2$), 13.0 (C$_5$<u>Me$_5$</u>) ppm. ^{19}F NMR (C$_6$D$_5$Br, 282.1 MHz, 293 K) -131.5 (m, *o*-C$_6$F$_5$), -162.1 (m, *p*-C$_6$F$_5$), -166.0 (m, *m*-C$_6$F$_5$) ppm. ^{11}B NMR (C$_6$D$_5$Br, 96.2 MHz, 293 K) -16.1 ppm. IR (NaCl plates, Nujol mull, cm^{-1}) 1643 (m), 1601 (w), 1514 (s), 1410 (s), 1340 (m), 1273 (m), 1210 (m), 1172 (w), 1150 (w), 1084 (s), 979 (s), 848 (w), 815 (w), 774 (m), 756 (m), 683 (w), 661 (m). Anal. found (calcd. for C$_{53}$H$_{56}$BF$_{20}$N$_5$Ti) C, 53.13 (52.97); H, 4.85 (4.70); N, 5.83 (5.83).

[Cp*Ti{NC(N(Xyl)CH$_2$)$_2$}{MeC(N^{i}Pr)$_2$}][BF$_{20}$] (45-[BF$_{20}$])

Cp*Ti{NC(N(Xyl)CH$_2$)$_2$}Me$_2$ (40 mg, 0.08 mmol) and ^{i}PrNCN^{i}Pr (10.0 mg, 12.2 μL, 0.08 mmol) were mixed together in fluorobenzene (10 ml). To this a solution of TBF$_{20}$ (73 mg, 0.08 mmol) in fluorobenzene (5 ml) was added. After 30 min pentane (20 mL) was added resulting in the formation of a brown oil. The pentane/fluorobenzene was decanted and the oil washed with pentane (10 ml). The remaining solvent was removed *in vacuo* to yield the product as a brown solid. Yield: 74 mg (72%). ^{1}H NMR (CD$_2$Cl$_2$, 299.9 MHz, 293 K) 7.15 (6H, s, C$_6$<u>H$_3$</u>Me$_2$), 3.82 (4H, s, C<u>H$_2$</u>C<u>H$_2$</u>), 3.31 (2H, sept, ^3J = 6.3 Hz, NC<u>H</u>Me$_2$), 2.41 (12H, s, C$_6$H$_3$<u>Me$_2$</u>), 2.18 (3H, s, <u>Me</u>C(N^{i}Pr)$_2$), 1.92 (15H, s, C$_5$<u>Me$_5$</u>), 0.97 (6H, d, ^3J = 6.3 Hz, NCH<u>Me$_2$</u>), 0.25 (6H, d, ^3J = 6.3 Hz, NCH<u>Me$_2$</u>) ppm. ^{13}C-{^{1}H} NMR (C$_6$D$_5$Br, 75.4 MHz, 293 K) 169.2 (Me<u>C</u>(N^{i}Pr)$_2$), 152.1 (N<u>C</u>(N(Xyl)CH$_2$)$_2$), 148.7 (br d, $^1J_{CF}$ = 241.7 Hz, *o*-<u>C</u>$_6$F$_5$), 139.0 (br d, $^1J_{CF}$ = 245.1 Hz, *p*-<u>C</u>$_6$F$_5$), 137.1 (*i*-<u>C</u>$_6$H$_5$Me$_2$), 136.9 (br d, $^1J_{CF}$ = 244.4 Hz, *m*-<u>C</u>$_6$F$_5$), 130.6 (<u>C</u>$_5$Me$_5$), 130.1 (*m*-<u>C</u>$_6$H$_5$Me$_2$), 129.8 (*p*-<u>C</u>$_6$H$_5$Me$_2$), 51.5 (N<u>C</u>HMe$_2$), 47.1 (<u>C</u>H$_2$<u>C</u>H$_2$), 25.8 (NCH<u>Me$_2$</u>), 25.7 (NCH<u>Me$_2$</u>), 18.9 (C$_6$H$_5$<u>Me$_2$</u>), 14.0 (<u>Me</u>C(N^{i}Pr)$_2$), 13.6 (C$_5$<u>Me$_5$</u>) ppm. ^{19}F NMR (CD$_2$Cl$_2$, 282.1 MHz, 293K) -133.0 (m, *o*-C$_6$F$_5$), -163.8 (m, *p*-C$_6$F$_5$), -167.6 (m, *m*-C$_5$F$_5$) ppm. ^{11}B NMR (CD$_2$Cl$_2$, 96.2 MHz, 293K) -16.2 ppm. IR (NaCl plates, Nujol mull, cm^{-1}) 1643 (w), 1598 (w), 1529 (m), 1513 (m), 1307 (m), 1261 (m), 1209 (w), 1086 (s), 1020 (m), 979 (m), 868 (w), 801 (m), 775 (w), 756 (w), 723 (m), 683

(w), 672 (w), 661 (w). Anal. found (calcd. for $C_{61}H_{54}BF_{20}N_5Ti$) C, 56.36 (56.54); H, 4.08 (4.20); N, 5.27 (5.40). Single crystals suitable for X-ray analysis were grown from a saturated CH_2Cl_2 solution at room temperature.

[Cp*Ti{NC(NMe$_2$)$_2$}{OC(Me)N^{t}Bu}][BF$_{20}$] (46-[BF$_{20}$])

Cp*Ti{NC(NMe$_2$)$_2$}Me$_2$ (500 mg, 1.53 mmol) and ^{t}BuNCO (0.17 ml, 151 mg, 1.53 mmol) were mixed together in fluorobenzene (10 ml). To this a solution of TBF_{20} (845 mg, 1.53 mmol) in fluorobenzene (10 ml) was added dropwise. After 30 min pentane (20 ml) was added resulting in the formation of a red oil. The pentane/fluorobenzene was decanted and the oil washed further with pentane (10 ml). The remaining solvent was removed *in vacuo* to yield a red solid as the product. Yield: 1.27 g (76%). ^{1}H NMR (CD_2Cl_2, 299.9 MHz, 293 K) 2.79 (12H, s, NC(N<u>Me</u>)$_2$), 2.37 (3H, s, OC(<u>Me</u>)N^{t}Bu), 2.14 (15H, s, C$_5$<u>Me</u>$_5$), 1.24 (9H, s, OC(Me)N^t<u>Bu</u>) ppm. ^{13}C-{^{1}H} NMR (CD_2Cl_2, 75.4 MHz, 293 K) 177.6 (O<u>C</u>(Me)N^{t}Bu), 161.9 (N<u>C</u>(NMe$_2$)$_2$), 148.7 (br d, $^1J_{CF}$ = 241.7 Hz, *o*-<u>C</u>$_6$F$_5$), 139.0 (br d, $^1J_{CF}$ = 245.1 Hz, *p*-<u>C</u>$_6$F$_5$), 136.9 (br d, $^1J_{CF}$ = 244.4 Hz, *m*-<u>C</u>$_6$F$_5$), 130.6 (<u>C</u>$_5$Me$_5$), 55.4 (N<u>C</u>Me$_3$), 40.8 (NC(N<u>Me</u>$_2$)$_2$), 31.0 (NC<u>Me</u>$_3$), 21.1 (OC(<u>Me</u>)N^{t}Bu), 12.7 (C$_5$<u>Me</u>$_5$) ppm. ^{19}F NMR (CD_2Cl_2, 282.1 MHz, 293K) -133.0 (m, *o*-C$_6$F$_5$), -163.7 (m, *p*-C$_6$F$_5$), -167.5 (m, *m*-C$_6$F$_5$) ppm. ^{11}B NMR (CD_2Cl_2, 96.2 MHZ, 293K) -16.1 ppm. IR (NaCl plates, Nujol mull, cm^{-1}) 1643 (w), 4596 (w), 1514 (s), 1419 (s), 1327 (m), 1261 (m), 1214 (w), 1155 (w), 1085 (s), 1021 (m), 979 (s), 862 (w), 796 (m), 775 (m), 769 (w), 756 (m), 684 (m), 661 (m). Anal. Found (calcd. for $C_{45}H_{39}BF_{20}N_4OTi$): C, 49.66 (49.56); H, 3.56 (3.60); N, 5.03 (5.14).

[Cp*Ti{NC(N^{i}BuMe)$_2$}{OC(Me)N^{t}Bu}][BF$_{20}$] (47-[BF$_{20}$])

Cp*Ti{NC(N^{i}BuMe)$_2$}Me$_2$ (108 mg, 0.26 mmol) and ^{t}BuNCO (30 μL, 26 mg, 0.26 mmol) were mixed together in fluorobenzene (10 ml). To this a solution of TBF_{20} (242 mg, 0.26 mmol) in fluorobenzene (5 ml) was added dropwise. After 30 min pentane (20 ml) was added resulting in the formation of a red oil. The pentane/fluorobenzene was decanted and the oil washed further with pentane (10 ml). The remaining solvent was removed *in vacuo* to yield a red solid as the product. Yield: 191 mg (74%). ^{1}H NMR (C_6D_5Br, 299.9 MHz, 293 K) 2.87 (2H, dd, ^2J = 13.0 Hz, ^3J = 8.6 Hz, NC<u>H</u>$_2$CHMe$_2$), 2.64 (6H, s, N<u>Me</u>), 2.61 (1H, dd, ^2J = 13.0 Hz, ^3J = 6.1 Hz NC<u>H</u>$_2$CHMe$_2$), 2.17 (3H, s, OC(<u>Me</u>)N^{t}Bu), 2.03 (15H, s, C$_5$<u>Me</u>$_5$), 1.72 (2H, m, NCH$_2$C<u>H</u>Me$_2$), 1.12 (9H, s, OC(Me)N^t<u>Bu</u>), 0.83 (6H, d, ^3J = 6.6 Hz, NCH$_2$CH<u>Me</u>$_2$),

0.79 (6H, d, ^{3}J = 6.6 Hz, NCH$_2$CH$\underline{\text{Me}}_2$) ppm. ^{13}C-{^{1}H} NMR (C_6D_5Br, 75.4 MHz, 293 K) 176.7 (O$\underline{\text{C}}$(Me)N^{t}Bu), 161.3 (N$\underline{\text{C}}$(N^{i}BuMe)$_2$), 148.9 (br d, $^{1}J_{CF}$ = 244.4 Hz, *o*-$\underline{\text{C}}_6F_5$), 138.6 (br d, $^{1}J_{CF}$ = 247.8 Hz , *p*-C_6F_5), 136.8 (br d, $^{1}J_{CF}$ = 249.0 Hz, *m*-C_6F_5), 130.0 ($\underline{\text{C}}_5\text{Me}_5$), 59.6 (N$\underline{\text{C}}H_2$CHMe$_2$), 54.6 (N$\underline{\text{C}}Me_3$), 38.8 (NC(N^{i}Bu$\underline{\text{Me}}$)$_2$), 30.4 (NC$\underline{\text{Me}}_3$), 26.7 (NCH$_2\underline{\text{C}}HMe_2$), 20.4 (OC($\underline{\text{Me}}$)N^{t}Bu), 19.9 (NCH$_2CH\underline{\text{Me}}_2$), 19.4 (NCH$_2CH\underline{\text{Me}}_2$), 12.3 ($\text{C}_5\underline{\text{Me}}_5$) ppm. ^{19}F NMR ($CD_2Cl_2$, 282.1 MHz, 293K) -131.5 (m, *o*-C_6F_5), -162.0 (m, *p*-C_6F_5), -165.9 (m, *m*-C_6F_5) ppm. ^{11}B NMR (CD_2Cl_2, 96.2 MHZ, 293K) -16.1 ppm. IR (NaCl plates, Nujol mull, cm^{-1}) 1643 (m), 1596 (w), 1513 (s), 1495 (s), 1411 (s), 1341 (s), 1272 (m), 1213 (w), 1153 (w), 1083 (s), 1056 (m), 1031 (w), 978 (s), 862 (w), 849 (w), 836 (w), 793 (w), 774 (w), 755 (m), 683 (w), 660 (w). Anal. Found (calcd. for $C_{51}H_{51}BF_{20}N_4OTi$): C, 52.27 (52.15); H, 4.43 (4.38); N, 4.67 (4.77).

[Cp*Ti{NC(NMe$_2$)$_2$}{BnC(N^{i}Pr)$_2$}][BF$_{20}$] (48-[BF$_{20}$])

Cp*Ti{NC(NMe$_2$)$_2$}Bn$_2$ (248 mg, 0.52 mmol) and ^{i}PrNCN^{i}Pr (80 µl, 65 mg, 0.52 mmol) were mixed together in fluorobenzene (10 ml). To this a solution of TBF_{20} (477 mg, 0.52 mmol) in fluorobenzene (10 ml) was added dropwise. After 30 min pentane (20 ml) was added resulting in the formation of a brown oil. The pentane/fluorobenzene was decanted and the oil washed further with pentane (10 ml). The remaining solvent was removed *in vacuo* to yield a brown solid as the product. Yield: 0.43 g (70%). ^{1}H NMR (C_6D_5Br, 299.9 MHz, 293 K) 7.20-6.70 (5H, m, CH$_2\underline{\text{Ph}}$), 3.65 (2H, s, C$\underline{\text{H}}_2$Ph), 3.40 (2H, sept, ^{3}J = 6.3 Hz, NC$\underline{\text{H}}$Me$_2$), 2.36 (12H, s, NC(N$\underline{\text{Me}}_2$)$_2$), 1.77 (15H, s, $\text{C}_5\underline{\text{Me}}_5$), 0.73 (6H, d, ^{3}J = 6.3 Hz, NCH$\underline{\text{Me}}_2$), 0.64 (6H, d, ^{3}J = 6.3 Hz, NCH$\underline{\text{Me}}_2$) ppm. ^{13}C-{^{1}H} NMR (C_6D_5Br, 75.4 MHz, 293 K) 168.8 (BnC(N^{i}Pr)$_2$), 161.3 (N$\underline{\text{C}}$(NMe$_2$)$_2$), 148.9 (br d, $^{1}J_{CF}$ = 244.4 Hz, *o*-$\underline{\text{C}}_6F_5$), 138.6 (br d, $^{1}J_{CF}$ = 247.8 Hz , *p*-C_6F_5), 136.8 (br d, $^{1}J_{CF}$ = 249.0 Hz, *m*-C_6F_5), 134.2 (*i*-Bn), 129.3 (*o*-Bn), 128.6 ($\underline{\text{C}}_5\text{Me}_5$) 127.9 (*m*-Bn), 126.2 (*p*-Bn), 50.7 (N$\underline{\text{C}}$HMe$_2$), 40.2 (NC(N$\underline{\text{Me}}_2$)$_2$), 32.9 ($\underline{\text{C}}$H$_2$Ph), 25.8 (N$\underline{\text{C}}$HMe$_2$), 24.9 (N$\underline{\text{C}}$HMe$_2$), 13.0 ($\text{C}_5\underline{\text{Me}}_5$) ppm. ^{19}F NMR ($C_6D_5Br$, 282.1 MHz, 293 K) -132.1 (m, *o*-C_6F_5), -162.6 (m, *p*-C_6F_5), -166.4 (m, *m*-C_6F_5) ppm. ^{11}B NMR (C_6D_5Br, 96.2 MHz, 293 K) -16.1 ppm. IR (NaCl plates, Nujol mull, cm^{-1}) 1643 (m), 1576 (w), 1559 (w), 1514 (s), 1420 (m), 1403 (s), 1343 (m), 1276 (m), 1204 (w), 1181 (w), 1149 (w), 1086 (m), 1026 (w), 852 (m), 774 (m), 756 (m), 768 (m), 728 (m), 703 (w), 683 (w), 661 (m). Anal. found (calcd. for $C_{53}H_{48}BF_{20}N_5Ti$) C, 53.36 (53.33); H, 3.97 (4.05); N, 5.69 (5.87).

NMR tube scale synthesis of [Cp*Ti{NC(NMe$_2$)$_2$}{OC(Bn)N^{t}Bu}][BF$_{20}$] (49-[BF$_{20}$])

To a solution of Cp*Ti{NC(NMe$_2$)$_2$}Bn$_2$ (20 mg, 0.04 mmol) and ^{t}BuNCO (4 mg, 5 µl, 0.04 mmol) in C_6D_5Br (0.5 ml) was added TBF_{20} (39 mg, 0.04 mmol) resulting in the formation of a red solution. The red solution was transferred to an NMR tube and the ^{1}H NMR spectrum recorded after 5 min. ^{1}H NMR (C_6D_5Br, 299.9 MHz, 293 K) 7.16-6.40 (5H, m, $C_6\underline{H}_5$), 3.65 (1H, d, ^2J = 14.5 Hz, C$\underline{H}_2$), 3.54 (1H, d, ^2J = 14.5 Hz, C$\underline{H}_2$), 2.27 (12H, s, N$\underline{Me}_2$), 1.67 (15H, s, $C_5\underline{Me}_5$), 0.99 (9H, s, ^{t}Bu) ppm.

[Cp*Ti{NC(NMe$_2$)$_2$}(NCMe$_2$)(NCMe)][BF$_{20}$] (50-[BF$_{20}$])

Cp*Ti{NC(NMe$_2$)$_2$}Me$_2$ (300 mg, 0.92 mmol) and 2 equivs MeCN (96 µl, 75 mg, 1.83 mmol) were mixed together in fluorobenzene (10 ml). To this a solution of TBF_{20} (845 mg, 0.92 mmol) in fluorobenzene (10 ml) was added. After 30 min pentane (20 ml) was added resulting in the formation of a red oil. The pentane/fluorobenzene was decanted and the oil washed further with pentane (10 ml). The remaining solvent was removed *in vacuo* to yield an orange solid as the product. Yield: 0.85g (86%). ^{1}H NMR (CD_2Cl_2, 299.9 MHz, 293 K) 2.80 (12H, s, NC(N$\underline{Me}$)$_2$), 2.41 (3H, s, $\underline{Me}$CN), 1.99 ($C_5\underline{Me}_5$), 1.95 (NC$\underline{Me}_2$) ppm. ^{13}C-{^{1}H} NMR (CD_2Cl_2, 75.4 MHz, 293 K) 179.1 (N$\underline{C}$Me$_2$), 159.8 (N$\underline{C}$(NMe)$_2$), 148.7 (br d, $^1J_{CF}$ = 241.7 Hz, *o*-$\underline{C}_6F_5$), 139.0 (br d, $^1J_{CF}$ = 245.1 Hz, *p*-$\underline{C}_6F_5$), 136.9 (br d, $^1J_{CF}$ = 244.4 Hz, *m*-$\underline{C}_6F_5$), 128.4 (Me$\underline{C}$N), 122.1 ($\underline{C}_5Me_5$), 40.3 (NC(N$\underline{Me}_2$)$_2$), 29.0 (NC$\underline{Me}_2$), 12.3 ($C_5\underline{Me}_5$), 3.4 ($\underline{Me}$CN) ppm. ^{19}F NMR (CD_2Cl_2, 282.1 MHz, 293K) -133.1 (m, *o*-C_6F_5), -163.7 (m, *p*-C_6F_5), -167.6 (m, *m*-C_6F_5) ppm. ^{11}B NMR (CD_2Cl_2, 96.2 MHZ, 293K) -16.1 ppm. IR (NaCl plates, Nujol mull, cm^{-1}) 2318 (w), 2289 (w), 1679 (w), 1643 (m), 1617 (w), 1514 (s), 1419 (s), 1405 (s), 1274 (m), 1199 (w), 1146 (w), 1084 (s), 978 (s), 904 (w), 856 (m), 804 (w), 775 (m), 768 (m), 756 (m), 726 (m), 684 (w), 661 (m). Anal. Found (calcd. for $C_{44}H_{36}BF_{20}N_5Ti$): C, 49.03 (49.23); H, 3.08 (3.38); N, 6.36 (6.58).

[Cp*Ti{NC(N(Xyl)CH$_2$)$_2$}(NCMe$_2$)(NCMe)][BF$_{20}$] (51-[BF$_{20}$])

Cp*Ti{NC(N(Xyl)CH$_2$)$_2$}Me$_2$ (40 mg, 0.08 mmol) and 2 equivs MeCN (8 µl, 7 mg, 0.16 mmol) were mixed together in fluorobenzene (10 ml). To this a solution of TBF_{20} (73 mg, 0.08 mmol) in fluorobenzene (10 ml) was added. After 30 min pentane (20 ml) was added resulting in the formation of a red oil. The pentane/fluorobenzene was decanted and the oil washed further with pentane (10 ml). The remaining solvent was

removed *in vacuo* to yield an orange solid as the product. Yield: 57 mg (58%) ^{1}H NMR (C_6D_5Br, 299.9 MHz, 293 K) 7.11-6.77 (6H, $C_6\underline{H}_3Me_2$), 3.29 (4H, s, $C\underline{H}_2C\underline{H}_2$), 2.10 (6H, s, $C_6H_3\underline{Me}Me$), 2.07 (6H, s, $C_6H_3Me\underline{Me}$), 1.57 (6H, s, $NC\underline{Me}_2$), 1.55 (3H, s, $\underline{Me}CN$), 1.37 (15H, s, $C_5\underline{Me}_5$) ppm. ^{13}C-{^{1}H} NMR (C_6D_5Br, 75.4 MHz, 293 K) 178.3 ($NC\underline{Me}_2$), 149.1 ($N\underline{C}(N(Xyl)CH_2)_2$), 148.9 (br d, $^{1}J_{CF}$ = 244.4 Hz, *o*-$\underline{C}_6F_5$), 138.6 (br d, $^{1}J_{CF}$ = 247.8 Hz, *p*-C_6F_5), 137.5 (*i*-$\underline{C}_6H_3Me_2$), 137.4 (*o*-$\underline{C}_6H_3Me_2$), 136.8 (br d, $^{1}J_{CF}$ = 249.0 Hz, *m*-$\underline{C}_6F_5$), 136.1 (*o*-$\underline{C}_6H_3Me_2$), 128.9 (*m*-$\underline{C}_6H_3Me_2$), 128.8 (*m*-$\underline{C}_6H_3Me_2$), 128.6 (*p*-$\underline{C}_6H_3Me_2$), ($Me\underline{C}N$), 121.9 ($C_5\underline{Me}_5$), 45.5 ($C\underline{H}_2C\underline{H}_2$), 28.6 ($NC\underline{Me}_2$), 18.0 ($C_6H_3\underline{Me}Me$), 17.9 ($C_6H_3Me\underline{Me}$), 11.5 ($C_5Me_5$), 2.6 ($\underline{Me}CN$) ppm. ^{19}F NMR ($C_6D_5Br$, 282.1 MHz, 293 K) -131.4 (m, *o*-C_6F_5), -162.0 (m, *p*-C_6F_5), -165.8 (m, *m*-C_6F_5) ppm. ^{11}B NMR (C_6D_5Br, 96.2 MHz, 293 K) -16.0 ppm. IR (NaCl plates, Nujol mull, cm^{-1}) 2289 (w), 1643 (w), 1552 (s), 1513 (s), 1303 (w), 1281 (m), 1198 (w), 1085 (m), 979 (s), 869 (w), 774 (w), 756 (w), 661 (w). Anal. found (calcd. for $C_{58}H_{46}BF_{20}N_5Ti$) C, 55.51 (55.66); H, 3.58 (3.70); N, 5.70 (5.60).

NMR tube scale reaction of Lewis base adducts with carbodiimide

The general procedure is as follows. The Lewis base stabilized cations **8**$^{+}$, **9**$^{+}$, **11**$^{+}$, **12**$^{+}$, **13**$^{+}$, **16**$^{+}$, **17**$^{+}$, **18**$^{+}$, **22**$^{+}$, **23**$^{+}$, **24**$^{+}$, **26**$^{+}$, **27**$^{+}$ or **28**$^{+}$ was dissolved in C_6D_5Br (0.5 ml). Following this 1 equiv of ^{i}PrNCN^{i}Pr was added and the reaction followed by ^{1}H NMR spectroscopy. THF adducts **9**$^{+}$, **13**$^{+}$, **18**$^{+}$, **24**$^{+}$ and **28**$^{+}$ reacted immediately with ^{i}PrNCN^{i}Pr to give the κ^2-amidinate species **35**$^{+}$, **37**$^{+}$, **43**$^{+}$, **44**$^{+}$ and **45**$^{+}$. Pyridine adducts **8**$^{+}$, **12**$^{+}$ and **17**$^{+}$, **23**$^{+}$ and **27**$^{+}$ also reacted with ^{i}PrNCN^{i}Pr but over the period of *ca.* 2 h in each case to yield the respective κ^2-amidinate supported species. $OPPh_3$ adducts **11**$^{+}$, **16**$^{+}$, **22**$^{+}$ and **26**$^{+}$ showed no reaction.

NMR tube scale synthesis of [Cp*Ti{NC(N^{i}Pr$_2$)Ph}{Me$_3$SiCC(Ph)Me}][BF$_{20}$] (52-[BF$_{20}$])

Cp*Ti{NC(N^{i}Pr$_2$)Ph}Me$_2$ (50 mg, 0.12 mmol) and $Me_3SiCCPh$ (21 mg, 24 μl, 0.12 mmol) were mixed together in C_6D_5Br (0.5 ml). To this TBF_{20} (111 mg, 0.12 mmol) was added resulting in the formation of a red solution. The red solution was transferred to an NMR tube and the NMR spectra recorded after 5 min. The product exists as a mixture of isomers (**52a**$^{+}$ and **52b**$^{+}$). The quoted integrals are self-consistent within each isomer. ^{1}H NMR (C_6D_5Br, 299.9 MHz, 293 K) 7.55-6.60 (20H, m, NC(N^{i}Pr$_2$)$\underline{Ph}$ and $Me_3SiCC(\underline{Ph})Me$, **52a**$^{+}$ and **52b**$^{+}$), 4.47 (2H, br, $NC\underline{H}Me_2$, **52a**$^{+}$ and **52b**$^{+}$), 3.42

(1H, sept, ^3J = 6.9 Hz, NC<u>H</u>Me$_2$, **52b**$^+$), 3.35 (1H, sept, ^3J = 6.9 Hz NC<u>H</u>Me$_2$, **52a**$^+$), 1.92 (3H, s, CC<u>Me</u>, **52a**$^+$), 1.68 (3H, s, CC<u>Me</u>, **52b**$^+$), 1.65 (15H, s, C$_5$<u>Me</u>$_5$, **52b**$^+$), 1.43 (15H, s, C$_5$<u>Me</u>$_5$, **52a**$^+$), 1.31 (3H, d, ^3J = 6.9 Hz, NCH<u>Me</u>$_2$, **52b**$^+$), 1.20 (3H, d, ^3J = 6.9 Hz, NCH<u>Me</u>$_2$, **52b**$^+$), 1.16 (3H, d, ^3J = 6.9 Hz, NCH<u>Me</u>$_2$, **52a**$^+$), 1.12 (3H, d, ^3J = 6.9 Hz, NCH<u>Me</u>$_2$, **52a**$^+$), 0.76 (9H, overlapping doublets, NCH<u>Me</u>$_2$, **52a**$^+$ and **52b**$^+$), 0.71 (3H, d, ^3J = 6.9 Hz, NCH<u>Me</u>$_2$, **52a**$^+$ and **52b**$^+$), -0.15 (9H, s, Si<u>Me</u>$_3$ **52a**$^+$), -0.52 (9H, s, Si<u>Me</u>$_3$ **52a**$^+$) ppm. ^{13}C-{^{1}H} NMR (C$_6$D$_5$Br, 75. MHz, 293 K) 236.1 (Ti<u>C</u>, **52a**$^+$), 230.2 (Ti<u>C</u>, **52b**$^+$), 170.5 (N<u>C</u>(N^{i}Pr$_2$)Ph, **52a**$^+$ and **52b**$^+$), 166.7 (C<u>C</u>Me, **52b**$^+$), 148.9 (br d, $^1J_{CF}$ = 244.4 Hz, *o*-<u>C</u>$_6$F$_5$), 144.2 (C<u>C</u>Me, **52a**$^+$), 138.6 (br d, $^1J_{CF}$ = 247.8 Hz , *p*-<u>C</u>$_6$F$_5$), 136.8 (br d, $^1J_{CF}$ = 249.0 Hz, *m*-<u>C</u>$_6$F$_5$), 138.7 (*i*-NC(N^{i}Pr$_2$)<u>Ph</u>, **52b**$^+$), 136.5 (*i*-NC(N^{i}Pr$_2$)<u>Ph</u>, **52a**$^+$), 131.5 (*i*-Me$_3$SiCC(<u>Ph</u>)Me, **52a**$^+$ or **52b**$^+$), 129.9 (<u>C</u>$_5$Me$_5$, **52a**$^+$), 129.3 (Ar), 128.5 (Ar), 127.4 (<u>C</u>$_5$Me$_5$, **52b**$^+$), 124.6 (Ar), 50.5 (NCH<u>Me</u>$_2$, **52a**$^+$ and **52b**$^+$), 49.7 (NCH<u>Me</u>$_2$, **52a**$^+$ and **52b**$^+$), 33.8 (CC<u>Me</u>, **52b**$^+$), 26.2 (CC<u>Me</u>, **52a**$^+$), 23.9 (NCH<u>Me</u>$_2$, **52a**$^+$ or **52b**$^+$), 21.8 (NCH<u>Me</u>$_2$, **52a**$^+$ or **52b**$^+$), 21.5 (NCH<u>Me</u>$_2$, **52a**$^+$ or **52b**$^+$), 21.4 (NCH<u>Me</u>$_2$, **52a**$^+$ or **52b**$^+$), 21.2 (NCH<u>Me</u>$_2$, **52a**$^+$ or **52b**$^+$), 21.0 (NCH<u>Me</u>$_2$, **52a**$^+$ or **52b**$^+$), 13.9 (C$_5$<u>Me</u>$_5$, **52a**$^+$), 13.5 (C$_5$<u>Me</u>$_5$, **52b**$^+$), 2.7 (Si<u>Me</u>$_3$, **52b**$^+$), 2.5 (Si<u>Me</u>$_3$, **52a**$^+$) ppm. Resonances labeled Ar could not be unambiguously assigned. ^{29}Si NMR (C$_6$D$_5$Br, 59.6 MHz, 293 K) -16.0 (**52a**$^+$), -43.2 (**52b**$^+$) ppm. ^{19}F NMR (C$_6$D$_5$Br, 282.1 MHz, 293 K) -131.5 (m, *o*-C$_6$F$_5$), -162.1 (m, *p*-C$_6$F$_5$), -165.8 (m, *m*-C$_6$F$_5$) ppm. ^{11}B NMR (C$_6$D$_5$Br, 96.2 MHz, 293 K) -16.1 ppm.

NMR tube scale synthesis of [Cp*Ti{NC(N^{i}Pr$_2$)Ar^{F2}}{Me$_3$SiCC(Ph)Me}][BF$_{20}$] (53-[BF$_{20}$])

Cp*Ti{NC(N^{i}Pr$_2$)Ar^{F2}}Me$_2$ (30 mg, 0.07 mmol) and Me$_3$SiCCPh (12 mg, 13 µl, 0.07 mmol) were mixed together in C$_6$D$_5$Br (0.5 ml). To this TBF$_{20}$ (61 mg, 0.07 mmol) was added resulting in the formation of a red solution. The red solution was transferred to an NMR tube and the spectrum recorded after 5 min. The product exists as a mixture of isomers (**53a**$^+$ and **53b**$^+$). The quoted integrals are self-consistent within each isomer. ^{1}H NMR (C$_6$D$_5$Br, 299.9 MHz, 293 K) 7.19-6.60 (16H, <u>Ar</u>^{F2} and Me$_3$SiCC(<u>Ph</u>)Me, **53a**$^+$ and **53b**$^+$), 4.60 (1H, br, NC<u>H</u>Me$_2$, **53a**$^+$), 3.59 (1H, br, NC<u>H</u>Me$_2$, **53b**$^+$), 3.37 (2H, sept, ^{3}J = 6.8 Hz, NC<u>H</u>Me$_2$, **53a**$^+$ and **53b**$^+$), 1.91 (3H, s, CC<u>Me</u>, **53a**$^+$), 1.71 (15H, s, C$_5$<u>Me</u>$_5$, **53b**$^+$), 1.52 (3H, s, CC<u>Me</u>, **53b**$^+$), 1.45 (15H, s, C$_5$<u>Me</u>$_5$, **53a**$^+$), 1.29 (3H, br, NCH<u>Me</u>$_2$, **53b**$^+$), 1.17 (3H, d, ^3J = 6.8 Hz, NCH<u>Me</u>$_2$, **53b**$^+$), 1.08 (3H, d, ^3J = 6.8 Hz, NCH<u>Me</u>$_2$, **53a**$^+$), 0.85 (3H, d, ^3J = 6.8 Hz, NCH<u>Me</u>$_2$,

53a$^+$), 0.82 (3H, m, NCH$\underline{Me}_2$, **53b**$^+$), -0.22 (9H, s, $SiMe_3$, **53a**$^+$), -0.46 (9H, s, **53b**$^+$) ppm. ^{13}C-{^1H} NMR (C_6D_5Br, 75.4 MHz, 293 K) 237.4 (Ti$\underline{C}$, **53a**$^+$), 230.8 (Ti$\underline{C}$, **53b**$^+$), 166.0 (C$\underline{C}$Me, **53b**$^+$), 158.4 (dd, $^1J_{CF}$ = 250.1 Hz, $^3J_{CF}$ = 6.8 Hz, *o*-$\underline{C}_6H_3F_2$, **53b**$^+$), 158.1 (dd, $^1J_{CF}$ = 250.1 Hz, $^3J_{CF}$ = 6.7 Hz, *o*-$\underline{C}_6H_3F_2$, **53a**$^+$), 156.7 (N$\underline{C}$(N^iPr_2)Ar^{F2}, **53b**$^+$), 156.2 (N$\underline{C}$(N^iPr_2)Ar^{F2}, **53a**$^+$), 148.9 (br d, $^1J_{CF}$ = 244.4 Hz, *o*-$\underline{C}_6F_5$), 144.2 (C$\underline{C}$Me, **53a**$^+$), 138.6 (br d, $^1J_{CF}$ = 247.8 Hz , *p*-$\underline{C}_6F_5$), 136.8 (br d, $^1J_{CF}$ = 249.0 Hz, *m*-$\underline{C}_6F_5$), 132.1 (*i*-$Me_3SiCC(\underline{Ph})Me$, **53a**$^+$ or **53b**$^+$), 130.3 ($\underline{C}_5Me_5$, **53a**$^+$), 128.7 (*o*-$Me_3SiCC(\underline{Ph})Me$, **53a**$^+$ and **53b**$^+$), 128.4 ($\underline{C}_5Me_5$, **53b**$^+$), 126.9 (*m*-$Me_3SiCC(\underline{Ph})Me$, **53a**$^+$ and **53b**$^+$), 125.2 (*p*-$Me_3SiCC(\underline{Ph})Me$, **53a**$^+$ and **53b**$^+$), 114.9 (t, $^2J_{CF}$ = 21.8 Hz, *i*-$\underline{C}_6H_3F_2$), 114.8 (t, $^2J_{CF}$ = 22.1 Hz, *i*-$\underline{C}_6H_3F_2$), 112.3 (overlapping m, *m*-$\underline{C}_6H_3F_2$), (TiC$\underline{C}$MePh, **53b**$^+$), (TiC$\underline{C}$MePh, **53a**$^+$), 49.6 (N$\underline{C}$HMe_2, **53a**$^+$), 49.1 (N$\underline{C}$HMe_2, **53b**$^+$), 33.5 (C$\underline{Me}$Ph, **53b**$^+$), 26.1 (C$\underline{Me}$Ph, **53a**$^+$), 21.8 (NCH$\underline{Me}_2$, **53a**$^+$ or **53b**$^+$), 20.4 (NCH$\underline{Me}_2$, **53a**$^+$ or **53b**$^+$), 20.3 (NCH$\underline{Me}_2$, **53a**$^+$ or **53b**$^+$), 20.1 (NCH$\underline{Me}_2$, **53a**$^+$ or **53b**$^+$), 20.0 (NCH$\underline{Me}_2$, **53a**$^+$ or **53b**$^+$), 12.6 ($C_5\underline{Me}_5$, **53a**$^+$), 12.4 ($C_5\underline{Me}_5$, **53b**$^+$), 1.5 (Si$\underline{Me}_3$, **53b**$^+$) 1.0 (Si$\underline{Me}_3$, **53a**$^+$) ppm. ^{29}Si NMR (C_6D_5Br, 59.6 MHz, 293 K) -15.8 (**53a**$^+$), -42.0 (**53b**$^+$) ppm. ^{19}F NMR (C_6D_5Br, 282.1 MHz, 293 K) -108.8 ($C_6H_3\underline{F}_2$, **53a**$^+$),-111.9 ($C_6H_3\underline{F}_2$, **53b**$^+$), -131.4 (m, *o*-C_6F_5), -162.0 (m, *p*-C_6F_5), -165.8 (m, *m*-C_6F_5) ppm. ^{11}B NMR (C_6D_5Br, 96.2 MHz, 293 K) -16.1 ppm.

[Cp*$_2$Ti$_2${NC(N^iPr_2)Ar^{F2}}$_2$(μ-Br)$_2$][BF_{20}]$_2$ (54-[BF_{20}])

[Cp*Ti{NC(N^iPr_2)Ar^{F2}}{$Me_3SiCC(Ph)Me$}][BF_{20}] (57 mg, 0.04 mmol) generated *in situ* in C_6D_5Br was left to stand for 2 h resulting in the formation of crystals of the product. The crystals were washed with pentane (5 ml) and dried *in vacuo* yielding the product as a brown solid. Yield: 47 mg (90%). IR (NaCl plates, Nujol mull, cm^{-1}). 1645 (w), 1533 (m), 1457 (s), 1421 (m), 1264 (w), 1086 (s), 1021 (m), 981 (m), 755 (m), 682 (w). Anal. found (calcd. for $C_{94}H_{66}B_2Br_2F_{44}N_4Ti_2$) C, 47.85 (47.75); H, 2.76 (2.81); N, 2.36 (2.37). Single crystals suitable for X-ray diffraction were grown from a C_6D_5Br solution at room temperature.

[Cp*Ti{NC(N^iPr_2)Ar^{F2}}{($Me_3SiCC(Ph)Me$)C($N^iPr)_2$}][BF_{20}] (55-[BF_{20}])

Cp*Ti{NC(N^iPr_2)Ar^{F2}}Me_2 (200 mg, 0.44 mmol) and TBF_{20} (408 mg, 0.44 mmol) were mixed together in fluorobenzene (10 ml) after 1 min $Me_3SiCCPh$ (77 mg, 87 μl, 0.44 mmol) was added. After another 5 min ^{i}PrNCN^{i}Pr (56 mg, 69 μl, 0.44 mmol) was added and the mixture was left for 10 min before pentane (10 mL) was added resulting

in the formation of a brown oil. The pentane/fluorobenzene was decanted and the solid washed further with pentane (10 ml). The solid was dried *in vacuo* yielding the product as a brown solid. Yield: 482 mg (77%). ^{1}H NMR (C_6D_5Br, 299.9 MHz, 293 K) 7.20-6.83 (8H, m, $C_6\underline{H}_3F_2$ and $C_6\underline{H}_5$), 4.68 (1H, br, κ^1-NC$\underline{H}$Me$_2$), 3.79 (2H, sept, ^{3}J = 6.30 Hz, κ^2-NC$\underline{H}$Me$_2$), 3.47 (1H, sept, ^{3}J = 6.8 Hz, κ^1-NC$\underline{H}$Me$_2$), 2.08 (15H, s, $C_5\underline{Me}_5$), 2.00 (3H, s, (Me$_3$SiCC(Ph)$\underline{Me}$)C(N^{i}Pr)$_2$), 1.12 (6H, d, ^{3}J = 6.8 Hz, κ^1-NCH$\underline{Me}_2$), 1.06 (3H, d, ^{3}J = 6.30 Hz, κ^2-NCH$\underline{Me}_2$), 0.95 (6H, d, ^{3}J = 6.8 Hz, κ^1-NCH$\underline{Me}_2$), 0.45 (3H, br, κ^2-NCH$\underline{Me}_2$), 0.00 (9H, s, Si$\underline{Me}_3$) ppm. ^{13}C-{^{1}H} NMR (C_6D_5Br, 75.4 MHz, 293 K) 171.7 (-$\underline{C}$(N^{i}Pr)$_2$), 158.2 (dd, $^{1}J_{CF}$ = 250 Hz, $^{3}J_{CF}$ = 7.0 Hz, *o*-$\underline{C}_6H_3F_2$), 156.4 (*i*-$\underline{C}_6H_5$), 155.7 (N$\underline{C}$(N^{i}Pr$_2$)Ar^{F2}) 148.9 (br d, $^{1}J_{CF}$ = 244.4 Hz, *o*-$\underline{C}_6F_5$), 142.3 (*o*-$\underline{C}_6H_5$), 138.6 (br d, $^{1}J_{CF}$ = 247.8 Hz , *p*-$\underline{C}_6F_5$), 136.8 (br d, $^{1}J_{CF}$ = 249.0 Hz, *m*-$\underline{C}_6F_5$), 130.8 ($\underline{C}_5Me_5$), 129.9 (Me$_3$Si$\underline{C}$C(Ph)Me), 128.4 (*m*-$\underline{C}_6H_5$), 126.0 (*p*-$\underline{C}_6H_5$), 114.8 (t, $^{2}J_{CF}$ = 21.0 Hz, *i*-$C_6\underline{H}_3F_2$), 112.0 (dd, $^{2}J_{CF}$ = 21.0 Hz, $^{4}J_{CF}$ = 3.0 Hz, *m*-$C_6\underline{H}_3F_2$), 52.3 (κ^2-N$\underline{C}$HMe$_2$), 49.4 (κ^1-N$\underline{C}$HMe$_2$), 49.0 (κ^1-N$\underline{C}$HMe$_2$), 28.2 (CC$\underline{Me}$), 26.1 (κ^1-N$\underline{C}$HMe$_2$), 24.6 (κ^2-N$\underline{C}$HMe$_2$), 21.9 (κ^1-N$\underline{C}$HMe$_2$), 20.6 (κ^2-N$\underline{C}$HMe$_2$), 13.0 ($C_5\underline{Me}_5$), 0.7 (Si$\underline{Me}_3$) ppm. ^{19}F NMR (C_6D_5Br, 282.1 MHz, 293 K) -108.7 ($C_6H_3\underline{F}_2$), -131.8 (m, *o*-C_6F_5), -162.1 (m, *p*-C_6F_5), -165.9 (m, *m*-C_6F_5) ppm. ^{11}B NMR (C_6D_5Br, 96.2 MHz, 293 K) -16.1 ppm. ^{29}Si NMR (C_6D_5Br, 59.6 MHz, 293 K) -8.5 ppm. IR (NaCl plates, Nujol mull, cm^{-1}) 1642 (w), 1623 (w), 1588 (w), 1512 (s), 1327 (m), 1274 (w), 1206 (w), 1137 (w), 1084 (m), 979 (m), 841 (w), 765 (w), 756 (w), 703 (w) , 683 (w). Anal. found (calcd. for $C_{66}H_{63}BF_{22}N_4SiTi$) C, 55.84 (55.94); H, 4.55 (4.48); N, 4.12 (3.95).

[Cp*Ti{NC(N^{i}Pr$_2$)Ph}{(Me$_3$SiCC(Ph)Me)C(N^{i}Pr)$_2$}][BF$_{20}$] (56-[BF$_{20}$])

Cp*Ti{NC(N^{i}Pr$_2$)Ph}Me$_2$ (100 mg, 0.24 mmol) and TBF$_{20}$ (222 ml, 0.24 mmol) were mixed together in fluorobenzene (10 ml) after 1 min Me$_3$SiCCPh (42 mg, 47 µl, 0.24 mmol) was added. After another 5 min ^{i}PrNCN^{i}Pr (30 mg, 37 µL, 0.24 mmol) was added and the mixture was left for 10 min before pentane (10 mL) was added resulting in the formation of a brown oil. The pentane/fluorobenzene was decanted and the oil washed further with pentane (10 ml). The remaining solvent was removed *in vacuo* yielding the product as a brown solid. Yield: 255 mg (77%). The product exists as a mixture of isomers (**56a**$^{+}$ and **56b**$^{+}$). The quoted integrals are self-consistent within each isomer. ^{1}H NMR (C_6D_5Br, 299.9 MHz, 293 K) 7.16-6.18 (20H, m, NC(N^{i}Pr$_2$)$\underline{Ph}$ and Me$_3$SiCC($\underline{Ph}$)Me, **56a**$^{+}$ and **56b**$^{+}$), 4.41 (2H, m, κ^1-NC$\underline{H}$Me$_2$, **56a**$^{+}$ and **56b**$^{+}$), (4H, m, κ^2-NC$\underline{H}$Me$_2$, **56a**$^{+}$ and **56b**$^{+}$), 3.27 (2H, m, κ^1-NC$\underline{H}$Me$_2$, **56a**$^{+}$ and **56b**$^{+}$), 1.90 (3H,

s, $Me_3SiCC(Ph)\underline{Me}$, **56b**$^+$), 1.88 (15H, s, $C_5\underline{Me}_5$, **56a**$^+$), 1.87 (3H, s, $Me_3SiCC(Ph)\underline{Me}$, **56a**$^+$), 1.85 (15H, s, $C_5\underline{Me}_5$, **56b**$^+$), 1.09 (6H, br, κ^1-$NCH\underline{Me}_2$, **56a**$^+$ and **56b**$^+$), 0.94 (12H, d, ^3J = 6.2 Hz, κ^2-$NCH\underline{Me}_2$, **56a**$^+$ and **56b**$^+$), 0.84 (6H, d, ^3J = 6.9 Hz, κ^1-$NCH\underline{Me}_2$, **56a**$^+$ and **56b**$^+$), 0.74 (6H, d, ^3J = 6.9 Hz, κ^1-$NCH\underline{Me}_2$, **56a**$^+$ and **56b**$^+$), 0.69 (6H, d, ^3J = 6.9 Hz, κ^1-$NCH\underline{Me}_2$, **56a**$^+$ and **56b**$^+$), 0.19 (6H, br , κ^2-$NCH\underline{Me}_2$, **56a**$^+$ and **56b**$^+$), -0.18 (9H, s, $Si\underline{Me}_3$, **56a**$^+$), -0.19 (9H, s, $Si\underline{Me}_3$, **56b**$^+$) ppm. ^{13}C-{^1H} NMR (C_6D_5Br, 75.4 MHz, 293 K) 52.1 (κ^2-$N\underline{C}HMe_2$ **56a**$^+$ and **56b**$^+$), 52.0 (κ^1-$N\underline{C}HMe_2$, **56a**$^+$ and isomer), 49.4 (κ^1-$N\underline{C}HMe_2$, **56a**$^+$ or **56b**$^+$), 49.1 (κ^1-$N\underline{C}HMe_2$, **56a**$^+$ or **56b**$^+$), 171.9 (-$\underline{C}(N^iPr)_2$, **56a**$^+$), 171.8 (-$\underline{C}(N^iPr)_2$, **56b**$^+$), 168.6 ($N\underline{C}(N^iPr_2)Ph$, **56b**$^+$), 168.5 ($N\underline{C}(N^iPr_2)Ph$, **56a**$^+$), 155.5 (*i*-$Me_3SiCC(\underline{Ph})Me$, **56b**$^+$), 155.1 (*i*-$Me_3SiCC(\underline{Ph})Me$, **56a**$^+$), 148.9 (br d, $^1J_{CF}$ = 244.4 Hz, *o*-$\underline{C}_6F_5$), 142.4 (*o*-$Me_3SiCC(\underline{Ph})Me$, **56b**$^+$), 142.1 (*o*-$Me_3SiCC(\underline{Ph})Me$, **56a**$^+$), 138.6 (br d, $^1J_{CF}$ = 247.8 Hz , *p*-$\underline{C}_6F_5$), 136.8 (br d, $^1J_{CF}$ = 249.0 Hz, *m*-$\underline{C}_6F_5$), 136.3 (*i*-$NC(N^iPr_2)\underline{Ph}$, **56a**$^+$), 136.1 (*i*-$NC(N^iPr_2)\underline{Ph}$, **56b**$^+$), 131.6 ($Me_3Si\underline{C}C(Ph)Me$, **56b**$^+$), 130.7 ($Me_3Si\underline{C}C(Ph)Me$, **56a**$^+$), 129.6 ($\underline{C}_5Me_5$, **56a**$^+$), 129.4 ($\underline{C}_5Me_5$, **56a**$^+$), 128.6 (Ar), 128.5 (Ar), 128.4 (Ar), 128.3 (Ar), 128.2 (Ar), 127.7 (Ar), 127.6 (Ar), 127.5 (Ar), 127.3 (Ar), 124.2 (*p*-$NC(N^iPr_2)\underline{Ph}$), 32.0 ($\kappa^1$-$NCH\underline{Me}_2$, **56a**$^+$ and **56b**$^+$), 28.9 ($CC\underline{Me}$, **56a**$^+$), 27.9 ($CC\underline{Me}$, **56b**$^+$), 26.3 (κ^1-$NCH\underline{Me}_2$, **56a**$^+$ and **56b**$^+$), 25.6 (κ^1-$NCH\underline{Me}_2$, **56a**$^+$ and **56b**$^+$), 24.6 (κ^2-$NCH\underline{Me}_2$, **56a**$^+$ and **56b**$^+$), 23.6 (κ^1-$NCH\underline{Me}_2$, **56a**$^+$ and **56b**$^+$), 23.1 (κ^1-$NCH\underline{Me}_2$, **56a**$^+$ and **56b**$^+$), 20.9 (κ^2-$NCH\underline{Me}_2$, **56a**$^+$ and **56b**$^+$), 13.4 ($C_5\underline{Me}_5$, **56a**$^+$ and **56b**$^+$), 0.94 ($Si\underline{Me}_3$, **56a**$^+$), 0.85 ($Si\underline{Me}_3$, **56b**$^+$) ppm. Resonances labeled Ar could not be unambiguously assigned. ^{29}Si NMR (C_6D_5Br, 59.6 MHz, 293 K) -7.7 and -8.1 ppm. ^{19}F NMR (C_6D_5Br, 282.1 MHz, 293 K) -108.7 ($C_6H_3\underline{F}_2$), -131.8 (m, *o*-C_6F_5), -162.1 (m, *p*-C_6F_5), -165.9 (m, *m*-C_6F_5) ppm. ^{11}B NMR (C_6D_5Br, 96.2 MHz, 293 K) -16.1 ppm. IR (NaCl plates, Nujol mull, cm^{-1}) 1642 (w), 1585 (w), 1513 (m), 1332 (w), 1274 (w), 1208 (w), 1137 (w), 1085 (m), 1028 (w), 978 (m), 841 (w), 788 (w), 775 (w), 684 (w). Anal. found (calcd. for $C_{66}H_{65}BF_{20}N_4SiTi$) C, 57.76 (57.40); H, 4.69 (4.74); N, 4.15 (4.06).

[Cp*Ti{NC(N^{i}Pr$_2$)Ph}{Ph$_2$PCC(Tol)Me}][BF$_{20}$] (57-[BF$_{20}$])

$Cp^*Ti\{NC(N^iPr_2)Ph\}Me_2$ (100 mg, 0.24 mmol) and $Ph_2PCCTol$ (72 mg, 0.24 mmol) were mixed together in fluorobenzene (10 ml). To this a solution of TBF_{20} (221 mg, 0.24 mmol) in fluorobenzene (5 ml) was added. After 2 h pentane (20 ml) was added resulting in the formation of a red oil. The pentane/fluorobenzene was decanted and the oil washed further with pentane (10 ml). The remaining solvent was removed *in*

vacuo yielding the product as a red solid. Yield: 219 mg (66%). ^{1}H NMR (C_6D_5Br, 299.9 MHz, 293 K) 7.50-6.68 (17H, m, Ar), 6.13 (2H, d , ^{3}J =6.6 Hz, *o*-Tol), 3.52 (1H, br, NC<u>H</u>Me_2), 3.37 (1H, sept, ^{3}J = 6.8 Hz, NC<u>H</u>Me_2), 2.04 (3H, s, C_6H_4<u>Me</u>), 1.89 (3H, d, $^{4}J_{PH}$= 1.8 Hz, Ph_2PCC(Tol)<u>Me</u>), 1.32 (15H, s, C_5<u>Me_5</u>), 0.98 (3H, d, ^{3}J = 6.8 Hz, NCH<u>Me_2</u>), 0.92 (3H, d, ^{3}J = 6.8 Hz, NCH<u>Me_2</u>), 0.67 (3H, d, ^{3}J = 6.8 Hz, NCH<u>Me_2</u>), 0.62 (3H, d, ^{3}J = 6.8 Hz, NCH<u>Me_2</u>) ppm. ^{13}C-{^{1}H} NMR (C_6D_5Br, 75.4 MHz, 293 K) 198.1 (Ti<u>C</u>, $^{1}J_{PC}$ = 101.5 Hz), 169.3 (N<u>C</u>($N^{i}Pr_2$)Ph), 165.2 (d, $^{2}J_{PC}$ = 12.8 Hz TiC<u>C</u>Me,), 148.9 (br d, $^{1}J_{CF}$ = 244.4 Hz, *o*-<u>C_6F_5</u>), 138.6 (br d, $^{1}J_{CF}$ = 247.8 Hz , *p*-<u>C_6F_5</u>), 136.8 (br d, $^{1}J_{CF}$ = 249.0 Hz, *m*-<u>C_6F_5</u>), 127.6 (<u>C_5Me_5</u>), 53.2 (N<u>C</u>HMe_2), 49.2 (N<u>C</u>HMe_2), 26.8 (d, $^{3}J_{PC}$ = 9.3 Hz, TiCC<u>Me</u>,), 21.4 (C_6H_4<u>Me</u>), 21.1 (NCH<u>Me_2</u>), 21.0 (NCH<u>Me_2</u>), 20.4 (NCH<u>Me_2</u>), 20.3 (NCH<u>Me_2</u>), 12.2 (C_5<u>Me_5</u>) ppm. ^{31}P-{^{1}H} NMR (C_6D_5Br, 121.4 MHz, 293 K) 28.0 ppm. ^{19}F NMR (C_6D_5Br, 282.1 MHz, 293 K) -131.8 (m, *o*-C_6F_5), -162.2 (m, *p*-C_6F_5), -166.0 (m, *m*-C_6F_5) ppm. ^{11}B NMR (C_6D_5Br, 96.2 MHz, 293 K) -16.1 ppm. IR (NaCl plates, Nujol mull, cm^{-1}) 1642 (w), 1512 (s), 1345 (m), 1261 (m), 1182(w), 1151 (w), 1084 (m), 1022 (w), 979 (s), 891 (w), 785 (w), 774(w), 738 (w), 723 (w), 683 (w), 660 (w). Anal. Found (calcd. for $BC_{69}F_{20}H_{54}N_2PTi$) C, 60.16 (60.02); H, 3.81 (3.94); N, 2.16 (2.03).

NMR tube scale synthesis of [Cp*Ti{NC($N^{i}Pr_2$)Ph}(CO_2){Ph_2PCC(Tol)Me}]-[BF_{20}] (58-[BF_{20}])

[Cp*Ti{NC($N^{i}Pr_2$)Ph}{Ph_2PCC(Tol)Me}][BF_{20}] (60 mg, 0.04 mmol) was dissolved in C_6D_5Br and the red solution was transferred to an NMR tube. This was then exposed to a CO_2 atmosphere at 1.25 atm for 10 min and then the NMR spectra recorded. ^{1}H NMR (C_6D_5Br, 299.9 MHz, 293 K) 7.85-6.83 (15H, NC($N^{i}Pr_2$)<u>Ph</u> and <u>Ph_2</u>PCC(Tol)Me), 6.61 (2H, d, ^{3}J = 7.6 Hz, *o*-Tol), 6.28 (2H, ^{3}J = 7.6 Hz, *m*-Tol), 3.53 (1H, br, NC<u>H</u>Me_2), 3.30 (1H, sept, ^{3}J = 6.9 Hz, NC<u>H</u>Me_2), 2.06 (3H, s, C_6H_4<u>Me</u>), 1.76 (3H, d, $^{4}J_{PH}$= 2.9 Hz, CC<u>Me</u>), 1.50 (15H, s, C_5<u>Me_5</u>), 0.96 (6H, d, ^{3}J = 6.9 NCH<u>Me_2</u>), 0.70 (6H, d, ^{3}J = 6.9, NCH<u>Me_2</u>) ppm. ^{13}C-{^{1}H} NMR (C_6D_5Br, 75.4 MHz, 293 K) 174.9 (d, $^{2}J_{PC}$ = 6.1 Hz, C<u>C</u>Me), 167.6 (N<u>C</u>($N^{i}Pr_2$)Ph), 166.0 (d, $^{1}J_{PC}$ = 121.3 Hz, O<u>C</u>O), 155.1 (d, $^{1}J_{PC}$ = 24.3 Hz, Ti<u>C</u>), 148.9 (br d, $^{1}J_{CF}$ = 244.4 Hz, *o*-<u>C_6F_5</u>), 142.3 ($^{3}J_{PC}$ = 27.9 Hz, *i*-<u>C_6H_4</u>Me), 140.4 (*i*-NC($N^{i}Pr_2$)<u>Ph</u>), 138.6 (br d, $^{1}J_{CF}$ = 247.8 Hz , *p*-<u>C_6F_5</u>), 136.8 (br d, $^{1}J_{CF}$ = 249.0 Hz, *m*-<u>C_6F_5</u>), 134.2 (*p*-P<u>Ph</u>$_2$), 133.0 (d, $^{2}J_{PC}$ = 9.0 Hz, *o*-P<u>Ph</u>$_2$), 130.1 (<u>C_5Me_5</u>), 129.9 (*m*-<u>C_6H_4</u>Me) 129.2 (*o*-NC($N^{i}Pr_2$)<u>Ph</u>), 128.8 (*m*-NC($N^{i}Pr_2$)<u>Ph</u>), 126.4 (*p*-NC($N^{i}Pr_2$)<u>Ph</u>), 52.7 (N<u>C</u>HMe_2), 31.0 (Ph_2PCC(Tol)<u>Me</u>,

coupling obscured by $[Ph_3C\underline{Me}]^+$), 21.4 ($C_6H_4\underline{Me}$), 20.4 ($NCH\underline{Me}_2$), 19.8 ($NCH\underline{Me}_2$), 12.5 ($C_5\underline{Me}_5$) ppm. ^{31}P-{^1H} NMR (C_6D_5Br, 121.4 MHz, 293 K) 25.9 ppm. ^{19}F NMR (C_6D_5Br, 282.1 MHz, 293 K) -131.5 (m, *o*-C_6F_5)), -161.9 (m, *p*-C_6F_5), -165.8 (m, *m*-C_6F_5) ppm. ^{11}B NMR (C_6D_5Br, 96.2 MHz, 293 K) -16.1 ppm.

[Cp*Ti{NC(N^{i}Pr$_2$)Ph}{(Ph$_2$PCC(Tol)Me)C(N^{i}Pr)$_2$}][BF$_{20}$] (59-[BF$_{20}$])

[Cp*Ti{NC(N^{i}Pr$_2$)Ph}{Ph$_2$PCC(Tol)Me}][BF$_{20}$] (500 mg, 0.36 mmol) and ^{i}PrNCN^{i}Pr (46 mg, 57 μl, 0.36 mmol) were mixed together in fluorobenzene (10 ml). After 30 min pentane (20 mL) was added resulting in the formation of a red oil. The pentane/fluorobenzene was decanted and the oil washed with pentane (10 ml). The remaining solvent was removed *in vacuo* yielding the product as a red solid. Yield: 349 mg (64%) ^1H NMR (C_6D_5Br, 299.9 MHz, 293 K) 7.45-6.67 (Ar, 15H), 4.36 (1H, br, κ^1-NC$\underline{H}$Me$_2$, 3.79 (2H, sept d., ^3J = 6.3 Hz, $^5J_{PH}$ = 1.7 Hz, κ^2-NC$\underline{H}$Me$_2$), 3.23 (1H, sept, ^3J = 6.9, κ^1-NC$\underline{H}$Me$_2$), 2.15 (3H, s, $C_6H_4\underline{Me}$), 1.86 (3H, d, $^4J_{PH}$ = 1.11 Hz, CC$\underline{Me}$), 1.77 (15H, s, $C_5\underline{Me}_5$), 0.90 (6H, d, ^3J = 6.9 Hz, κ^1-NC$\underline{H}$Me$_2$), 0.71 (6H, d, ^3J = 6.9 Hz, κ^2-NCH$\underline{Me}_2$), 0.60 (6H, d, ^3J = 6.3 Hz, κ^1-NC$\underline{H}$Me$_2$), -0.05 (6H, d, ^3J = 6.3 Hz, κ^2-NCH$\underline{Me}_2$) ppm. ^{13}C-{^1H} NMR (C_6D_5Br, 75.4 MHz, 293 K) 170.8, (d, $^2J_{PC}$ = 33.5 Hz, -$\underline{C}$(N^{i}Pr)$_2$), 168.2 (N$\underline{C}$(N^{i}Pr$_2$)Ph), 156.9 (d, $^4J_{PC}$ = 4.12 Hz, *o*-$\underline{C}_6H_4$Me), 139.2 (d, $^2J_{PC}$ = 28.1 Hz, C$\underline{C}$Me), 136.3 (*i*-NC(N^{i}Pr$_2$)$\underline{Ph}$), 134.9 (d, $^3J_{PC}$ = 16.0 Hz, *i*-$\underline{C}_6H_4$Me), 132.7 (d, ^3J = 19.5, *m*-P$\underline{Ph}_2$), 129.1 ($\underline{C}_5Me_5$), 129.0 ($\underline{C}$CMe), 128.1 (*m*-NC(N^{i}Pr$_2$)$\underline{Ph}$), 127.8 (d, $^4J_{PC}$ = 3.6 Hz, *p*-P$\underline{Ph}_2$), 124.2 (d, $^4J_{PC}$ = 3.9 Hz, *o*-$\underline{C}_6H_4$Me), 121.8 (d, $^1J_{PC}$ = 42.1 Hz, *i*-P$\underline{Ph}_2$), 115.8 (d, $^2J_{PC}$ = 21.1 Hz, *o*-P$\underline{Ph}_2$), (κ^2-N$\underline{C}$HMe$_2$), 49.1 (κ^1-N$\underline{C}$HMe$_2$), 25.8 (Ph$_2$PCC(Tol)$\underline{Me}$), 25.4 (κ^1-N$\underline{C}$HMe$_2$), 25.0 (κ^2-N$\underline{C}$HMe$_2$), 23.6 (κ^2-N$\underline{C}$HMe$_2$), 21.2 ($C_6H_4\underline{Me}$), 21.0 (κ^1-N$\underline{C}$HMe$_2$), 13.2 ($C_5\underline{Me}_5$) ppm. ^{31}P-{^1H} NMR (C_6D_5Br, 121.4 MHz, 293 K) -6.1 ppm. IR (NaCl plates, Nujol mull, cm^{-1}) 1642 (w), 1585 (w), 1513 (s), 1490 (m), 1332 (m), 1274 (w), 1208 (w), 1137 (w), 1085 (m), 1028 (w), 980 (s), 842 (w), 789 (w), 756 (w), 684 (w). ^{19}F NMR (C_6D_5Br, 282.1 MHz, 293 K) -131.5 (m, *o*-C_6F_5), -162.1 (m, *p*-C_6F_5), -166.0 (m, *m*-C_6F_5) ppm. ^{11}B NMR (C_6D_5Br, 96.2 MHz, 293 K) -16.0 ppm. Anal. Found (calcd. for $C_{76}H_{68}BF_{20}N_4PTi$): C, 60.35 (60.57); H, 4.71 (4.55); N, 3.88 (3.72).

5.7 General polymerisation procedure

Polymerisation testing was carried out at Lanxess Elastomers, The Netherlands, by Mr Ralph Franssen, Mr Philip Kenyon, Mr John van de Moosdijk, Mr. Hans Leduc, Ms Emma de Koning and Dr Richard Scott under the supervision of Drs Alexandra Berthoud and Martin Zuideveld.

5.8 Reagents, cocatalysts and scavengers

Tri*iso*butylaluminium (TiBA, 10 wt.% Al *n*-hexanes solution) was purchased from Akzo Nobel and dosed as 0.10 M solutions in *n*-hexanes. 4-Methyl-2,6-di-*tert*-butylphenol (BHT, > 99.0 %) was purchased from Sigma-Aldrich and dosed as a 0.20 M solution in *n*-hexanes. *Iso*butylaluminoxane (IBAO-65), 3.5 wt.% Al *n*-hexanes solution) was purchased from Akzo Nobel and dosed as 0.10 M solutions in *n*-hexanes. The catalyst precursor solutions were dosed as 1.0 mM solutions in toluene or *n*-hexanes. $[Ph_3C][BF_{20}]$ was dosed as a 2.0 mM solution in toluene. The feed streams (ethylene, propylene, *n*-hexanes, hydrogen, nitrogen) were purified by contacting with various adsorption media to remove impurities such as water, oxygen and polar compounds. Nitrogen, ethylene and hydrogen were purified using 4Å molecular sieves (Merck). Propylene and 2,2,4,6,6-pentamethylheptane (PMH) were purified using Molsieves 13-X (Merck). Nitrogen, ethylene and propylene were further purified with a copper catalyst (BTS R311 (BASF)). The PMH solvent was additionally stripped with nitrogen. In order to avoid mass transfer limitation problems, the total polymer yield in each polymerisation was limited to approximately 10 g after a total polymerisation time of 10 min. The total aluminium concentration in the reactor was kept above 0.45 mM to ensure efficient scavenging.

5.9 Ethylene-propylene copolymerisation

Ethylene-propylene batch copolymerisation reactions were carried out in a 2 L autoclave equipped with a double intermig stirrer and baffles. The reaction temperature was set to 90 °C and regulated by a Lauda LTH303 Thermostat. Ethylene and propylene monomers were continuously fed to the gas cap of the reactor during the conditioning period and the polymerisation time. The total monomer flow was kept constant during each experiment (600 NL/h). The pressure of the reactor was kept constant by a back-pressure valve. In an inert atmosphere of nitrogen (1.8 bar) the reactor was filled with 950 ml of PMH solvent, BHT and TiBA (BHT:TiBA, 2.22:1)

or IBAO-65. It was heated to 90 °C while stirring at 1350 rpm, pressurised to 7 bar by feeding ethylene and propylene and conditioned by applying a fixed ratio of ethylene and propylene for 15 min. The catalyst components were then added as PMH solutions to the reactor and the catalyst vessel was rinsed with an additional 50 mL of PMH. $[Ph_3C][BF_{20}]$ or BF_{15} was added directly after the precatalyst was dosed. After 10 min of polymerisation time the monomer flow was stopped and the solution was carefully transferred to a 2 L Erlenmeyer flask, containing a solution of Irganox-1076 in isopropanol and dried over night at 100 °C under reduced pressure (< 20 mbar). The polymers were analysed for molecular weight distribution (GPC) and composition (FT-IR).

5.10 X-ray data collection and processing parameters

Crystals were mounted on glass fibres using perfluoropolyether oil and cooled rapidly in a stream of dinitrogen gas (150 K) from an Oxford Cryostreams unit. Diffraction data were measured using an Enraf-Nonius KappaCCD diffractometer or Agilent Technologies Supernova diffractometer using Mo-κα or Cu-κα, respectively. As appropriate, absorption and decay corrections were applied to the data and equivalent reflections merged.[43] The structures were solved with SIR92[44] or Superflip[45] and further refinements and all other crystallographic calculations were performed using the CRYSTALS[46] program suite. Other details of structure solutions and refinements (CIF data) are provided in the CD Appendix.

5.11 References

1. A. B. Pangborn, M. A. Giardello, R. H. Grubbs, R. K. Rosen and F. J. Timmers, *Organometallics*, 1996, **15**, 1518-1520.
2. R. Scott, *DPhil Thesis, University of Oxford*, 2013.
3. A. D. Miller, S. A. Johnson, K. A. Tupper, J. L. McBee and T. D. Tilley, *Organometallics*, 2009, **28**, 1252-1262.
4. E. G. Ijpeij, B. Coussens, M. A. Zuideveld, G. H. J. van Doremaele, P. Mountford, M. Lutz and A. L. Spek, *Chem. Commun.*, 2010, **46**, 3339-3341.
5. C. Fonseca Guerra, J. G. Snijders, G. te Velde and E. J. Baerends, *Theor. Chem. Acc.*, 1998, **99**, 391-403.
6. G. te Velde, F. M. Bickelhaupt, E. J. Baerends, C. Fonseca Guerra, S. J. A. van Gisbergen, J. G. Snijders and T. Ziegler, *J. Comput. Chem.*, 2001, **22**, 931-967.

7. *ADF2013, SCM, Theoretical Chemistry, Vrije Universiteit, Amsterdam, The Netherlands*, 2013.
8. S. H. Vosko, L. Wilk and M. Nusair, *Can. J. Phys*, 1980, **58**, 1200.
9. A. D. Becke, *Phys. Rev. A*, 1988, **38**, 3098-3100.
10. A. D. Becke, *J. Chem. Phys.*, 1988, **88**, 1053-1062.
11. J. P. Perdew and W. Yue, *Phys. Rev. B*, 1986, **33**, 8800-8802.
12. J. I. Rodríguez, R. F. W. Bader, P. W. Ayers, C. Michel, A. W. Götz and C. Bo, *Chem. Phys. Lett.*, 2009, **472**, 149-152.
13. J. I. Rodríguez, *J. Comput. Chem.*, 2013, **34**, 681-686.
14. G. W. T. M. J. Frisch, H. B. Schlegel, G. E. Scuseria, M. A. Robb, J. R. Cheeseman, G. Scalmani, V. Barone, B. Mennucci, G. A. Petersson, H. Nakatsuji, M. Caricato, X. Li, H. P. Hratchian, A. F. Izmaylov, J. Bloino, G. Zheng, J. L. Sonnenberg, , M. E. M. Hada, K. Toyota, R. Fukuda, J. Hasegawa, M. Ishida, T. Nakajima, Y. Honda, O. Kitao, H. Nakai, T. Vreven, J. A. Montgomery, Jr., J. E. Peralta, F. Ogliaro, M. Bearpark, J. J. Heyd, E. Brothers, K. N. Kudin, V. N. Staroverov, R. Kobayashi,, K. R. J. Normand, A. Rendell, J. C. Burant, S. S. Iyengar, J. Tomasi, M. Cossi, N. Rega, J. M. Millam, M. Klene, J. E. Knox, J. B. Cross, V. Bakken, C. Adamo, J. Jaramillo, R. Gomperts, R. E. Stratmann, O. Yazyev, A. J. Austin, R. Cammi, and J. W. O. C. Pomelli, R. L. Martin, K. Morokuma, V. G. Zakrzewski, G. A. Voth, P. Salvador, J. J. Dannenberg, S. Dapprich, A. D. Daniels, Ö. Farkas, J. B. Foresman, J. V. Ortiz, J. Cioslowski, and D. J. Fox, , *Gaussian 09*, Gaussian, Inc., Wallingford CT, 2009.
15. R. Ahlrichs, M. Bär, M. Häser, H. Horn and C. Kölmel, *Chem. Phys. Lett.*, 1989, **162**, 165-169.
16. O. Treutler and R. Ahlrichs, *J. Chem. Phys.*, 1995, **102**, 346-354.
17. M. B. R. Ahlrichs, H.-P. Baron, R. Bauernschmitt, S. Bocker,, K. E. M. Ehrig, S. Elliott, F. Furche, F. Haase, M. Haser, C., H. H. Hattig, C. Huber, U. Huniar, M. Kattannek, A. K ¨ ohn, C., M. K. Kolmel, K. May, C. Ochsenfeld, H. Ohm, A. Schafer, , O. T. U. Schneider, K. Tsereteli, B. Unterreiner, M. von and F. W. Arnim, P. Weis, H. Weiss Turbomole Version 5, January 2002, Theoretical Chemistry Group, University of Karlsruhe.
18. C. Lee, W. Yang and R. G. Parr, *Phys. Rev. B*, 1988, **37**, 785-789.
19. A. D. Becke, *J. Chem. Phys.*, 1993, **98**, 1372-1377.

20. A. D. Becke, *J. Chem. Phys.*, 1993, **98**, 5648-5652.
21. Y. Zhao and D. Truhlar, *Theor. Chem. Acc.*, 2008, **120**, 215-241.
22. A. Schäfer, H. Horn and R. Ahlrichs, *J. Chem. Phys.*, 1992, **97**, 2571-2577.
23. T. H. Dunning Jr. and P. J. Hay, *Modern Theoretical Chemistry*, H. F. Schaefer III edn., Plenum, New York, 1977.
24. P. J. Hay and W. R. Wadt, *J. Chem. Phys.*, 1985, **82**, 270-283.
25. W. R. Wadt and P. J. Hay, *J. Chem. Phys.*, 1985, **82**, 284-298.
26. P. J. Hay and W. R. Wadt, *J. Chem. Phys.*, 1985, **82**, 299-310.
27. A. Schäfer, C. Huber and R. Ahlrichs, *J. Chem. Phys.*, 1994, **100**, 5829-5835.
28. J. P. Perdew and Y. Wang, *Phys. Rev. B*, 1992, **45**, 13244-13249.
29. P. D. Bolton, E. Clot, N. Adams, S. R. Dubberley, A. R. Cowley and P. Mountford, *Organometallics*, 2006, **25**, 2806-2825.
30. D. Andrae, U. Häußermann, M. Dolg, H. Stoll and H. Preuß, *Theor. Chim. Acta*, 1990, **77**, 123-141.
31. A. W. Ehlers, M. Böhme, S. Dapprich, A. Gobbi, A. Höllwarth, V. Jonas, K. F. Köhler, R. Stegmann, A. Veldkamp and G. Frenking, *Chem. Phys. Lett.*, 1993, **208**, 111-114.
32. A. Bergner, M. Dolg, W. Kuchle, H. Stoll and H. Preuss, *Mol. Phys.*, 1993, **30**, 1431.
33. A. Hollwarth, H. Bohme, S. Dapprich, A. W. Ehlers, A. Gobbi, V. Jonas, K. F. Kohler, R. Stagmann, A. Veldkamp and G. Frenking, *Chem. Phys. Lett.*, 1993, **203**, 237.
34. P. C. Hariharan and J. A. Pople, *Theor. Chim. Acta*, 1973, **28**, 213-222.
35. W. Kutzelnigg, U. Fleischer and M. Schindler, *IGLOO-II*, Springer-Verlag: Berlin, 1990.
36. T. H. Dunning, *J. Chem. Phys.*, 1989, **90**, 1007-1023.
37. R. A. Kendall, T. H. Dunning and R. J. Harrison, *J. Chem. Phys.*, 1992, **96**, 6796-6806.
38. K. A. Peterson, D. E. Woon and T. H. Dunning, *J. Chem. Phys.*, 1994, **100**, 7410-7415.
39. D. E. Woon and T. H. Dunning, *J. Chem. Phys.*, 1993, **98**, 1358-1371.
40. V. Barone, *Recent Advances in Density Functional Methods, Part I, Ed. D. P. Chong*, 1996, World Scientific Publ. Co., Singapore, .

41. E. G. Ijpeij, P. J. H. Windmuller, H. J. Arts, F. Van der Burgt, G. H. J. Van Doremaele and M. A. Zuideveld, *LANXESS ELASTOMERS, WO/2005/090418*, 2005.
42. W. P. Kretschmer, *Stichting Dutch Polymer Institute, US20040192541A1*, 2004.
43. Z. Otwinowski and W. Minor, *Processing of X-ray Diffraction Data Collected in Oscillation Mode*, Academic Press, New York, 1997.
44. A. Altomare, G. Cascarano, C. Giacovazzo and A. Guagliardi, *J. Appl. Crystallogr.*, 1994, **27**, 1045-1050.
45. L. Platinus and G. Chapuis, *J. Appl. Cryst.*, 2007, **40**, 284.
46. P. W. Betteridge, J. R. Carruthers, R. I. Cooper, K. Prout and D. J. Watkin, *J. Appl. Crystallogr.*, 2003, **36**, 1487.